Computational Investigation of Condensed Phase Properties of Ionic Systems

by

Tae Bum Lee

A dissertation submitted to the Graduate Faculty of
Auburn University
in partial fulfillment of the
requirements for the Degree of
Doctor of Philosophy

Auburn, Alabama
May 7, 2012

Keyword: ab intio, solvation, multi-anion, pK_a, lattice energy, redox potential

Approved by

Michael L. McKee, Chair, Professor of Department of Chemistry and Biochemistry
J. Vincent Ortiz, Ruth W. Molette Professor of Department of Chemistry and Biochemistry
German Mills, Associate Professor of Department of Chemistry and Biochemistry
Orlando Acevedo, Assistant Professor of Department of Chemistry and Biochemistry

Abstract

Four computational studies have been performed with various computational techniques including density functional theory, post-HF theory, and implicit solvation modeling to investigate the dehydrogenation mechanism of $LiNH_2BH_3(s)$, acid dissociation constants (pK_{a1}, pK_{a2}, and pK_{a3}) of polyprotic acids, the dissolution free energy of alkali-metal dianion salts (M_2X_1), and redox potentials of polyboranes. Theoretical background and computational methodology in these studies are introduced in chapter 1. Chapter 2-5 present four different studies exploring condensed-phase properties of inorganic materials including reaction mechanisms.

Chapter 2 reports on the formation of $LiNH_2BH_3$ from $(LiH)_4$ and NH_3BH_3 and their subsequent dehydrogenation. The free energy of activation for loss of H_2 is reduced from 37.2 kcal/mol in NH_3BH_3 to 11.0 kcal/mol in $(LiH)_4 + NH_3BH_3$. Further, H_2 elimination from the $(LiNH_2BH_3)_2$ dimer is predicted to be much easier than from the monomer which may suggest that a cooperative H_2-loss mechanism is possible in solid $LiNH_2BH_3$.

Chapter 3 reports a systematic study of $\Delta G_{aq}/pK_a$ for monoprotic, diprotic, and triprotic acids based on DFT/aug-cc-pVTZ combined with CPCM and SMD solvation modeling. All DFT/cavity set combinations considered showed similar accuracy for $\Delta G_{aq}^1/pK_{a1}$ (70% within ±2.5 kcal/mol of experiment) while only the M05-2X/Pauling cavity combination gave reasonable results for $\Delta G_{aq}^2/pK_{a2}$ when both pK_a values are separated by more than three units (70% within ±5.0 kcal/mol of experiment).

Chapter 4 reports on the dissolution Gibbs free energies (ΔG^o_{diss}) of salts (M_2X_1) using the Conductor-like Polarizable Continuum Model (CPCM) solvation modeling. The absolute solvation free energies of the alkali metal cations ($\Delta G_{solv}(M^+)$) come from the literature, which coincide well with half reduction potential versus SHE data. Lattice free energies (ΔG_{latt}) of salts were determined by three different approaches: (1) volumetric, (2) a cohesive Gibbs free energy (ΔG_{coh}) plus gaseous dissociation free energy (ΔG_{gas}), and (3) the Born-Haber cycle. Only the M05-2X/Pauling combination with the three different methods for estimating ΔG_{latt} yields the expected negative dissolution free energies (ΔG^o_{diss}) of M_2SO_4.

Chapter 5 reports the reduction potentials (E^o_{Red} versus SHE) of *hypercloso* boron hydrides B_nH_n (n=6-13) and $B_{12}X_{12}$ (X=F, Cl, OH, and CH_3) with CPCM and SMD solvation modeling. The E^o_{Red} of $B_nH_n^{-/2-}$ (n=6-12) with the G4/M06-2X/Pauling (energy/solvation/cavity) combination agrees within 0.2 V of experimental values. The experimental oxidative stability ($E_{1/2}$) of $B_nX_n^{2-}$ (X=F, Cl, OH, and CH_3) is usually located between the values predicted using the B3LYP and M06-2X functionals. The disproportionation free energies (ΔG_{dpro}) of $2B_nH_n^- \rightarrow B_nH_n + B_nH_n^{2-}$ reveal that the stabilities of $B_nH_n^-$ (n=6-13) to disproportionation decrease in the order $B_8H_8^- > B_9H_9^- > B_{11}H_{11}^- > B_{10}H_{10}^-$. The spin densities in $B_{12}X_{12}^-$ (X=F, Cl, OH, and CH_3) tend to delocalize on the boron atoms rather than on the exterior functional groups. The partitioning of $\Delta G_{solv}(B_nH_n^{2-})$ over spheres allows a rationalization of the nonlinear correlation between $\Delta G_{E.A.}$ and E^o_{Red} for $B_6H_6^{-/2-}$, $B_{11}H_{11}^{-/2-}$, and $B_{13}H_{13}^{-/2-}$.

Acknowledgments

Without the following people's help, I would have had trouble to pursue my academic research career in Auburn. My fearless leader, Dr. McKee guided me into the appropriate direction with technical advice and insight for interpretation. For the reaction kinetics in condensed phase, advice from Dr. Mills was helpful to understand my computational results in the $LiNH_2BH_3$ for hydrogen storage project. Dr. John Gorden gave me the interpretation of alkali metal crystal structure for my computation. The advice about solution chemistry from Dr. Stanbury was also important to my research. Dr. Cammarata guided me in the interpretation of cyclic voltammetry and redox potential literature data. The electron affinity from the electron propagator theory was successfully done with the help of Dr. Dolgounitcheva and Dr. El Zein. Dr. Patkowski gave a valuable guide about molecular interactions and helped me with the modification of Grimme's dispersion potential. I deeply appreciate Dr Webb's review for all of my manuscripts for publication, which are each now a chapter in my dissertation.

All my research committee (Dr. McKee, Dr. Ortiz, Dr. Mills, and Dr. Acevedo) reminded me what I knew and what I did not know. Beside my dissertation research topic, Dr. Anne Gorden, Dr. Stewart Schneller, and Dr. Christian Goldsmith presented several chances to join collaboration research with them. I would like to thank all of staff in Department of Chemistry and Biochemistry for their hospitality and kindness.

Style manual or journal manual used: Journal of American Chemical Society

Computer software used: MS word for Mac 2011, gnuplot 4.2, CS ChemDraw Ultra 9.0, and

Molecule 1.3.5d

Table of Contents

List of Tables

x

List of Figures

Chapter 1

Chapter 2

List of Schemes

List of Abbreviations

DFT   Density Functional Theory

LDA   Local Density Approximation

GGA   Generalized Gradient Approximation

ACM   Adiabatic Connection Method

HOMO   Highest Occupied Molecular Orbital

LUMO   Lowest Unoccupied Molecular Orbital

OVGF   Outer Valence Green Function

SCRF   Self-Consistent Reaction Field

PCM   Polarizable Continuum Model

CPCM   Conductor-like Polarizable Continuum Model

MP2   Møller-Plesset at the second-order

CCSD(T)   Coupled-Cluster Single and Double excitation fully and Triple excitation with
            perturbation theory

IRC   Intrinsic Reaction Coordinates

SHE   Standard Hydrogen Electrode

NIST   National Institute of Standards and Technology

ZPE   Zero Point Energy

QCISD(T)   Quadratic Configuration Interaction with Single and Double Excitations and Triple
            Excitations added Perturbatively

SAPT   Symmetry Adapted Perturbation Theory

ESR   Electron Spin Resonance

Chapter 1

General Introduction

1.1 Density functional theory

Density functional theory (DFT) has become a "household tool" for chemists. However, the dawn of density functional theory for chemical science took a series of stepwise advances. If the energy of an electronic system can be separated into a kinetic and potential part, the classical potential energy is the simplest form while the kinetic energy of continuous charge distribution is less obvious. Thomas and Fermi used fermion statistical mechanics to derive the kinetic energy for the uniform electron gas system as

$$T[\rho(r)] = \frac{3}{10}(3\pi^2)^{2/3} \int \rho^{5/3}(r)dr$$

(1)

T is a function of the density while the density itself is a function of the 3-D spatial coordinates. A function whose argument is also a function is called a 'functional' and the T becomes a 'density functional'. However, the Thomas-Fermi equation with variational principle is of no use in modern chemistry since all molecules are unstable relative to dissociation into their constituent atoms. With a simple approximations of exchange energy (e.x. Thomas-Fermi-Dirac model), the early DFT methods were applied widely in the solid-state physics community. One major approximation in the early stage of density functional theory is the interelectronic repulsion, which is associated with exchange and correlation. The density functional theory applies the concept of 'hole function ($h(r_1;r_2)$)' to correct the energetic errors (eq 2).

$$\langle\Psi| \sum_{i<j}^{electron} \frac{1}{r_{ij}}|\Psi\rangle = \frac{1}{2}\int\int\frac{\rho(r_1)\rho(r_2)}{|r_1-r_2|}dr_1dr_2 + \frac{1}{2}\int\int\frac{\rho(r_1)h(r_1;r_2)}{|r_1-r_2|}dr_1dr_2$$

(2)

The exact quantum mechanical interelectronic repulsion (left hand side of eq 2) is described with the correction for classical repulsion with the hole function, $h(r_1;r_2)$ (eq 2). In the one-electron case, the function $h(r1;r2)$ is clearly the negative of the density but the exact form of $h(r_1;r_2)$ in the many-electron case becomes hard to determine. However, the hole functions in many electron systems account for exchange and correlations as well as the self-interaction error. The electron-electron repulsion (self-interaction error) in the one-electron system can be solved in a Hartree-Fock scheme but the representation of the exchange energy constitutes a major obstacle in density functional theory. In order to apply DFT methods in the chemical sciences, the variational principle should be proved. If we have some well-behaved candidate density for the integration of N electrons, this density can be a candidate wavefunction and Hamiltonian (Hohenberg-Kohn first theorem). The energy expectation value is given by

$$\langle\Psi_{candidate}|H_{candidate}|\Psi_{candidate}\rangle = E_{candidate} \geq E_0$$

(3)

where E_0 means the ground state energy. The challenge is how to select a well-behaved density itself while the mappings from density onto the Hamiltonian and wavefunction is available. The machinery to determine the energy directly without recourse to the wavefunction is needed and the introduction of Kohn-Sham self-consistent field method is proposed.

Kohn-Sham scheme is operationally a variant of Hartree-Fock method, where the complicated Hartree-Fock exchange operator is replaced by much simpler density functional.[1] The Hartree-Fock is a deliberately approximate theory, which is motivated by an ability to solve

2

the relevant equations exactly. DFT is an exact theory but the relevant equations should be

solved approximately since the key operator has an unknown form. Integration of the exchange-

correlation functional lies at the heart of DFT and gives it an enormous edge, in terms of

computational efficiency over the Hartree-Fock based *ab initio* method. The ground state energy

E is a functional of ρ and the total energy can be expressed as:

$$E[\rho] = T_s[\rho] + V_{ext}[\rho] + J[\rho] + E_{xc}[\rho] \tag{4}$$

The key to DFT development is the approximate functionals of $E_{xc}[\rho]$ while $T_s[\rho]$ is the kinetic

energy of an independent electron, $V_{ext}[\rho]$ is the potential energy in the field of the nuclei

including external perturbation, and $J[\rho]$ is the total Coulomb interaction. However, there is no

systematic way to improve $E_{xc}[\rho]$. The first success of DFT for practical purposes came with the

use of the local density approximation (LDA), in which the function for the uniform electron gas

density ρ is integrated over the whole space:

$$E_{xc}^{LDA} = \sum_{\sigma} \int \epsilon_{xc}^{unif}(\rho_\sigma)\rho_\sigma(r)^{4/3} dr \tag{5}$$

Incorporation of the uniform exchange-correlation energy distribution per unit volume is

responsible for the early success of DFT in solid-state physics but the uniform electron gas

model frequently produces unsatisfactory results in chemical applications. The most distinct

improvement of the LDA approach is achieved by introduction of thr electron density gradient

∇ρ, which is suitable to present non-uniformity of atomic and molecular densities. The

correction is collectively referred to as generalized gradient approximation (GGA), which is

3

expressed in terms of an enhancement factor over the exchange-correlation energy of the uniform electron gas. The total exchange-correlation energy takes the form:

$$E_{xc}^{GGA} = E_{xc}^{LDA} - \sum_{\sigma} \int F_{xc}^{GGA}[\rho_{\sigma}, \nabla\rho_{\sigma}]\rho_{\sigma}(r)^{4/3} dr$$

(6)

Due to the absence of a unique function for F_{xc}^{GGA}, a number of GGA exchange-correlation functionals have been proposed. In practice, the $E_{xc}[\rho]$ can be presented as the sum of an exchange functional (E_x) and a correlation functional (E_c) which depend on the electron density. Therefore, any exchange functional can be combined with various correlation functionals. The separation of exchange functional introduces the application of the Hartree-Fock exchange term with the DFT correlation functional, the so-called hybrid DFT method. For hybridization, a useful method is to apply the extent of interelectronic interaction, λ through the Hellmann-Feynman theorem (eq 7).

$$E_{XC} = \int_0^1 \langle \Psi(\lambda)|V_{XC}(\lambda)|\Psi(\lambda)\rangle d\lambda$$

(7)

Figure 1 describes the decomposition of exchange-correlation energy with the variable, λ. The area **A** can be produced with the Hartree-Fock exchange (E_C^{HF}) since the expectation value of V_{XC} is the exact exchange for the non-interacting system and can be computed in a Hartree-Fock calculation (Figure 1). The remaining area (**B**) is a portion of $\langle \Psi(1)|V_{XC}(1)|\Psi(1)\rangle - E_X^{HF}$, which is the second rectangle on top of **A** (Figure 1). The challenge is that not only do we not know the portion (z) but also the expectation value of the full interacting exchange-correlation potential. If

4

the empirical constant of z is to be optimized, a convenient approximation of E_{XC} can be

establilshed. The total area under the expectation value (V_{XC}) curve in Figure 1 (**A+B**) is given

by

$$E_{XC} = E_X^{HF} + z(E_{XC}^{DFT} - E_X^{HF})$$

(8)

$$E_{XC} = (1-a)E_{XC}^{DFT} + aE_X^{HF}$$

(9)
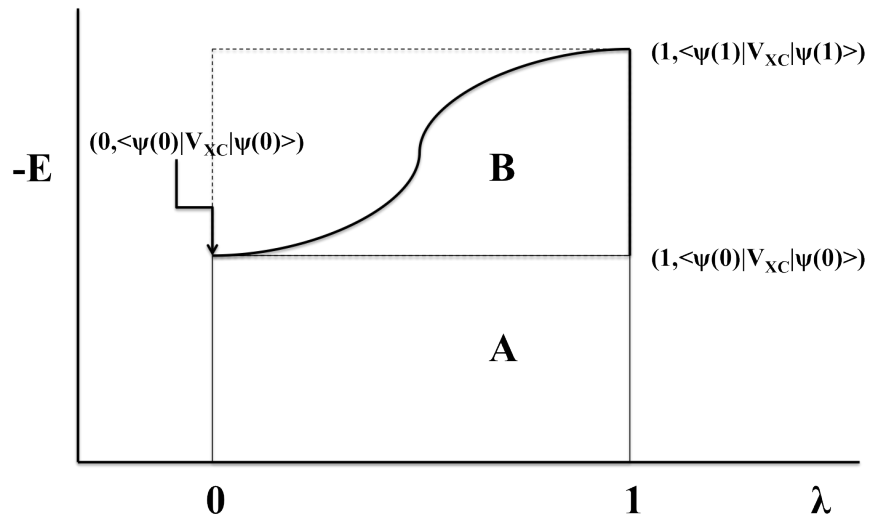
Figure 1. Schematic diagram for the evaluation of exchange-correlation energy (E_{XC}). The area

under the curve is the sum of expectation value of Hartree-Fock exchange operator for

non-interacting system and the corresponding value from an approximated DFT

calculation for $\langle\psi(1)|V_{XC}(1)|\psi(1)\rangle$.

where another variable a=1-z is defined (eq 8 and 9). This analysis is also called the adabatic

connection method (ACM) and we can conveniently connect the non-interacting and fully

interacting state. The most primitive constant is a=0.5 so called half-half method and later one

applies multiple constants to the ababatic connection method. One of the proposed three-parameter functional is given with the introduction of LSDA (Local Spin Density Approximation) term and Becke 88 exchange functional (eq 10).

$$E_{XC}^{B3PW91} = (1-a)E_X^{LSDA} + aE_X^{HF} + b\Delta E_X^B + E_C^{LSDA} + c\Delta E_C^{PW91} \qquad (10)$$

The LYP (Lee-Yang-Parr correlation) functional, which is designed to compute the full correlation energy, replaces the PW91 functional and the most popular hybrid DFT method emerges so called B3LYP (eq 11).

$$E_{XC}^{B3PW91} = (1-a)E_X^{LSDA} + aE_X^{HF} + b\Delta E_X^B + (1-c)E_C^{LSDA} + c\Delta E_C^{LYP} \qquad (11)$$

Without reoptimization of the three parameters in eq 10, the BLYP method presents remarkabley good performance in the early stage of DFT applications for general chemical research. The serendipitous success in computational chemistry is very rare but the overall performance of BLYP for molecular science has been impressive until the issue of intermolecular interaction emerged.

1.2 Meta-GGA functional

The ultimate goal of DFT method development is the generation of a totally non-local density functional and the logical next step in functional improvement is to take into account the second derivatives of the electron density, ie., the Laplacian. Such functionals are termed meta-GGA functionals. However, numerically stable calculation of the Laplacian of density is

techanically challenging. An alternative meta-GGA is implemented with the introduction of the kinetic energy density τ, which is defined as:

$$\tau_\sigma(r) = \frac{1}{2} \sum_i^{occup} |\nabla \Psi_{i\sigma}(r)|^2$$

(12)

$$E_{xc}^{m-GGA} = E_{xc}^{LDA} - \sum_\sigma \int F_{xc}^{GGA}[\rho_\sigma, \nabla\rho_\sigma, \tau]\rho_\sigma(r)^{4/3} dr$$

(13)

where the Ψ is self-consistently determined from Kohn-Sham orbitals. The Truhlar group performed the most active development of meta-GGA functionals, which is represented by M05, M05-2X, M06, and M06-2X.[2] Truhlar group's meta-GGA method also applies hybrid DFT scheme with the Hartree-Fock exchange term:

$$E_{xc}^{hybrid} = \frac{X}{100} E_x^{HF} + (1 - \frac{X}{100})E_x^{DFT} + E_c^{DFT}$$

(14)

$$E_{xc}^{hybrid} = E_x^{HF} + (1 - \frac{X}{100})(E_x^{DFT} - E_x^{HF}) + E_c^{DFT}$$

(15)

Where E_x^{HF} is the nonlocal Hartree-Fock exchange energy, X is the percentage of Hartree-Fock exchange in the hybrid functional, E_x^{DFT} is the local DFT exchange energy and E_c^{DFT} is the local DFT correlation energy. E_c^{DFT} gives the dynamical correlation energy and the nondynamical correlation energy is contained in (1-X/100)($E_x^{DFT} - E_x^{HF}$). The optimization of X along with the parameters in new functionals is the main task in hybrid meta-GGA development. With the

improvement of the thermochemistry, kinetics, and reaction barrier height, and transition metal chemistry the most important impact of meta-GGA approach is the advanced description of intermolecular interactions, which is governed by the medium range correlation energy. The B3LYP functional is known to be good for the determination of molecular geometry but the isomerization energy calculation is beyond the current chemical accuracy.[3] Non-covalent interactions in molecular systems are almost ubiquitous in every chemical applications and the meta-GGA approach presents an alternative calculation method for dispersion interactions using affordable computational resources.

1.3 Dispersion correction for density functional theory

A general drawback of all common GGA functionals including hybrid DFT functionals is that they cannot describe long-range electron-correlations. The long-range electron-correlation is responsible for the van der Waals (dispersion) force of many chemical systems. Practically any conventional DFT can be modified with the empirical correction for dispersion with a $C_6 \cdot R^{-6}$ term, which is so called DFT-D. The successful application of DFT-D needs consistent atomic parameters (C_6 coefficients) for all elements of the periodic table. The GGA functionals for DFT-D method are pure GGA functionals while the meta-GGA functionals frequently use a hybrid approach together with Hartree-Fock method.[3] The total energy of DFT-D is given by

$$E_{DFT-D} = E_{KS-DFT} + E_{disp} \tag{16}$$

Where E_{KS-DFT} is usually the Kohn-Sham energy and E_{disp} is an empirical dispersion energy given by

$$E_{disp} = -s_6 \sum_{i=1}^{N} \sum_{j=i+1}^{N} \frac{C_6^{ij}}{R_{ij}^6} f_{dmp}(R_{ij})$$

(17)

N is the number of atoms in the system. C_6^{ij} is the dispersion coefficient for atom pair ij while s_6 is a global scaling factor which depends on the choice of density fuctionals. The calculation of C_6^{ij} is available from the geometric mean ($C_6^{ij} = \sqrt{C_6^i C_6^j}$) of the form. R_{ij} is an interatomic distance. The incorporation of the damping function for small R_{ij} is mandatory to avoid near-singularities. The $f_{dmp}(R_{ij})$ is given by

$$f_{dmp}(R_{ij}) = \frac{1}{1 + e^{-d(R_{ij}/R_r - 1)}}$$

(18)

where R_r is the sum of atomic van der Waals radii. Grimme's group has developed a C_6 parameter for atoms and a s_6 scale factor for GGA functionals.[4] Since the dispersion interaction is important to the interaction in crystal, DFT-D/planewave approach[5] is applied for the periodic boundary system with the real space summation scheme for dispersion interaction given by

$$E_{disp} = -\frac{1}{2} \sum_{ij} C_{6ij} [\sum_{\vec{R}} |\vec{r_{ij}} + \vec{R}|^{-6} f_{damp}(|\vec{r_{ij}} + \vec{R}|)]$$

(19)

$$f_{damp}(|\vec{r_{ij}} + \vec{R}|) = s_6[1 + exp[-d(\frac{|\vec{r_{ij}} + \vec{R}|}{r_0} - 1)]]^{-1}$$

(20)

where $\vec{r_{ij}} = (\vec{r_j} - \vec{r_i})$ is the atom-atom distance vector, $\vec{R} = (l\vec{a} + m\vec{b} + n\vec{c})$ is the lattice vector. Parameter d tunes the steepness of the damping function. In order to cover long-range dispersive interactions, the inner summation of eq 11 runs over the lattice parameters until the $|\vec{r_{ij}} + \vec{R}|$ becomes larger than 100 Å.

1.4 Pseudopotential

Hellmann[8] introduced first the approximation of pseudopotential with orthogonality to all the core states. The pseudopotential approximation has been popular since the complicated effects of the motion of core electrons of an atom are replaced with a simplified effective potential (Figure 2).
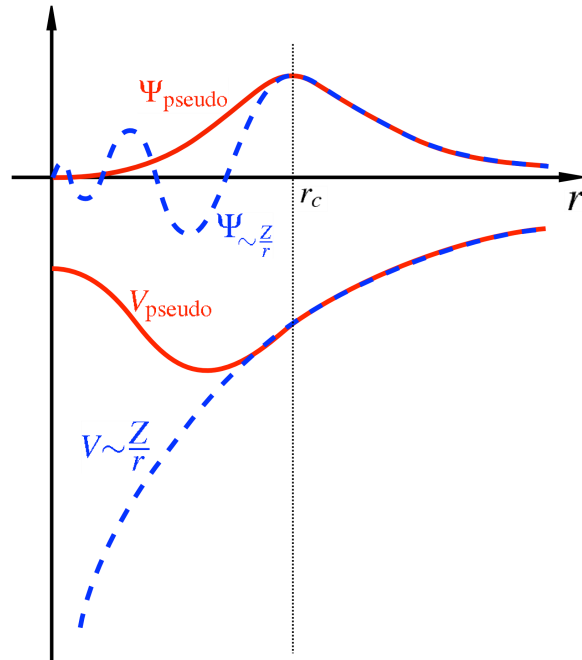
Figure 2. The wavefunction in the Coulomb potential of the nucleus (blue) and pseudopotential (red). At a certain cutoff (r_c), the real and pseudo wavefunction and potentials match each other.

10

The nuclei are rigid non-polarizable (frozen) ion cores while the valence electrons are described with nodeless pseudo-wavefunctions. The pseudopotential approach successfully applied to condensed phase properties including solution state because using a pseudopotential reduces the size of the basis set and the number of electrons. Recent development of relativistic pseudopotentials allows application to heavy-atom systems.[9] The general idea behind the pseudopotential approximation is that the exact Hamiltonian (H_{exact}) can be replaced with an effective Hamiltonian (H_{pp}) with a pseudopotential operator V_{pp}. For example, the molecular pseudo-Hamiltonian (H_v) is given by

$$H_v = -\frac{1}{2}\sum_i^{n_v}\nabla_i^2 + \sum_i^{n_v}\sum_a^{n_c}[V_{pp}^a(r_{ai}) - \frac{Q_a}{r_{ai}}] + \sum_{a<b}^{N_c}\frac{Q_aQ_b}{r_{ab}}$$ (21)

with n_v the number of valence electrons and N_c the number of cores (nuclei), and the indices a,b are applied to all cores, Q_a is the charge of core a and the last term of eq 21 is the classical core-core repulsion induced by point charges. Here V_{pp} is the one-electron pseudopotential operator, which separates valence eletrons from core region. The pure ionic core part of the pseudopotential ($V_l^{PP,ion}(r)$) is represented with Hartree, exchange-correlation, and screened pseudopotential ($V_l^{PP,scr}(r)$) terms.

$$V_l^{PP,ion}(r) = V_l^{PP,scr}(r) - V_{Hartree}^{PP}(r) - V_{xc}^{PP}(r)$$ (22)

$$V_l^{PP,scr}(r) = \epsilon_l - \frac{l(l+1)}{2r^2} + \frac{1}{2r\varphi_l^{PP}(r)}\frac{d^2}{dr^2}r\varphi_l^{PP}(r)$$ (23)

It should be noted that different pseudopotentials should be used for different exchange-correlation functionals. Norm-conserving pseudopotentials, which are originated from the orthogonalized planewave approximation,[10] are constructed from Kohn-Sham rather than Hartree-Fock equations and are dependent on the functionals used. The norm-conserving pseudopotential enforces the condition that no significant overlaps exist between core and valence wavefunctions. The nonlinear core correction[11] or semicore electron inclusion[12] deals with a situation where overlap is non-negligible. If all above works well, the norm of pseudopotential is identical to its corresponding all-electron wavefunction.[13] The development of ultrasoft pseudopotential introduces a relaxation of the norm-conserving constraint with the reduction of basis set.[14] However, incorporation of norm-conserving pseudopotential and ultra-soft pseudopotential is applicable to any system.

1.5 G4 level of theory – a composite method

Accurate prediction of thermochemistry data has been attempted using various high-level *ab initio* computations. The Gaussian-n(Gn) theories (n=1,2,3 and now 4) employ a series of calculations with different levels of accuracy and basis sets to approach exact energy of system.[6] The Gaussian-4 (G4) theory is a composite method with a sequence of well-defined *ab initio* calculations.[7] The each steps in G4 theory are as follows.

(1) The molecular geometry of equilibrium structure is obtained by B3LYP/6-31G(2df,p) while G3 theory use the MP2(full)/6-31G* level.

(2) The harmonic frequency of equilibrium structure is calculated using B3LYP/6-31G(2df,p) and scaled by an empirical factor of 0.9854. The zero-point energy (ZPE) uses this harmonic frequency calculation.

(3) The new step in G4 is the Hartree-Fock energy limit (HF/limit). HF/limit uses two-point extrapolartion scheme and Dunning's aug-cc-pv(n)z basis sets ($E_{HF/limit}(n,n+1) = (E_{HF/n+1} - E_{HF/n} \exp(-\alpha))/(1-\exp(-\alpha))$). The best n is 4 and $\alpha =1.63$ is adequate for the G3/05 test set.

(4) 4 single-point energy calcualtions are incorporated after the MP4/6-31G(d) calculation. A correction for diffuse function ($\Delta E(+) = E[MP4/6-31+G(d)] – E[MP4/6-31G(d)]$), a correction for higher polarization function ($\Delta E(2df,p) = E[MP4/6-31G(2df,p)] – E[MP4/6-31G(d)]$), a correction for correlation effects beyond a fourth-order perturbation theory using cupled cluster theory ($\Delta E(CC) = E[CCSD(T)/6-31G(d)] – E[MP4/6-31G(d)]$), and a correction for larger basis set effects including the nonadditivity from basis set extension, diffuse fuction, and polarization function ($\Delta E(G3LargeXP) = E[MP2(full)/G3LargeXP] – E[MP2/6-31G(2df,p)] – E[MP2/6-31+G(d)] + E[MP2/6-31G(d)]$) are applied.

(5) The energy in step 4 is combined with a correction for the HF limit (step 3). The computed atomic spin-orbit corrections $\Delta E(SO)$ for first and second row of element are applied while experimental spin-orbit correction are applied for third row atomic species. The combined energy is $E(combined) = E[MP4/6-31G(d)] + \Delta E(+) + \Delta E(2df,p) + \Delta E(CC) + \Delta E(G3LargeXP) + \Delta E(HF) + \Delta E(SO)$.

(6) The electronic energy of G4 level of theory (E_e) is the sum of E(combind) and E(HLC). The form of HLC is the same as for the G3 theory except for two additional parameters

(A' and E). The A' parameter accounts for deficiencies in pairs of electrons in the case

of radical molecular species and ions. The value of E is determined by minimization of

the root mean square deviation of the energies in G5/03 test set.

(7) Finally, the total energy at 0 K is obtained using ZPE from step 2, E_0(G4) = E_e(G4) +

E(ZPE). Here the energy E_0 is referred to as the "G4 energy".

1.6 Electron propagator thery

Ionization energy and electron affinity are indispensable properties in chemistry and

physics. Koopmans[15] proposed that the first ionization energy of a molecule was equal to the

negative of the orbital energy of the HOMO level. However, the Koopmans Theorem is based

on restricted Hartee-Fock theory and the frozen orbital approximation should be applied which

means the orbitals of the ions are identical to those of the neutral molecule. Thus, the main

source of error from Koopmans Theorem comes from the orbital relaxiation and electron

correlation. The introduction of electron propagator coupled with Dyson orbitals includes the so

called self-energy (energy-dependent nonlocal operator) and advances the computation of

electron binding energy (eq 15).[16]

$$[f + \sum(\epsilon_i)]\phi_i^{Dyson}(x) = \epsilon_i\phi_i^{Dyson}(x) \tag{24}$$

The nonlocal operator $\sum^{(\epsilon_i)}$ describes electron relaxation and correlation which is neglected by the

Hartree-Fock operator, f. For electron binding energy, the Dyson orbitals are given by

$$\phi_i^{IP,Dyson}(x_N) = \sqrt{N}\int \Psi_N\Psi_{i,N\pm1}^* dx_{N\pm1} \tag{25}$$

Here, Dyson orbital describes the wavefunction of N-electron and N±1 electron and makes it possible to compute the ionization energy/electron affinity from a single-point calculation since the eigenvalue ϵ_i of Dyson equation (eq 24) corresponds to electron binding energy of molecule. Still, the off-diagonal matrix elements of the self-energy operator in the HF basis remain and leads to the simpler quasi-particle espression (diagonal approximation).[17] The electron binding energy in the quasi-particle approximation reads $\epsilon_i^{HF} + \sum_{ii}(E) = E$ where ϵ_i^{HF} is the ith canonical Hartree-Fock energy. The outer valence Green's function (OVGF) method is one of the popular approaches with electron propagator theory now. It is natural to introduce an indicator of the qualitative validity of this approximation, pole strength p_i defined as follows;

$$p_i = \int |\phi_i^{Dyson}(x)|^2 dx \qquad (26)$$

The Dyson orbital within the diagonal approximation is simply proportional to a normalized, canonical Hartree-Fock orbital such that

$$\phi_i^{Dyson}(x) = \sqrt{p_i}\psi_i^{HF}(x) \qquad (27)$$

The pole strength takes values between zero and unity. If the Koopmans theorem works well for the ioninzation process, pole strength is very close to 1.0 while less than 0.85 needs nondiagonal analysis of energy poles. A similar idea to Koopmans theorem exists in DFT method for relating the exact first vertical ionization energy and electron affinity to the HOMO and LUMO energies. However, the error is much larger than that of the Koopmans theorem (> 2.0 eV) and greatly depends on the choice of exchange-correlation functional.[18] OVGF theory can estimate the

15

electron attachment energy of monoanion to form dianion using β–LUMO orbital energy and it provides an alternative way to determine electron affinity of dianion when the electron attachment of monoanion to form dianion is unstable.

1.7 Implicit solvation modeling

An explicit treatment of solvent would require that 100s-1000s of solvent molecules surround the solute. In a continuum model, the charge distribution of the solvent is replaced with a continuous electric field that represents a statistical average over all solvent degrees of freedom at thermal equilibrium. For polar solute and solvent, the electrostatic interaction with induction is dominant but the cavitation, exchange repulsion, and dispersion attraction also play a role. Since the short-range interaction (cavitation, repulsion, and dispersion) is of quantum nature, *ab initio* computation is usually combined with the continuum model for solvation. The bulk dielectric constant ϵ, which is a macroscopic measurement of polarizability, is applied to the continuous polarizable medium. With the presence of a dielectric, the electrostatic potential between solute and solvent is screened (weakened) and the simplest representation of the solvation free energy (ΔG_{solv}) is given by

$$\Delta G_{solv} = -\frac{1}{2}(\frac{\epsilon - 1}{\epsilon})\frac{Q^2}{R}$$
(28)

where Q is a point charge and R is the cavity radius.[19] Instead of a charge, one can apply a dipolar distribution having a dipole moment μ, which is so called Kirkwood-Onsager equation in atomic units (eq 29).[20]

$$\Delta G_{solv} = -\frac{1}{2}[\frac{(2\epsilon - 1)}{(2\epsilon + 1)}]\frac{\mu^2}{R^3}$$

(29)

The solute dipole moment is $\mu = \mu_0, + \alpha F$ where μ_0 is the permanent solute dipole moment determined in the gas-phase. The αF term is the additional solute moment that is induced by the reaction field F. Thus, the mutual polarization between solute and solvent continues until a self-consistent equilibrium is achieved. This introduces the notion of a self-consistent reaction field (SCRF). The nature of self-consistent in a continuum model is easy to apply to the Schrodinger equation (eq 30).

$$\{H - \frac{1}{2}(\frac{2(\epsilon - 1)}{(2\epsilon + 1})\frac{< \Psi|\mu|\Psi >}{a^3}\} = E\Psi$$

(30)

For the usual gas-phase Hamiltonian (H), the Hartree-Fock and DFT operators can be easily applied with the perturbation of solvation (eq 30). However, it should be noted that the ΔG_{solv} in eq 28, 29, and 30 is purely electrostatic with polarization and the determination of R still arbitary.

One of the standard implicit solvation models is the polarizable continuum model (PCM) which was developed by the Tomasi group.[21] A distinct advantage of the PCM model over the Kirkwood-Onsager equation is that the non-electrostatic interaction is applied to the determination of ΔG_{solv} (eq 31).

$$\Delta G_{solv} = \Delta G_{cav} + \Delta G_{elec} + \Delta G_{disp} + \Delta G_{rep} + \Delta G_{tm}$$

(31)

The terms ΔG_{elec}, ΔG_{disp}, and ΔG_{rep} originate from the QM level treatment of polarization, induction, and electron exchange contributions while ΔG_{cav} needs geometrical nuclear parameters to define the shape and size.[22] ΔG_{tm} represents a thermal motion contribution given by

$$\Delta G_{tm} = RTln(\frac{q_{rot,g}q_{vib,g}}{q_{rot,s}q_{vib,s}}) - RTln(\frac{n_{solute,g}\Lambda_{solute,g}}{n_{solute,s}\Lambda_{solute,s}}) + P\Delta V \qquad (32)$$

Terms q_{rot} and q_{vib} are the micropartition functions of the rotation and vibration states of the solute. n_{solute} is the numerical density of the solute while Λ_{solute} means the momentum partition function. The last $P\Delta V$ term is negligible in most case since its value is normally less than 0.001 kcal/mol.[23] The first two terms in eq 32 are also negligible unless the solvation process accompanies the chemical association or dissociation process with relatively weak interactions.[24] Thus, ΔG_{tm} is usually ignored for the any popular derivatives of the PCM approach.

For ΔG_{cav}, the scaled particle theory (SPT) based on the surface tension of solute has been successfully applied in numerous cases.[25] After charging the portion of solute (cavity), the solvent density is kept constant to guarantee that the cavity volume is infinitely small with respect to the bulk solvent. The remaining issue is how to determine the boundary between the solute and solvent, the so called cavity radii. Histocally, simple spherical and ellipsoidal shapes were applied but these simple models ignored many of the stereochemical details of the molecule (eq 28 and 29).[19,20] Still, the generalized Born model is popular in the biochemistry community because of its simple and fast analytical solution of the electrostatic equations. In the original version of PCM model, the cavity radii (R_α) is proportional to the van ver Waals radii (eq 33).

$$R_\alpha = f R_\alpha^{(vdW)}$$

$$(33)$$

An initially proposed factor of $f = 1.2$ was used to evaluate the electrostatic term with neutral solutes.[24] However, the existence of a sharp corner-like crevice can lead an infinite electric field, which is a problem when evaluating numerical solution. The solvent accesible surface (SAS) rolls a probe sphere (radius of solvent) on van der Waals surface (VWS), originated from Bondi's atomic radii set (Figure 2).[26] Since the SAS traces out the surface defined by the center of the rolling probe, the SAS surface nauturally removes the inaccessible crevices. The solvent excluded surface (SES) use the surface defined by the inward facing part of the probe instead of the center while the crevices are smoothed with reentrant surface (thick black line in Figure 3).
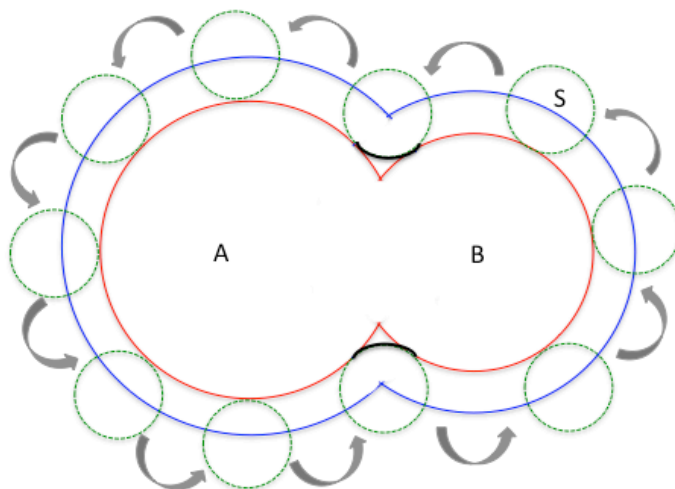
Figure 3. Illustration of the cavities based on interlocking spheres. The solvent accessible surface (SAS) rolls a probe sphere (solvent, dotted green) over the solute spheres, tracing out the surface defined by the center of the rolling probe. The solvent excluded surface (SES) traces out the inward facing part of the probe. The reentrant surfaces (black) remove the inaccessible crevices and also smooth out the cavity shape.

The first and most famous algorithm to calculate the SES has been proposed by Connolly, which is called the Connolly surface.[27] This region, which is enclosed in the SES but not in VWS, is called the solvent excluded volume. The Connolly algorithm is applied directly to any molecular modeling fields but it has been rarely used in combination with the PCM model since the good graphical rendering needs substaintial computational resources. GEPOL method[28] and tessellation technique[29] are applied to build a cavity boundary using SES. In the GEPOL approach, the solvent excluded volume is approximated by a set of supplementary spheres, which are defined through a recursive algorithm. The number, position, and radius of these spheres are changed with the molecular geometry. The generated molecular surface should be suitable to the boundary element method to build reaction field. The partitioning of surface makes tesserae (a function of surface area, sampling point $\vec{s}$ and a unit outword vector $\hat{n}$ at the sampling point). Partitioning of a sphere with respect to the molecular symmetry enables a symmetry-reduced cavity and the PCM method can consider the molecular symmetry restriction in solvation. Alternatively, one can generate the cavity surface using a constant solute electron density. This method has the avantage of smoothing the surface and the solute molecule automatically determines the shape. However, the only parameter, the isosurface of electron density contour level, is arbitrary even though 0.001 au is generally accepted.

Different algorithms for slightly differnet physical and mathmetical models have been proposed to determine the solvation charges q_i with the general expression given by $\mathbf{Dq} = \mathbf{-b}$ where the column vector q collects the solvation charges.[22] $\mathbf{D}$ is a square matrix of dimensions equal to the number of tesserae, depending on the dielectric constant (ε) and on the tesserae geometrical parameters. It represents the electrostatic interaction matrix between the

polarization charges. In the dielectic polarizable continuum model (DPCM), the matix element D_{ij} contains the electrostatic field that q_i exerts on q_j. D_{ij} depends on the inverse of the square modulus of the distance between the charges $|r_{ij}|^2$ while the column matrix **b** collects the normal components of the solute electrostatic field on tesserae. For conductor-like polarizable continuum model (CPCM), the matrix element D_{ij} contains electrostatic potential between q_i and q_j charges and it depends on the inverse of the modulus of the distance $|r_{ij}|$ while the column matrix b collects the solute electrostatic potential on the tesserae. D_{ij} for the integral equation formalism PCM (IEFPCM) is a combination of the potential and electrostatic field between charges. The column matrix **b** for IEFPCM can contain either solute potential or solute potential plus electrostatice fields on tesserae. For a high dielectric solvent with insignificant charge penetration, CPCM and IEFPCM give nearly the same results using similar way of cavity construction, while DPCM gives better results than CPCM. However, the determination of the cavity is the most important factor in many cases. Bondi[26] and Pauling tabulated van der Waals radii sets for atoms using crystallographic data. Later, the atomic radii for UFF force field were applied to tabulate the atomic radii, which was missing in Bondi and Pauling tabulation (UFF cavity set).[31] In the united atom model, hydrogens are enclosed in the sphere of the heavy atom to which they are bonded. The UA0 model is the united atom model with heavy atom radii (every atom radii except hydrogen radii) of UFF force field. The UAHF and UAKS models are the united atom models on radii optimized for HF/6-31G(d) and PBEPBE/6-31G(d) levels of theory respectively. All radii for cavity generation is based on the neutral atomic volume while the Pauling model, actually Merz-Kollman radii (not the van der Waals radii by Pauling) is defined to determine the electrostatic potential of ions.[32]

1.8 Thermodynamic properties – macroscopic and microscopic connection

One needs to connect the results from electronic structure calculation to the thermodynamic ensemble properties like enthalpy and free energy. The first step in the transition from the microscopic to the macroscopic regime is initiated with the Born-Oppenheimer potential energy surface, which is classically constructed although the energies of various points are determined from QM calculations. The motion of the nuclei on this surface is accounted for in a QM method and the energy is tied up in molecular vibration since the lowest vibrational energy level for any bound vibration is not zero even when close to absolute zero (0 K). With the harmonic oscillator approximation, the internal energy at 0 K (U_0) for a molecule is given by

$$U_0 = E_{elec} + \sum_i^{mode} \frac{1}{2}h\omega_i \tag{34}$$

where E_{elec} is the energy of the stationary point on the Born-Oppenheimer potential energy surface. ω_i is the vibrational frequency and h is the Plank constant. The sum of all vibrational energies in eq 34 defines the zero-point vibrational energy (ZPVE). For the canonical ensemble (N,V,T), the partition function from the ideal gas model can be written as

$$q(N, V, T) = \frac{[q(V,T)]^N}{N!} \tag{35}$$

$$q(V, T) = q_{elec}(T)q_{trans}(V, T)q_{rot}(T)q_{vib}(T) \tag{36}$$

where q represents the molecular partion function. For a large value of N (quantum mechanically indistinguishable particles), using Stirling's approximation, the molecular partition function becomes additive with following terms (eq 37).

$$\ln[Q(N,V,T)] \approx N\{\ln[q_{elec}(T)] + \ln[q_{trans}(V,T)] + \ln[q_{rot}(T)] + \ln[q_{vib}(T)]\} - N\ln N + N \quad (37)$$

The simplest partition function to be calculated is the electronic partition function (q_{elec}) since it makes no significant contribution to closed-shell singlet molecules at temperature below thousands of degrees. If I define the ground state for each energy component to have an energy of zero, the electronic component of internal energy U and entropy S are given by

$$U_{elec} = 0 \quad (38)$$

$$S_{elec} = R\ln(2S+1) \quad (39)$$

where R is the gas constant ($N_A k_B = R$) and S is the spin multiplicity. Thus, for closed-shell singlet states, S_{elec} always becomes zero. However, the q_{trans} and q_{rot} molecular partition function are free of any requirement to perform an electronic structure calculation. For an ideal, the q_{trans} and q_{rot} for non-linear molecule contribute 3/2RT each to overall molecular partition function while the entropy contribution is given by

$$S^o_{trans} = R(ln[(\frac{2\pi M k_B T}{h^2})^{3/2} V^o] + \frac{3}{2}) \quad (40)$$

$$S_{rot}^o = R(ln[\frac{\sqrt{\pi I_A I_B I_C}}{\sigma}(\frac{8\pi^2 k_B T}{h^2})^{3/2}] + \frac{3}{2})$$

(41)

where M is the molecular mass and I_A, I_B, and I_C are the principal moments of inertia. The pure rotations in molecule itself are represented σ. S^o denotes the standard state given by one mole of an ideal gas at 298K and 1 atm pressure (V^o =24.5 L). Thus, the most important molecular partition function for evaluation of an ensemble quantity through ab intio computation is the vibrational partition function. Using the harmonic oscillator assumption, the full vibrational partition function can be expressed as

$$q_{vib}(T) = \prod_{i=1}^{3N-6} (\frac{1}{1 - e^{-h\omega_i/k_B T}})$$

(42)

For a linear molecule, the upper limit of the product series would be 3N-5. The vibrational components of the internal energy and entropy are given by

$$U_{vib} = R \sum_{i=1}^{3N-6} \frac{h\omega_i}{k_B(e^{h\omega_i/k_B T} - 1)}$$

(43)

$$S_{vib} = R \sum_{i=1}^{3N-6} [\frac{h\omega_i}{k_B T(e^{h\omega_i/k_B T} - 1)} - ln(1 - e^{-h\omega_i/k_B T})]$$

(44)

Based on optimized geometry, the vibration frequencies from any practical *ab initio* computation can yield the contribution of the vibrational partition function for internal energy and entropy.

The sum of eq 39, 40, 41, and 44 represents the absolute entropy (S^o), which is directly

comparable to experimental values.

1.9 References

(1)   (a) Kohn, W.; Sham, J. L. *Phys. Rev.* **1965**, *140*, A1133.

(2)   (a) Zhao, Y.; Schultz, N. E.; Truhlar, D. G. *J. Chem. Theory Comput.* **2006**, *2*, 364. (b) Zhao, Y.; Truhlar, D. G. *Theor. Chem. Acc.* **2008**, *120*, 215. (c) Zhao, Y.; Truhlar, D. G. *Acc. Chem. Res.* **2008**, *41*, 157.

(3)   Grimme, S. *J. Comp. Chem.* **2004**, *25*, 1463.

(4)   Grimme, S. *J. Comp. Chem.* **2006**, *27*, 1787.

(5)   Barone, V.; Casarin, M.; Forrer, D.; Pavone, M.; Sambi, M.; Vittadini, A. *J. Comp. Chem.* **2008**, *30*, 934.

(6)   (a) Pople, J. A.; Head-Gordon, M.; Fox, D. J.; Raghavachari, K.; Curtiss, L. A. *J. Chem. Phys.* **1989**, *90*, 5622. (b) Curtiss, L. A.; Raghavachari, K.; Redfern, P. C.; Rassolov, V.; Pople, J. A. *J. Chem. Phys.* **1998**, *109*, 7764.

(7)   Curtiss, L. A.; Redfern, P. C.; Raghavachari, K. *J. Chem. Phys.* **2007**, *126*, 084108.

(8)   Hellmann, H. *J. Chem. Phys.* **1935**, *3*, 61.

(9)   Schwerdtfeger, P. *ChemPhysChem* **2011**, *12*, 3143.

(10)   (a) Herring, C. *Phys. Rev.* **1940**, *57*, 1169. (b) Focher, P.; Rastri, A.; Covi, M.; Bachelet, G. B. *Phys. Rev. B* **1991**, *44*, 8486.

(11)   Louie, S. G.; Froyen, S.; Cohen, M. L. *Phys. Rev. B* **1982**, *26*, 1738.

(12)   Reis, C. L; Pacheco, J. M.; Martins, J. L. *Phys. Rev. B* **2003**, *68*, 155111.

(13)   Bachelet, G. B.; Hamann, D. R.; Schlüter, M. *Phys. Rev. B* **1982**, *26*, 4199.

(14)   Vanderbilt, D. *Phys. Rev. B* **1990**, *41*, 7892.

(15)   Koopmans, T. *Phys.* **1934**, *1*, 104.

(16)   (a) Cedebaum, L. S. *J. Phys. B* **1975**, *8*, 280. (b) Simons, J. *Ann. Rev. Phys. Chem.* **1977**, *28*, 15. (c) Ortiz, J. V. *J. Chem. Phys.* **1996**, *104*, 7599. (d) Ortiz, J. V. *Adv. Quantum Chem.* **1999**, *33*, 35.

(17)   (a) Ohrn, Y.; Born, G. *Adv. Quantum Chem.* **1981**, *13*, 1. (b) Cederbaum, L. S.; Domcke, W.; Schirmer, J.; von Niessen, W. *Adv. Chem. Phys.* **1986**, 1*04*, 7599.

(18)   (a) Politzer, P.; Abu-Awwad, F. *Theor. Chem. Acc.* **1998**, *99*, 83. (b) Hamel, S.; Duffy, P.; Casida, M. E.; Salahub, D. R. *J. Elect. Spec. Pheno.* **2002**, *123*, 345.

(19)   (a) Born, M. *Z. Phys.* **1920**, *1*, 45.

(20)   (a) Kirkwood, J. G. *J. Chem. Phys.* **1934**, *2*, 351. (b) Onsager, L. *J. Am. Chem. Soc.* **1936**, *58*, 1486.

(21)   Miertus, S.; Scrocco, E.; Tomasi, J. *Chem. Phys.* **1981**, *55*, 117.

(22)   (a) Mennucci, B.; Cammi, R. *Continuum Solvation Models in Chemical Physics*; Wiley, Chichester, **2007**. (b) Rega, N.; Cossi, M.; Barone, V. *J. Comp. Chem.* **1999**, *20*, 1186.

(23)   Ben-Naim, A.; Marcus, Y. *J. Chem. Phys.* **1984**, *81*, 2016.

(24)   Tomasi, J.; Persico, M. *Chem. Rev.* **1994**, *94*, 2027.

(25)   (a) Ulig, H. H. *J. Phys. Chem.* **1937**, *41*, 1215. (b) Pierotti, R. A. *Chem. Rev. B* **1976**, *76*, 712. (c) Carbo, R. *Current Aspects of Quantum Chemistry*; Elsevier, Amsterdam, **1982**

(26)   Bondi, A. *J. Phys. Chem.* **1964**, *68*, 441.

(27)   Connolly. M. L. *J. Appl. Cryst.* **1983**, *16*, 548.

(28)   Pascual-Ahuir, J. L.; Silla, E.; Tunon, I. *J. Comp. Chem.* **1994**, *15*, 1127.

(29)   Pomelli, C. S.; Tomasi, J. *Theo. Chem. Acc.* **1998**, *99*, 34.

(30)   Pauling, L. *The Nature of Chemical Bond, 3rd*; Cornell University Press, Ithaca, **1960**

(31)   Rappe, A. K.; Casewit, C. J.; Colwell, K. S.; Goddard, W. A.; Skiff, W. M. *J. Am. Chem. Soc.* **1992**, *114*, 10024.

(32)   Besler, B. H.; Merz, K. M.; Kollman, P. A. *J. Comp. Chem.* **1990**, *11*, 431.

Chapter 2

Mechanistic Study of LiNH$_2$BH$_3$ Formation from (LiH)$_4$ + NH$_3$BH$_3$ and Subsequent

Dehydrogenation

2.1 Introduction

Hydrogen is ubiquitous, but bottling this gas may be the most challenging step for a

hydrogen economy because the low density (and boiling point) of H$_2$ makes it difficult to store in

compressed or liquefied form. Ammoniaborane (NH$_3$BH$_3$) is attracting a great deal of attention

as a chemical storage system. It contains 19.6 wt% of H$_2$, which is larger than the 9.0 wt% target

set by the U.S. Department of Energy for 2015.[1] Unlike CH$_3$CH$_3$, the first dehydrogenation of

the NH$_3$BH$_3$ molecule is exothermic due to the conversion of an N-B dative bond into an N=B

double bond.[2,3] However, this exothermic character vanishes as more hydrogen is generated

since aminoborane (H$_2$N=BH$_2$) and iminoborane (HN≡BH), which have multiple bonds between

nitrogen and boron, become endothermic for hydrogen release.[2] In terms of reversibility,

NH$_3$BH$_3$ still requires further study to improve sustainable hydrogen storage systems. By using

solid state quantum simulation, Miranda and Ceder[4] showed that dehydrogenation from both the

polymeric ammoniaborane and cyclotriborazane were exothermic (approximately -10 kcal/mol),

implying that rehydrogenation may be difficult at moderate H$_2$ pressures. Thus, the full amount

of hydrogen in NH$_3$BH$_3$ may not be available as a relevant energy source. Some recent studies

have attempted to improve hydrogen generation from NH$_3$BH$_3$ through a catalytic process.[3,5-8]

However, these storage systems, which need solvent or catalyst, have a significantly lower

storage capacity. Meanwhile, LiH/LiNH$_2$ mixture and their derivatives are also attracting

attention as hydrogen storage systems,[9-14] and several mechanistic studies have appeared.[14-16]

Typically, dehydrogenations in these systems are achived through a ball-milling process, which does not require a solvent for operation. However, high thermal stability limits their use as a practical storage system. Many attempts have been made to lower the thermodynamic barriers of these hydride or amide derivatives through high-pressure polymorphism,[17] self-catalyzing material,[18] mixed alkali metal,[19] partial substitution of Li by K or Mg,[20] vacancies on the surface,[21] autocatalysis of NH_2BH_2,[22] and N-heterocyclic carbene[23] but still only partial successes have been reported. Recently, Xiong et al.[24] reported a new storage system using ball milling of NH_3BH_3 and LiH powder (Table 1), through formation of a lithium amidoborane ($LiNH_2BH_3$) crystal. This process generates about 15.6 wt% of hydrogen ($NH_3BH_3 + LiH \rightarrow LiN{\equiv}BH + 2H_2$) at 90 °C which is a milestone for practical application of chemical storage, since polymer electrolyte membrane (PEM) fuel cells are limited by this operation temperature.[25] Kang et al.[26] used a similar temperature (100 ~ 120 °C) to achieve a 10.4 wt% dehydrogenation from a ball-milling process (Table 1).

Table 1. Reported H_2 wt% for the Thermal Decomposition from $NH_3BH_3 + LiH^a$

Decomposition	Xiong et al.[b]	Kang et al.[c]
loss of 1st H_2	5.2 wt% at 90°C	5.2 wt% at 100°C
loss of 2nd H_2	5.2 wt% at 90°C	5.2 wt% at 100°C
loss of 3rd H_2	5.2 wt% at 90°C	4.1 wt% at 200°C[d]

[a]Kang et al. used $NH_3BH_3 + LiH$ as their reference to calculate H_2 wt% while Xiong et al. used $LiNH_2BH_3$ to report H_2 wt%. Thus, the value of 10.9 wt% reported by Xiong et al. corresponds to the 2nd and 3rd dehydrogenation in this table with $LiNH_2BH_3$ as the reference. [b]Reference 24. [c]Reference 26. [d]Calculated from the reported reaction of $NH_3BH_3 + LiH \rightarrow LiNBH_{1.4} + 2.8H_2$. The isothermal decomposition behavior was not reported at 200°C.

However, they reported that a higher temperature was required to reach the final product ($LiNBH_{1.4}$) which would correspond to a total wt % of 14.5. Thus, the two experimental studies

report very similar results for the loss of the first two hydrogen molecules, but differ on the loss

of the third hydrogen. In both studies, $LiNH_2BH_3$ does not generate borazine derivatives, which

are undesirable by-products for hydrogen storage. Typically, NH_3BH_3, which tends to hydrolyze

in acid (a process catalyzed by metals or promoted by solid acids), is very stable in neutral or

basic aqueous solution.[1] Dixon and co-workers have suggested several catalytic processes using

the Lewis acid BH_3,[27] alane,[28] acid initiation of NH_3BH_3,[29] $(NH_3BH_3)_2$,[30] and ammonia

triborane.[31] Interestingly, a LiH and NH_3BH_3 mixture can generate three molar equivalents of H_2

without additional catalyst, which is advantageous since the catalyst would lower the wt%

capacity of H_2 storage. Here, a thorough study of the mechanism of $LiNH_2BH_3$ formation and its

subsequent dehydrogenation is presented based on *ab initio* computational quantum chemistry

where the formation of $LiNH_2BH_3$ and the number of reversible dehydrogenation steps available

from its decomposition are explored. Hopefully, this study can provide clues for advancing

hydrogen storage, either through solid-state dehydrogenation or its catalytic promotion.

2.2 Computational Details

    Due to the systematic underestimation of reaction barrier heights by density functional

theory (DFT) and overestimation of barrier heights by the MP2 formalism, all stationary points

are calculated at the CCSD(T)/6-311++G(3d,2p)//MP2/6-311++G(2d,p) level using the

Gaussian03 package.[32] Simplified intrinsic reaction coordinates (IRC) are used to confirm the

identity of reactant and product from a transition state. The nature of the stationary points was

determined with vibrational analysis at the MP2 level. Zero-point energies, heat capacity

corrections, and TΔS contributions at the MP2/6-311++G(2d,p) level were combined with

single-point energies at the CCSD(T)/6-311++G(3d,2p) level to yield free energies at 298 K.

This level of theory is expected to yield a potential energy surface within about 1 kcal/mol of the complete basis set limit.[30] Unless otherwise indicated energy values in the text will be free energies at 298 K. Figures will present relative free energies at 298 K followed by enthalpies at 298 K in parentheses.

2.3 Results

The reaction of $NH_3BH_3(s)$ + LiH(s) in the ball-milling process at 90 °C releases one mole of H_2 per mole from a 1:1 mixture of NH_3BH_3 and LiH (eq 1).[24] NaH, which has the same ability to generate hydrogen through the formation of $NaNH_2BH_3$, has a smaller total weight capacity (7.5 wt%) than $LiNH_2BH_3$ (10.9 wt%) under the same conditions.

$$NH_3BH_3(s) + LiH(s) \rightarrow LiNH_2BH_3(s) + H_2(g) \qquad\qquad (1)$$
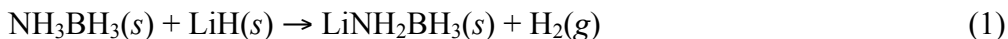
The nature of solid NH_3BH_3 and LiH are very different. In NH_3BH_3 the intermolecular interactions (dispersion plus dihydrogen bonding) are much weaker than in solid LiH where the ionic interactions result in an experimental lattice energy of 217.9 kcal/mol.[33] Morrison and Siddick[34] used a PW-DFT method to calculate a sublimation energy NH_3BH_3 of 18.2 kcal/mol. More recently, Matus et al.[35] determined an experimental value of 25 ± 3 kcal/mol for the sublimation of NH_3BH_3 from extrapolated vapor pressure data to 298 K. Such a large molecular cohesive energy of NH_3BH_3 is consistent with the low vapor pressure observed for solid NH_3BH_3, <1 μm at ambient temperature.[36] Thus, sublimation of NH_3BH_3 is not expected during $LiNH_2BH_3$ formation and dehydrogenation. Furthermore, NH_3BH_3/LiH can also undergo dehydrogenation in THF to form $LiNH_2BH_3$ and further dehydrogenation to form [LiN≡BH].[37]

31

The activation barrier of dehydrogenation from LiH/NH_3BH_3 in this study[37] (11.1 kcal/mol) is in excellent accord with our calculated value (see below, $\Delta H^{\ddagger} = 12.4$ kcal/mol, **1→TS1/3**).

The cohesion of LiH clusters up to $(LiH)_{10}$ was computed (Table 2) to determine the binding of smaller LiH units within a larger cluster. It was found that sublimation of small LiH cluster will not be involved in $LiNH_2BH_3$ formation since the dissociation energy is at least 35.5 kcal/mol ($(LiH)_{10} \rightarrow (LiH)_6 + (LiH)_4$). However, we suggest that the $(LiH)_4$ cluster unit may represent a useful model of the activated surface of the LiH crystal. Several *ab initio* calculations have shown that the cubic $(LiH)_4$ (T_d symmetry) is the most stable LiH cluster.[38]

Table 2. Reaction Enthalpies and Free Energies (kcal/mol and 298K) of LiH and NaH Cluster at the CCSD(T)/6-311++G(3d,2p)//MP2/6-311++G(2d,p) level

Decomposition	ΔG	ΔH	Decomposition	ΔG	ΔH
$(LiH)_2 \rightarrow LiH + LiH$	37.5	46.4	$(NaH)_2 \rightarrow NaH + NaH$	27.6	36.3
$(LiH)_4 \rightarrow (LiH)_2+(LiH)_2$	34.1	46.4	$(NaH)_4 \rightarrow (NaH)_2+(NaH)_2$	28.4	40.5
$(LiH)_6 \rightarrow (LiH)_4+(LiH)_2$	34.0	44.3	$(NaH)_6 \rightarrow (NaH)_4+(NaH)_2$	30.2	40.0
$(LiH)_8 \rightarrow (LiH)_4+(LiH)_4$	30.0	39.5	$(NaH)_8 \rightarrow (NaH)_4+(NaH)_4$	29.0	38.3
$(LiH)_8 \rightarrow (LiH)_6+(LiH)_2$	30.0	41.7	$(NaH)_8 \rightarrow (NaH)_6+(NaH)_2$	27.2	48.7
$(LiH)_{10} \rightarrow (LiH)_6+(LiH)_4$	27.0	36.5			
$(LiH)_{10} \rightarrow (LiH)_8+(LiH)_2$	31.4	41.3			

If the reaction of NH_3BH_3 and LiH takes place through solid-to-solid contact, the most likely path is through the transfer of one NH_3BH_3 unit to the surface of the LiH crystal. Indeed, the calculated adsorption enthalpy ($\Delta H(298K)$) of NH_3BH_3 on the $(LiH)_4$ cluster is 17.1 kcal/mol

(Figure 1 and eq 2) which compensates the sublimation energy[35] of NH_3BH_3 (25 ± 3 kcal/mol).
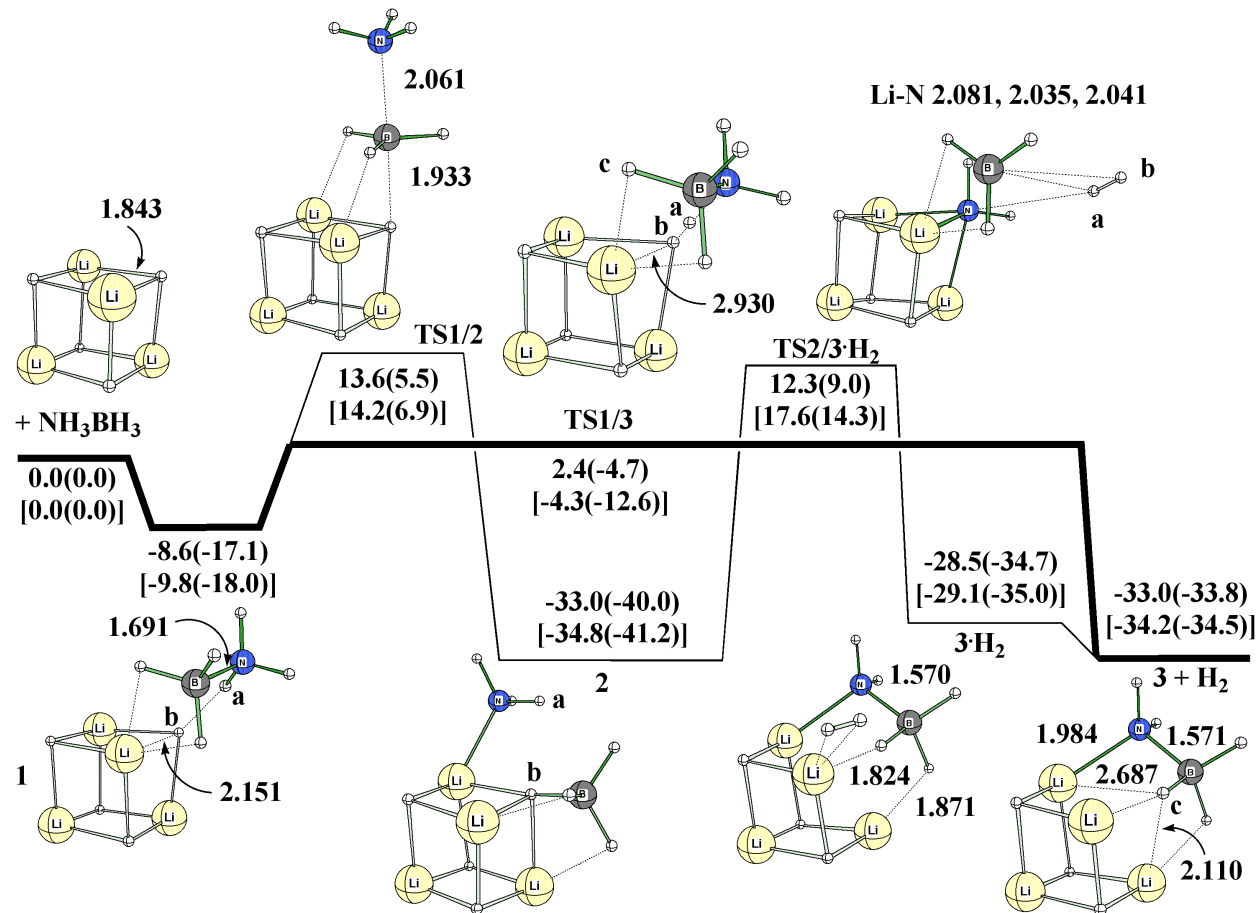
Figure 1. Free energy surface for the reaction of $(LiH)_4 + NH_3BH_3$. Free energies (kcal/mol) are relative to $(LiH)_4 + NH_3BH_3$ at 298 K. The values in parentheses are enthalpies (kcal/mol) relative to $(LiH)_4 + NH_3BH_3$ at 298 K. The values in bracket are free energies and enthalpies for the $(NaH)_4 + NH_3BH_3$ reaction pathway. Distances are in units of Angstroms.

The $(LiH)_4 \cdot NH_3BH_3$ complex (**1**) has a small 11.0 kcal/mol free energy barrier ($\Delta G^{\ddagger}$) to formation of the $(LiH)_3 \cdot LiNH_2BH_3$ complex (**3** + H_2) through **TS1/3**. A larger cluster model

$((LiH)_8$ rather than $(LiH)_4$) was tested for the reactions presented in Figure 1 and found to yield (at the B3LYP/6-31G(d) level) nearly the same energies (Figure 2).

$$(LiH)_4 + NH_3BH_3 \rightarrow (LiH)_4 \cdot NH_3BH_3 \; (\mathbf{1}) \rightarrow \; (LiH)_3 \cdot LiNH_2BH_3 \; (\mathbf{3}) + H_2 \qquad (2)$$
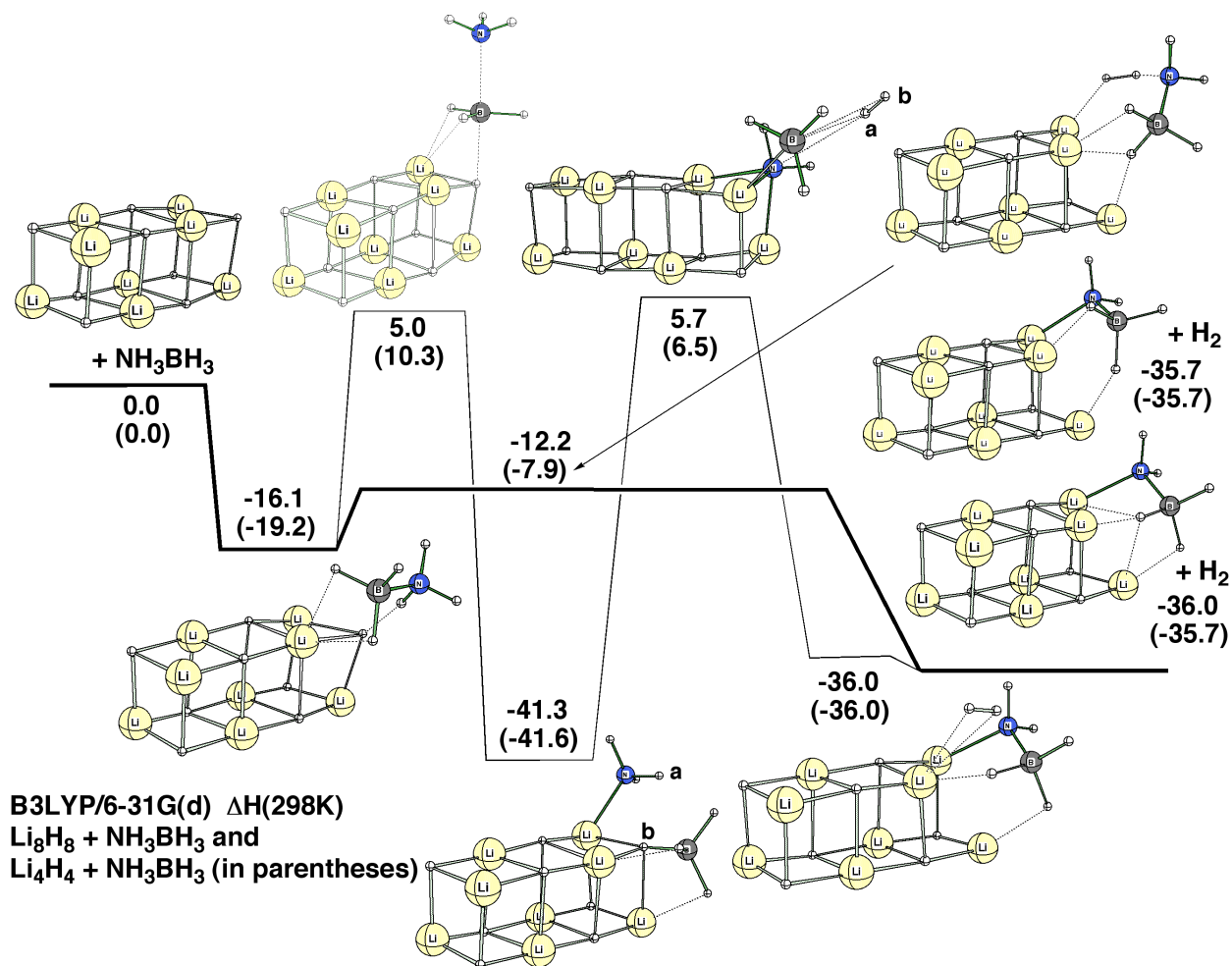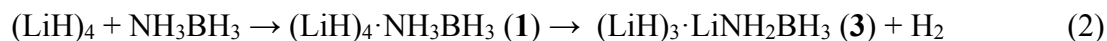
Figure 2. The enthalpy surface for the reaction of $(LiH)_8 + NH_3BH_3$.

Since dehydrogenation of NH_3BH_3 has also been observed with NaH powder, the reaction profile was also calculated for $(NaH)_4 + NH_3BH_3$. In Figure 1 $\Delta G(\Delta H)$ values given in brackets. In $(NaH)_4$, the free energy barrier is about half of $(LiH)_4$ ($\mathbf{1} \rightarrow \mathbf{TS1/3}$; $\Delta G^{\ddagger} = 5.5$ versus 11.0 kcal/mol) which may be due to weaker Na-H (relative to Li-H) bonding. The electron-

donating power of the alkali metal is critical to promote amidoborane formation. This interpretation is confirmed by a study of MgH_2/NH_3BH_3 where the lower ionicity of MgH_2 reduces the strength of the $H^{\delta-}...H^{\delta+}$ Coulombic attraction such that Mg^{2+}-substituted derivative of NH_3BH_3 are not observed.[39]

An alternative pathway to **3** involves initial cleavage of the N-B bond where the enthalpic barrier (**1** → **TS1/2** → **2**) is 22.2 kcal/mol, slightly smaller than the N-B dative bond dissociation energy (27.5 ± 0.5 kcal/mol).[40] The product, $NH_3 \cdot (LiH_4)_4 \cdot BH_3$ (**2**) is significantly more stable than **1** (ΔG=-24.4 kcal/mol). Given the four similar bond lengths around the boron atom, **2** could also be viewed as a salt between $[NH_3 \cdot Li_4H_3]^+$ and $[BH_4]^-$. If **2** were formed from **1**, dehydrogenation would be much more difficult because the free energy barrier for **2** → **3** + H_2 conversion is 45.3 kcal/mol.

Wu et al.[41] described the NH_3BH_3/LiH reaction as a competition between H^- and $NH_2BH_3^-$. Hydride is a stronger base than $NH_2BH_3^-$ which is demonstrated by the free energy change of -24.4 kcal/mol for the reaction **1** → **3** + H_2. Thus, the N-B bond dissociation mechanism for dehydrogenation from LiH/NH_3BH_3 through **TS1/2** and **TS2/3·H_2** cannot compete with dehydrogenation through the **TS1/3** without N-B bond dissociation. A key to avoiding borazine formation comes from the much lower activation barrier of **TS1/3** than direct H_2 elimination from NH_3BH_3. If initial dehydrogenation occurred first, as suggested from previous work on isolated NH_3BH_3,[42] then subsequent formation of borazine from NH_2BH_2 could not be avoided. Autrey and co-workers[43,44] used NMR analysis to propose a decomposition mechanism of NH_3BH_3 in the solid state and solution through the formation of $[NH_3BH_2NH_3]^+[BH_4]^-$, the so called DADB (diammoniate of diborane). Based on their studies, a pathway of dehydrogenation from DADB cannot avoid the formation of cyclic borazine in both

solution and solid. In the present mechanism, BH_4^- and NH_2BH_2 intermediates are not formed, rather H_2 is formed through the recombination of a Lewis acid/base pair. A Li-N distance of 1.984 Å in **3** agrees well with the distance in solid $LiNH_2BH_3$ (2.032 Å) and a shortened N-B distance of 1.571 Å in **3** (Figure 1) agrees well with the distance in solid $LiNH_2BH_3$ (1.561 Å).[41] The formation of a second $LiNH_2BH_3$ follows the same mechanism as the previous one, i.e. **3** + $NH_3BH_3 \rightarrow$ **6** + H_2 (Figure 3), but with a lower free energy barrier for the $H^{\delta-}...H^{\delta+}$ formation in **TS4/5** (**4** $\rightarrow$ **TS4/5,** $\Delta G^{\ddagger}$=8.4 kcal/mol) relative to **TS1/3** (**1** $\rightarrow$ **TS1/3**, $\Delta G^{\ddagger}$=11.0 kcal/mol).
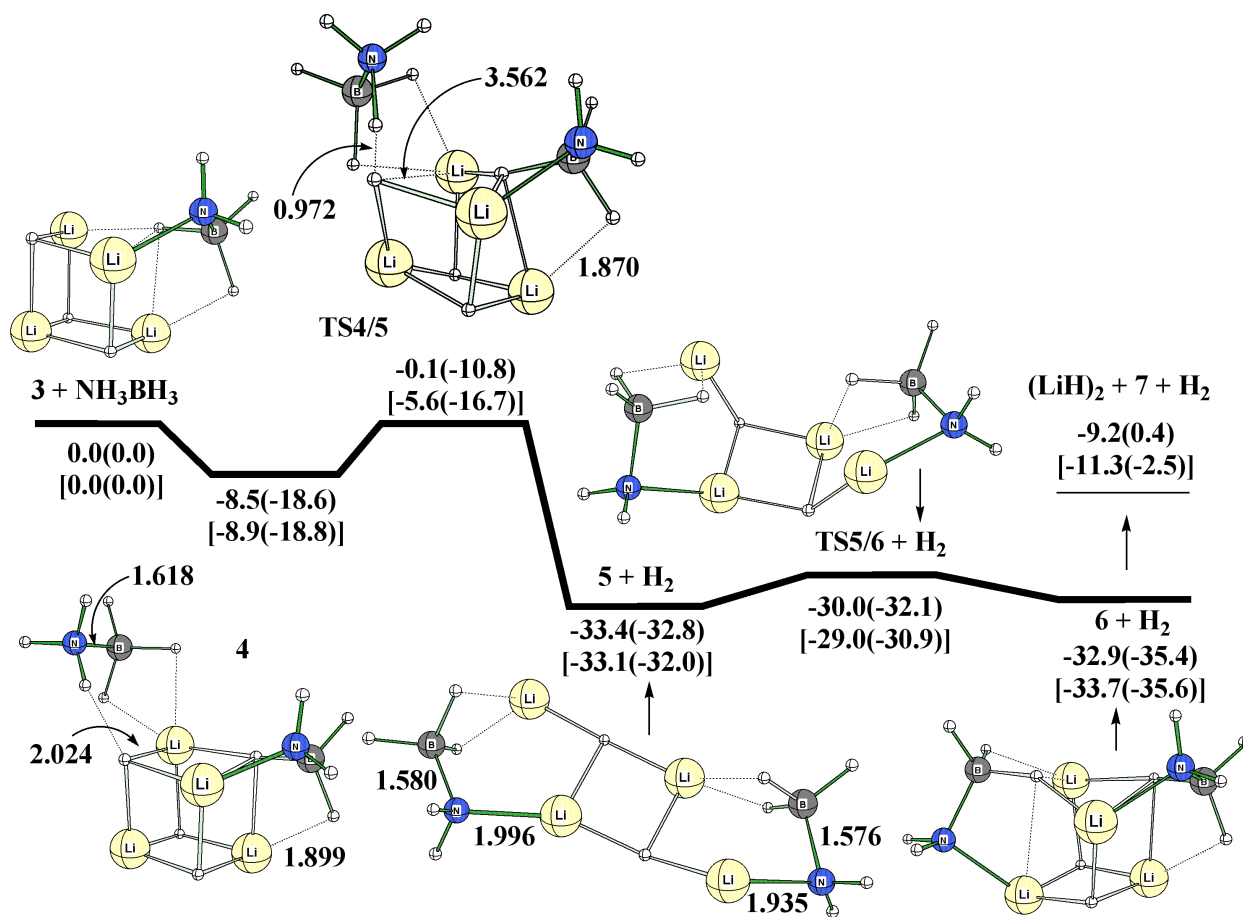
Figure 3. Free energy surface for the reaction of $(LiH)_3 \cdot LiNH_2BH_3$ (**3**) + NH_3BH_3.

The product of dehydrogenation, **5**, has a rather flat Li-H network with a very small free energy barrier (**5** + **H₂** → **TS5/6** + **H₂**, $\Delta G^{\ddagger}$ = 3.4 kcal/mol) to generate a more cube-like structure (**6** + **H₂**). Reaction of $(NaH)_4$ with a second NH_3BH_3 molecule follows the same mechanism as for $(LiH)_4$ ($\Delta G(\Delta H)$ values for $(NaH)_4$ given in brackets in Figure 3) but with a smaller free energy barrier for **4** → **TS4/5** ($\Delta G^{\ddagger}$ = 3.3 kcal/mol) as compared to $(LiH)_4$ ($\Delta G^{\ddagger}$ = 8.4 kcal/mol). Thus, the free energy barrier for H_2 elimination from the addition of both NH_3BH_3 molecules to $(NaH)_4$ is about one half of that for $(LiH)_4$. However, the reaction of NaH with NH_3BH_3 is almost explosive, while that of LiH with NH_3BH_3 takes about 4 hours for complete reaction.[24] The lattice energy of NaH is 186.9 kcal/mol, which is not significantly smaller than LiH (217.9 kcal/mol[33]). However, the mechanical strength difference between NaH and LiH may be a factor for the difference in kinetics since NaH has a smaller bulk modulus compared to that of LiH (19.4 versus 32.2 GPa, respectively).[45,46] In addition, since the ball-milling process involves mechanical activation without solvent, the greater brittleness of NaH and low activation barrier may be a sufficient explanation for the large difference in reaction kinetics.

One can understand **3** as a cation-anion bound complex of $[Li_4H_3]^+[NH_2BH_3]^-$ where the LiH distance (2.687 Å) clearly shows disruption of the cubic LiH lattice (Figure 1). This LiH bond-breaking enables the detachment of $LiNH_2BH_3$ from the LiH cluster as described in Figure 4 (**3** → **TS3/B** → **B** → $LiNH_2BH_3$ + $(LiH)_3$). The transition state for elimination of $LiNH_2BH_3$ **TS3/B** is reached by rotating the NH_2Li group 180° around the N-B bond to form eclipsed $LiNH_2BH_3$ complexed with the $(LiH)_3$ cluster, **B**. The final geometry of the $(LiH)_3$ cluster has D_{3h} symmetry as previously reported.[38] However, this process is very endergonic and the free energy barrier to **TS3/B** from **3** ($\Delta G^{\ddagger}$ = 27.7 kcal/mol) is much higher than the free energy barrier to **TS4/5** from **4** ($\Delta G^{\ddagger}$ = 8.4 kcal/mol) after the second NH_3BH_3 adsorption (Figure 3).
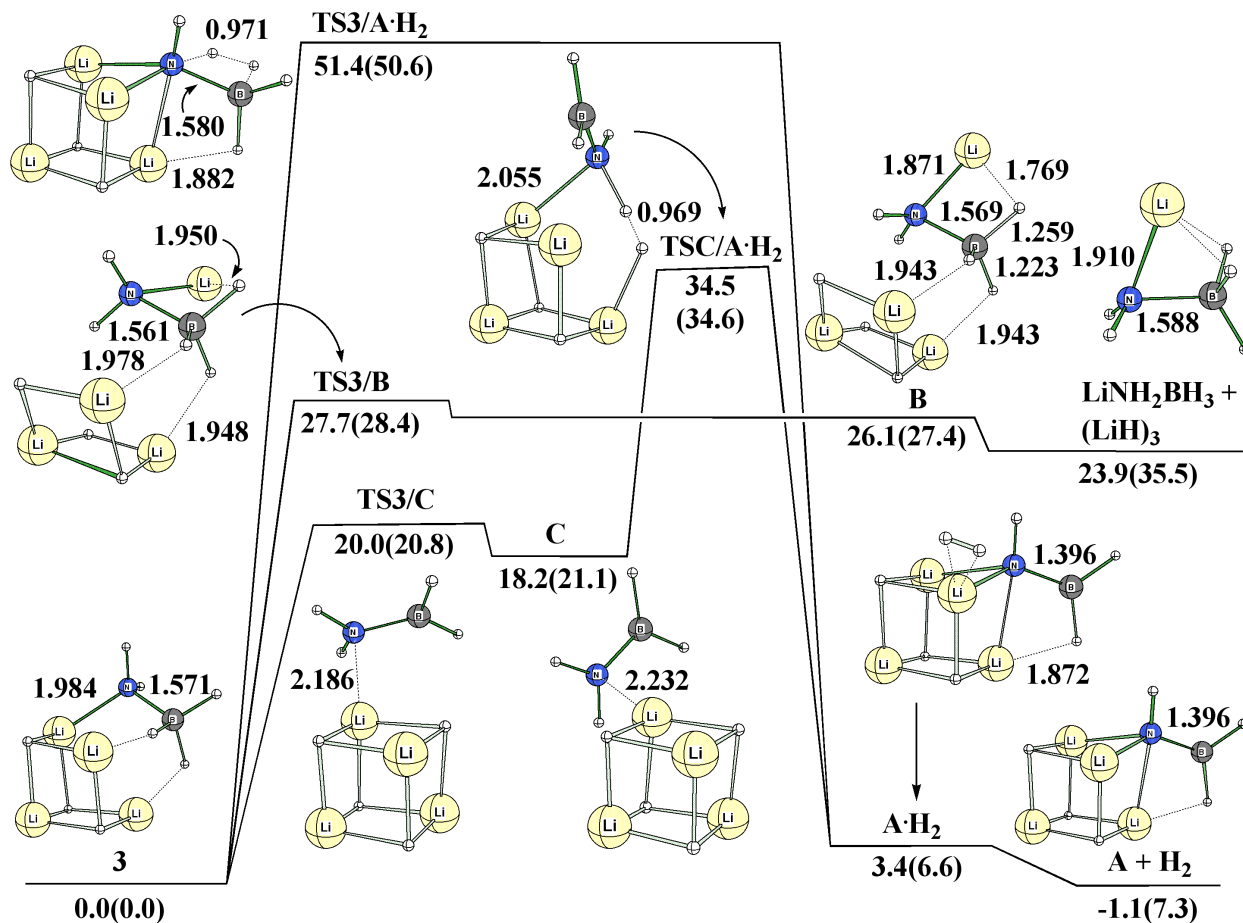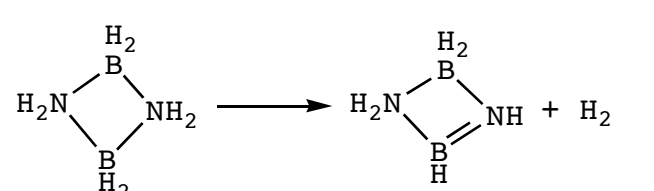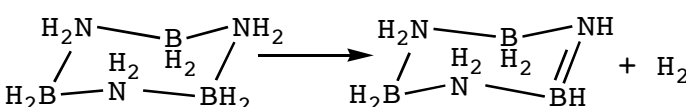
Figure 4. A comparison of free energy surface of **3** for dehydrogenation and formation of

        $LiNH_2BH_3 + H_2$.

Therefore, dissociation of $LiNH_2BH_3$ from the crystal is not likely. The possibility of concerted

dehydrogenation from the N-B bond of **3** was also investigated but the free energy barrier to H_2

release via **TS3/A·H₂** was much too high ($\Delta G^{\ddagger} = 51.4$ kcal/mol) to be competitive. A

mechanism through the intermediate, **C** (**3** → **TS3/C** → **C** → **TSC/A·H₂** → **A·H₂**) was also

considered but the free energy barrier from **3** to **TSC/A·H₂** ($\Delta G^{\ddagger} = 34.5$ kcal/mol) is still too

large to compete with addition and dehydrogenation of another NH_3BH_3 (**4** → **TS4/5**, $\Delta G^{\ddagger} = 8.4$

kcal/mol). Thus, the formation of multiple $LiNH_2BH_3$ units on $(LiH)_4$ is much more favorable

than concerted dehydrogenation from a single $LiNH_2BH_3$ on $(LiH)_4$, which explains why the $LiNH_2BH_3$ crystal is formed during the dehydrogenation experiment.

A major issue of hydrogen storage is its reversibility. For ammonia borane the first dehydrogenation is exothermic by 6.1 kcal/mol in the gas phase (Table 3). Miranda and Ceder[4] used DFT with solid-state modeling to calculate that the reaction was also exothermic in the solid solid state by 10 kcal/mol. Wu et al.[41] reported that dehydrogenation of $LiNH_2BH_3$ was not reversible while Kang et al.[26] reported the dehydrogenation reaction enthalpy was less exothermic than that for neat NH_3BH_3. However, to date, all the efforts for restoring the hydride $(NH_3BH_3 + LiH)$ have failed.[24,26,41,47] In the present mechanism, $LiNH_2BH_3$ formation is exergonic for the first two steps, $(LiH)_4 + NH_3BH_3 \rightarrow 3 + H_2$ and $3 + NH_3BH_3 \rightarrow 6 + H_2$ (Figures 1 and 2, $\Delta G = -33.0$ and -32.9 kcal/mol, respectively). The corresponding steps are slightly more exergonic for $(NaH)_4$ than $(LiH)_4$ ($\Delta G = -34.2$ and -33.7 kcal/mol, respectively).

Table 3. Reaction Enthalpies and Free Energies (kcal/mol and 298K) of Aminoborane Oligomers at the CCSD(T)/6-311++G(3d,2p)//MP2/6-311++G(2d,p) level

Equation	TS		Reaction	
	$\Delta G^{\ddagger}$	$\Delta H^{\ddagger}$	ΔG	ΔH
$NH_3-BH_3 \longrightarrow H_2N = BH_2 + H_2$	37.6	38.0	-15.0	-6.1
$H_2N = BH_2 \longrightarrow HN \equiv BH + H_2$	74.2	74.0	23.1	31.0
(cyclic) $\longrightarrow$ (cyclic) $+ H_2$	62.8	63.0	9.6	18.4
(ring) $\longrightarrow$ (ring) $+ H_2$	54.4	54.9	1.9	11.4

39

Thus, given the large exergonic/exothermic nature of the $NH_3BH_3 + (LiH)_4 \rightarrow LiNH_2BH_3 + H_2$ reaction, its reversibility is even more difficult than for $NH_3BH_3 \rightarrow NH_2BH_2 + H_2$. Bowden et al.[48] studied hydrogen generation from the methyl derivative. A recent theoretical study showed that $CH_3NH_2BH_3$ does not enhance dehydrogenation but does improve reversibility.[49]

For the catalytic dehydrogenation of NH_3BH_3, $Ni(NHC)_2$ activated, Ruthenium catalyzed,[50,51] and Lewis acid BH_3 catalyzed dehydrogenations are known.[25] Ionic liquids also catalyze dehydrogenation of NH_3BH_3.[52] However, these systems do not show increased hydrogen generation from NH_2BH_2. Another dehydrogenation pathway (eq 3), using gaseous NH_3 and LiH, was calculated to have an activation barrier of $\Delta H^{\ddagger} = 16.3$ kcal/mol at the CCSD(T) level.[15] This pathway will be unpractical due to the energy requirements to sublime LiH units from the LiH crystal (Table 2). Comparing with the activation barrier between LiH/NH_3 ($\Delta H^{\ddagger} = 16.3$ kcal/mol) and $(LiH)_4/NH_3BH_3$ (Figure 1, $\Delta H^{\ddagger} = 12.4$ kcal/mol), the latter is lower than former.

$$LiH(g) + NH_3(g) \rightarrow LiNH_2(g) + H_2(g) \qquad\qquad (3)$$

Chen et al.[9a] found a 7 wt% reversible hydrogen storage using $LiNH_2(s) + LiH(s)$ but the operation conditions for this dehydrogenation require over 200 ^{o}C. The authors proposed a polar mechanism with the formation of an $LiNH_2 \cdot LiH$ intermediate. Aguey-Zinsou et al.[16] also investigated the $LiNH_2/LiH$ system and detected the existence of $Li_2NH_2^+$ and a penta-coordinated nitrogen Li_2NH_3 as intermediates using thermal analysis and FTIR. The loss of H_2 from $(LiH)_n \cdot LiNH_2$ can be compared to the free energy barrier for the conversion of

$(LiH)_3 \cdot LiNH_2BH_3$ (**3**) to **TSC/A·H$_2$** (Figure 4, 34.5 kcal/mol) where the large barrier explains the high temperature need for the reaction.

Several studies of the $LiNH_2/LiBH_4$ solid state system have appeared including dehydrogenation.[53-56] In general hydrogen storage systems involving $LiBH_4$ have a bottleneck due to its high thermal stability. At the standard level of theory in this study, the free energy for $LiBH_4$ decomposition (51.6 kcal/mol) shows why it is not easy to dehydrogenate the hydride (eq 4). Purewal et al.[57] suggested a combination of ScH_2 and $LiBH_4$ for

$$LiBH_4 \rightarrow LiH + BH_3 \quad \Delta G=51.6 \text{ kcal/mol (298K)} \hspace{3cm} (4)$$
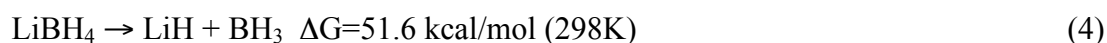
hydrogen storage but, while the operation temperature is over 450 ^{o}C, they do observe that $LiBH_4$ decomposes into LiH as the final desorption product. Thus, dehydrogenation cannot easily occur if $LiBH_4$ is formed.

The existence of the Lewis acid BH_3 is critical to eliminate H with a low activation barrier. Thus, for $(LiH)_3 \cdot LiNH_2BH_3$ (**3**), in the first step Li^+ acts as a relay agent that facilitates transfer of a hydride ion from BH_3 to the LiH cluster (Figure 4, **3** $\rightarrow$ **TS3/C** $\rightarrow$ **C**), while in the second step (**C** $\rightarrow$ **TSC/A·H$_2$** $\rightarrow$ **A·H$_2$**) the hydride ion combines with the acidic proton on nitrogen to form H_2. A corresponding mechanism for $(LiH)_3 \cdot LiNH_2$ would not be possible because a hydride ion cannot be transferred.

Recently, Hügle et al.[58] reported that a mixture of hydrazine borane ($NH_2NH_2BH_3$) and LiH generated 12 wt% of H_2 at 150 ^{o}C (three H_2 molecules from a $N_2H_4BH_3$/LiH mixture, which has 15.0 wt% hydrogen in total) without an induction period. The dehydrogenation behavior of hydrazine borane may be enhanced by LiH, which enables formation of $Li^+(N_2H_3BH_3^-)$.

However, the more rapid kinetics of the $N_2H_4BH_3$/LiH mixture may be related to the low cohesive energy in the $N_2H_4BH_3$ lattice since the melting point of $N_2H_4BH_3$ is lower than that for NH_3BH_3 (61 $^{\circ}$C and 110 $^{\circ}$C[23], respectively). Initial addition of $NH_2NH_2BH_3$ to $(LiH)_4$ and elimination of H_2 follows the same mechanism as that for NH_3BH_3 except that the H_2 elimination step has a lower free energy barrier ($\Delta G^{\ddagger} = 1.1$ kcal/mol at B3LYP/6-31G(d), see Figure 5)
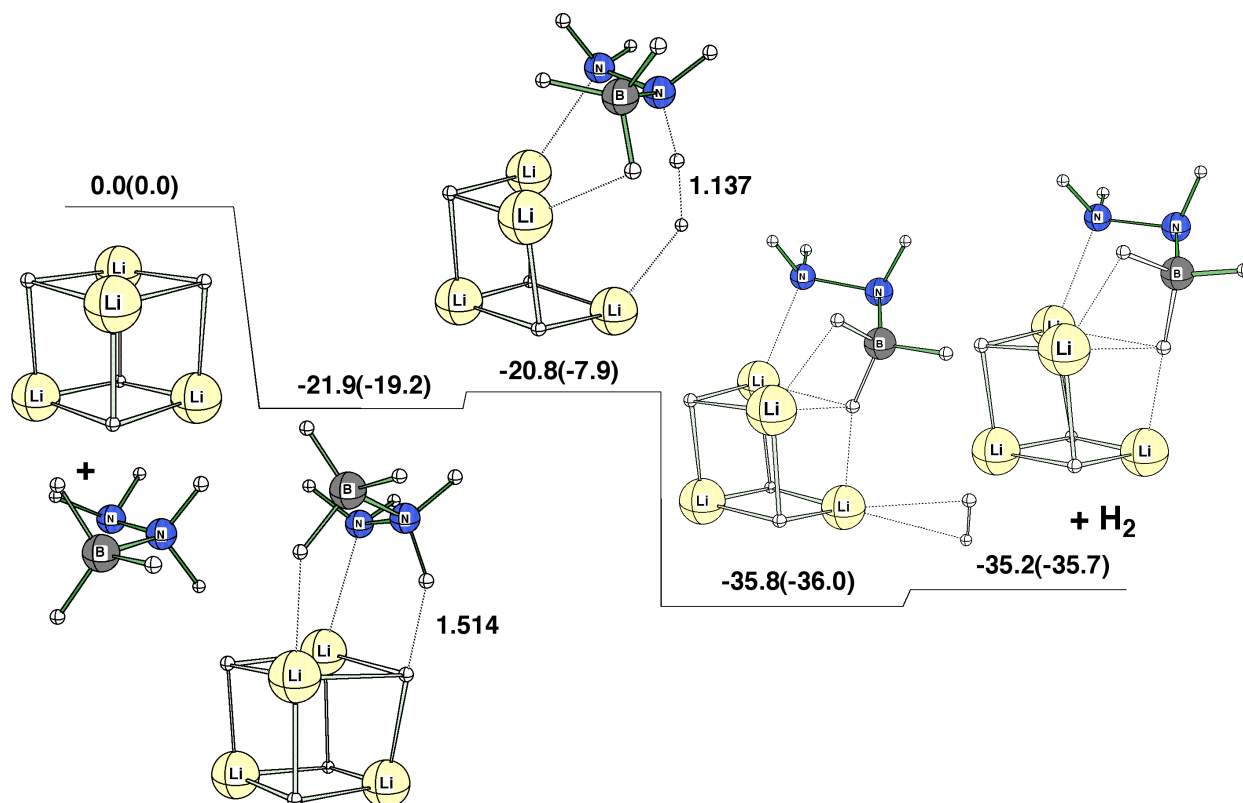
Figure 5. The enthalpy surface for the reaction of $(LiH)_4 + NH_2NH_2BH_3$. ΔH(298K) values for $(LiH)_4 + NH_3BH_3$ in parentheses.

The crystal structure of the involving two $LiNH_2BH_3$ molecules (**7**) resembles that of $LiBH_2NH_3$ where two interacting Li^+ cations and a hydrogen atom from BH_3 are in a zigzag arrangement.[41] In the crystal, the distances between Li and hydrogen of BH_3 are 1.976 Å and 2.116 Å while the corresponding distances in **7** (C_{2h} symmetry) are 1.838 Å. The interaction

between two LiNH$_2$BH$_3$ units is very strong as shown in eq 5a where the intermolecular Li-H distance is 1.838 Å (Figure 6), which is shorter than that of (LiH)$_4$ cluster (Figure 1).

2LiNH$_2$BH$_3$ → c-(LiNH=BH$_2$)$_2$ (**7**) ΔG=-26.0 kcal/mol   (5a)

c-(LiNH$_2$BH$_3$)$_2$ (**7**) → LiNH$_2$BH$_3$ + NH$_2$BH$_2$ + LiH   (5b)

LiNH$_2$BH$_3$ + NH$_2$BH$_2$ + LiH → Li$_2$N$_2$B$_2$H$_8$ (**9**) + H$_2$(H$_2$#1)   (5c)
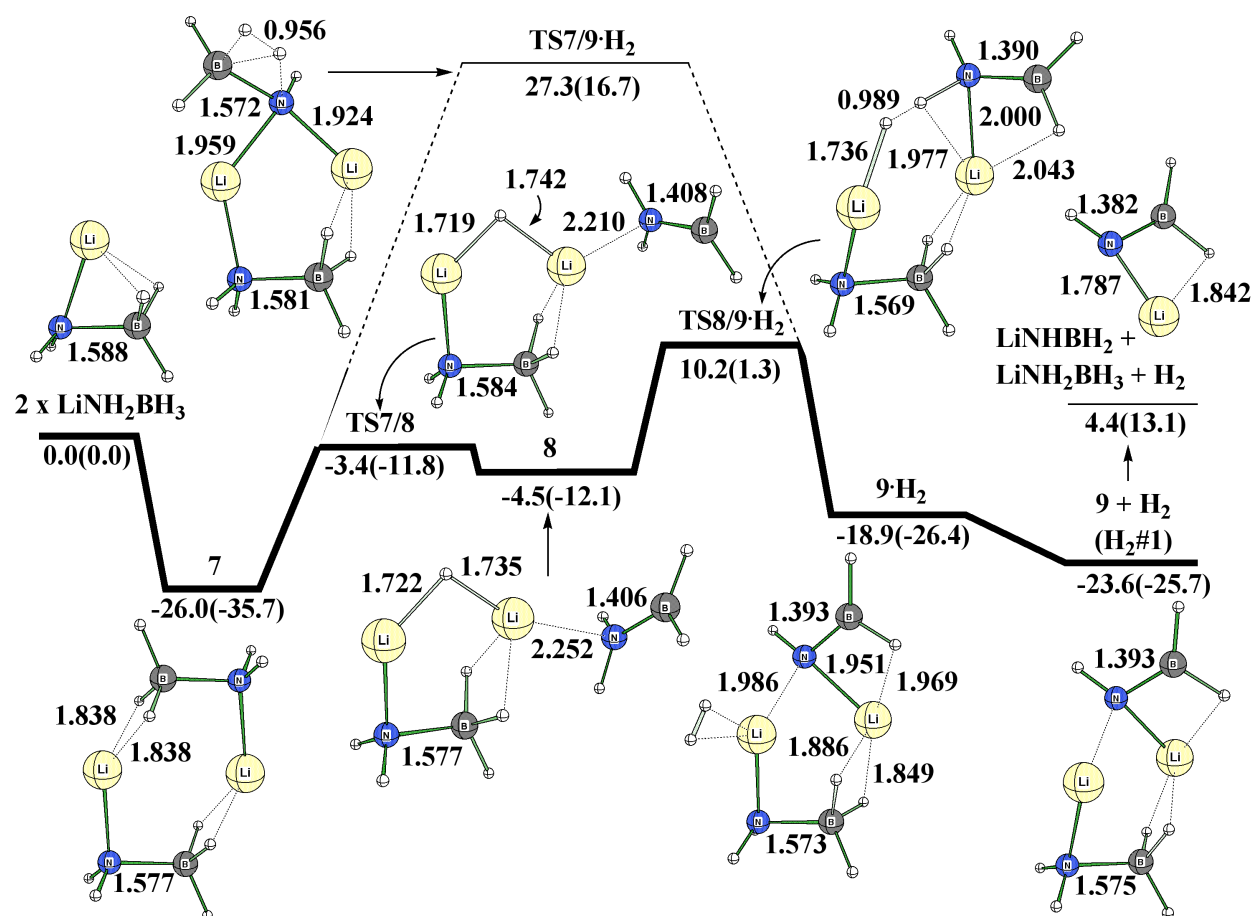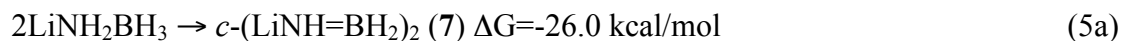
Figure 6. Dehydrogenation from a complex of two LiNH$_2$BH$_3$ molecules (**7**).

43

In order to get one mole of H_2 from $LiNH_2BH_3$, two H_2 molecules should be generated from the $LiNH_2BH_3$ dimer.[59] The first dehydrogenation mechanism is summarized as shown in eqs 5b and 5c ($H_2\#1$ indicates the first H_2 molecule generated from $(LiNH_2BH_3)_2$ dimer; later steps generate $H_2\#2$, $H_2\#3$, and $H_2\#4$). However, a one-step dehydrogenation through **TS7/9·H₂** is very unfavorable ($\mathbf{7 \rightarrow TS7/9 \cdot H_2 \rightarrow 9 \cdot H_2}$, $\Delta G^{\ddagger} = 53.3$ kcal/mol) compared to a two-step mechanism ($\mathbf{7 \rightarrow TS7/8 \rightarrow 8 \rightarrow TS8/9 \cdot H_2 \rightarrow 9 \cdot H_2}$, $\Delta G^{\ddagger} = 36.2$ kcal/mol) (Figure 6). One may compare this enthalpy barrier ($\Delta H^{\ddagger} = 37.0$ kcal/mol) of the two-step mechanism with the first dehydrogenation from NH_3BH_3, which is $\Delta H^{\ddagger} = 33.8$ kcal/mol at the CCSD(T)/CBS level[27] or $\Delta H^{\ddagger} = 36.4$ kcal/mol obtained using DFT.[60] However, the sublimation enthalpy of the NH_3BH_3 crystal (25 ± 3 kcal/mol) should be added to the NH_3BH_3 dehydrogenation barrier to make a fair comparison since **7** represents solid $LiNH_2BH_3$. Nguyen et al.[30] report the dehydrogenation enthalpy barrier of 44.5 kcal/mol to 59.4 kcal/mol for $(NH_3BH_3)_2$, which exhibits the same topology as **7**. Thus, the first dehydrogenation of $LiNH_2BH_3$ through a two-step mechanism is energetically lower than dehydrogenation of NH_3BH_3.

A N-B bond distance of 1.572 Å in **TS7/9·H₂** indicates a single-bond character. However, the N-B bond distances in **TS7/8** and **TS8/9·H₂** are 1.408 Å and 1.390 Å, which indicate a double-bond character. The formation of a Li-H-Li bridge in **TS7/8** weakens one of the Li-N bonds in one $LiNH_2BH_3$ unit where NH_2BH_2 is bound to the Li^+ cation in **8**. Breaking a Li-H bond ($1.735 \rightarrow 2.470$ Å) and forming a H-H bond (0.989 Å) in **TS8/9·H₂** enables dehydrogenation and formation of the complex **9·H₂**. This two-step mechanism ($\mathbf{7 \rightarrow 8 \rightarrow 9 \cdot H_2}$) lowers the free energy barrier by 17.1 kcal/mol when compared with the one-step dehydrogenation. The first dehydrogenation product, a complex of $LiNH_2BH_3$ and $LiNH=BH_2$ **9**, has stronger intermolecular interactions than in the complex of two $LiNH_2BH_3$ molecules **7** (**7**

→ 2xLiNH$_2$BH$_3$, ΔG = -26.0 kcal/mol and **9**+H$_2$ → LiNH=BH$_2$ + LiNH$_2$BH$_3$ + H$_2$, ΔG = -28.0 kcal/mol, respectively).

The second dehydrogenation of LiNH$_2$BH$_3$ starting from **9** follows the formation of a Li-H-Li bridge in **TS9/10** (Figure 7) where NH$_2$BH$_2$ is again bound to the Li$^+$ cation in **10**. Thus, the second dehydrogenation (loss of H$_2$#2) from **9** (**9** → **10** → **11**, eq 6a) follows the same pathway as the previous dehydrogenation (**7** → **8** → **9**, eq 5b) using Li$^+$ as a relay agent for hydride.
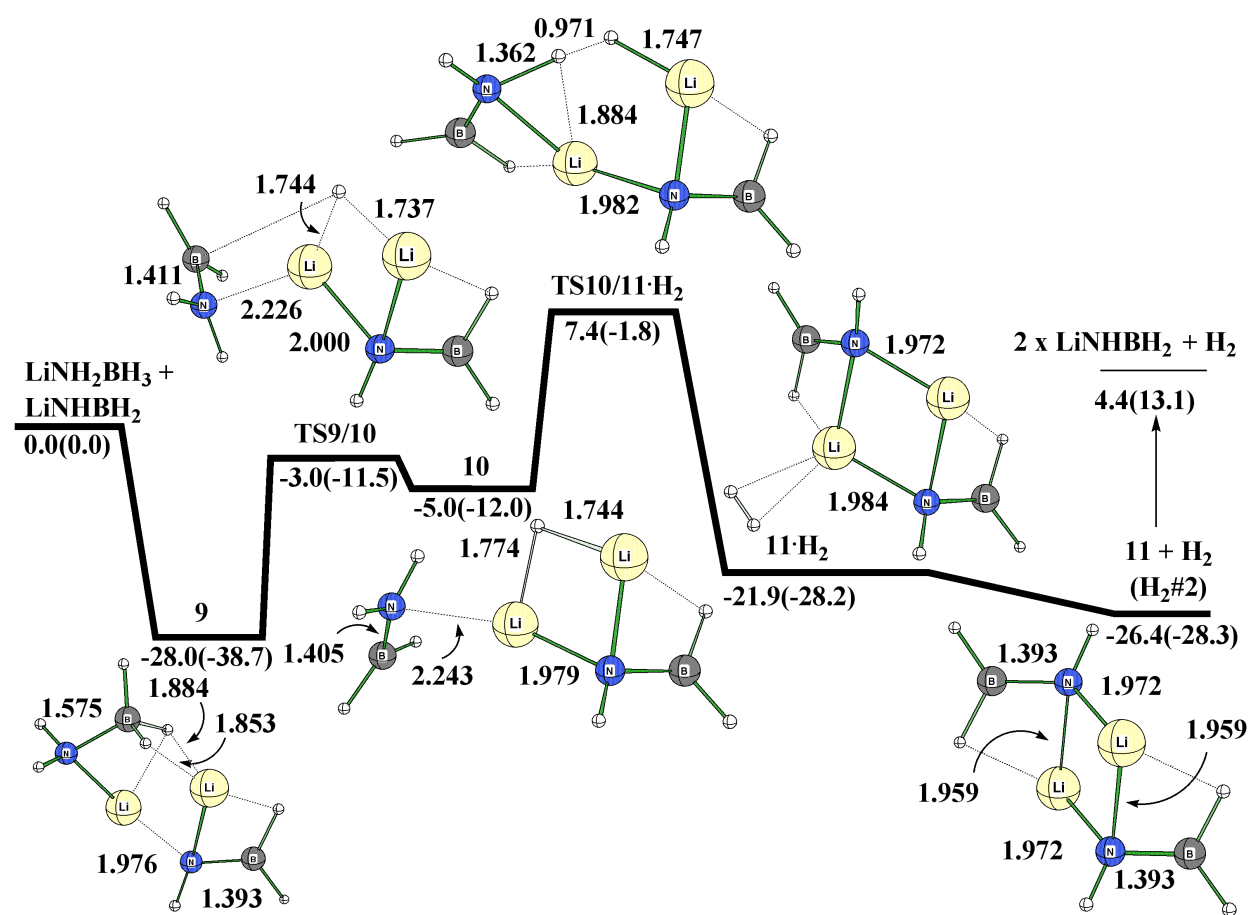
Figure 7. Dehydrogenation from a complex of LiNH$_2$BH$_3$ and LiNH=BH$_2$ molecules (**9**).

45

The enthalpy dehydrogenation barrier from **9** to **TS10/11·H₂** ($\Delta H^{\ddagger} = 40.5$ kcal/mol) is still lower than for $(NH_3BH_3)_2$. Dehydrogenation of $LiNH_2BH_3$ is slightly endergonic, ($\Delta G = 2.4$ kcal/mol **7** → **9**+H₂, Figure 6 and $\Delta G = 1.6$ kcal/mol **9** → **11**+H₂, Figure 7) while the dehydrogenation from $(LiH)_4$ and NH_3BH_3 is very exergonic ($\Delta G = -33.0$ kcal/mol **1**→**3**+H₂, Figure 1 and $\Delta G = -32.9$ kcal/mol **3** + NH_3BH_3 → **6**+H₂, Figure 3). The final product of the dehydrogenation from the $LiNH_2BH_3$ complex, **11**, is a complex between two $LiNH=BH_2$ units with a square Li-N network and two N=B double bonds. One may observe increasingly stronger intermolecular interactions between two units in the complexes **7**, **9**, and **11** ($\Delta G = -26.0$, -28.0, and -30.8 kcal/mol, respectively) as H₂ is released. The complex **11** (C_i symmetry) requires further rearrangement to achieve dehydrogenation (loss of H₂#3 and H₂#4) since the Li^+ cation in the Li-N network is not free to act as a relay agent for hydride ions.

$$Li_2N_2B_2H_8 \ (\mathbf{9}) \rightarrow LiNH=BH_2 + NH_2BH_2 + LiH \tag{6a}$$

$$LiNH=BH_2 + NH_2BH_2 + LiH \rightarrow c\text{-}(LiNH=BH_2)_2 \ (\mathbf{11}) + H_2 \ (H_2\#2) \tag{6b}$$
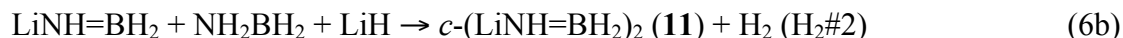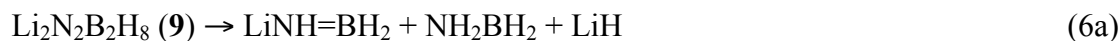
Before proceeding to the third dehydrogenation (loss of H₂#3) from **11**, it is valuable to compare dehydrogenation from a single $LiNH_2BH_3$ molecule (eq 5 and Figure 8) to form $LiNH=BH_2$ as a final product. The one-step dehydrogenation through **TSLiNH₂BH₃/LiNHBH₂·H₂** has a very unfavorable free energy barrier ($\Delta G^{\ddagger} = 60.2$ kcal/mol) with a N-B single bond distance (1.536 Å) and the process **LiNH₂BH₃** → **LiNH₂BH₂** + H₂ exhibiting a slight endergonic nature ($\Delta G = 4.4$ kcal/mol, Figure 8). The two-step dehydrogenation occurs with a lower free energy barrier (**LiNH₂BH₃** → **TSLiNH₂BH₃/D** → **D** → **TSD/LiNH₂BH₂·H₂** → **LiNH₂BH₂** + H₂, $\Delta G^{\ddagger} = 30.3$ kcal/mol) than the one-step

dehydrogenation and is analogous to the two-step dehydrogenation of **7** to **9** ($\Delta G^{\ddagger} = 29.4$ kcal/mol, Figure 6)**.**
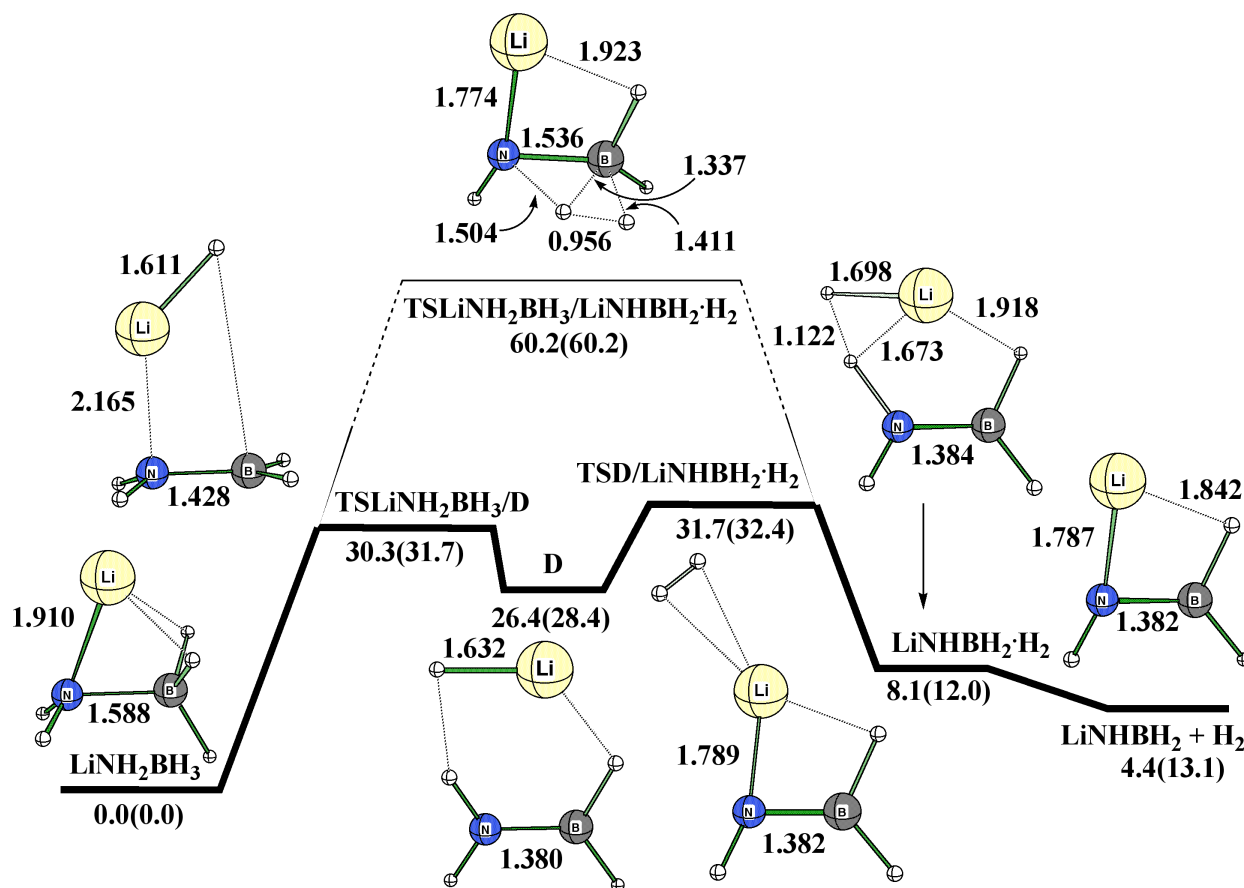
Figure 8. One-step dehydrogenation (**TSLiNH₂BH₃/LiNHBH₂·H₂**) and a two-step

    dehydrogenation (**TSLiNH₂BH₃/D → D → TSD/LiNHBH₂·H₂**) pathway of a single

    LiNH₂BH₃ molecule.

Therefore, dehydrogenation of LiNH₂BH₃ is not promoted by the formation of the (LiNH₂BH₃)₂ dimer but by the Li⁺ relay (Li-H-Li moiety) mechanism. Staubitz et al.[3] showed that dimerization of ammoniaborane were reduced when functional groups such as methyl are added to the nitrogen atom.

The rearrangement of **11** (eq 7) starts by replacing a Li-N bond with a N-B bond as shown in **TS11/12** and **12** (Figure 9). The Li$^+$ cation can establish a strong Li-H interaction with the hydrogen of the BH$_2$ group in **TS11/12** (1.846 Å), which is similar to the Li-H distances in the (LiH)$_4$ cluster (1.843 Å).
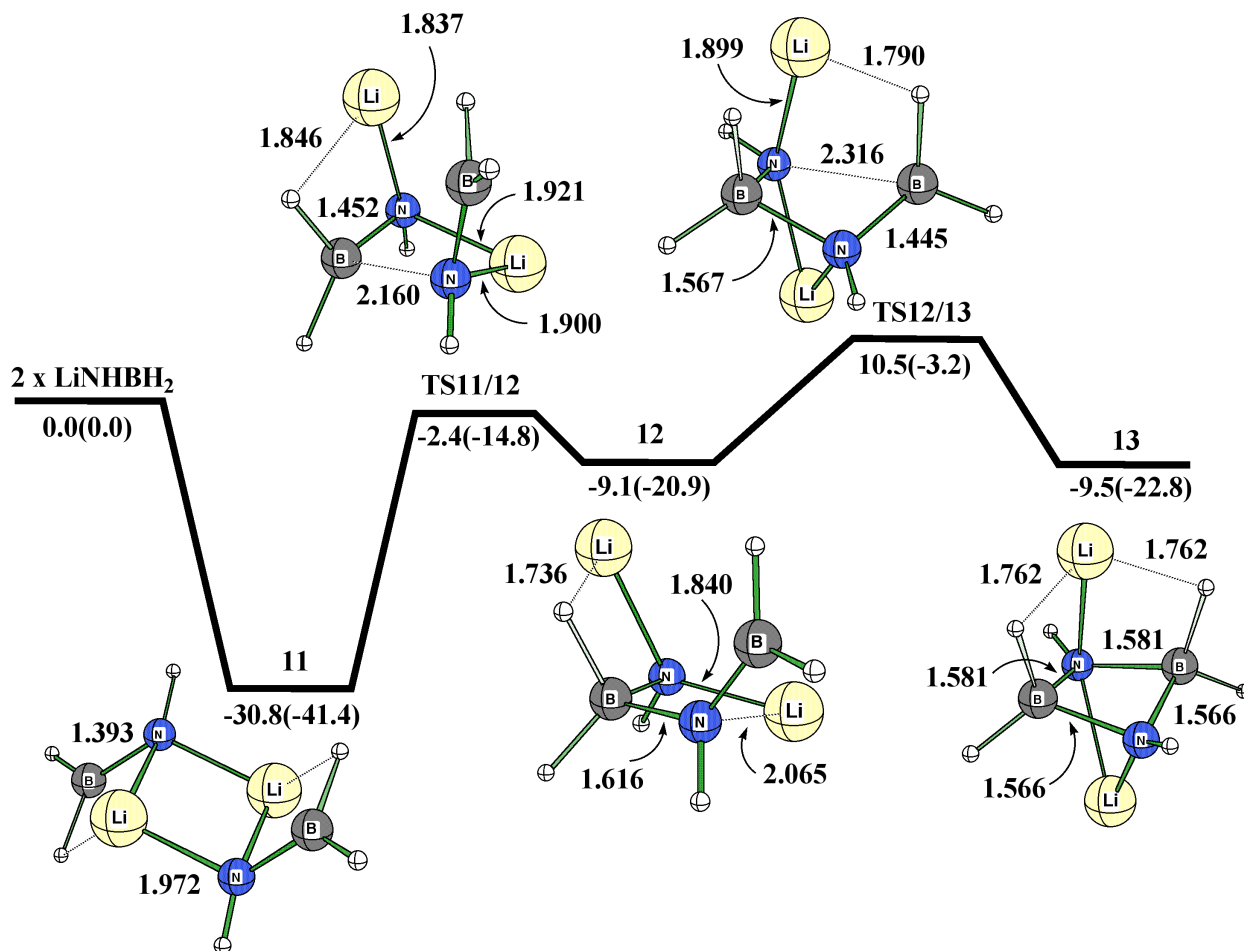
Figure 9. Rearrangement process of a (LiNH=BH$_2$)$_2$ complex (**11**).

The second Li-N interaction is replaced by a N-B bond in a reaction requiring 19.6 kcal/mol of free energy (**12** → **TS12/13**) which is smaller than the first Li-N → N-B replacement (ΔG = 28.4 kcal/mol, **11** → **TS11/12**). The relatively small free energy barrier arises due to two interactions

of the Li^+ cation with the nitrogen atom and a strong LiH bond (1.790 Å) in **TS12/13**. In the

final cyclic N-B bonded complex (**13**), the N-B bond lengths are 1.566 Å and 1.581 Å (Figure 9).

$$c\text{-}(LiNH=BH_2)_2 \rightarrow Li_2N_2B_2H_6 \tag{7}$$

It should be pointed out that the reaction **11**→**13** is strongly endergonic (21.3 kcal/mol) which

suggests that the Li^+ cation movement in the $LiNH=BH_2$ bulk matrix is disfavored. The final

dehydrogenation generates amorphous LiN≡BH with one mole of H_2 released (eq 8).[24]

$$LiNH=BH_2(s) \rightarrow LiN\equiv BH(s) + H_2(g) \tag{8}$$

The reaction of two $LiNH=BH_2$ units (**13**) may follow a similar pathway as the reaction of two

$LiNH_2BH_3$ units as shown in eq 9a and eq 9b.

$$Li_2N_2B_2H_6 (\textbf{13}) \rightarrow LiN_2B_2H_5 + LiH \tag{9a}$$

$$LiN_2B_2H_5 + LiH \rightarrow Li_2N_2B_2H_4 (\textbf{15}) + H_2 (H_2\#3) \tag{9b}$$
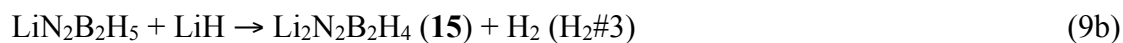
In the pathway **13** → **15**, the role of Li^+ as a relay agent for hydride ion can be

recognized. The Li^+ cation in **TS13/14** abstracts a hydride from one BH_2 group and interacts

with a hydrogen atom of the other BH_2 group while the N-B bond in **14** shortens (1.566 → 1.442

Å) due to rehybridization (sp^3→sp^2) around the boron atom. As hydride is relayed in

TS14/15·H$_2$, the LiH unit swings around to abstract a H^+ from nitrogen to form the product

complex **15·H₂** where H_2 is coordinated to lithium. The final product **15** has a Li^+ cation

coordinated to two nitrogen atoms and one hydrogen atom of the BH_2 group (Figure 10).
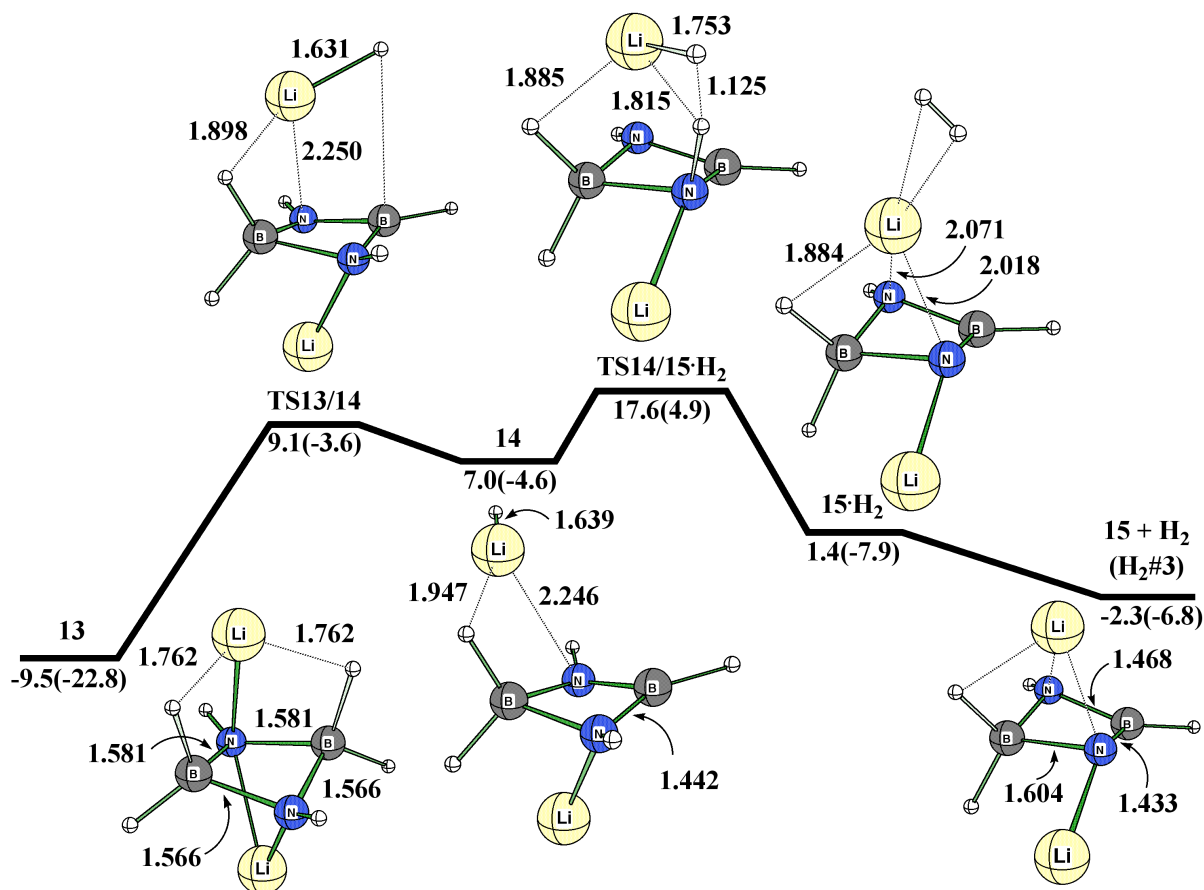
Figure 10. Dehydrogenation of a (LiNH=BH₂)₂ complex (**13**).

The dehydrogenation process for H₂#3 shows a very endergonic nature (**11** → **15**+H_2, ΔG=28.5

kcal/mol) while dehydrogenation steps of H₂#1 and H₂#2 are almost thermoneutral.

A discrepancy between two experimental studies[24,26] (Table 1) involves release of H₂#3

and H₂#4 in the NH₃BH₃/Li system. Based upon the observation from Kang et al.[26] 10.4 wt% of

H_2 release is available after 2.5 hours at 120^oC or after 5 hours at 100^oC. However, an additional

0.8H_2 equivalence (total 14.5 wt% of H_2 from NH₃BH₃/LiH) is only available at 200^oC, which

corresponds to all of H₂#3 and a partial amount of H₂#4. The fourth H_2 (H_2#4) is essential to achieve over 10 wt% of H_2 from $LiNH_2BH_3$ in our calculations since dehydrogenation of H_2#1, H_2#2, and H_2#3 coresponds to 8.4 wt% from $(LiNH_2BH_3)_2$. In order to achieve a one molar equivalent dehydrogenation (loss of H_2#3) from eq 9b, one more H_2 molecule should be available from $Li_2N_2B_2H_6$ (Figure 11).
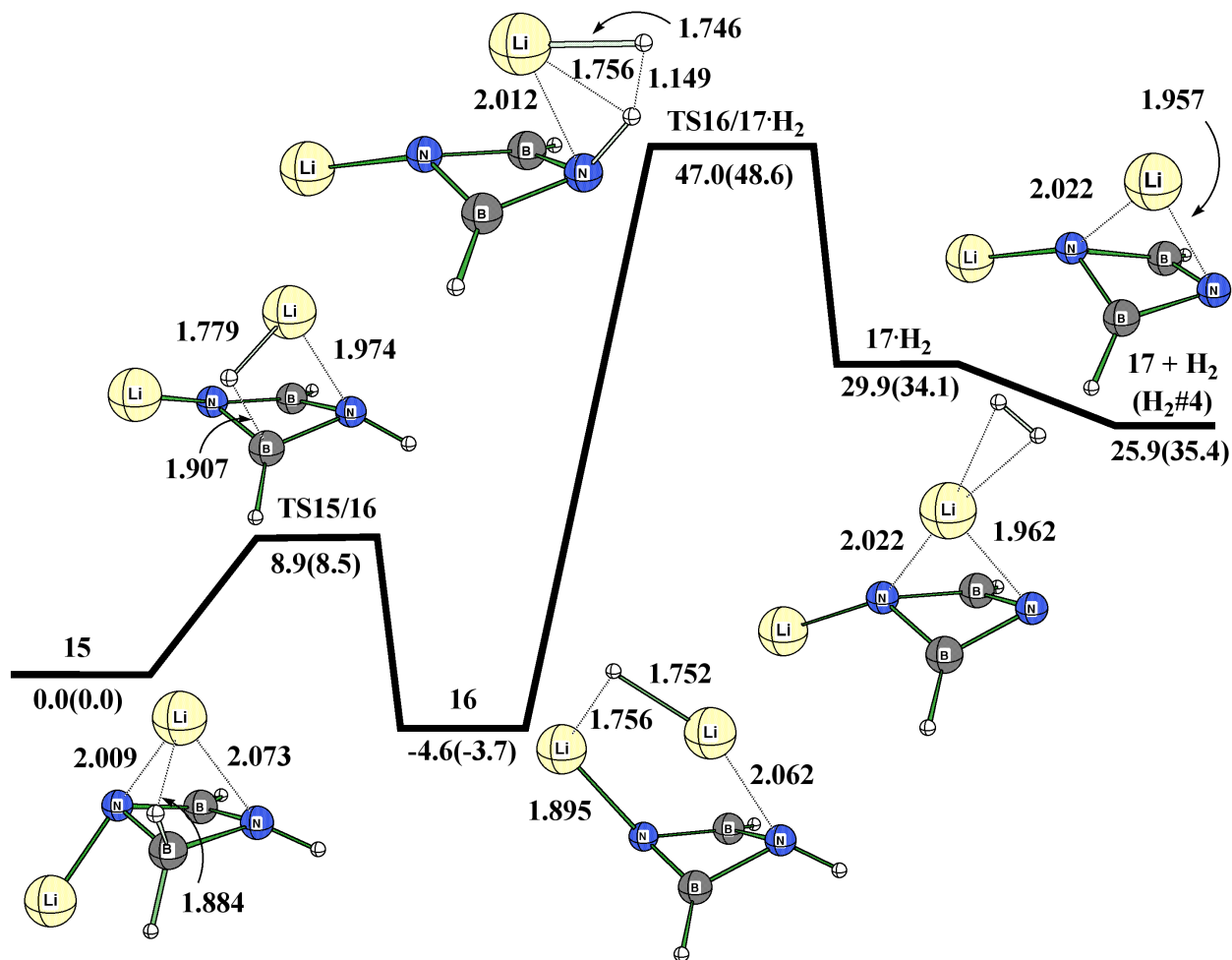
Figure 11. Dehydrogenation of $Li_2N_2B_2H_4$ (**15**)

Dehydrogenation (loss of H_2#4) of **16** is very difficult ($\Delta G^{\ddagger} = 51.6$ kcal/mol) where the Li^+ relay agent transfers a hydride ion from boron to nitrogen to form the product complex **17·H₂**. The distances between the Li^+ cation and nitrogen in **TS16/17·H₂** are 2.012 Å and 2.407

Å (2.407 Å is not shown explicitly in **TS16/17·H$_2$**). The two-step reaction presented by eq 10a and eq 10b summarizes the second dehydrogenation (loss of H$_2$#4) from Li$_2$N$_2$B$_2$H$_4$ (**18**).

$$\text{Li}_2\text{N}_2\text{B}_2\text{H}_4 \ (\textbf{15}) \rightarrow \text{LiN}_2\text{B}_2\text{H}_3 + \text{LiH} \ (\textbf{16}) \tag{10a}$$

$$\text{LiN}_2\text{B}_2\text{H}_3 + \text{LiH} \ (\textbf{16}) \rightarrow \text{Li}_2\text{N}_2\text{B}_2\text{H}_2 \ (\textbf{17}) + \text{H}_2 \ (\text{H}_2\#4) \tag{10b}$$

While high, the free energy barrier of the step **16** → **TS16/17·H$_2$** ($\Delta G^{\ddagger}$=51.6 kcal/mol) is still significantly lower than the barrier NH$_2$BH$_2$ → HN≡BH + H$_2$ ($\Delta G^{\ddagger}$=74.2 kcal/mol). Thus, dehydrogenation of NH$_2$BH$_2$, N$_2$B$_2$H$_8$, c-N$_3$B$_3$H$_{12}$ have much higher free energy barriers than the step **13** → **TS14/15·H$_2$** ($\Delta G^{\ddagger}$ = 27.2 kcal/mol) and **16** → **TS16/17·H$_2$** ($\Delta G^{\ddagger}$ = 51.6 kcal/mol). Li et el.[61] studied several structures of H(H$_2$N=BH$_2$)$_n$H oligomers but did not investigate the dehydrogenation mechanism for hydrogen storage applications. In experiments by Xiong et al., about 8 wt% of hydrogen is released within one hour, which would corresponding to the release of H$_2$#1, H$_2$#2, and H$_2$#3 from (LiNH$_2$BH$_3$)$_2$ which gives results in a 8.2 wt% change. After 19 hours 3 additional wt% of hydrogen is released which would corresponding to the release of H$_2$#4 from (LiNH$_2$BH$_3$)$_2$ (2.7 additional wt%).[24] Both the increasing free energy barriers and the endergonic nature of the last dehydrogenation steps explain the early saturation and the slow kinetics of subsequent LiNH$_2$BH$_3$ dehydrogenation. One concern is the unfavorable pathway between **15** and **17**+H$_2$ (Figure 11) since it becomes more strongly endothermic (ΔH = 35.4 kcal/mol, Table 4) than a pathway between **11** and **15**+H$_2$ (ΔH = 34.6 kcal/mol, Table 4). From the report of Miranda and Ceder,[4] dehydrogenation from NH$_3$BH$_3$ is exothermic in both the gas-phase (ΔH = -5.7 kcal/mol)[2] and solid-state (ΔH = -1.6 kcal/mol) while dehydrogenation from

NH_2BH_2 is strongly endothermic in the gas-phase (30.3 kcal/mol) but exothermic in the solid-state (-9.6 kcal/mol).

Table 4.   Reaction Enthalpies and Free energies (kcal/mol and 298K) for each steps at the CCSD(T)/6-311++G(3d2p)//MP2/6-311++G(2d,p) level

Dehydrogenation	Equation	TS		Reaction	
		$\Delta G^{\ddagger}$	$\Delta H^{\ddagger}$	ΔG	ΔH
$NH_3BH_3+(LiH)_4 \rightarrow LiNH_2BH_3+H_2$	$\mathbf{1\rightarrow TS1/3\rightarrow 3}+H_2$	11.0	12.4	-24.4	-16.7
	$\mathbf{4\rightarrow TS4/5\rightarrow 5}+H_2$	8.4	7.8	-24.9	-14.2
	$\mathbf{5}+H_2\rightarrow \mathbf{TS5/6}+H_2\rightarrow \mathbf{6}+H_2$	3.4	0.7	0.5	-2.6
$LiNH_2BH_3 \rightarrow LiNH=BH_2+H_2$	$\mathbf{7\rightarrow TS7/8\rightarrow 8}$	22.6	23.9	21.5	23.6
	$\mathbf{8\rightarrow TS8/9\rightarrow 9}+H_2$	14.7	13.4	-19.1	-13.6
	$\mathbf{9\rightarrow TS9/10\rightarrow 10}$	25.0	27.2	23.0	26.7
	$\mathbf{10\rightarrow TS10/11\rightarrow 11}+H_2$	12.4	10.2	-21.4	-16.3
$LiNH=BH_2 \rightarrow LiN\equiv BH+H_2$	$\mathbf{11\rightarrow TS11/12\rightarrow 12}$	28.4	26.6	21.7	20.5
	$\mathbf{12\rightarrow TS12/13\rightarrow 13}$	19.6	17.7	-0.4	-1.9
	$\mathbf{13\rightarrow TS13/14\rightarrow 14}$	18.6	19.2	16.5	18.2
	$\mathbf{14\rightarrow TS14/15\rightarrow 15}+H_2$	10.6	9.5	-9.3	-2.2
	$\mathbf{15\rightarrow TS15/16\rightarrow 16}$	8.9	8.5	-4.6	-3.7
	$\mathbf{16\rightarrow TS26/17\rightarrow 17}+H_2$	51.6	52.3	30.5	39.1

In addition, a recent experimental thermal analysis shows a distinct two-step exothermic decomposition accompanied by the generation of 2.2 mol H_2/mol from NH_3BH_3 powder.[62] Therefore, hydrogen loss from solid-state NH_2BH_2 has a significant enthalpy contribution from lattice stabilization of the product, amounting to as much as 39.9 kcal/mol (30.3+9.6). Such an increase in lattice stabilization is not found in the dehydrogenation of NH_3BH_3. However, lattice stabilization of $LiNH_2BH_3$ and products of its dehydrogenation might be stronger than those of

NH$_3$BH$_3$ due to the ionic character of LiNH$_2$BH$_3$ and its dehydrogenation products (Table 5). If one assumes that hydrogen loss from LiNH$_2$BH$_3$ and LiNH=BH$_2$ would roughly parallel that from NH$_3$BH$_3$ and NH$_2$BH$_2$, the energetics of hydrogen loss from LiNH=BH$_2$ might be seriously underestimated.

Table 5.   Atomic Charges from Natural Bond Orbital Analysis at the MP2/6-11++G(2d,p) level

NH$_3$-BH$_3$	B	-0.12	LiNH$_2$-BH$_3$	B	-0.16
	N	-0.83		N	-1.13
				Li	0.84
NH$_2$=BH$_2$	B	0.45	LiNH=BH$_2$	B	0.30
	N	-1.00		N	-1.21
				Li	0.84
HN≡BH	B	0.63	LiN≡BH	B	0.51
	N	-0.97		N	-1.34
				Li	0.92

In order to compensate for the increase in reaction endergonicity during the dehydrogenation of (LiNH=BH$_2$)$_2$ in solid state, I assume that the loss of H$_2$#3 and H$_2$#4 are accompanied by a decrease in lattice free energy amounting 20 kcal/mol for each step. (Table 6). Thus, loss of H$_2$#1 (**7 → 9** + H$_2$) and H$_2$#2 (**9 → 11** + H$_2$) is nearly thermoneutral, while H$_2$#3 would be thermoneutral if increased lattice energy stabilization was included. Thus, the three initial H$_2$-loss steps are consistent with rapid evolution of 8 wt% of hydrogen.[24] Loss of H$_2$#4 has a more unfavorable free energy/enthalpy change (ΔH = 70.0 - 40 kcal/mol, ΔG = 54.4 - 40 kcal/mol) and, while observed, the evolution of 3 additional wt% of H$_2$ is much slower. During the revision process of this article, a quantum mechanical study for the dehydrogenation mechanism for loss of H$_2$#1 and H$_2$#2 from (LiNH$_2$BH$_3$)$_2$ was published by Kim et al (Figure 12).[63] They identified two mechanism for loss of H$_2$#1 and H$_2$#2, the "L" pathway which corresponds to the

mechanism in our manuscript, and the "L*" pathway, a new mechanism where a new N-B bond is formed before the loss of $H_2\#1$ (Figure 12).

Table 6. Reaction Enthalpies and Free energies (kcal/mol) for each Step at the CCSD(T)/6-311++G(3d,2p)//MP2/6-311++G(2d,p) level

	$\Delta G(298K)$	$\Delta G(365K)$[a]	DLS[b]	Best estimate for solid LiNH$_2$BH$_3$ at $\Delta G(365K)$	$\Delta H(298K)$
$7 \rightarrow 9+H_2$	2.4	0.7	0.0	0.7	10.0
$7 \rightarrow 11+2H_2$	4.0	0.3	0.0	0.3	20.4
$7 \rightarrow 15+3H_2$	32.5	27.5	20.0[c]	7.5	55.0
$7 \rightarrow 17+4H_2$	58.4	51.2	40.0[d]	11.2	90.4
$NH_3BH_3 \rightarrow$ HN≡BH+2H$_2$	8.2	4.5			24.7
$LiNH_2BH_3 \rightarrow$ LiN≡BH+2H$_2$	21.7	17.8			39.1

[a]Experimental condition of ref. 24. [b]Differential Lattice energy Stabilization (see text). [c]The free energy change for the reaction in solid is increased by 20 kcal/mol due to the larger lattice energy of product-solid compared to the lattice energy of the reactant-solid. [d]The free energy change for the reaction in solid is increased by 20 kcal/mol relative to **15**+3H$_2$ to account for differential lattice energy stabilization. The total change with respect to **7** is 40 kcal/mol.

I have re-computed all of the transition states and intermediates in their "L" and "L*" pathways at our standard level of theory and have extended the "L*" pathway to include elimination of $H_2\#3$ (Figure 12). The "L" pathway corresponds to our Li$^+$ relay mechanism (Li-H-Li moiety) and is consistent with our mechanism between **7** to **11**+H$_2$ with minor differences in geometry of **1'**, **T1t**, **T2h**, and **4t** (their notation). Their enthalpy values for reaction pathway "L" agree with our values to within about 2 kcal/mol except for **11** (**5H$_2$** in their notation) which I calculate to be 20.6 kcal/mol less stable than **7** (LiNH$_2$BH$_3$)$_2$ while they report **5H$_2$** (their notation) is 30.3 kcal/mol less stable than (LiNH$_2$BH$_3$)$_2$ (**1** in their notation).
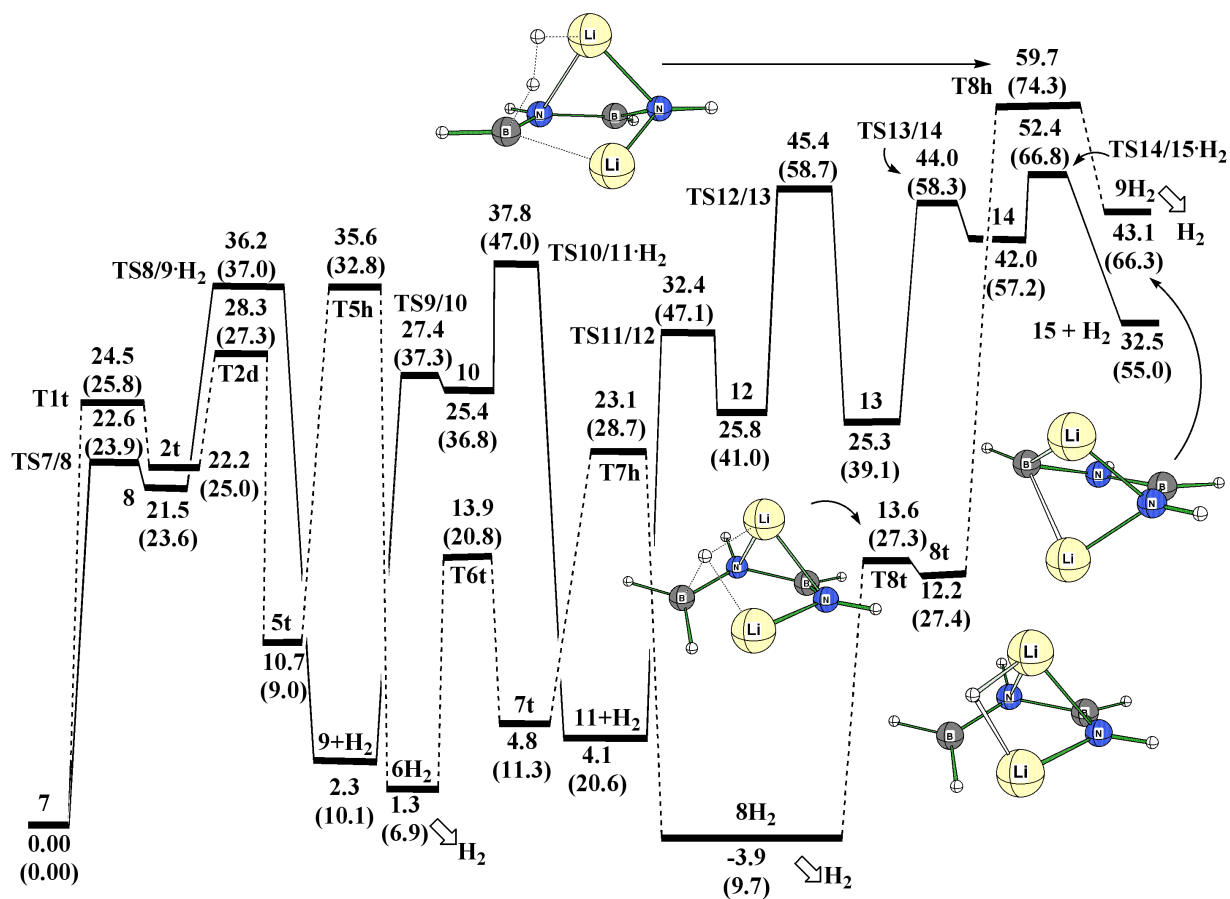
Figure 12. Free energy surface of dehydrogenation from $(LiNH_2BH_3)_2$ dimer (H_2#1, H_2#2, and H_2#3). Free energies and enthalpies (kcal/mol) are relative to **7** at 298 K. The values in parentheses are enthalpies (kcal/mol) relative to **7** at 298 K. Dotted lines represent pathway from Ref. 63.

In terms of enthalpy, pathway "L*" is slightly more favorable than pathway "L" but **TS8/9·H₂** (Pathway L) and **T5h** (Pathway L*) are within 0.6 kcal/mol in terms of free energy. A chain N-B bond is formed early in the "L*" pathway while a cyclic N-B bond is formed in the "L" pathway. Thus, this N-B bond chain formation might be a key to understand the difference from the two experimental studies for H_2#3 and H_2#4 release from $(LiNH_2BH_3)_2$.[24,26]

2.4 Conclusions

The formation of $LiNH_2BH_3$ crystal from $(LiH)_4 + NH_3BH_3$ and its stepwise dehydrogenation mechanism is investigated through an *ab initio* study. A competition mechanism between H^- and $NH_2BH_3^-$ is proposed to explain $LiNH_2BH_3$ formation during the ball-milling process. Exchange of the $NH_2BH_3^-$ and H^- positions is possible at the edge of cubic $(LiH)_4$ geometry, which represent the active surface of bulk LiH crystal. The dehydrogenation of $LiNH_2BH_3$ is facilitated by relaying a hydride ion from boron to Li^+, which then abstracts a H^+ from NH_3 to form H_2. Thus, Li^+ plays a key role by carrying the hydride ion from boron to nitrogen. The rearrangement of the $(LiNH=BH_2)_2$ complex to $Li_2N_2B_2H_6$, which requires the replacement of Li-N bonds by N-B bonds, is necessary for the third and fourth equimolecular dehydrogenation. If differential lattice energy effects in the dehydrogenation of $(LiNH_2BH_3)_2$ dimer are sufficiently large, the present results suggest that four molecules of H_2 from $(LiNH_2BH_3)_2$ dimer may be reversibly available, which corresponds to 10.9 wt% of hydrogen.

2.5 References

(1) (a) Marder, T. B. *Angew. Chem. Int. Ed.* **2007**, *46*, 8116. (b) Hamilton, C. W.; Baker, T.; Staubitz, A.; Manners, I. *Chem. Soc. Rev.* **2009**, *38*, 279.

(2) Dixon, D. A.; Gutowski, M. *J. Phys. Chem. A* **2005**, *109*, 5129.

(3) Staubitz, A.; Besora, M.; Harvey, J. N.; Manners, I. *Inorg. Chem.* **2008**, *47*, 5910.

(4) Miranda, C.; Ceder, G. *J. Chem. Phys.* **2007,** *126*, 184703.

(5) Cheng, F.; Ma, H.; Li, Y.; Chen, J. *Inorg. Chem.* **2007,** *46*, 788.

(6) Allouti, F.; Siebert, W.; Himmel, H.-J. *Inorg. Chem.* **2008**, *47*, 7631.

(7) (a) Peng, B.; Chen, J. *Energy Environ. Sci.* **2008**, *1*, 479. (b) Chen, P.; Zhun, M. *Materials Today* **2008**, *11*, 36.

(8) (a) Staubitz, A.; Soto, P. A.; Manners, I. *Angew. Chem. Int. Ed.* **2008,** *47*, 6212. (b) Kalidindi, S. B.; Indirani, M.; Jagirdar, B. R. *Inorg. Chem.* **2008,** *47*, 7424.

(9) (a) Chen, P.; Xiong, Z.; Luo, J.; Lin, J.; Tan, K. L. *Nature* **2002**, *420*, 302. (b) Chen, P.; Xiong, Z.; Yang, L.; Wu, G.; Luo, W. *J. Phys. Chem. B* **2006**, *110*, 14221. (c) Chen, P.; Xiong, Z.; Luo, J.; Lin, J.; Tan, K. L. *J. Phys. Chem. B* **2003**, *107*, 10967.

(10) (a) Leng, H. Y.; Ichikawa, T.; Hino, S.; Hanada, N.; Isobe, S.; Fujii, H. *J. Phys. B.* **2004**, *108*, 8763. (b) Isobe, S.; Ichikawa, T.; Hino, S.; Fujii, H. *J. Phys. Chem. B* **2005**, *109*, 14855. (c) Hanada, N.; Ichikawa, T.; Fujii, H. *J. Phys. Chem. B* **2005**, *109*, 7188. (d) Leng, H.; Ichikawa, T.; Fujii, H. *J. Phys. Chem. B* **2006**, *110*, 12964.

(11) (a) Shaw, L. L.; Ren, R.; Markmaitree, T.; Osborn, W. *J. Alloys Compd.* **2008,** *448*, 263. (b) Ortiz, A. L.; Osborn, W.; Markmaitree, T.; Shaw, L. L. *J. Alloys Compd.* **2008**, *454*, 297.

(12) (a) Wu, H. *J. Am. Chem. Soc.* **2008,** *130*, 6515. (b) Baldé, C. P.; Hereijgers, B. P. C.; Bitter, J. H.; de Jong, K. P. *J. Am. Chem. Soc.* **2008**, *130*, 6761.

(13) Li, L.; Yao, X.; Sun, C.; Du, A.; Cheng, L.; Zhu, Z.; Yu, C.; Zou, J.; Smith, S. C.; Wang, P.; Cheng, H.-M.; Frost, R. L.; Lu, G. Q. *Adv. Funct. Mater.* **2009**, *19*, 265.

(14) (a) Shaw, L. L.; Osborn, W.; Markmaitree, T.; Wan, X. *J. Power Sources* **2008,** *177*, 500. (b) Ichikawa, T.; Hanada, N.; Isobe, S.; Leng, H. Y.; Fujii, H. *J. Phys. Chem. B* **2004**, *108*, 7887.

(15) Kar, T.; Scheiner, S.; Li, L. *THEOCHEM* **2008**, *857*, 111.

(16) Aguey-Zinsou, K.-F.; Yao, J.; Guo, Z. X. *J. Phys. Chem. B* **2007**, *111*, 12531.

(17)   Filinchuk, Y.; Chernyshov, D.; Nevidomskyy, A.; Dmitriev, V. *Angew. Chem. Int. Ed.* **2008,** *47*, 529.

(18)   Yang, J.; Sudik, A.; Siegel, D. J.; Halliday, D.; Drews, A. D.; Carter, R. O.; Wolverton, C.; Lewis, G. J.; Sachtler, J. W.; Low, J. J.; Faheem, S. A.; Lesch, D. A.; Ozolinš, V. *Angew. Chem. Int. Ed.* **2008,** *47*, 882.

(19)   Nickels, E. A.; Jones, M. O.; David, W. I. F.; Johnson, S. R.; Lowton, R. L.; Sommariva, M. S.; Edwards, P. P. *Angew. Chem. Int. Ed.* **2008,** *47*, 2817.

(20)   Zhang, C.; Alavi, A. *J. Phys. Chem. B* **2006**, *110*, 7139.

(21)   Du, A. J.; Smith, S. C.; Yao, X. D.; Lu, G. Q. *J. Phys. Chem. C* **2007**, *111*, 12124.

(22)   Zimmerman, P. M.; Paul, A.; Zhang, Z.; Musgrave, C. B. *Inorg. Chem.* **2009**, *48*, 1069.

(23)   (a) Zimmerman, P. M.; Paul, A.; Zhang, Z.; Musgrave, C. B. *Angew. Chem. Int. Ed.* **2009**, *48*, 2201. (b) Zimmerman, P. M.; Paul, A.; Musgrave, C. B. *Inorg. Chem.* **2009**, *48, 5418*.

(24)   Xiong, Z.; Yong, C. K.; Wu, G.; Chen, P.; Shaw, W.; Karkamkar, A.; Autrey, T.; Jones, M. O.; Johnson, S. R.; Edwards, P. P.; David, W. I. F. *Nat. Mater.* **2008**, *7*, 138.

(25)   Benedetto, S. D.; Carewska, M.; Cento, C.; Gislon, P.; Pasquali, M.; Scaccia, S.; Prosini, P. P. *Thermochim. Acta* **2006**, *441*, 184.

(26)   Kang, X.; Fang, Z.; Kong, L.; Cheng, H.; Yao, X.; Lu, G.; Wang, P. *Adv. Mat.* **2008**, *20*, 2756.

(27)   Nguyen, M. T.; Nguyen, V. S.; Matus, M. H.; Gopakumar, G.; Dixon, D. A. *J. Phys. Chem. A* **2007**, *111*, 679.

(28)   Nguyen, V. S.; Matus, M. H.; Ngan, V. T.; Nguyen, M. T.; Dixon, D. A. *J. Phys. Chem. C* **2008**, *112*, 5662.

(29)   Stephens, F. H.; Baker, R. T.; Matus, M. H.; Grant, D. J.; Dixon, D. A. *Angew. Chem. Int. Ed.* **2007**, *46*, 746.

(30)   Nguyen, V. S.; Matus, M. H.; Grant, D. J.; Nguyen, M. T.; Dixon, D. A. *J. Phys. Chem. A* **2007**, *111*, 8844.

(31)   Nguyen, V. S.; Matus, M. H.; Nguyen, M. T.; Dixon, D. A. *J. Phys. Chem. C* **2007**, *111*, 9603.

(32)   Frisch, M. J. T., G. W.; Schlegel, H. B.; Scuseria, G. E.; Robb, M. A.; Cheeseman, J. R.; Montgomery, Jr., J. A.; Vreven, T.; Kudin, K. N.; Burant, J. C.; Millam, J. M.; Iyengar,

S. S.; Tomasi, J.; Barone, V.; Mennucci, B.; Cossi, M.; Scalmani, G.; Rega, N.; Petersson, G. A.; Nakatsuji, H.; Hada, M.; Ehara, M.; Toyota, K.; Fukuda, R.; Hasegawa, J.; Ishida, M.; Nakajima, T.; Honda, Y.; Kitao, O.; Nakai, H.; Klene, M.; Li, X.; Knox, J. E.; Hratchian, H. P.; Cross, J. B.; Bakken, V.; Adamo, C.; Jaramillo, J.; Gomperts, R.; Stratmann, R. E.; Yazyev, O.; Austin, A. J.; Cammi, R.; Pomelli, C.; Ochterski, J. W.; Ayala, P. Y.; Morokuma, K.; Voth, G. A.; Salvador, P.; Dannenberg, J. J.; Zakrzewski, V. G.; Dapprich, S.; Daniels, A. D.; Strain, M. C.; Farkas, O.; Malick, D. K.; Rabuck, A. D.; Raghavachari, K.; Foresman, J. B.; Ortiz, J. V.; Cui, Q.; Baboul, A. G.; Clifford, S.; Cioslowski, J.; Stefanov, B. B.; Liu, G.; Liashenko, A.; Piskorz, P.; Komaromi, I.; Martin, R. L.; Fox, D. J.; Keith, T.; Al-Laham, M. A.; Peng, C. Y.; Nanayakkara, A.; Challacombe, M.; Gill, P. M. W.; Johnson, B.; Chen, W.; Wong, M. W.; Gonzalez, C.; Pople, J. A.; *Gaussian03*, Revision E.01; Gaussian, Inc: Wallingford CT, 2004.

(33)   Rioux, F. *J. Chem. Edu.* **1977**, *54*, 555.

(34)   Morrison, C. A.; Siddick, M. M. *Angew. Chem. Int. Ed.* **2004,** *116*, 4884.

(35)   Matus, M. H.; Anderson, K. D.; Camaioni, D. M.; Autrey, T.; Dixon, D. A. *J. Phys. Chem.* **2007,** *111*, 4411.

(36)   Alton, E. R.; Brown, R. D.; Carter, J. C.; Taylor, R. C. *J. Am. Chem. Soc.* **1959**, *81*, 3550.

(37)   Xiong, Z.; Chua, Y. S.; Wu, G.; Xu, W.; Chen, P.; Shaw, W.; Karkamkar, A.; Linehan, J.; Smurthwaite, T.; Autry, T. *Chem. Commun.* **2008**, 5595.

(38)   (a) Wang, X.; Andrews, L. *J. Phys. Chem. A* **2007,** *111*, 6008. (b) Bertolus, M.; Brenner, V.; Millie, P. *J. Chem. Phys.* **2001**, *115*, 4070. (c) Kato, H.; Hirao, K.; Nishida, I.; Kimoto, K.; Akagi, K. *J. Phys. Chem.* **1981**, *85*, 3391. (d) Kato, H.; Hirao, K.; Akagi, K. *Inorg. Chem.* **1981**, *20*, 3659.

(39)   Kang, X.; Ma, L.; Fang, Z,; Gao, L.; Luo, J.; Wang, S.; Wang, P. *Phys. Chem. Chem. Phys.* **2009**, *11*, 2507.

(40)   Plumley, J. A.; Evanseck, J. D. *J. Chem. Theory Comput.* **2008**, *4*, 1249.

(41)   Wu, H.; Zhou, W.; Yildirim, T. *J. Am. Chem. Soc.* **2008**, *130*, 14834.

(42)   Stephens, F. H.; Pons, V.; Baker, R. T. *Dalton trans.* **2007**, *25*, 2613.

(43)   Stowe, A. C.; Shaw, W. J.; Linehan, J. C.; Schmid, B.; Autrey, T. *Phys. Chem. Chem. Phys.* **2007,** *9*, 1831.

(44)   Shaw, W. J.; Linehan, J. C.; Szymczak, N. K.; Heldebrant, D. J.; Yonker, C.; Camaioni, D. M.; Baker, R. T.; Autrey, T. *Angew. Chem. Int. Ed.* **2008**, *47*, 7493.

(45)   Loubeyre, P.; Le Toullec, R.; Hanfland, M.; Ulivi, L.; Datchi, F.; Hausermann, D. *Phys. Rev. B* **1998,** *57*, 10403.

(46)   Duclos, S. J.; Vohra, Y. K.; Ruoff, A. L.; Filipek, S.; Baranowski, B. *Phys. Rev. B* **1987,** *36*, 7664.

(47)   For a recent study about restoring the hydrogen capacity of a depleted hydride, see: Davis, B, L.; Dixon, D. A.; Garner, E. B.; Gordon, J. C.; Matus, M. H.; Scott, B.; Stephens F. H. *Angew. Chem. Int. Ed.* **2009**, *48*, 6812.

(48)   Bowden, M. E.; Brown, I. W. M.; Gainsford, G. J.; Wong, H. *Inorg. Chim. Acta* **2008,** *361*, 2147.

(49)   Sun, C.-H.; Yao, X.-D.; Du, A.-J.; Li, L.; Smith, S.; Lu, G.-Q. *Phys. Chem. Chem. Phys.* **2008,** *10*, 6104.

(50)   Yang, X.; Hall, M. B. *J. Am. Chem. Soc.* **2008**, *130*, 1798.

(51)   Blaquiere, N.; Diallo-Garcia, S.; Gorelsky, S. I.; Black, D. A.; Fagnou, K. *J. Am. Chem. Soc.* **2008**, *130*, 14034.

(52)   Bluhm, M. E.; Bradley, M. G.; Butterick III, R.; Kusari, U.; Sneddon, L. G. *J. Am. Chem. Soc.* **2006**, *128*, 7748.

(53)   Noritake, T.; Aoki, M.; Towata, S.; Ninomiya, A.; Nakamori, Y.; Orimo, S. *Appl. Phys. A* **2006**, *83*, 277.

(54)   Chater, P. A.; David, W. I. F.; Johnson, S. R.; Edwards, P. P.; Anderson P. A. *Chem. Commun.* **2006**, *23*, 2439.

(55)   Chater, P. A.; David, W. I. F.; Anderson, P. A. *Chem. Commun.* **2007**, *45*, 4770.

(56)   Siegel, D.; Wolverton, C. *Phys. Rev. B* **2007,** *75*, 014101.

(57)   Purewal, J.; Hwang, S.-J.; Bowman, R. C.; Rönnebro, E.; Fultz, B.; Ahn, C. *J. Phys. Chem. C* **2008**, *112*, 8481

(58)   Hügle, T; Kühnel, M. F.; Lentz, D. *J. Am. Chem. Soc* **2009**, *131*, 7444.

(59)   While I consider the $(LiNH_2BH_3)_2$ dimer as the minimum reactive species of solid $LiNH_2BH_3$, the minimum unit may be larger, i.e. trimer or tetramer.

(60)   Nutt, W. R.; McKee, M. L. *Inorg. Chem.* **2007,** *46*, 7633.

(61)   Li, J.; Kathmann, S. M.; Schenter, G. K.; Gutowski, M. *J. Phys. Chem. C* **2007**, *111*, 3294.

(62)   Baitalow, F.; Baumann, J.; Wolf, G.; Jaenicke-Röβler, K.; Leitner, G. *Thermochim. Acta* **2002**, *391*, 159.

(63)   Kim, D. Y.; Singh, N. J.; Lee, H. M.; Kim, K. S. *Chem. Eur. J.* **2009**, *15*, 5598.

Chapter 3

Dependence of pK$_a$ on Solute Cavity for Diprotic and Triprotic Acids

3.1 Introduction

Aqueous proton dissociation is important for many chemical and biological reactions and has motivated the development of many implicit solvation models to calculate reliable free energy of acid dissociation or acid dissociation constant (ΔG_{aq}/pK$_a$) values.[1–7] For practical computations in aqueous solution, high level ab initio quantum theory is usually combined with an implicit solvation model, such as the polarizable continuum model (PCM). In addition, several PCM-based studies have been applied successfully for the calculation of ΔG_{aq}/pK$_a$ values in non-aqueous media.[8,9] PCM-based solvation models can also be used to calculate redox potentials with some reliability.[10,11] The combination of density functional theory with PCM is useful for the practical computation of a broad range of molecular species in solution.[12,13] Time dependent DFT combined with the PCM solvation model enables theoretical determination of ΔG_{aq}/pK$_a$ in excited states.[14] A theoretical structure–property relationship between pK$_a$ and Bader's atoms in molecules (AIM) is also available through DFT/PCM solvation modeling.[15] An accurate prediction of ΔG_{aq}/pK$_a$ in solution enables appropriate interpretation of overlapping pK$_a$ regions in experiment.[16] Despite practical success for various chemical systems, general guidelines for the prediction of aqueous ΔG_{aq}/pK$_a$ have not been well described. For example, the choice of cavity definition has not been specified in many cases.[8,12,16,17] Therefore, it is difficult to compare different calculations in order to access the best choice of cavity sizes. Tomasi,[4] who has performed pioneering work in the field of PCM-based solvation modeling, has

63

indicated that a coherent choice of solvation model should be maintained and that comparisons among results obtained from different cavity models should be avoided. Takano and Houk[18] have reported a systematic benchmark study where they investigated the choice of radii for computing molecular cavities. They suggested DFT/6-31+G(d) combined with the CPCM method as suitable for calculation of pK_a for typical monoprotic organic molecules because this method was well balanced in terms of computation time and accuracy. In their study, the UAKS cavity model showed the best performance among several cavity models. However, Król et al.[19] suggested that the Pauling cavity set, which is actually the Merz–Kollman radii set,[20] showed best performance for the pK_a prediction of polyprotic acids among the UAHF, UAKS, and Pauling sets. However, their results were only for fluorescein and its derivatives using the PBE1PBE/6-311+G(2d,2p)//PBE1PBE/6-31+G(d) method. Fernández et al.[21] have reported better predictions with a Pauling cavity set over the UAKS cavity set for ammonia oxide ($^+NH_3O^-$), which is a zwitterionic tautomer of hydroxylamine (NH_2OH). A recent study addressed several major issues of implicit solvation modeling including thermodynamic cycles of free energy perturbation, choice of basis set, cavity definition, and electronic energy calculation.[22] The gaseous energy of the proton is critical since an error of 1.36 kcal/mol in ΔG_{aq} produces an error of 1 pK_a unit. Several gas-phase acid dissociation free energy (ΔG_{gas}) prediction studies used computationally demanding methods like CCSD(T)/CBS or MP2/aug-cc-pVTZ.[23,24] Liptak and Shields[24] suggested that the DFT/aug-cc-pVTZ method can be a quite reasonable choice for pK_a prediction as compared to other higher-level computation methods when used in combination with the experimental value of $\Delta G_{gas}(H^+)$ (-6.28 kcal/mol). While free energy calculations in the gas phase are quite straightforward, in solution perturbation Hamiltonian must be used to obtain the free energy of solution (ΔG_{aq}). Sadlej-Sosnowska[22]

found the ΔG_{aq} values using $\Delta G_{solv}(H_3O^+)$ were slightly better than ΔG_{aq} using $\Delta G_{solv}(H^+)$. However, the simplest and most straightforward description (Scheme 1) is obtained when $\Delta G_{solv}(H^+)$ is used in the free energy cycle.

$$H_2A(g,\ 1\ atm) \xrightarrow{\Delta G_{gas}{}^1} HA^-(g,\ 1\ atm)\ +\ H^+(g,\ 1\ atm)$$

$$\uparrow -\Delta G_{solv}{}^1(H_2A) \qquad\qquad \downarrow \Delta G_{solv}{}^1(HA^-) \qquad\qquad \downarrow \Delta G_{solv}(H^+)$$

$$H_2A(aq,\ 1\ M) \xrightarrow{\Delta G_{aq}{}^1} HA^-(aq,\ 1\ M)\ +\ H^+(aq,\ 1\ M)$$

$$HA^-(g,\ 1\ atm) \xrightarrow{\Delta G_{gas}{}^2} A^{2-}(g,\ 1\ atm)\ +\ H^+(g,\ 1\ atm)$$

$$\uparrow -\Delta G_{solv}{}^2(HA^-) \qquad\qquad \downarrow \Delta G_{solv}{}^2(A^{2-}) \qquad\qquad \downarrow \Delta G_{solv}(H^+)$$

$$HA^-(aq,\ 1\ M) \xrightarrow{\Delta G_{aq}{}^2} A^{2-}(aq,\ 1\ M)\ +\ H^+(aq,\ 1\ M)$$
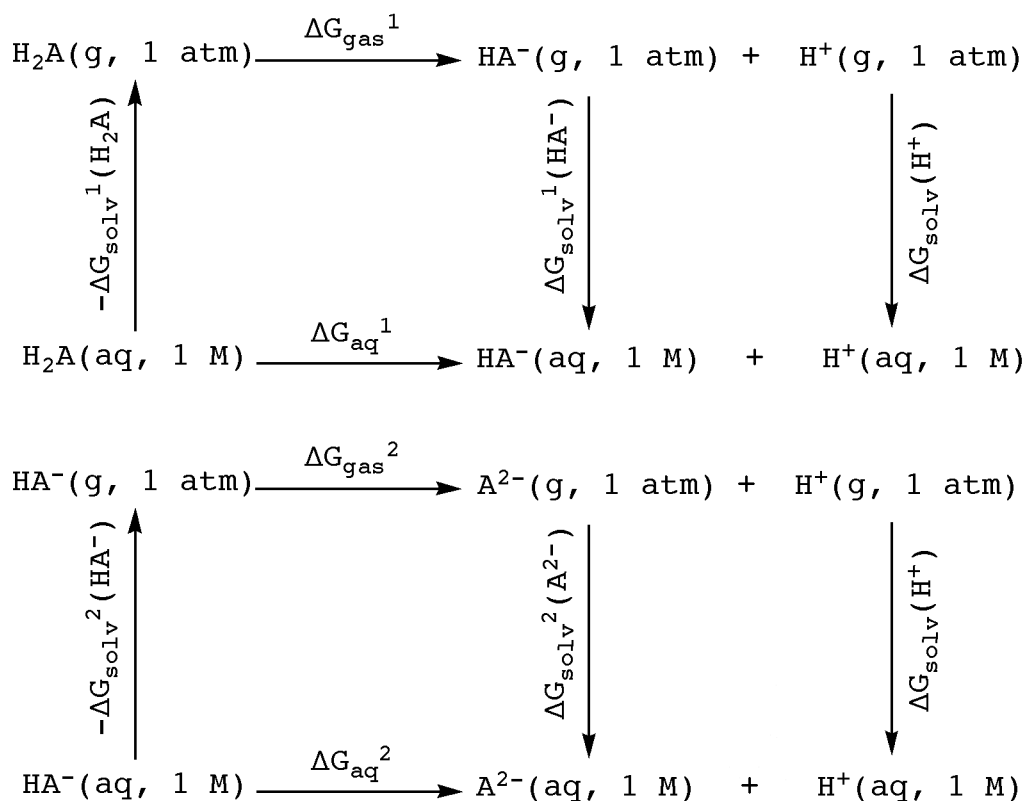
Scheme 1. Thermodynamic cycle for free energy change in solution.

After several theoretical studies and much debate, the best experimental value of $\Delta G_{solv}(H^+)$ from 1 atm to the 1 M standard state is accepted to be -264.0 kcal mol^{-1}.[25–27] Energy changes due to geometry optimization in solution usually make a minor contribution to $\Delta G_{aq}/pK_a$.[18,22] Thompson et al.[28] suggested that the experimental uncertainty in ΔG_{aq} for neutral molecules is around 0.2 kcal/mol, while for ionic species it is 4 to 5 kcal/mol (2.9 to 3.7 pK_a units) at ambient conditions. Takano and Houk[18] found that the UAKS cavity model gave the smallest deviation from experiment of the free energy of solvation (ΔG_{solv}) for neutral molecules

(1.35 kcal/mol) while the Pauling cavity model yield the smallest deviation for anions (2.73

kcal/mol). However, the deviation from experiment of free energies of solvation using the

Pauling radii was larger for neutral species (3.49 kcal/mol) than those obtained from the UAKS

or UFF radii (1.35 and 2.82 kcal/mol, respectively). Thus, a better prediction using Pauling

cavity is expected for pK_{a2} since the step $HA^- \rightarrow H^+ + A^{2-}$ needs only solvation calculations for

anions. Pratuangdejkul et al.[29] reported that PCM/UAHF method with the B3LYP/6-31+G(d,p)

failed to give reliable pK_{a2} values for 5-hydrotryptamine while a cluster-continuum model

including three water molecules was successful. Solvation results are also available for cavities

based on charge-dependent atomic radii.[30] In addition to choice of cavity set, Cossi et al.[2,31]

expressed concern about the choice of basis set and level of calculation. As a result, not only the

cavity model but also the electronic energy calculation should be chosen carefully in PCM-based

solvation modeling. Efforts to improve the predicted solvation free energy have usually

concentrated on improving the description of the solute–solvent boundary (isodensity contour

level, cavity radius, and explicit water incorporation). Casasnovas et al.[32] improved predictions

for ΔG_{aq1} and ΔG_{aq2} for pyridine derivatives by including one explicit water molecule. The

solute–water interactions over the additional surface area for the composite system allowed a

better description of the overall dissociation process. Chipman[33] reported that no single common

contour values led to acceptable solvation free energies of anions in his test sets. The SSC(V)PE

method with isodensity contour cavities agreed well with experimental solvation energies for

neutrals/cations but underestimated the solvation energy of anions. These results suggest that a

seamless and universal definition of any dielectric continuum theory without parameterization

may be difficult. Guthrie and Povar[34] were also skeptical about the accuracy of currently

available IPCM solvation models, since the prediction of $\Delta G_{aq}/pK_a$ for highly polar or

polyfunctional compounds failed to achieve reliable results without additional parameterization. Nevertheless, these compounds are of great interest and experimental data is scarce. Ho and Coote[35,36] suggested a proton exchange scheme with the CPCM/UAKS method rather than the direct method (Scheme 1) for pK_a prediction. However, an accurate solvation free energy of a reference acid is a prerequisite. For a broad range of acid species, a direct method like Scheme 1 combined with an adequate cavity set can be sufficient for reasonable predictions of $\Delta G_{aq}/pK_a$. Here, I perform a systematic study to find a proper cavity set for the prediction of $\Delta G_{aq}/pK_a$ with a test set of diprotic and triprotic acids. Our comparisons reveal the importance and sensitivity of cavity choice to the solvation free energy (ΔG_{solv}) computation along with the evaluation of several popular DFT functionals.
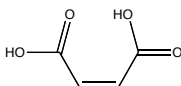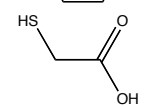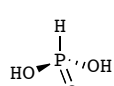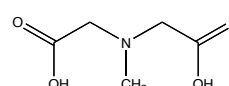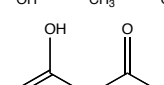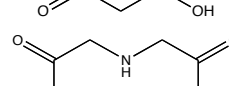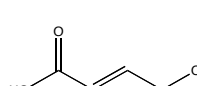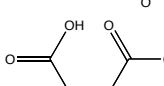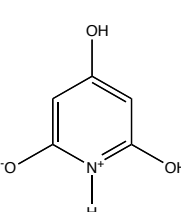
3.2 Computational Details

B3LYP, PBE (PBEPBE in G03 keyword), BVP86, and M05-2X DFT functionals were combined with the aug-cc-pVTZ basis set to calculate acid dissociation constants (pK_a) from diprotic to triprotic acids. Zero-point energies, heat capacity corrections, and TDS contributions are combined with single-point energies at the same level to yield free energies at 298 K. A conductor-like polarizable continuum model (CPCM)[30] method was used with the dielectric constant of water (e = 78.39) and gas-phase optimized geometries to compute solvation free energies (ΔG_{solv}). Four different cavity models (UFF, UAKS, Pauling, and Klamt) were used with the gaseous free energy of the proton (-6.28 kcal/mol) and the experimental aqueous free energy of the proton at 1 M (-264.0 kcal/mol). The latter value includes a standard state correction of 1.89 kcal/mol to an often cited value of -265.9 kcal/mol for a change of state of product from 1 atm to 1 M. No symmetry restrictions were made on the cavity, and the cavity

surface was optimized with the tesserae area of 0.1 Å^2. For the COSMO solvation model, I use the Klamt cavity set with polarization charges through a linear scaling iterative method.[13a] Geometries and gaseous free energies for the four cavity models were obtained using Gaussion03.[37] The Truhlar/Cramer group has recently developed the SMD model[38] and implemented it into Gaussian 09.[39] I applied the SMD method to our test sets when the radii for atomic species were available. The choice of test molecules for diprotic and triprotic acids are much more difficult than for monoprotic acids since reliable literature data are sparse for the polyprotic acids.[40] The test sets were chosen using the following considerations (Table 1). First, pK$_{a1}$ should be smaller than pK$_{a2}$, indicating that K$_{a1}$ > K$_{a2}$. Second, the difference of pK$_{a1}$ and pK$_{a2}$ should be at least 3 pK$_a$ units (4.1 kcal/mol) in order to maintain exclusive acid dissociation for each stepwise deprotonation. If the difference between the pK$_a$ values is less than two pK$_a$ units, the two dissociations are not independent of one another, and the base from the first acid dissociation may react with the proton of second acid dissociation. Third, the size of test molecule should not be too large to carry out *ab initio* computations with the aug-cc-pVTZ basis set. Fourth, species having tautomers were not chosen for the test set.

Selected acids show a broad range of acidity and include several organic/inorganic species (**A** to **M** in Table 1). For comparison, I select four more polyprotic acids, fumaric, succinic, H$_2$Fe(CO)$_4$, and 2,4,6-trihydroxypyridine (**N** to **Q** in Table 1). The first two acids (**N** and **O**) have a 2 kcal/mol or greater interval between ΔG_{aq}^1 and ΔG_{aq}^2. The third and fourth acids (**P** and **Q**) have low-lying d-orbitals, while the last acid (**Q**) has various structures for each acid dissociation step (Scheme 2). I expect a comparison between the two test sets (**A** to **M** and **N** to **Q**) can reveal the predictive power of each cavity set.

Table 1.   List of diprotic and triprotic acids with corresponding experimental ΔG_{aq}^1, ΔG_{aq}^2, and ΔG_{aq}^3 values (kcal/mol at 298.15 K) in present study[a]

Polyprotic acids	Chemical structure	ΔG_{aq}^1	ΔG_{aq}^2	ΔG_{aq}^3
Sulfuric H_2SO_4 (**A**)		-13.6^b	2.7	
Oxalic $H_2C_2O_4$ (**B**)		1.8^c	5.8	
Sulfurous H_2SO_3 (**C**)		2.4	9.8^d	
Maleic $H_2C_4H_2O_4$ (**D**)		2.6	9.0	
Thioglycolic $H_2C_2H_2O_2S$ (**E**)		2.7	14.1	
Phosphorous H_3PO_3 (**F**)		2.7	9.0	
Phosphoric H_3PO_4 (**G**)		2.9	9.8	16.8
Arsenic H_3AsO_4 (**H**)		3.0	9.5	17.7
Methylimino diacetic $H_2C_5H_7NO_4$ (**I**)		3.8	13.9	
Malonic $H_2C_3H_2O_4$ (**J**)		3.9	7.8	
Imino diacetic $H_2C_4H_5NO_4$ (**K**)		4.1	13.5	
Carbonic H_2CO_3 (**L**)		5.3^e	14.1^e	
Vanadic H_3VO_4 (**M**)		5.5^f	11.7^g	19.5^g
Fumaric $H_2C_4H_2O_4$ (**N**)		4.1	6.2	
Succinic $H_2C_4H_4O_4$ (**O**)		5.7	7.5	
Iron(II) tetracarbonyl hydride $H_2Fe(CO)_4$ (**P**)		6.0	19.1	
2,4,6-trihydroxy pyridine $H_3C_5H_2N_1O_3$ (**Q**)		6.3	12.3	17.7

[a]Experimental value based on pK_{a1}, pK_{a2}, and pK_{a3} values in Ref. 32. [b]Ref. 43b. [c]Ref. 65. [d]Ref. 66. [e]Ref. 54 and Ref. 67. [f]Ref. 68. [g]Ref. 57.

To determine the lowest free energy ($G_{aq} = G_{gas} + \Delta G_{solv}$) in flexible conformers, I performed geometry optimization in the gas phase followed by CPCM solvation calculations using B3LYP/6-31G(d,p) combined with the UFF cavity set.
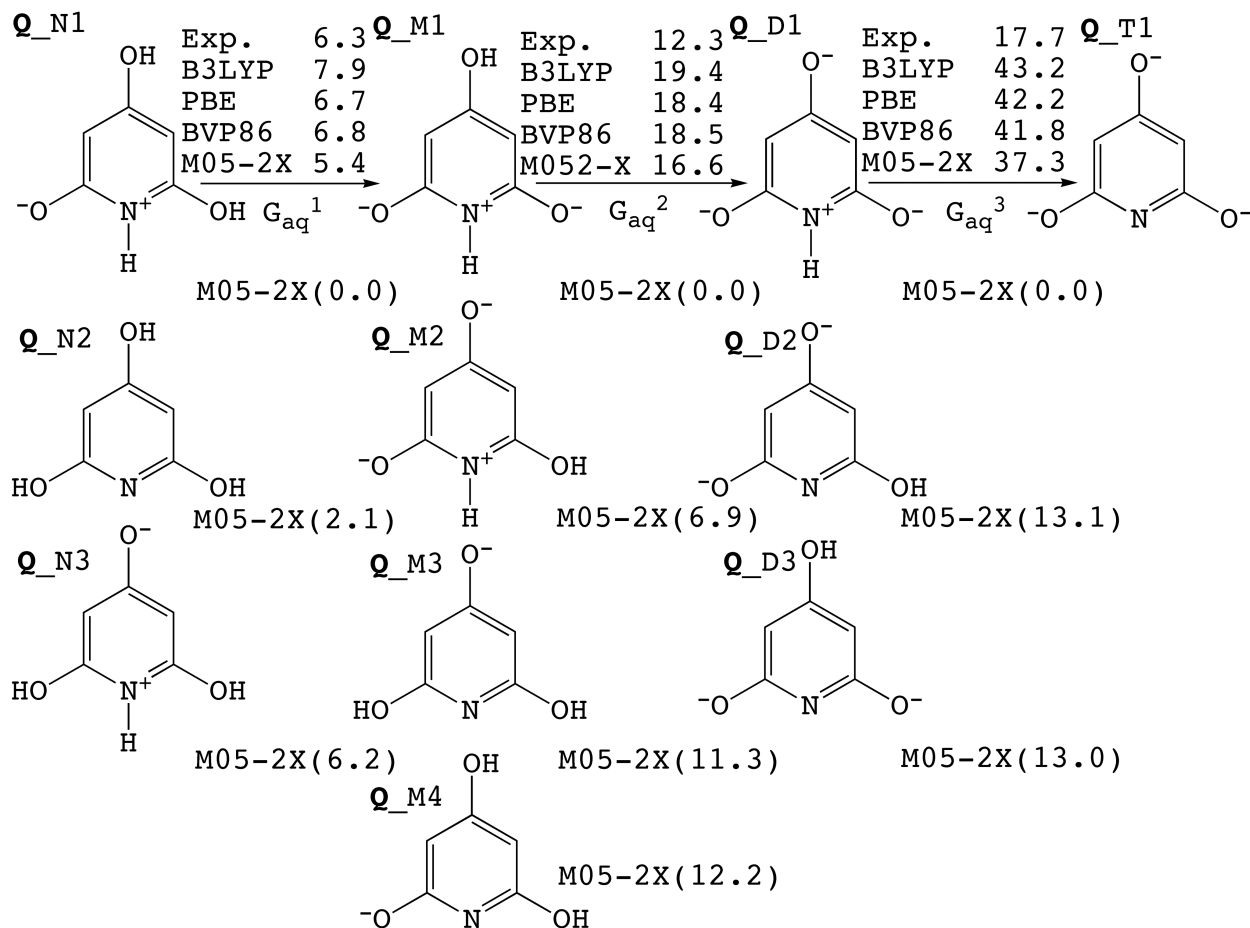
Scheme 2. First, second, and third free energies of dissociation (ΔG_{aq}^1, ΔG_{aq}^2, and ΔG_{aq}^3) in

kcal/mol at 298.15 K for 2,4,6-trihydroxypyridine (**Q**). All results in here were

obtained with the Pauling cavity set. Values in parentheses are stabilities in kcal/mol

relative to the most stable conformer.

In some cases, the conformer with lowest value of G_{aq} was not the conformer with lowest G_{gas}. I decided not to include an entropy correction for a Boltzmann average of multiple conformers because the Pulay group found the correction was small (0.12 of a pK_a unit).[41] However, the difference between the two conformers with lowest values of G_{aq} was at least 2 kcal/mol in our test sets. For UFF, UAKS, Pauling, and Klamt cavity sets, the solvation free energy (ΔG_{solv}) comes from the energy difference between the gaseous and aqueous state (SCFVAC keyword in Gaussian03). For SMD, the solvation free energy results from the energy difference between the gaseous and aqueous state since the non-electrostatic energy is already included in the total solution energy. For triprotic acids, the cc-pVTZ basis set (rather than the aug-cc-pVTZ) was used for $\Delta G_{aq}^3/pK_{a3}$ calculations because I observed unreasonable orbital populations for the trianion when diffuse functions were included. In order to make consistent comparisons, the dianion (HA^{2-}) was calculated with the aug-cc-pVTZ basis set for the step H_2A^- $\rightarrow H^+ + HA^{2-}$ and calculated again with the cc-pVTZ basis set for the step $HA^{2-} \rightarrow H^+ + A^{3-}$. For H_3VO_4, the Dunning basis set for the vanadium atom came from the basis set exchange project.[42] With a standard thermodynamic relation ($\Delta G_{aq} = \Delta G^o$ and $K = K_a$ convention in this study)

$$\Delta G_{aq} = -RT\ln K_a \tag{1}$$

gives

$$pK_a = \Delta G_{aq}/2.303RT \tag{2}$$

At ambient conditions in kcal/mol, the pK_a can be represented by the following simple relationship:

$$pK_a = \Delta G_{aq}/1.364 \qquad (3)$$

All values discussed below are free energies in kcal/mol unless noted, where pK_a is obtained from eqn (3). The free energy of acid dissociation (ΔG_{aq}), which can be converted directly into pK_a, is the sum of the free energy of dissociation in the gas phase (ΔG_{gas}) and the change of free energy of solvation ($\Delta\Delta G_{solv}$) (eqn (4)).

$$\Delta G_{aq} = \Delta G_{gas} + \Delta\Delta G_{solv} \qquad (4)$$

Since the free energy of gas-phase dissociation ($HA(g) \rightarrow H^+(g) + A^-(g)$) by the same DFT functional is identical with every cavity model set (geometries were not reoptimized in solution), the difference of the free energy of acid dissocation (ΔG_{aq}) results only from the change of free energy of solvation ($\Delta\Delta G_{solv}$) for each cavity set. All differences in our free energies of solution (ΔG_{aq}) originate from the differences between the free energy of solvation (ΔG_{solv}) for the anion and the neutral acid ($\Delta G_{solv}(A^-) - \Delta G_{solv}(HA)$) because I use the literature value for $\Delta G_{solv}(H^+)$ = -264.0 kcal/mol in eqn (5).

$$\Delta\Delta G_{solv} = \Delta G_{solv}(H^+) + \Delta G_{solv}(A^-) - \Delta G_{solv}(HA) \qquad (5)$$

3.3 Results

The results of a systematic survey of polyprotic acids (**A** to **M**) with various combinations for CPCM and SMD solvation modeling are shown in Tables 2 and 3.

Table 2. First Free Energies of Dissociation (ΔG_{aq}^{1}) in kcal/mol at 298.15 K for Some Polyprotic Acids

		A	B	C	D	E	F	G	H	I	J	K	L	M
Cavity	Exp.[a]	-13.6	1.8	2.4	2.6	2.7	2.7	2.9	3.0	3.8	3.9	4.1	5.3	5.5
UFF	B3LYP	-14.0	2.1	-0.4	-0.9	9.1	4.0	2.7	6.1	2.4	1.0	3.7	5.3	3.6
	PBE	-14.6	0.5	-1.5	-3.5	6.2	2.4	1.3	4.6	-1.9	-2.8	-2.4	4.5	3.6
	BVP86	-14.2	1.1	-1.2	-4.4	6.4	2.7	1.6	5.1	-1.8	-2.5	-2.0	4.7	4.2
	M05-2X	-17.1	0.0	-1.9	-5.5	7.8	2.7	1.0	5.1	-0.7	-2.3	0.2	3.4	2.2
UAKS	B3LYP	-11.5	2.7	2.6	1.8	10.0	5.6	5.7	8.1	4.7	3.7	6.5	6.9	5.1
	PBE	-12.3	2.1	1.2	-0.4	8.5	4.4	4.6	7.0	2.5	0.8	2.7	6.6	4.9
	BVP86	-11.9	2.5	1.6	-0.2	8.7	4.7	4.9	7.7	2.7	1.1	3.4	6.7	5.4
	M05-2X	-14.3	0.9	1.5	-2.0	8.9	4.6	4.3	6.9	2.0	1.2	3.6	5.1	3.5
Pauling	B3LYP	-12.8	4.8	-0.3	2.2	9.9	4.2	3.1	6.3	4.5	3.2	5.7	5.1	6.1
	PBE	-13.3	3.5	-0.9	-0.1	7.4	3.1	2.2	5.5	2.5	-0.1	2.6	5.2	6.0
	BVP86	-13.1	3.9	-0.8	0.0	7.5	3.2	2.4	5.8	2.6	0.0	2.8	5.3	6.3
	M05-2X	-16.2	2.7	-2.6	-2.1	7.7	2.5	0.6	4.3	1.9	0.5	1.8	2.9	3.9
Klamt	B3LYP	-12.8	2.4	0.5	-0.1	10.6	4.7	3.8	7.2	3.4	1.7	5.2	6.4	4.1
	PBE	-13.4	1.3	-0.7	-2.6	8.1	3.7	2.8	5.7	-1.3	-1.8	0.6	5.2	3.4
	BVP86	-13.1	2.0	-0.4	-2.4	8.4	3.9	3.2	6.3	-1.1	-1.5	-1.2	5.4	4.8
	M05-2X	-15.9	0.7	-1.2	-4.1	8.9	3.9	2.5	6.2	-0.4	-1.4	0.8	4.4	2.5
SMD	B3LYP	-13.6	2.1	-0.7	0.6	9.5	4.2	3.7		4.1	2.4	3.7	5.2	
	PBE	-14.3	1.0	-1.5	-1.6	7.6	2.9	2.6		1.8	-0.8	0.4	4.8	
	BVP86	-14.0	1.6	-0.2	-1.5	7.7	3.1	2.7		1.8	-0.6	0.6	4.8	
	M05-2X	-16.8	0.3	-2.2	-3.6	9.2	2.9	1.9		1.0	-0.7	0.1	2.8	

[a]Experimental value based on pK_{a1}.

The first acidity dissociation constant of H_2SO_4 is not well-known (pK_a varies from -2 to -10)[43] while the second acidity dissociation constant is well established in the literature.

Table 3. Second Free Energies of Dissociation (ΔG_{aq}^2) in kcal/mol at 298.15 K for Some polyprotic Acids

Cavity		A	B	C[b]	D	E	F	G[b]	H[b]	I	J	K	L	M
Cavity	Exp.[a]	2.7	5.8	9.8	9.0	14.1	9.0	9.8	9.5	13.9	7.8	13.5	14.1	11.7
UFF	B3LYP	12.9	12.1	24.4	26.1	22.1	22.2	21.8	22.4	22.9	24.0	18.6	31.8	27.8
	PBE	14.3	12.3	24.2	27.1	22.3	21.0	21.1	21.1	24.3	27.2	21.4	31.4	26.0
	BVP86	14.2	12.4	24.3	27.4	22.2	21.0	21.1	21.4	24.6	27.3	21.5	31.4	25.7
	M05-2X	9.4	9.3	22.0	26.3	19.2	20.6	19.6	20.0	22.3	23.2	16.8	29.6	25.7
UAKS	B3LYP	11.9	10.5	28.1	19.3	19.3	23.2	24.1	22.9	18.6	17.8	15.0	27.8	25.8
	PBE	13.6	10.8	27.7	20.9	20.0	22.2	23.2	22.0	20.1	21.4	18.6	27.4	24.5
	BVP86	13.4	10.8	27.9	21.1	19.9	22.1	23.2	22.0	20.3	21.2	18.1	27.2	24.3
	M05-2X	8.0	7.5	25.8	18.5	16.0	21.5	21.8	20.7	17.1	16.3	13.4	24.9	23.4
Pauling	B3LYP	5.9	8.5	17.4	21.2	20.2	15.9	15.5	16.7	17.5	18.8	14.0	22.8	22.6
	PBE	8.1	8.5	17.4	22.2	21.0	15.3	15.0	16.0	18.7	21.6	16.8	22.6	21.5
	BVP86	7.8	8.4	17.5	22.4	20.9	15.1	14.9	16.0	18.6	21.5	16.9	22.4	21.2
	M05-2X	1.9	4.8	13.9	19.7	16.6	13.5	12.3	13.6	14.2	16.2	11.7	19.3	19.8
Klamt	B3LYP	12.6	12.2	24.0	25.4	24.2	22.3	22.3	22.5	23.2	23.9	18.2	31.6	27.4
	PBE	13.9	12.4	23.9	26.5	25.0	21.1	21.4	21.2	24.4	26.9	20.1	31.3	25.9
	BVP86	13.9	12.3	24.0	26.8	24.9	21.1	21.2	21.3	24.7	26.9	20.9	31.2	25.1
	M05-2X	9.1	9.4	21.6	25.0	21.5	20.7	19.8	20.1	22.3	22.9	17.5	29.4	25.6
SMD	B3LYP	10.9	9.0	23.4	19.9	26.7	18.2	18.0		18.1	18.1	14.7	25.3	
	PBE	12.7	9.1	23.4	21.1	27.1	17.4	17.2		19.6	21.1	17.6	24.9	
	BVP86	12.5	9.0	22.5	21.3	27.1	17.3	17.2		19.7	21.0	17.6	24.7	
	M05-2X	7.2	5.6	20.6	18.6	23.6	16.2	15.1		16.2	16.4	13.2	22.4	

[a]Experimental value based on pK_{a2}. [b]The ΔG_{aq}^2 values at the CBS-QB3/CPCM level[59] for H_2SO_3 (**C**), H_3PO_4 (**G**), and H_3AsO_4 (**H**) are 26.5, 27.2, and 24.1 kcal/mol, respectively.

The Dixon group reported the free energy of dissociation (ΔG_{aq}) for pK_{a1} of H_2SO_4 (**A**) using the CCSD(T)/CBS limit[44] as fluctuating between -4.67 and -11.65 kcal/mol (pK_{a1} = -3.4 to -8.5)

where the free energy of dissociation (ΔG_{aq}) depended greatly on the cavity contour level for the anion HSO_4^-. They suggested the best value of pK_{a1} to be between -6 and -8 and favored the low end of this range (i.e. the first acid dissociation free energy, $\Delta G_{aq}^1 = -10.9$ kcal/mol; $pK_{a1} = -8$). Our ΔG_{aq}^1 values for H_2SO_4 with the DFT/UAKS cavity set (except for the M05-2X functional) agree with that of the Dixon group within 1.4 kcal/mol (Table 2). I believe that the difference arises mainly from the free energy of the proton in solution since they used $\Delta G_{solv}(H^+) = -262.4$ kcal/mol at 1 M while I used -264.0 kcal/mol. For the second acid dissociation free energy (ΔG_{aq}^2) of H_2SO_4, the Pauling cavity set with the M05-2X functional gave a value in good agreement with experiment while the Pauling cavity set with B3LYP, PBE, and BVP86 functionals yielded a larger discrepancy ($\Delta G_{aq}^2 = 7.3$ kcal/mol (average of three DFT methods) versus 2.7 kcal/mol, see Table 3).

Oxalic acid (**B**) and malonic acid (**J**) have relatively small gaps between $\Delta G_{aq}^1/pK_{a1}$ and $\Delta G_{aq}^2/pK_{a2}$ values. An assessment of the pK_a gap is useful to determine the robustness of the cavity model for polyprotic acids. Acceptable values of the first acid dissociation ($\Delta G_{aq}^1/pK_{a1}$) of oxalic acid (**B**) were obtained with the UAKS, Pauling, and Klamt cavity sets while a reasonable value of the second acid dissociation ($\Delta G_{aq}^2/pK_{a2}$) resulted using the M05-2X/Pauling or M05-2X/SMD method. The first acid dissociation ($\Delta G_{aq}^1/pK_{a1}$) of malonic acid (**J**) is acceptable with the B3LYP functional while the second acid dissociation ($\Delta G_{aq}^2/pK_{a2}$) is too large with every combination of DFT and cavity set. Using the B3LYP/UAKS and M05-2X/Pauling methods for ΔG_{aq}^1 and ΔG_{aq}^2, respectively, the calculated gaps in oxalic acid (**B**) and malonic acid (**J**) are 2.1 and 12.5 kcal/mol, respectively compared to experimental values of 4.0 and 3.9 kcal/mol (Tables 2 and 3).

For H_2SO_3 (**C**) the calculation of pK_a is not straightforward because the existence of molecular H_2SO_3 in aqueous solution is still under debate ($H_2SO_3 \rightarrow H_2O + SO_2$).[45] Since our free energy cycle uses gaseous geometries, I report ΔG_{aq} based on a H_2SO_3 (**C**) geometry without considering the step $SO_2 + H_2O$. In addition, the ΔG_{aq} value based on a free-energy cycle of $SO_2 + H_2O \rightarrow H^+ + SO_3^-$ deviates more from experiment than a cycle based on H_2SO_3 (**C**) (data not presented). Additionally, the solution behavior of H_2SO_3 (**C**) is quite complicated where a dimer can form followed by decomposition pathways.[46] However, a comparison between calculated and experimental ΔG_{aq}^1 of H_2SO_3 (**C**) using DFT/UAKS method (ΔG_{aq}^1 = 1.7 versus 2.4 kcal/mol, Table 2) and the second free energy of dissociation ΔG_{aq}^2 using M05-2X/Pauling method (ΔG_{aq}^2 = 13.9 versus 9.8 kcal/mol, Table 3) agrees well with experiment.

The prediction of ΔG_{aq}^1 for maleic acid (**D**) is within 2.5 kcal/mol of experiment using the B3LYP/UAKS, B3LYP/Pauling, or B3LYP/SMD methods while none of the methods predict ΔG_{aq}^2 to within 5 kcal/mol of experiment (Tables 2 and 3). Fumaric acid (**N**, Table 4) is an isomer of maleic acid (**D**) and has a relatively narrow gap between pK_{a1} and pK_{a2}. Maleic acid (**D**) has strong intramolecular hydrogen bonding in the neutral and monoanion form while fumaric acid (**N**) does not. Thus, I compare the results of maleic acid (**D**) and fumaric acid (**N**) to investigate the effect of the intramolecular hydrogen bond with acid dissociation free energy (ΔG_{aq}^1 and ΔG_{aq}^2). Succinic acid (**O**) is also compared to see the effect of conjugation on acid dissociation free energies (ΔG_{aq}^1 and ΔG_{aq}^2). Table 4 shows the ΔG_{aq}^1 of fumaric acid (**N**) is in reasonable agreement with experiment using any DFT/solvation method except the B3LYP functional while the calculated ΔG_{aq}^2 of fumaric acid (**N**) gives a good result with the M052-X functional (M05-2X/Pauling or M05-2X/SMD). The ΔG_{aq}^1 value for succinic acid (**O**) is best with the B3LYP functional while every method fails to give a reasonable value for ΔG_{aq}^2 (Table

76

3 and 4). I interpret these deviations to be due to intramolecular hydrogen bonding of the succinic acid (**O**) monoanion. Thioglycolic acid (**E**) has one carboxylic group and one thiol group. None of methods gives a reasonable value for $\Delta G_{aq}{}^1$ of thioglycolic acid (**E**) while the M05-2X/UAKS or M05-2X/Pauling cavity set gives acceptable values for $\Delta G_{aq}{}^2$ (16.0 or 16.6 kcal/mol, Table 3).

Table 4. First and Second Free Energies of Dissociation ($\Delta G_{aq}{}^1$, $\Delta G_{aq}{}^2$) in kcal/mol at 298.15 K for Fumaric acid (**N**), Succinic acid (**O**), Iron(II) tetracarbonyl hydride (**P**), and 2,4,6-trihydroxypyridine (**Q**)

		N		O		P		Q	
		$\Delta G_{aq}{}^1$	$\Delta G_{aq}{}^2$	$\Delta G_{aq}{}^1$	$\Delta G_{aq}{}^2$	$\Delta G_{aq}{}^1$	$\Delta G_{aq}{}^2$	$\Delta G_{aq}{}^1$	$\Delta G_{aq}{}^2$
Cavity	Exp.[a]	4.1	6.2	5.7	7.5	6.0	19.1	6.3	12.3
UFF	B3LYP	8.0	11.9	2.3	23.0	4.6	27.8	6.2	23.4
	PBE	4.9	12.4	-0.6	24.9	-2.7	20.8	4.8	22.2
	BVP86	5.2	12.5	-0.3	25.0	-2.1	21.9	5.1	22.3
	M05-2X	5.2	9.7	-1.2	22.4	12.7	33.2	4.3	20.9
	M05					2.1	27.2		
UAKS	B3LYP	7.9	11.2	5.1	16.3	4.0	28.2	9.1	23.7
	PBE	6.4	11.9	2.8	18.9	-3.7	21.2	7.9	22.7
	BVP86	6.7	12.0	3.1	18.8	-3.1	22.0	8.2	22.9
	M05-2X	5.8	8.7	2.2	15.1	11.8	33.5	7.1	21.4
	M05					1.5	27.3		
Pauling	B3LYP	9.0	9.8	4.0	17.2	10.9	26.4	7.9	19.4
	PBE	7.0	9.9	1.5	19.2	2.3	19.1	6.7	18.4
	BVP86	7.1	9.9	-1.2	19.3	2.9	19.3	6.8	18.5
	M05-2X	5.4	7.2	-0.2	15.3	18.3	30.3	5.4	16.6
	M05					7.6	24.9		
Klamt	B3LYP	8.5	12.6	2.9	22.6	4.3	29.0	7.5	24.4
	PBE	4.9	13.0	0.6	24.3	-2.8	21.7	6.1	22.6
	BVP86	6.4	13.1	0.9	24.4	-2.3	23.7	6.4	23.5
	M05-2X	5.9	10.2	0.0	21.8	12.4	34.3	5.6	22.2
	M05					1.9	28.0		
SMD	B3LYP	7.5	9.9	4.1	17.2			7.6	21.0
	PBE	5.4	10.4	1.4	19.3			6.4	20.0
	BVP86	5.6	10.4	1.6	19.3			6.6	20.0
	M05-2X	4.6	7.2	0.8	15.7			5.4	18.3

[a]Experimental value based on pK_{a1} and pK_{a2}.

A prediction of ΔG_{aq}^1 for H_3PO_3 (**F**) and H_3PO_4 (**G**) is acceptable regardless of DFT functional and solvation model. However, the prediction of ΔG_{aq}^2 for these two acids clearly shows that the Pauling cavity is the only acceptable choice regardless of functional (best value is obtained with the M05-2X/Pauling method, see Tables 2 and 3). Alexeev et al.[44a] reported the ΔG_{aq}^1 of H_3PO_4 (**G**) as 3.46 kcal/mol, which can be compared with 4.9 kcal/mol by DFT/UAKS method and 2.1 kcal/mol by DFT/Pauling method (Table 2, averaged over four functionals). For ΔG_{aq}^2 of H_3PO_4 (**G**), the Pauling cavity set gives the only acceptable results (ΔG_{aq}^2=12.3 kcal/mol averaged over four functional) compared to experiment (ΔG_{aq}^2=9.8 kcal/mol). DFT/UFF and DFT/Pauling methods were in good agreement with experiment for ΔG_{aq}^1 of H_3AsO_4 (**H**), while only M05-2X/Pauling gave reasonable results for ΔG_{aq}^2 (Tables 2 and 3). Experimental and calculated free energies of solvation ΔG_{solv} for phosphoric acid and related anions can be compared. Previous two studies reported ΔG_{solv} of H_3PO_4 (**G**) to be between -8.1 kcal/mol (reported value[47] of -10 kcal/mol is corrected by 1.89 to account for a change of state) and -12.8 kcal/mol.[47,48a] In the present study, the Pauling cavity set gives the most negative ΔG_{solv} (-19.6 to -22.4 kcal/mol) while other cavity sets give values between -7.7 and -16.4 kcal/mol. The experimental free energy of solvation (ΔG_{solv}) for $H_2PO_4^-$ is -66.1 ± 8.0 kcal/mol (reported value of -68 kcal/mol is corrected by 1.89 to account for a change of state).[47] Previous calculated values of -82.9 and -84.6 kcal/mol have been reported for $\Delta G_{solv}(H_2PO_4^-)$ with PCM solvation modeling using B3LYP/6-31G(d) and B3LYP/6-311++G** methods, respectively (cavity set and standard state not specified).[48b] Smaller calculated values of -62.6 and -60.7 kcal/mol have been reported with the UAHF cavity set using MP2/6-31+G(d,p)//HF6-31+G(d,p) and G3B3//HF/6-31+G(d,p) level of theory, respectively (reported value corrected to account for

change of state).[48a] Our $\Delta G_{solv}(H_2PO_4^-)$ values based on the Pauling cavity set give free energies between -72.4 kcal/mol and -78.1 kcal/mol, which are somewhat more negative than those of other cavity sets (-61.4 to -70.8 kcal/mol including SMD).

For the dianion HPO_4^{2-} Flórián and Warshel[47] suggested a value of -245 ±15 kcal/mol for ΔG_{solv} based on the Langevin dipole model. They considered the value of -273.1 kcal/mol, based on the PCM/Pauling method, to be too negative. However, this value was computed with a smaller radius for phosphorus than the current default in the Pauling cavity set (1.80 versus 1.90Å). In the current study, two sets of values are available for $\Delta G_{solv}(HPO_4^{2-})$. Those calculated with the cc-pVTZ basis set are about 6 to 15 kcal/mol more negative than with the aug-cc-pVTZ basis set for the same DFT/cavity set. For the cc-pVTZ basis, the Pauling cavity set gives values of $\Delta G_{solv}(HPO_4^{2-})$ between -255.3 and -260.7 kcal/mol, somewhat more negative than with other cavity sets (-230.6 to -249.0 kcal/mol).

I expand our assessment of cavity models to the triprotic acids H_3PO_4 (**G**), H_3AsO_4 (**H**), and H_3VO_4 (**M**) in Table 5, which summarizes free energies of dissociation (ΔG_{aq}^3). In general, all DFT/cavity combinations underestimate the acidity for ΔG_{aq}^3 of H_3PO_4 (**G**). Marcus[49] reported an experimental $\Delta G_{solv}(PO_4^{3-})$ value of -664.7 kcal/mol, which is much more negative than the calculated values based on PCM solvation modeling. It should be pointed out that his value for $\Delta G_{solv}(H_2PO_4^-)$ is also much more negative than the experimental result (-115.0 versus -66.1 ± 8[47] kcal mol_1). Flórián and Warshel[47] reported -592.1 kcal/mol for $\Delta G_{solv}(PO_4^{3-})$ based on the PCM/Pauling method with a 1.8 Å vdW radius for phosphorus. They suggested a value of -534.1 ± 20 kcal/mol for $\Delta G_{solv}(PO_4^{3-})$ based on their Langevin dipole method. In this study, the $\Delta G_{solv}(PO_4^{3-})$ values from the Pauling cavity set and cc-pVTZ basis set are between -565.6 to -569.6 kcal/mol while other cavity sets give values between -526.3 and -551.0 kcal/mol.

A technical difficulty arose in the treatment of trianions like PO_4^{3-} since the third excess electron is not binding ($PO_4^{2-} + e^- \rightarrow PO_4^{3-}$).[50] Thus, the environment confers stability to PO_4^{3-} in water.[48,51,52] Computationally, the instability of PO_4^{3-} in the gas phase is manifested by unreasonable orbital populations of diffuse functions.

Table 5. Third Free Energies of Dissociation (ΔG_{aq}^3) in kcal/mol at 298.15 K for Some

Polyprotic Acids

Cavity		G^b	H^b	M	Q
	Exp.[a]	16.8	17.7	19.5	17.7
UFF	B3LYP	50.6	48.9	49.4	54.7
	PBE	50.7	49.0	47.2	54.2
	BVP86	49.9	48.3	46.9	53.2
	M05-2X	45.3	43.4	46.6	48.5
UAKS	B3LYP	45.5	44.5	38.2	48.2
	PBE	45.7	45.4	36.7	47.4
	BVP86	44.9	44.5	36.2	46.8
	M05-2X	40.1	38.8	39.9	45.4
Pauling	B3LYP	32.4	32.7	35.8	43.2
	PBE	32.5	33.0	34.3	42.2
	BVP86	31.8	32.3	33.6	41.8
	M05-2X	27.2	27.1	37.4	37.3
Klamt	B3LYP	50.1	49.1	48.3	55.7
	PBE	50.2	49.2	46.0	54.6
	BVP86	49.4	48.5	45.7	53.2
	M05-2X	44.6	43.6	45.4	48.6
SMD	B3LYP	39.4			47.4
	PBE	39.6			46.5
	BVP86	38.8			45.9
	M05-2X	34.1			41.3

[a]Experimental value based on pK_a. [b]The ΔG_{aq}^3 values at the CBS-QB3/CPCM level[59] for H_3PO_4(**G**) and H_3AsO_4 (**H**) are 40.7 and 39.1 kcal/mol, respectively.

On the other hand, diffuse functions are regarded as a prerequisite to describe negatively charge systems such as PO_4^{3-}.[46] With the augmented Dunning basis set (aug-cc-pVTZ), PO_4^{3-} has 0.72 e^- in diffuse phosphorus p functions and a total of 1.26 e^- in diffuse oxygen p functions. To circumvent this problem, I computed trianions without diffuse functions by using the cc-pVTZ basis set. In Table 3 the first and second free energy of dissociation (ΔG_{aq}^1 and ΔG_{aq}^2) use the aug-cc-pVTZ basis set while the third free energy of dissociation (ΔG_{aq}^3) uses the cc-pVTZ basis set. None of the cavity sets are successful in reproducing ΔG_{aq}^3 of H_3PO_4 (**G**). Smiechowski[48a] reproduced successfully ΔG_{aq}^2 and ΔG_{aq}^3 of H_3PO_4 (**G**) using the cluster-continuum approximation (several explicit water molecules were bound to the solute). However, the same method failed to reproduce ΔG_{aq}^1 of H_3PO_4 (**G**) quantitatively. Tang et al.[52] also report the $\Delta G_{aq}/pK_a$ value for H_3PO_4 (**G**) using a cluster-continuum model with the PBE/COSMO method. Five explicit water molecules provide the best model for evaluating $\Delta G_{aq}^2/pK_{a2}$ and $\Delta G_{aq}^3/pK_{a3}$ of H_3PO_4 (**G**) while two explicit water molecules were optimal for evaluation of $\Delta G_{aq}^1/pK_{a1}$.

     I assessed the effect of augmentation in the Dunning basis set for H_3PO_4 (**G**) (see Table 6) by comparing gaseous state optimization using the cc-pVTZ basis set with solution-state optimization using the aug-cc-pVTZ basis set. In the CPCM optimization of HPO_4^{2-} and PO_4^{3-} with the aug-cc-pVTZ basis set, the occupation of diffusion functions was within reasonable limits. For the gas-phase energy (needed to compute ΔG_{gas} in Scheme 1), the unperturbed energy was taken from the CPCM calculation. Vibrational frequencies obtained from the CPCM/DFT/aug-cc-pVTZ method were used to compute the thermal corrections and TDS contribution to obtain ΔG_{gas} in Scheme 1. The geometry change between gas-phase cc-pVTZ and solution-phase aug-cc-pVTZ optimizations was less than 0.02 Å in P–O distances. The ΔG_{gas} values for the step $HPO_4^{2-} \rightarrow H^+ + PO_4^{3-}$ from the aug-cc-pVTZ solution optimization

were significantly more negative as compared to the cc-pVTZ results (Table 6, up to 36.2

kcal/mol) which is to be expected since diffuse functions are more important for the trianion than

for the dianion. However, the difference was offset to some extent by the fact that free energies

of solvation favored the reaction more with the cc-pVTZ basis set as compared to the aug-cc-

pVTZ basis set. Overall, the ΔG_{aq} values for the third dissociation step were more negative by

about 10 kcal/mol when the aug-cc-pVTZ basis set was used with solution-state optimizations

relative to using cc-pVTZ with gas-phase optimizations.

Table 6. Free Energies of Dissociation (ΔG_{aq}^{3}) in kcal/mol at 298.15 K for $HPO_4^{2-} \rightarrow H^+ + PO_4^{3-}$

Cavity Model	DFT	cc-pVTZ (gas phase optimization)			aug-cc-pVTZ (solution phase optimization)		
		ΔG_{gas}	$\Delta\Delta G_{solv}$	ΔG_{aq}	ΔG_{gas}	$\Delta\Delta G_{solv}$	$\Delta G_{aq}{}^{a}$
UFF	B3LYP	606.2	-555.6	50.6	570.0	-531.1	38.8(11.8)
	PBE	607.1	-560.7	50.7	564.2	-527.2	36.8(13.9)
	BVP86	606.0	-573.8	49.9	564.5	-527.6	36.7(13.2)
	M05-2X	600.1	-556.1	45.3	573.7	-536.7	36.8(8.5)
UAKS	B3LYP	606.2	-573.8	45.5	570.0	-534.1	35.6(9.9)
	PBE	607.1	-556.1	45.7	564.2	-529.8	34.0(11.7)
	BVP86	606.0	-556.4	44.9	564.5	-530.3	33.8(11.1)
	M05-2X	600.1	-561.4	40.1	573.7	-539.8	33.5(6.6)
Pauling	B3LYP	606.2	-556.4	32.4	570.0	-541.8	28.1(4.3)
	PBE	607.1	-561.4	32.5	564.2	-537.2	26.8(5.7)
	BVP86	606.0	-574.6	31.8	564.5	-537.6	26.7(5.1)
	M05-2X	600.1	-556.9	27.2	573.7	-548.4	25.1(2.1)

[a] Difference between ΔG_{aq} by gas phase optimization and ΔG_{aq} by solution phase optimization.

H$_3$AsO$_4$ (**H**) shows the same trend in ΔG_{aq} as H$_3$PO$_4$ (see Tables 2, 3, and 5). The ΔG_{aq}

values with the Pauling cavity set are acceptable for the second dissociation step but are too

positive for the third dissociation step. Consistently, the M05-2X/Pauling method yields the best

agreement with experimental $\Delta G_{aq}/pK_a$ values of H_3AsO_4 (**H**) but is too positive for the third

step (ΔG_{aq}^3) by 9.4 kcal/mol. The corresponding errors for ΔG_{aq}^3 obtained from the other cavity

sets were much larger, up to 31.5 kcal/mol. The prediction of ΔG_{aq}^1 and ΔG_{aq}^2 for

methyliminodiacetic acid (**I**) and iminodiacetic acid (**K**) using the DFT/UAKS and M05-

2X/Pauling methods are in acceptable agreement with experiment. However, the ΔG_{aq}^1 for

malonic acid (**J**) from the B3LYP/UAKS method gives good agreement while other DFT/UAKS

combinations overestimate the acidity of malonic acid (**J**) (Tables 2 and 3). The DFT/Pauling

cavity set also shows a similar trend of DFT dependency. ΔG_{aq}^2 for malonic acid (**J**) by any

method yields too positive (weak acidic) even though M05-2X/Pauling still gives the least

positive ΔG_{aq}^2 value (16.2 kcal/mol). The underestimation of acidity (too positive ΔG_{aq}^2) for

malonic acid (**J**) may be related to the small gap between ΔG_{aq}^1 and ΔG_{aq}^2 (3.9 kcal/mol).

An intramolecular hydrogen bond is found in the monoanions of maleic acid (**D**),

thioglycolic acid (**E**), malonic acid (**J**), methyliminodiacetic acid (**I**), and iminodiacetic acid (**K**).

The ΔG_{aq}^2 of larger monoanions with intramolecular hydrogen bonds (**I**, **K**) are well reproduced,

while the ΔG_{aq}^2 of smaller monoanions with intramolecular hydrogen bonds (**D**, **J**, and **O**) are

significantly underestimated. The M05-2X/Pauling and M05-2X/SMD methods reproduce the

experimental ΔG_{aq}^2 value for oxalic acid (**B**), the smallest dicarboxylic acid considered (Table 3)

and for fumaric acid (**N**, Table 4). Due to the effect of intramolecular hydrogen bonds, a narrow

pK_a interval, and the size of the anion, it is not easy to make any correlation or trend for the

prediction of ΔG_{aq}^2 for **B**, **D**, **E**, **I**, **J**, **K**, **N**, and **O**.

The existence of CO_2 in aqueous solution influences the experimental $\Delta G_{aq}^1/pK_{a1}$ of

H_2CO_3 (**L**) ($H_2CO_3 \rightarrow H_2O + CO_2$). Tossell[53] investigated ΔG_{aq} of $H_2CO_3 \rightarrow H^+ + HCO_3^-$ with

the influence of $CO_2 + H_2O \rightarrow H^+ + HCO_3^-$. I use $\Delta G_{aq}^1 = 5.3$ kcal/mol ($pK_{a1} = 3.9$) as an

experimental value where the effect of perturbation of CO_2 in water has been removed.[54] In our study, all DFT/cavity methods give reasonable free energies of dissociation (2.8 to 6.9 kcal/mol, Table 2). The Dixon group used $\Delta G_{aq}^1 = 8.7$ kcal/mol ($pK_{a1}=6.4$) as an experimental value.[44a] Their best prediction was 8.65 kcal/mol with an anion contour level of 0.0022 using the fully polarizable continuum model (FPCM) method. Very recently, Wang et al.[55] reported $\Delta G_{aq}^1 = 5.1$ kcal/mol ($pK_{a1}= 3.7$) through the consideration of hydration/dehydration rates and equilibrium constant of CO_2 in aqueous media. Gao et al.[56] performed over fourteen combinations of implicit solvation including the QM/MM approach for pK_a of bicarbonate (HCO_3^-). Their predicted ΔG_{aq} values vary from 11.5 to 37.5 kcal/mol depending upon methods. Tossell[53] reported $\Delta G_{aq}^1 = 9.8$ kcal/mol (14.8 kcal/mol after correcting for $\Delta G_{solv}(H^+)$ change of state) of H_2CO_3 based on the step $CO_2 \cdot H_2O \rightarrow H^+ + HCO_3^-$, which is still far from the experimental value. It is worth noting that the consideration of a special interaction between solute and water, while important, may actually lead to poorer agreement with experimental data when explicitly included.[35,53,56] For ΔG_{aq}^2, the M05-2X/Pauling method gives the smallest ΔG_{aq}^2 (19.3 kcal/mol) and M05-2X/SMD method yields 22.4 kcal/mol (Table 3).

The experimental ΔG_{aq} values for the three dissociation steps in H_3VO_4 (**M**) are in question,[57] due to the complex aqueous behavior of H_3VO_4 (**M**). For various pH regions, multiple anionic species are possible such as $H_2V_{10}O_{28}^{4-}$, $H_2VO_4^-$, $V_4O_{12}^{4-}$, $HV_{10}O_{28}^{5-}$, HVO_4^{2-}, and $V_2O_7^{4-}$.[43a,58] Thus, the formation of isopolyanions ($[M_xO_y]^{n-}$) enables diverse dissociated speices. Nevertheless, any DFT/cavity method gives good agreement with experimental data for ΔG_{aq}^1 while M05-2X/UFF and M05-2X/Klamt results deviate from the measured data by only 3.3 and 3.0 kcal/mol for ΔG_{aq}^1 (Table 2). For ΔG_{aq}^2, the difference between experiment and DFT/Pauling values becomes larger than 8 kcal/mol for all methods (Table 3). The deviation

from the experimental ΔG_{aq}^3 value for H_3PO_4 (**G**), H_3AsO_4 (**H**), and H_3VO_4 (**M**) with the M05-2X/Pauling method is about 15 kcal/mol too large (Table 5).

Zimmermann and Tossell[59] performed CPCM solvation modeling (radii = UAHF) combined with one explicit water molecule for pK_a predictions of H_2SO_3 (**C**), H_3PO_4 (**H**), and H_3AsO_4 (**G**). Using a linear fit equation (0.42907 × pKa - 0.23), they reproduced pK_{a1} and pK_{a2} of these polyprotic acids. However, the individual values for $\Delta G_{aq}^2/pK_{a2}$ and $\Delta G_{aq}^3/pK_{a3}$ were still far from the literature data (Tables 3 and 5). Incorporation of an explicit water molecule did not improve predictions of ΔG_{aq}^1, ΔG_{aq}^2, and ΔG_{aq}^3 since the ΔG_{aq} value by CPCM + explicit water molecules differed from the CPCM approach by less than 3 kcal/mol. The incorporation of explicit water molecules shifts ΔG_{aq}^2 of H_2SO_3 5.1 kcal/mol more acidic (31.6 → 26.5 kcal/mol) still far from the literature value of 9.8 kcal/mol. Their linear fit equation may need a more comprehensive test in order to make it general for polyprotic acids. For a series of oxoacids (H_3PO_4 (**H**), H_3AsO_4 (**G**), and H_3VO_4 (**M**)), the unsigned average error of ΔG_{aq}^3 from the M05-2X/Pauling method is only 4.4 kcal/mol if 15 kcal/mol is subtracted from our third dissociation step.

$H_2Fe(CO)_4$ (**P**) is the only test molecule with a partially filled set of d electrons on one atom. The neutral form has C_{2v} symmetry while the monoanion has C_{3v} symmetry and the dianion has T_d symmetry. While the effect of the different DFT functionals on ΔG_{aq} is much larger than that for a non d-electron system, B3LYP/UFF, B3LYP/UAKS and B3LYP/Klamt methods yielded reasonable predictions for ΔG_{aq}^1. However, only the PBE or BVP86 functional with any cavity provided a ± 5.0 kcal/mol accuracy for ΔG_{aq}^2. For both ΔG_{aq}^1 and ΔG_{aq}^2, the M05-2X functional greatly underestimated the acidity (ΔG_{aq} too large) with every cavity set (Table 4). In order to access the accuracy of the DFT results in the gas phase for $H_2Fe(CO)_4$, I

applied G4(MP2) theory, recently extended to transition metal containing systems by Mayhall et al.[60] At the G4(MP2) level $\Delta G_{gas}{}^1$ is 306.2 kcal/mol while $\Delta G_{gas}{}^1$ obtained from B3LYP, PBE, BVP86, and M05-2X functionals are 310.7, 303.5, 304.2, and 319.1 kcal/mol, respectively. Also, $\Delta G_{gas}{}^2$ evaluated from G4MP2 is 437.1 kcal/mol while the $\Delta G_{gas}{}^2$ values resulting from B3LYP, PBE, BVP86, and M05-2X functionals are 429.0, 421.9, 422.9, and 437.1 kcal/mol, respectively. Because Zhao and Truhlar[61] recommended the M05 functional for 3d transition metal systems rather than the M05-2X functional, I also applied the M05 functional with the four cavity sets (Table 4). The $\Delta G_{aq}{}^1$ value from the M05/Pauling method (7.6 kcal/mol) is close to the experimental value of 6.0 kcal/mol while the $\Delta G_{aq}{}^2$ value (24.9 kcal/mol) is larger than experiment by 5.8 kcal/mol (Table 4).

2,4,6-trihydroxypyridine (**Q**) is a triprotic acid and may exist in several zwitterionic forms in solution (Scheme 2). In order to determine the most stable solution form, I calculated the geometry with the DFT/aug-cc-pVTZ method and its solvation energy with UFF, UAKS, Pauling, and Klamt cavity sets. The most stable form of each neutral, monoanionic, and dianionic form is selected by the aqueous solution free energy with the Pauling cavity set ($G_{aq} = G_{gas} + \Delta G_{solv}$). In all cavity sets, **Q_N1**, **Q_M1**, **Q_D1**, and **Q_T1** are the most stable forms. The $\Delta G_{aq}{}^1$ value of 2,4,6-trihydroxypyridine (**Q**) is well reproduced by every approach except when B3LYP/UAKS is used while $\Delta G_{aq}{}^2$ is within 5 kcal/mol of the experimental value when the M05-2X/Pauling is employed (Table 4). With the B3LYP, PBE, and BVP86 functionals, $\Delta G_{aq}{}^3$ obtained from the Pauling cavity set of 2,4,6-trihydroxypyridine (**Q**) is too large by over 24 kcal/mol (Table 5), while $\Delta G_{aq}{}^3$ from the M05-2X/Pauling method is too large by almost 20 kcal/mol.

Fig. 1 shows a deviation of ΔG_{aq}^1 using the UAKS cavity set for polyprotic acids **A** through **M**. Regardless of acidity, every DFT/UAKS method yields nine reasonable predictions of ΔG_{aq}^1 (±2.5 kcal/mol) in thirteen acids test set which indicates that no DFT functional is clearly superior for the prediction of ΔG_{aq}^1.
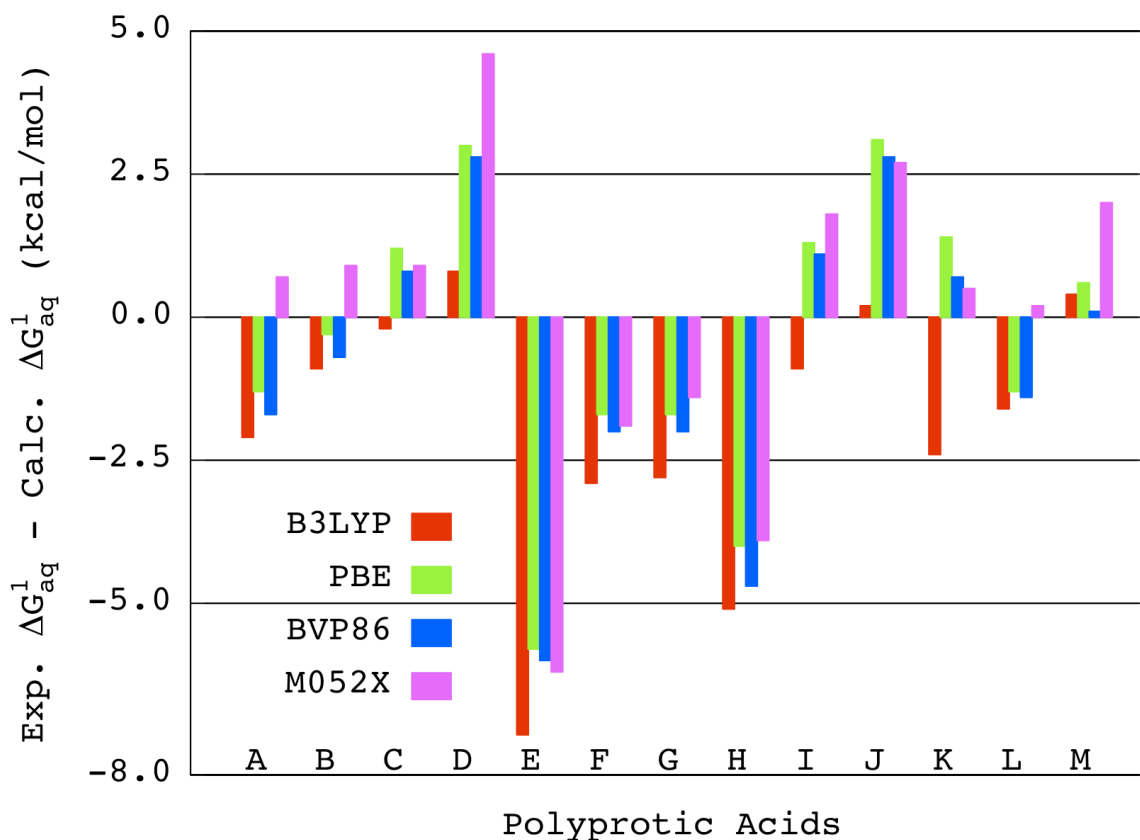
Figure 1. Performance of the UAKS cavity set for the first acid dissociation free energy prediction (ΔG_{aq}^1).

For the same acids, Fig. 2 shows the deviation of ΔG_{aq}^1 from the experimental data using the Pauling cavity set for polyprotic acids **A** through **M** (nine out of thirteen within ±2.5 kcal/mol). Takano and Houk[18] suggested the UAKS was the best choice for evaluation of ΔG_{aq}^1/pK_{a1}. However, our results indicate that the Pauling cavity set performs equally well at

predicting $\Delta G_{aq}^1/pK_{a1}$ for our test set since every DFT/Pauling method yields nine reasonable predictions of ΔG_{aq}^1 (within ±2.5 kcal/mol). The Merz group attempted to determine a reliable solvation free energy of 60 ionic species using a Poisson–Boltzmann and IEFPCM model combined by five explicit water molecules.[62] An unsigned average error in their test set of anion species was 2.1 kcal/mol.
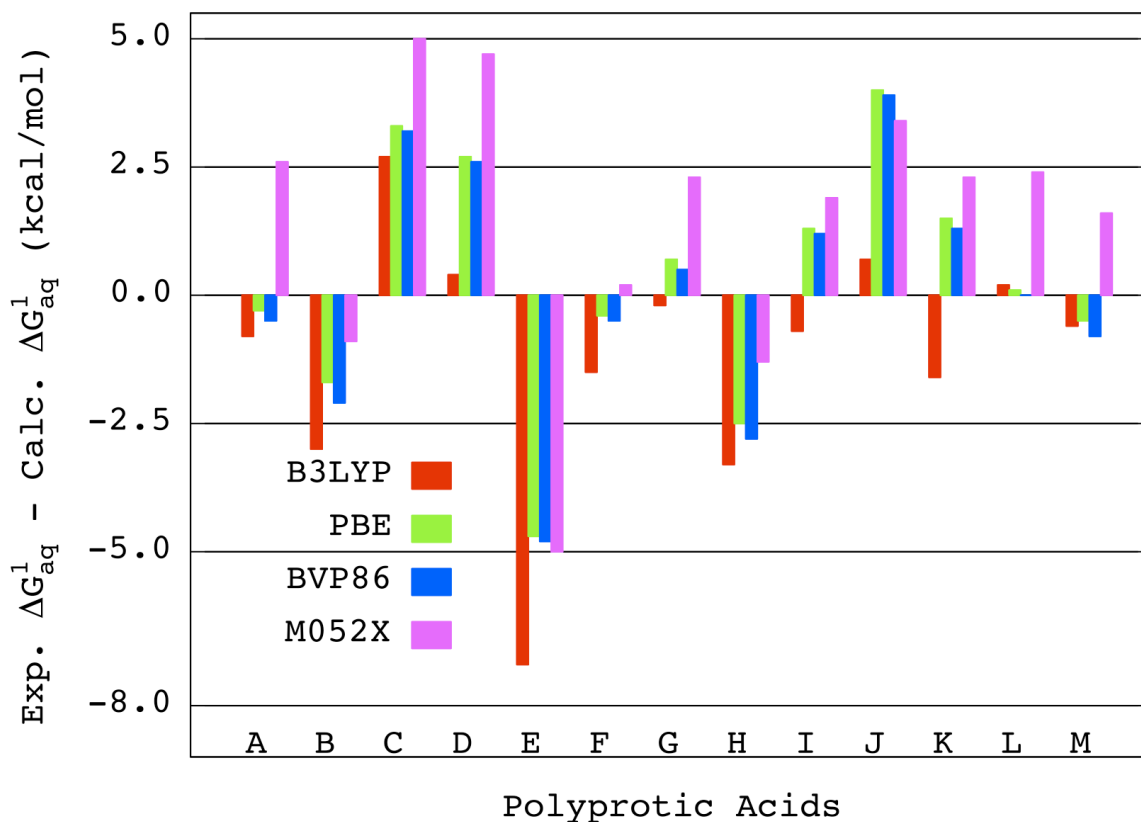
Figure 2. Performance of the Pauling cavity set for the first acid dissociation free energy prediction (ΔG_{aq}^1).

I expect a solute coordinated by several water molecules in implicit solvation model would improve the accuracy of $\Delta G_{aq}^1/pK_{a1}$ prediction for specific acids and indeed the accuracy is somewhat better than the results for our test set. However, I feel that the DFT/UAKS and

DFT/Pauling approaches can be useful tools for $\Delta G_{aq}^{1}/pK_{a1}$. Recently, Zhang et al.[63] established a standard linear regression fit for pK_{a1} (i.e. $pK_a(f) = \alpha_f \Delta H + \beta_f$). The role of DFT functionals in their study was only modest while solution optimization, choice of basis set, and fitting parameters were more important. They found the pure DFT functional (OLYP) to be more efficient than a hybrid functional for continuum solvation modeling, and B3LYP was not the best choice for the prediction of pK_a in small organic acids, which agrees with our observation.

For $\Delta G_{aq}^{2}/pK_{a2}$, the DFT/UAKS approach always underestimated the acidity of our test set (Fig. 3). Except for **B**, **E**, **I**, and **K**, the calculated ΔG_{aq}^{2} values deviate by more than 5.0 kcal/mol from experiment.
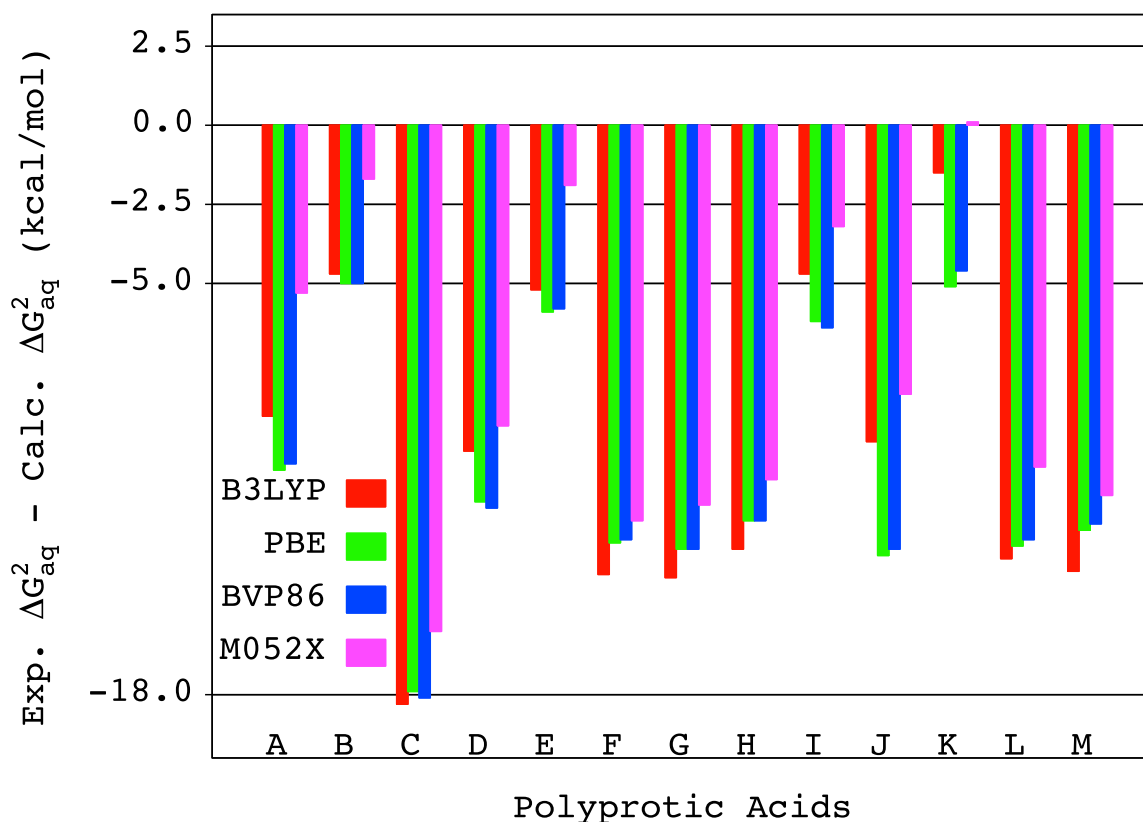
Figure 3. Performance of the UAKS cavity set for the second acid dissociation free energy prediction (ΔG_{aq}^{2}).

The M05-2X/UAKS method predicted only four acids within ±5.0 kcal/mol of experiment. However, the M05-2X/Pauling approach yields nine reasonable predictions of ΔG_{aq}^2/pK_{a2} with reliable accuracy (±5.0 kcal/mol of experiment). The other three DFT functionals yields only three or four reasonable predictions with ±5.0 kcal/mol of accuracy (Fig. 4). Since the solvation free energies of dianions are much larger than those of monoanions, the uncertainty in the calculated solvation free energy of dianions is expected to dominate the uncertainty of the calculated ΔG_{aq}^2 values. For **D**, **J**, **L**, and **M**, specific solute–water interactions may be important in the dianion, which is beyond the implicit solvation model used here.
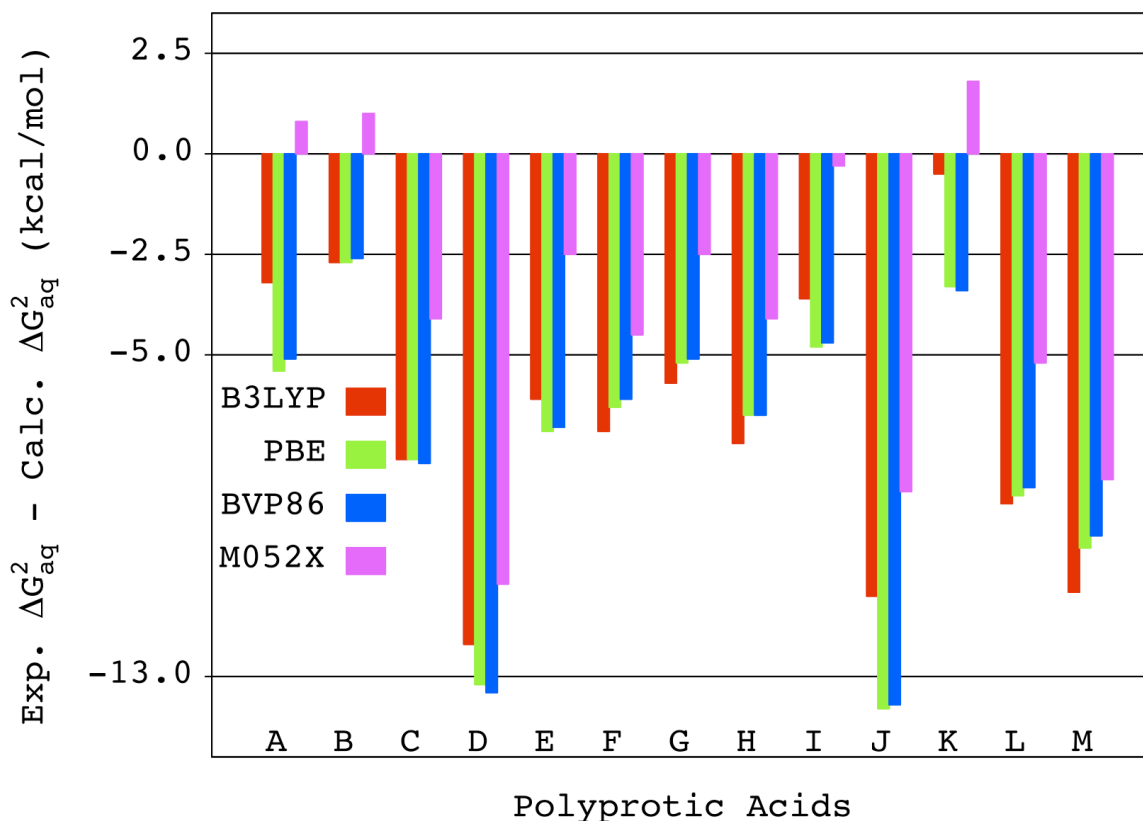
Figure 4. Performance of the Pauling cavity set for the second acid dissociation free energy prediction (ΔG_{aq}^2).

For multi-acid dissociation processes, the choice of cavity model with the CPCM method becomes critical for a reasonable prediction of solution free energies. The default cavity radii of each atom in the cavity set are tabulated in Appendix 1. However, the molecular environment modifies the actual radii of the UAKS model. Verdolino et al.[64] modified the scale factor in the UFF cavity sets for the prediction of pK_{a1} and pK_{a2}.
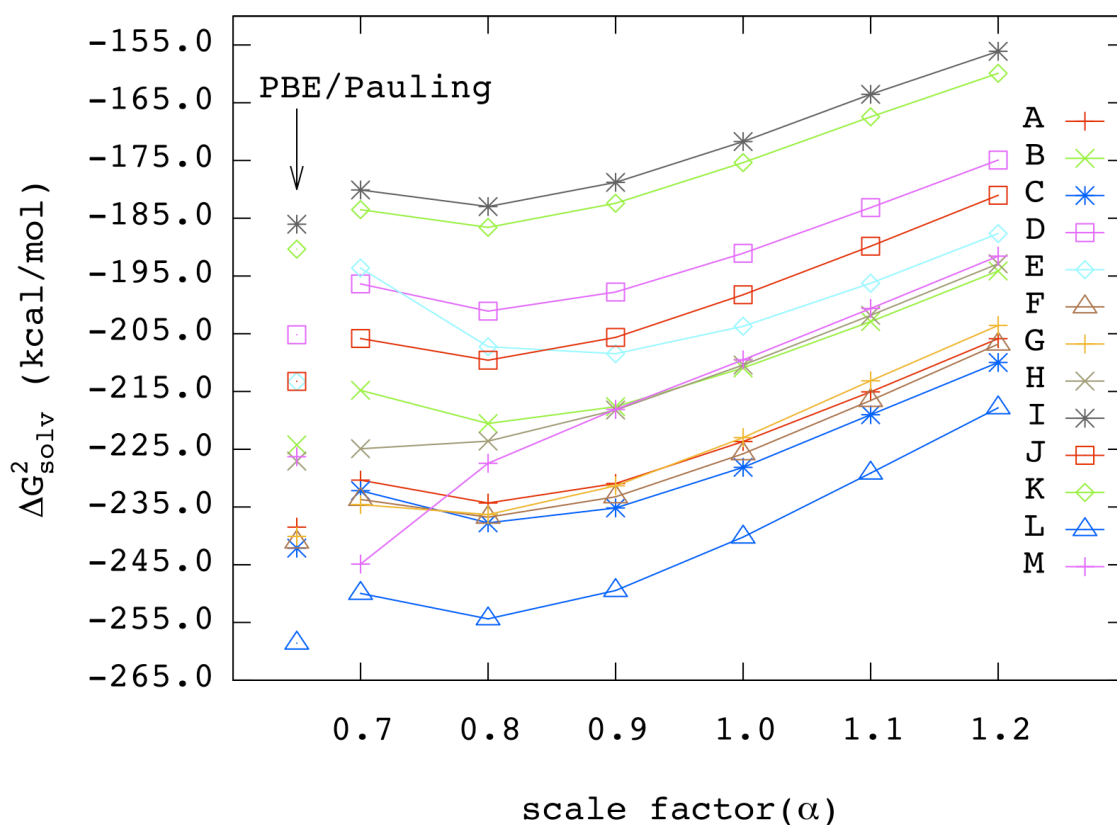
Figure 5. Free energies of solvation (ΔG_{solv}^2) for dianions using different scale factors on PBE/aug-cc-pVTZ with Pauling cavity.

The original purpose of a scale factor (default = 1.2 in G03) was to allow a transition between solute and bulk solvent.[3b] For pK_{a1}, a modified scale factor of 0.9 was chosen to reproduce the experimental data while a scale factor of 0.8 was chosen for pK_{a2}.[64] In our test set, smaller scale

factors for the UFF cavity set produced larger solvation free energies (ΔG_{solv}) and decreased pK_a (Fig. 5). However, solvation free energies from the smallest scale factor for the UFF cavity set (0.7) were still insufficient to match the solvation free energies from the Pauling cavity set. In fact, the 0.7 scale factor did not indicate a systematic approach of solvation free energies to the Pauling cavity set (Fig. 5) and probably represents an unrealistically small scale factor. Verdolino et al.[64] did not study the effect of scale factors for dianions since they investigated pK_{a1} of HA$^+$(aq) $\rightarrow$ A(aq) + H$^+$(aq) and pK_{a2} of HA(aq) $\rightarrow$ A$^-$(aq) + H$^+$(aq). Our tests show that a simple adjustment of the scale factor is not an adequate solution to modify the calculated dianion solvation free energies.

3.4 Conclusions

For five well-known cavity model sets (UFF, UAKS, Pauling, Klamt, and SMD), ΔG_{aq}/pK_a calculations were made for monoprotic, diprotic, and triprotic acids. The performance for ΔG_{aq}^1/pK_{a1} with the UAKS cavity set and Pauling cavity set was similar for all DFT functionals considered. However, the performance for ΔG_{aq}^2/pK_{a2} with the M05-2X/Pauling cavity was clearly superior to other combinations. All considered DFT/cavity set combinations underestimated ΔG_{aq}^2 with narrow ΔG_{aq}/pK_a intervals (less than 4 kcal/mol) between first and second dissociations. One exception was fumaric acid (**N**), which does not experience intramolecular hydrogen bond in the monoanionic form. For triprotic acids, all cavity sets predicted too positive a ΔG_{aq}^3, the best being the Pauling cavity set.

The free energy cycle based on the experimental value of ΔG_{solv}(H$^+$) enables simple but robust predictions for a broad range of acids. However, a universal or seamless methodology to calculate the free energy of solution (ΔG_{aq}) for pK_a prediction is still a goal. At this time I

suggest the M05-2X/Pauling combination as the method of choice for calculating ΔG_{aq}^{1} and ΔG_{aq}^{2} of diprotic acids whose pK_a values are separated by at least three units (4.1 kcal/mol). For triprotic acids, the M05-2X/Pauling combination is still reasonable for ΔG_{aq}^{1} and ΔG_{aq}^{2} but 15 kcal/mol should be subtracted from ΔG_{aq}^{3}.

3.5 References

(1)   Fortunelli, A.; Tomasi, J. *Chem. Phys. Lett.* **1994**, *231*, 34.

(2)   Cossi, M; Barone, V.; Cammi R.; Tomasi, J. *Chem. Phys. Lett.* **1996**, *255*, 327.

(3)   (a) Foresman, J. B.; Keith, T. A.; Wiberg, K. B.; Snoonian, J. ; Frisch, M. J. *J. Phys. Chem.* **1996**, *100*, 16098. (b) Barone, V.; Cossi, M.; Tomasi, J. *J. Chem. Phys.* **1997**, *107*, 3210. (c) Barone, V.; Cossi, M. *J. Phys. Chem. A* **1998**, *102*, 1995.

(4)   Tomasi, J.; Mennucci B.; Cammi, R. *Chem. Rev.* **2005**, *105*, 2999.

(5)   Marenich, A. V.; Cramer, C. J.; Truhlar, D. G. *J. Phys. Chem. B* **2009**, *113*, 4538.

(6)   Marenich, A. V.; Cramer, C. J.; Truhlar, D. G. *J. Phys. Chem. B* **2009**, *113*, 6378.

(7)   Cramer, C. J.; Truhlar, D. G. *Acc. Chem. Res.* **2008**, *41*, 760.

(8)   (a) Fu, Y.; Liu, L.; Li, R. C.; Liu R.; Guo, Q. X. *J. Am. Chem. Soc.* **2004**, *126*, 814. (b) Magill, A.M.; Cavell K. J.; Yates, B. F. *J. Am. Chem. Soc.* **2004**, *126*, 8717.

(9)   Ding, F. Z.; Smith, J. M.; Wang, H. B. *J. Org. Chem.* **2009**, *74*, 2679.

(10)   Dutton, A. S.; Fukuto J. M.; Houk, K. N. *Inorg. Chem.* **2005**, *44*, 4024.

(11)   Roy, L. E.; Jakubikova, E.; Guthrie M. G.; Batista, E. R. *J. Phys. Chem. A* **2009**, *113*, 6745.

(12)   (a) Tran N. L.; Colvin, M. E. *THEOCHEM* **2000**, *532*, 127. (b) Namazian, M.; Halvani S.; Noorbala, M. R. *THEOCHEM* **2004**, *711*, 13.

(13)   (a) Klamt, A.; Eckert, F.; Diedenhofen M.; Beck, M. E. *J. Phys. Chem. A* **2003**, *107*, 9380. (b) Lu, H.; Chen X.; Zhan, C. G. *J. Phys. Chem. B* **2007**, *111*, 10599. (c) Govender, K. K.; Cukrowski, I. *J. Phys. Chem. A* **2009**, *113*, 3639.

(14)   Jacquemin, D.; Perpete, E. A.; Ciofini, I.; Adamo, C. *J. Phys. Chem. A* **2008**, *112*, 794.

(15)   Adam, K. R. *J. Phys. Chem. A* **2002**, *106*, 11963.

(16)   Aschi, M.; D'Archivio, A. A.; Fontana, A.; Formiglio, A. *J. Org. Chem.* **2008**, *73*, 3411.

(17)   Benson, M. T.; Moser, M. L.; Peterman, D. R.; Dinescu, A. *THEOCHEM* **2008**, *867*, 71.

(18)   Takano, Y.; Houk, K. N. *J. Chem. Theory Comput.* **2005**, *1*, 70.

(19)   Król, M.; Wrona, M.; Page C. S.; Bates, P. A. *J. Chem. Theory Comput.* **2006**, *2*, 1520.

(20)   Lide, D. R. *CRC Handbook of Chemistry and Physics*; CRC Press: New York, 2005.

(21)   Fernández, M. I.; Canle, M.; García, M. V.; Santaballa, J. A. *Chem. Phys. Lett.* **2010**, *490*, 159.

(22)   Sadlej-Sosnowska, N. *Theor. Chem. Acc.* **2007**, *118*, 281.

(23)   (a) Rustad, J. R.; Dixon, D. A.; Kubicki, J. D.; Felmy, A. R. *J. Phys. Chem. A* **2000**, *104*, 4051. (b) He, X.; Fusti-Molnar, L.; Merz, K. M. *J. Phys. Chem. A* **2009**, *113*, 10096.

(24)   Liptak, M. D.; Shields, G. C. *Int. J. Quantum Chem.* **2005**, *105*, 580.

(25)   (a) Tissandier, M. D.; Cowen, K. A.; Feng, W. Y.; Gundlach, E.; Cohen, M. H.; Earhart, A. D.; Coe, J. V.; Tuttle, T. R. *J. Phys. Chem. A* **1998**, *102*, 7787. (b) Zhan, C.-G.; Dixon, D. A. *J. Phys. Chem. A* **2001**, *105*, 11534. (c) Pliego, J. R. *Chem. Phys. Lett.* **2003**, *367*, 145. (d) da Silva, C. O.; da Silva E. C.; Nascimento, M. A. C. *Chem. Phys. Lett.* **2003**, *381*, 244. (e) Pliego, J. R. *Chem. Phys. Lett.* **2003**, *381*, 246.

(26)   Palascak, M. W.; Shields, G. C. *J. Phys. Chem. A* **2004**, *108*, 3692.

(27)   Camaioni, D. M.; Schwerdtfeger, C. A. *J. Phys. Chem. A* **2005**, *109*, 10795.

(28)   Thompson, J. D.; Cramer, C. J.; Truhlar, D. G. *J. Phys. Chem. A* **2004**, *108*, 6532.

(29)   Pratuangdejkul, J.; Nosoongnoen, W.; Guérin, G.-A.; Loric, S.; Conti, M.; Launay, J.-M.; Manivet, P. *Chem. Phys. Lett.* **2006**, *420*, 538.

(30)   (a) Stefanovich, E. V.; Truong, T. N. *Chem. Phys. Lett.* **1995**, *244*, 65. (b) Aguilar, M. A.; Delvalle, F. J. O. *Chem. Phys.* **1989**, *129*, 439. (c) Rashin, A. A.; Namboodiri, K. *J. Phys. Chem.* **1987**, *91*, 6003.

(31)   Cossi, M.; Rega, N.; Scalmani, G.; Barone, V.; *J. Comput. Chem.* **2003**, *24*, 669.

(32)   Casasnovas, R.; Frau, J.; Ortega-Castro, J.; Salvá, A.; Donoso, J.; Muñoz, F. *THEOCHEM* **2009**, *912*, 5.

(33)   Chipman, D. M. *J. Phys. Chem. A* **2002**, *106*, 7413.

(34)   Guthrie, J. P.; Povar, I. *Can. J. Chem.* **2009**, *87*, 1154.

(35)   Ho, J.; Coote, M. L. *Theor. Chem. Acc.* **2010**, *125*, 3.

(36)   Ho, J.; Coote, M. L. *J. Chem. Theory Comput.* **2009**, *5*, 295.

(37)   Frisch, M. J. T., G. W.; Schlegel, H. B.; Scuseria, G. E.; Robb, M. A.; Cheeseman, J. R.; Montgomery, Jr., J. A.; Vreven, T.; Kudin, K. N.; Burant, J. C.; Millam, J. M.; Iyengar, S. S.; Tomasi, J.; Barone, V.; Mennucci, B.; Cossi, M.; Scalmani, G.; Rega, N.; Petersson, G. A.; Nakatsuji, H.; Hada, M.; Ehara, M.; Toyota, K.; Fukuda, R.; Hasegawa, J.; Ishida, M.; Nakajima, T.; Honda, Y.; Kitao, O.; Nakai, H.; Klene, M.; Li, X.; Knox, J. E.; Hratchian, H. P.; Cross, J. B.; Bakken, V.; Adamo, C.; Jaramillo, J.; Gomperts, R.; Stratmann, R. E.; Yazyev, O.; Austin, A. J.; Cammi, R.; Pomelli, C.; Ochterski, J. W.; Ayala, P. Y.; Morokuma, K.; Voth, G. A.; Salvador, P.; Dannenberg, J. J.; Zakrzewski,

V. G.; Dapprich, S.; Daniels, A. D.; Strain, M. C.; Farkas, O.; Malick, D. K.; Rabuck, A. D.; Raghavachari, K.; Foresman, J. B.; Ortiz, J. V.; Cui, Q.; Baboul, A. G.; Clifford, S.; Cioslowski, J.; Stefanov, B. B.; Liu, G.; Liashenko, A.; Piskorz, P.; Komaromi, I.; Martin, R. L.; Fox, D. J.; Keith, T.; Al-Laham, M. A.; Peng, C. Y.; Nanayakkara, A.; Challacombe, M.; Gill, P. M. W.; Johnson, B.; Chen, W.; Wong, M. W.; Gonzalez, C.; Pople, J. A. *Gaussian03*, Revision E.01; Gaussian, Inc: Wallingford CT, 2004.

(38)   Marenich, A. V.; Cramer, C. J.; Truhlar, D. G. *J. Phys. Chem. B* **2009**, *113*, 6378.

(39)   Frisch, M. J.; Trucks, G. W.; Schlegel, H. B.; Scuseria, G. E.; Robb, M. A.; Cheeseman, J. R.; Scalmani, G.; Barone, V.; Mennucci, B.; Petersson, G. A.; Nakatsuji, H.; Caricato, M.; Li, X.; Hratchian, H. P.; Izmaylov, A. F.; Bloino, J.; Zheng, G.; Sonnenberg, J. L.; Hada, M.; Ehara, M.; Toyota, K.; Fukuda, R.; Hasegawa, J.; Ishida, M.; Nakajima, T.; Honda, Y.; Kitao, O.; Nakai, H.; Vreven, T.; Montgomery Jr., J. A.; Peralta, J. E.; Ogliaro, F.; Bearpark, M.; Heyd, J. J.; Brothers, E.; Kudin, K. N.; Staroverov, V. N.; Kobayashi, R.; Normand, J.; Raghavachari, K.; Rendell, A.; Burant, J. C.; Iyengar, S. S. ; Tomasi, J.; Cossi, M.; Rega, N.; Millam, J. M.; Klene, M.; Knox, J. E.; Cross, J. B.; Bakken, V.; Adamo, C.; Jaramillo, J.; Gomperts, R.; Stratmann, R. E.; Yazyev, O.; Austin, A. J.; Cammi, R., Pomelli, C., Ochterski, J.; Martin, R. L., Morokuma, K.; Zakrzewski, V. G.; Voth, G. A.; Salvador, P.; Dannenberg, J. J.; Dapprich, S.; Daniels, A. D.; Farkas, O.; Foresman, J. B.; Ortiz, J. V.; Cioslowski J.; Fox, D. J. *Gaussian 09*, Revision A.2; Gaussian, Inc.: Wallingford CT, 2009.

(40)   Peterson, B. R. http://research.chem.psu.edu/brpgroup/pKa_compilation.pdf accessed on April 12, 2010.

(41)   Zhang, S.; Baker, J.; Pulay, P. *J. Phys. Chem. A* **2010**, *114*, 432.

(42)   (a) Feller, D. *J. Comput. Chem.* **1996**, *17*, 1571. (b) Schuchardt, K. L.; Didier, B. T.; Elsethagen, T.; Sun, L. S.; Gurumoorthi, V.; Chase, J.; Li J.; Windus, T. L. *J. Chem. Inf. Model.* **2007**, *47*, 1045.

(43)   (a) Atkins, P.; Overton, T.; Rourke, J.; Weller M.; Armstrong, F. *Inorganic Chemistry*; W. H. Freeman and Company: New York, 2006. (b) Smith, M.; March, J. *March's advanced organic chemistry: reactions, mechanisms, and structure*; Wiley-Interscience, Hoboken: New Jerzy, 2007. (c) Bruckenstein, S.; Kolthoff, I. M. *Treatise on Analytical Chemistry*; Interscience Encyclopedia: New York, 1959.

(44)   (a) Alexeev, Y.; Windus, T. L.; Zhan, C.-G.; Dixon, D. A. *Int. J. Quantum Chem.* **2005**, *102*, 775. (b) Gutowski, K. E.; Dixon, D. A. *J. Phys. Chem. A* **2006**, *110*, 12044.

(45)   (a) Sülzle, D.; Verhoeven, M.; Terlouw, J. K.; Schwarz, H. *Angew. Chem., Int. Ed.* **1988**, *27*, 1533. (b) William, J. L. *Modern Inorganic Chemistry*; McGraw-Hill: New York, 1991.

(46)   (a) Voegele, A. E.; Tautermann, C. S.; Loerting, T.; Hallbrucker, A.; Mayer, E.; Liedl, K. R. *Chem. Eur. J.* **2002**, *8*, 5644. (b) Voegele, A. F.; Tautermann, C. S.; Rauch, C.; Loerting, T.; Liedl, K. R. *J. Phys. Chem. A* **2004**, *108*, 3859.

(47)   Florián, J.; Warshel, A. *J. Phys. Chem. B* **1997**, *101*, 5583.

(48)   (a) Smiechowski, M. *J. Mol. Struct.* **2009**, *924*, 170. (b) Brandán, S. A.; Díaz, S. B.; Picot, R. C.; Disalvo, E. A.; Altabef, A. B. *Spectrochim. Acta, Part A* **2007**, *66*, 1152.

(49)   Marcus, Y. *Ion Properties*; Marcel Dekker Inc: New York, 1997.

(50)   Boldyrev, A. I. ; Simons, J. *J. Phys. Chem.* **1994**, *98*, 2298.

(51)   Pye, C. C.; Rudolph, W. W. *J. Phys. Chem. A* **2003**, *107*, 8746.

(52)   Tang, E.; Di Tommaso, D.; de Leeuw, N. H. *J. Chem. Phys.* **2009**, *130*, 234502.

(53)   Tossell, J. A. *Geochim. Cosmochim. Acta* **2005**, *69*, 5647.

(54)   Bell, R. P. *The proton in chemistry*; Cornell University Press: Ithaca, 1973.

(55)   Wang, X.; Conway, W.; Burns, R.; McCann, N.; Maeder, M. *J. Phys. Chem. A* **2010**, *114*, 1734.

(56)   Gao, D. Q.; Svoronos, P.; Wong, P. K.; Maddalena, D.; Hwang, J.; Walker, H. *J. Phys. Chem. A* **2005**, *109*, 10776.

(57)   Bickmore, B. R.; Tadanier, C. J.; Rosso, K. M.; Monn, W. D.; Eggett, D. L. *Geochim. Cosmochim. Acta* **2004**, *68*, 2025.

(58)   Housecroft, C. E.; Sharpe, A. G. *Inorganic Chemistry*; Prentice Hall: London, 2004.

(59)   Zimmermann, M. D.; Tossell, J. A. *J. Phys. Chem. A* **2009**, *113*, 5105.

(60)   Mayhall, N. J.; Raghavachari, K.; Redfern, P. C.; Curtiss, L. A. *J. Phys. Chem. A* **2009**, *113*, 5170.

(61)   Zhao, Y.; Truhlar, D. G. *J. Chem. Phys.* **2006**, *124*, 224105.

(62)   da Silva, E. F.; Svendsen, H. F.; Merz, K. M. *J. Phys. Chem. A* **2009**, *113*, 6404.

(63)   Zhang, S.; Baker, J.; Pulay, P. *J. Phys. Chem. A* **2010**, *114*, 425.

(64)   Verdolino, V.; Cammi, R.; Munk, B. H.; Schlegel, H. B. *J. Phys. Chem. B* **2008**, *112*, 16860.

(65)   Schwartz, L. M.; Howard, L. O. *J. Phys. Chem.* **1970**, *74*, 4374.

(66)   Jencks, W.P. http://evans.harvard.edu/pdf/evans_pKa_table.pdf accessed on May 7, 2010.

(67)   Rich, R. L. *Inorganic Reactions in Water*; Springer: Berlin, 2007.

(68)   Baes, C. F.; Mesmer, R. E. *The Hydrolysis of Cations*; John & Wiley: New York, 1976.

Chapter 4

Dissolution Thermochemistry of Alkali Metal Dianion Salts (M_2X_1, M=Li^+, Na^+, and K^+ with

X=CO_3^{2-}, SO_4^{2-}, $C_8H_8^{2-}$, and $B_{12}H_{12}^{2-}$)

4.1 Introduction

Solvation Gibbs free energies (ΔG_{solv}) contribute greatly to solubility, solution reactivity, adsorption of ionic species, and stability of biomolecules. For neutral organic species, experimental partition coefficients allow the calculation of ΔG_{solv} with 0.2 kcal/mol of uncertainty.[1] On the other hand, experimental ΔG_{solv} values of individual cations or anions are not directly available and in many cases the uncertainty is substantial (4 to 5 kcal/mol).[1] Alkali metal cations, which play a key role in biology, have widely varying reported values of ΔG_{solv} (Table 1).[2] The absolute ΔG_{solv} of Li^+, Na^+, and K^+ vary from -104.1 to -144.3 kcal/mol, -76.8 to -116.5 kcal/mol, and -59.6 to -85.4 kcal/mol, respectively.[3] Latimer[4] estimated ΔG_{solv} of alkali metal cations using a thermodynamic cycle which included sublimation energy, ionization energy and reduction potential. However, the entropy of solids, electron/ion convention, and standard reduction potential were not accurately known at that time. Tissandier et al.[3d] presented a cluster-pair approximation to get the absolute ΔG_{solv} of alkali metal cations. Kelly et al.[3i] applied the same method to determine the absolute ΔG_{solv} of alkali metal cations with the electron convention/Fermi-Dirac statistics. Donald and Williams[3l] performed an even more comprehensive cluster-pair approximation and reported slightly modified ΔG_{solv} of alkali metal cations based on -263.4 kcal/mol of $\Delta G_{solv}(H^+)$ at 1 atm standard state (Table 1).

Table 1. Absolute hydration free energies (ΔG_{solv}, kcal/mol) of alkali metal cations (Li^+, Na^+, K^+) in literature[a]

Reference	Absolute hydration free energy (ΔG_{solv})		
	Li^+	Na^+	K^+
3o	-122.1	-98.4	-80.6
3n	-122.1	-98.2	-80.6
3a	-123.5	-98.6	-80.8
3p	-113.5	-87.2	-70.5
3c[b]	-144.3	-116.5	
3d	-126.5	-101.3	-84.1
3e	-115.4	-96.3	-79.6
3f	-126.0		
3g	-124.9	-99.7	-82.5
3h	-118.6	-94.2	
3m			-68.6
3i	**-126.5**	**-101.3**	**-84.1**
3j[b]	-120.8	-92.3	-75.5
3q	-123.1	-96.6	-79.4
3k	-111.8	-86.8	-68.8
3k	-104.1	-76.8	-59.6
3k	-112.8	-87.5	-65.0
3l	-127.8	-102.6	-85.4
3r	-120.5	-96.3	-78.6
This work[c]	-126.6	-101.1	-83.8

[a]The standard state of 1 atm for gas and 1 M for aqueous solution. The reported values with 1M standard state for gas and solution are converted to the values with the standard state of 1 atm of gas and 1 M for aqueous solution using a +1.89 kcal/mol correction. [b]The standard state information is not shown clearly. [C]The SHE 4.281 eV is applied. See Scheme 4 for details. The values used (in bold) for $\Delta G_{solv}(M^+)$ are from reference 3i

The CPCM (Conductor-like Polarizable Continuum Model)[5] is combined with *ab initio* computations to determine ΔG_{solv} of neutral and ionic species. In a benchmark study of CPCM, Takano and Houk[6] found that the mean absolute deviations of aqueous ΔG_{solv} for ionic species

varied between 2.73 and 9.30 kcal/mol depending on the choice of the cavity set. The Pauling cavity set had the smallest deviation (2.73 kcal/mol) for ionic species while the same cavity set showed 3.49 kcal/mol of deviation for neutral species. Takano and Houk[6] recommended the UAKS cavity set for the prediction of pK_{a1} since it had the smallest deviation for neutral species (1.35 kcal/mol) and a small deviation for anions (3.21 kcal/mol). However, Chipman[7] reported that no single electronic isodensity contour value for solute cavity led to acceptable values of ΔG_{solv} for anions in his test sets. Król et al.[8] suggested that the Pauling cavity set was best for pK_a predictions of polyprotic acids. Fernández et al.[9] found that the Pauling cavity set was better than the UAKS cavity set for the pK_a calculation of ammonia oxide ($^+NH_3O^-$). I found the Pauling cavity set combined with the M05-2X functional to be the most suitable for the $\Delta G_{aq2}/pK_{a2}$ prediction in aqueous media.[10] The CPCM method with a proper choice of a cavity set can yield solvation free energies (ΔG_{solv}) of anions within about ±5 kcal/mol of experimental values.[1]

Many *ab initio* computations based on periodic or extended cluster models have been performed for organic crystal lattice energy.[11] Dispersion interactions, which are the main intermolecular contribution to the organic crystal lattice energy, are not described properly with traditional DFT methods. The Grimme group[11b,12] have developed an empirically parameterized dispersion correction which is implemented in several packages for periodic systems. For the Born-Haber cycle of M_2CO_3 and M_2SO_4 ($M = Li^+$, Na^+, and K^+), determining the second electron affinity is also a challenge (Scheme 1).[13] Most thermodynamic properties are well known from the literature or can be computed by established methods (Scheme 1). On the other hand, small dianions such as CO_3^{2-} and SO_4^{2-} are known to be stable in water but unstable or metastable in the gas phase due to the unbound nature of the second electron.[10,14] Many approaches have been

101

presented to calculate the second electron affinity (negative affinity) using chemical hardness,[15] an anion bound by a potential wall,[16] and the stabilization exerted by a polar solvent.[17] Jensen[18] reported that the lack of long-range dispersion in the exchange-correlation DFT functional led to poor performance for calculating electron affinities. The electron affinities (negative electron affinity, $-\Delta H_{0K}$) of CO_3^- and SO_4^- are known to be -87.6 kcal/mol and -37.0 kcal/mol, respectively from the literature.[19] The electron affinity of SO_4^- by the MP2/CBS method was -25.4 kcal/mol[20] while the Simons group[21] reported SO_4^{2-} was vertically unstable by 25.8 kcal/mol.
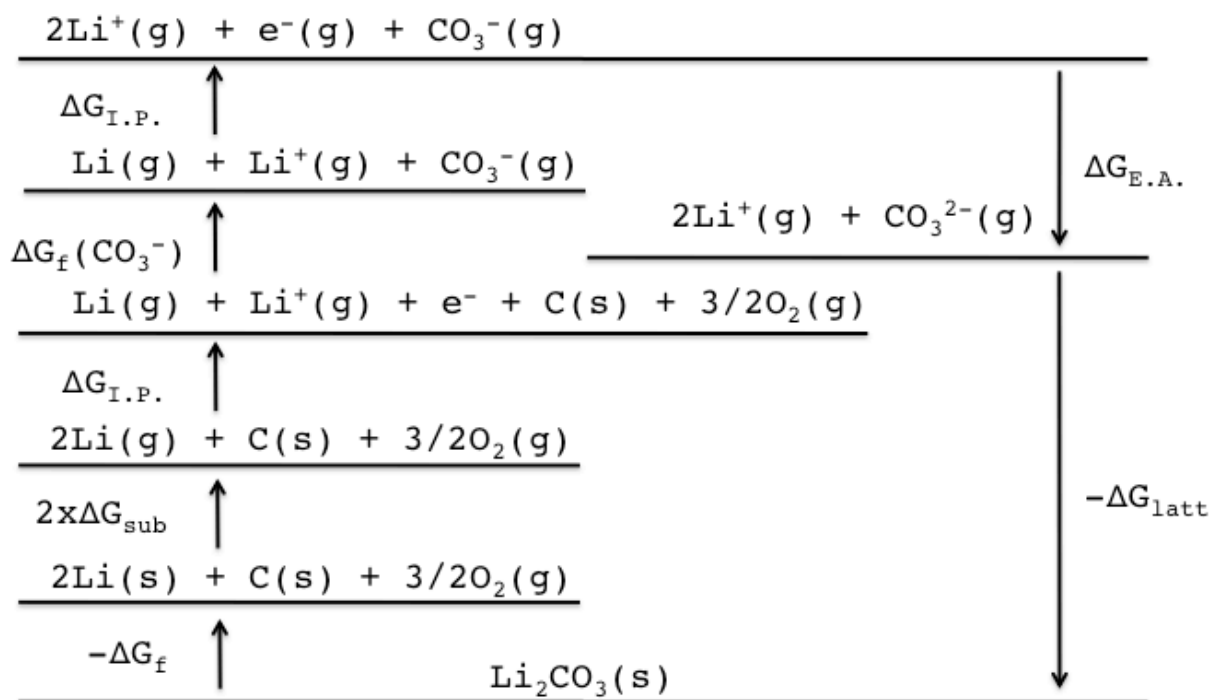
Scheme 1. Born-Haber cycle for Li_2CO_3.

Over the last ten years, the Jenkins group[22] developed a volumetric approach for the lattice energy of ionic crystals including an empirical formula for entropy estimation. Several studies have used this volumetric approach to determine the lattice energy of ionic crystals

because the equation is very easy to apply.[23] The lattice enthalpies of M_2CO_3 and M_2SO_4 (M =

Li^+, Na^+, and K^+) are available in the literature based on this volumetric approach as well as the

Born-Fajans-Haber cycle.[24] In fact, I consider the volumetric approach is more reliable because

the heat of formation for $CO_3^{2-}(g)$ and $SO_4^{2-}(g)$ are uncertain.[24] However, the choice of ionic

volume is critical to determine the lattice energy. For $K_2B_{12}Cl_{12}$, 0.010 nm^3 for the K^+ volume[23d]

gives 250.7 kcal/mol of lattice energy while 0.0277 nm^3 by a recent study[22h] gives 294.6

kcal/mol of lattice energy, a difference of 43.9 kcal/mol.

If the formation Gibbs free energy differences ($\Delta\Delta G_f = \Delta\Delta H_f - T\Delta S$) between gas and

solid are available, a thermodynamic triangle can be constructed to estimate ΔG_{latt} (Scheme 2).

Calculating the gaseous dissociation energy (ΔG_{gas}) of an ionic molecule by *ab initio* quantum

chemistry is straightforward. In addition, many papers are beginning to appear on the calculation

of ΔH_f in the solid.[25] I also define a cohesive free energy of the crystal (ΔG_{coh}), which can

replace $\Delta\Delta G_f$ in Scheme 2. With the optimized geometry of the gaseous ionic molecule and the

optimized crystal structure, the cohesion energy of the crystal can be estimated by computation.
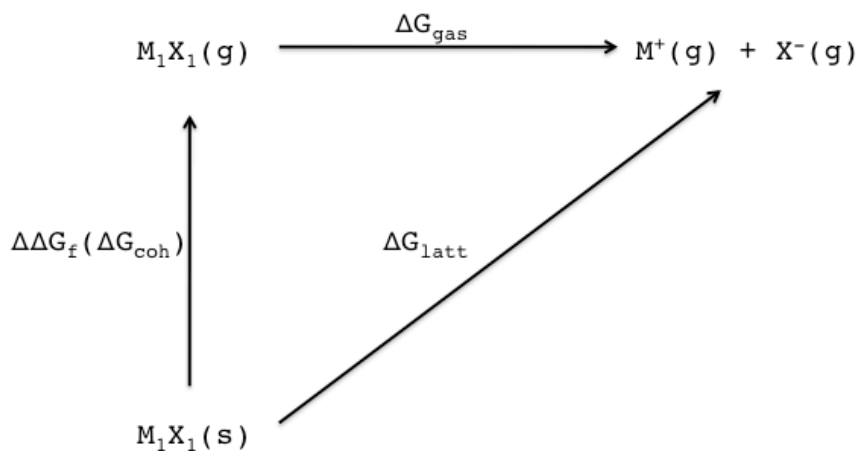
Scheme 2. Lattice free energy of crystal by the sum of free energy difference ($\Delta\Delta G = \Delta\Delta H_f -$

TΔS) between gas and solid followed by gaseous dissociation free energy (ΔG_{gas}).

I set up a thermodynamic cycle for the dissolution of alkali metal cations (Li^+, Na^+, and K^+) with several dianions (CO_3^{2-}, SO_4^{2-}, $C_8H_8^{2-}$, and $B_{12}H_{12}^{2-}$) in Scheme 3. At equilibrium, ΔG_{diss} is always 0 while $\Delta G^o{}_{diss}$ is given by $-RTlnK_{sp}$ ($\Delta G_{diss} = \Delta G^o{}_{diss} + RTlnK_{sp}$, where K_{sp} is solubility constant). With ΔH_f for aqueous ions and solids and entropies for aqueous ions and salts, $\Delta G^o{}_{diss}$ values of M_2CO_3 ($M=Li^+$, Na^+, and K^+) in infinitely dilute solutions are between -7.1 (K_2CO_3) to 4.3 kcal/mol (Li_2CO_3) while for M_2SO_4 ($M=Li^+$, Na^+, and K^+) they are between -2.3 (Li_2SO_4) to 2.0 kcal/mol (K_2SO_4) (Table 2).[24b]

$$2M^+(g) \quad + \quad X^{2-}(g)$$

$$\Delta G_{1att}$$

$$2*\Delta G_{solv}(M^+) \qquad \Delta G_{solv}(X^{2-})$$

$$M_2X_1 \ (solid) \xrightarrow{\ \Delta G^o{}_{diss}\ } 2M^+(aq) + X^{2-}(aq)$$
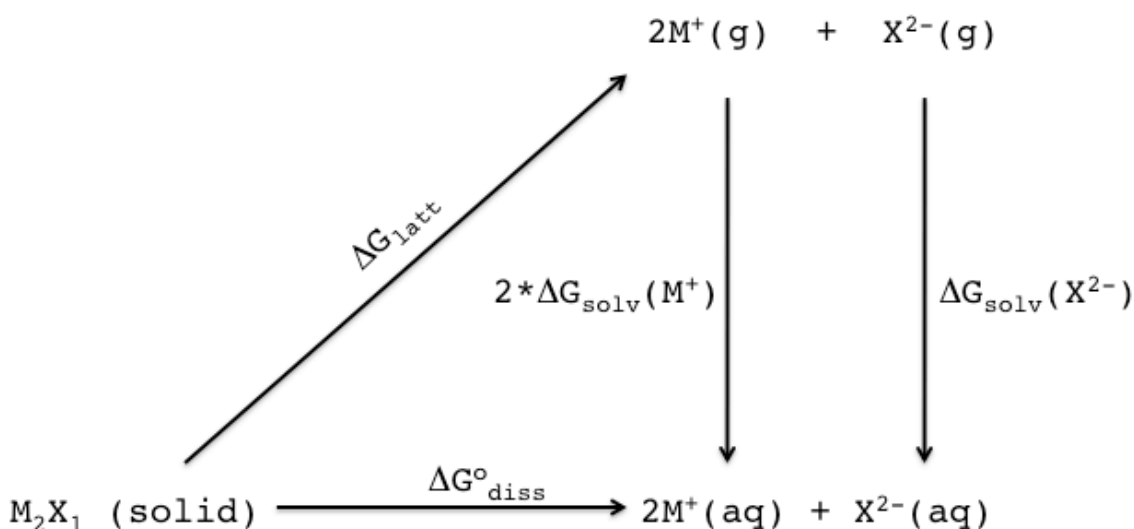
Scheme 3. Thermodynamic cycle for the dissolution of M_2X_1 (M_2X_1, $M=Li^+$, Na^+, and K^+ with $X=CO_3^{2-}$, SO_4^{2-}, $C_8H_8^{2-}$, and $B_{12}H_{12}^{2-}$) salts.

The solubilities of M_2CO_3, M_2SO_4, and $M_2B_{12}H_{12}$ ($M = Li^+$, Na^+, and K^+) vary greatly while $\Delta G^o{}_{diss}$ values are within ±5 kcal/mol of 0 (Table 2).[26] All $M_2B_{12}H_{12}$ salts ($M = Li^+$, Na^+, and K^+)

are known to be very soluble in water and stable in dilute acids but the solubility decreases sharply from lithium to the cesium salt.[23c,27-28]

Table 2. Experimental dissolution enthalpies (ΔH^o_{diss}) and free energies (ΔG^o_{diss}) (kcal/mol) of M_2CO_3 (M=Li^+, Na^+, and K^+), M_2SO_4 (M=Li^+, Na^+, and K^+), and $M_2B_{12}H_{12}$ (M=Li^+, Na^+, K^+, Rb^+, and Cs^+)

Dissolution reaction	$\Delta H^o_{diss}{}^a$	$\Delta G^o_{diss}{}^b$	$\Delta G^o_{diss}{}^c$
$Li_2CO_3(s) \rightarrow 2Li^+(aq) + CO_3^{2-}(aq)$	-4.3	4.3	2.2
$Na_2CO_3(s) \rightarrow 2Na^+(aq) + CO_3^{2-}(aq)$	-6.4	-1.1	-2.1
$K_2CO_3(s) \rightarrow 2K^+(aq) + CO_3^{2-}(aq)$	-7.6	-7.1	-4.5
$Li_2SO_4(s) \rightarrow 2Li^+(aq) + SO_4^{2-}(aq)$	-7.2	-2.3	$-2.4(-0.1)^d$
$Na_2SO_4(s) \rightarrow 2Na^+(aq) + SO_4^{2-}(aq)$	-0.5	0.4	$-1.4(1.7)^d$
$K_2SO_4(s) \rightarrow 2K^+(aq) + SO_4^{2-}(aq)$	5.6	2.0	$-0.2(2.4)^d$
$Li_2B_{12}H_{12}(s) \rightarrow 2Li^+(aq) + B_{12}H_{12}^{2-}(aq)$			-2.7^e
$Na_2B_{12}H_{12}(s) \rightarrow 2Na^+(aq) + B_{12}H_{12}^{2-}(aq)$			-2.6^e
$K_2B_{12}H_{12}(s) \rightarrow 2K^+(aq) + B_{12}H_{12}^{2-}(aq)$			-1.9^e
$Rb_2B_{12}H_{12}(s) \rightarrow 2Rb^+(aq) + B_{12}H_{12}^{2-}(aq)$			1.4^e
$Cs_2B_{12}H_{12}(s) \rightarrow 2Cs^+(aq) + B_{12}H_{12}^{2-}(aq)$			4.0^e

[a]The ΔH^o_{diss} is taken as the difference in the aqueous heat of formation (standard state is hypothetical ideal solution with molality m = 1 mol/kg) in reference 24b and the solid state heat of formation in the NIST webbook. [b]Free energy of the solid (ΔG) is taken as the heat of formation for the solid state (ΔH_f) plus the entropy term (-$T\Delta S$) while the entropy for the aqueous ion comes from reference 24b. [c]The ΔG^o_{diss} comes from the K_{sp} (ΔG=-$RTlnK_{sp}$) with concentration from solubility data. [d]The values in parentheses are determined using solubility data with activity coefficient (Guendouzi, M. E.; Mounir, A.; Dinane, A. *J. Chem. Thermodynamics* **2003**, *35*, 209-220). For solubility of Na_2SO_4, a value of 20g/100g water applied for 25°C solubility. [e]The ΔG^o_{diss} comes from the K_{sp} (ΔG=-$RTlnK_{sp}$) with concentration (activity coefficients are not used) from solubility data in reference 27.

The value of ΔG^o_{diss} can be determined more accurately using activity coefficients rather than concentrations but the adjusted ΔG^o_{diss} for M_2SO_4 (M=Li^+, Na^+, and K^+) still remains within ±5

kcal/mol of 0 (Table 2). The maximum difference in ΔG^o_{diss} for M_2SO_4 (M=Li^+, Na^+, and K^+)

between using concentrations and activities is 2.6 kcal/mol (Table 2). In this work, I determine

ΔG^o_{diss} through *ab initio* computation for lattice free energy (ΔG_{latt}) and solvation free energy

(ΔG_{solv}). It is well known that solubilities of salts can be rationalized by considering lattice and

hydration enthalpies. Our intention is to combine experiment and theory to evaluate dissolution

free energies and to determine a methodology that gives results most consistent with experiment.

4.2 Computational Details

The B3LYP, PBE, BVP86, and M05-2X[29] DFT functionals are applied with the aug-cc-

pVTZ basis set to calculate ΔG_{gas} ($M_2X_1(g) \rightarrow 2M^+(g) + X^{2-}(g)$). Zero-point energies, heat

capacity corrections, and TΔS contributions are combined with single-point energies at the same

level to yield free energies at 298 K. For potassium-containing systems, the 6-311++G(3df,2pd)

basis set was used. The ΔG_{gas} values were applied in Scheme 2 for the estimation of ΔG_{latt}.

The conductor-like polarizable continuum model (CPCM)[5] was applied with the

dielectric constant of water (ε=78.39) and the SCFVAC Gaussian03 keyword on gas-phase

optimized geometries to compute ΔG_{solv}. For atomic radii in CPCM, I tested three cavity models

(UFF, UAKS, and Pauling).[10]   No symmetry restrictions were made on the cavity, and the cavity

surface was fit with tesserae of average area 0.1 Å^2. Geometries, gaseous free energies, and

solvation free energies for the three cavity models were obtained using Gaussian03.[30] Since the

$\Delta G_{solv}(X^{2-})$ values by *ab initio* calculations are based on the standard state of 1 atm (24.47

liters/mol), I used a factor of +1.89 kcal/mol to convert to the standard state of 1 M (1 liter/mol).

In Scheme 4, I evaluate ΔG_{solv} of Li^+, Na^+, and K^+ using the standard reduction potentials

of alkali metal cations,[31] including correction for electron/ion convention[32] and standard state

conversion.[33] The determination of the absolute ΔG_{solv} of alkali metal cations depends on the

choice of standard hydrogen electrode (SHE) potential. Reiss and Heller[34] reported 4.43 eV

while Donald et al.[35] suggested 4.2 ± 0.4 eV and proposed 4.11 eV using nanodrops in the gas

phase. However, Isse and Gennaro[36] reported 4.281 eV using the real potential, $\alpha_{aq}(H^+)$ $(\alpha_{aq}(H^+)$

$= \Delta G_{aq}(H^+) + F\chi^{aq}$, where χ^{aq} is the surface potential of water. In the electrochemical approach,

the difference between E^o(SHE) and the half reduction potential of each alkali metal cation

$(E^o(M/M^+))$ determines the free energy change (ΔG_{redox}) of the step $M(s) \rightarrow M^+(aq) + e^-(g)$

(Scheme 4).

Thermodynamic way

$$M(s) \xrightarrow{\Delta G_{sub}} M(g) \xrightarrow{\Delta G_{I.P.}} M^+(g) + e^-(g) \xrightarrow{\Delta G_{solv}} M^+(aq) + e^-(g)$$

30.3(Li)	124.7(Li)	-126.6(Li)
18.3(Na)	118.9(Na)	-101.1(Na)
14.5(K)	100.5(K)	-83.8(K)

$$\Delta G_{redox} = E^o(SHE) - E^o(M/M^+)$$

28.4(Li)
36.1(Na)
31.2(K)
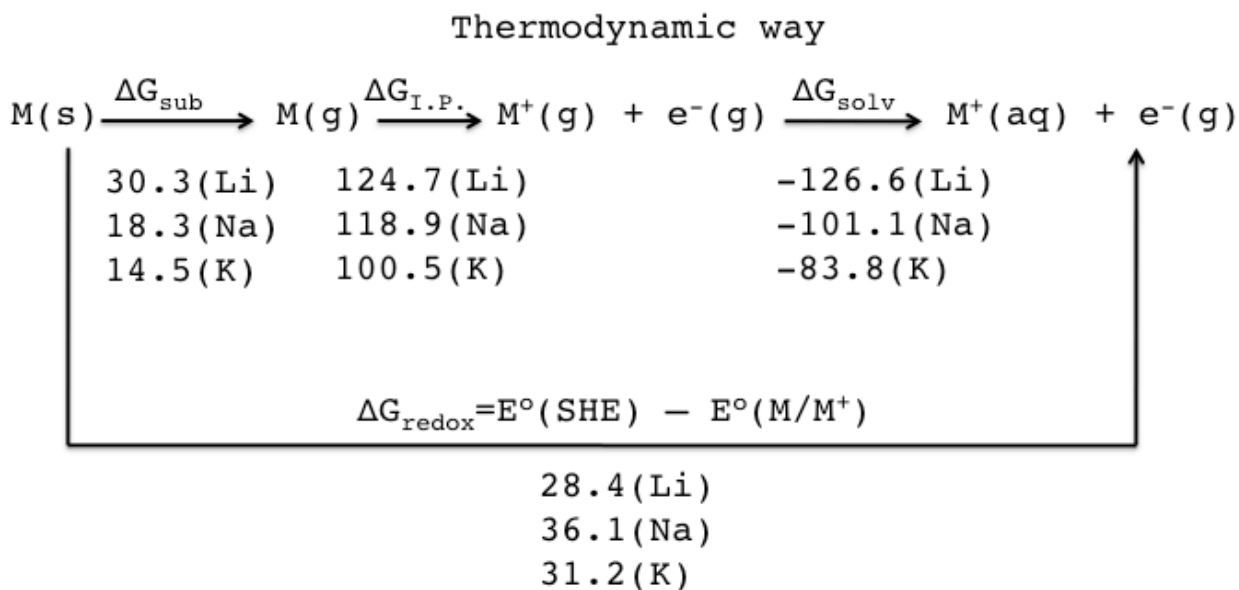
Scheme 4. Thermodynamic cycle for the evaluation of absolute ΔG_{solv} of M (M = Li$^+$, Na$^+$, and

K$^+$) (ΔG_{sub}, $\Delta G_{I.P.}$, ΔG_{redox} and ΔG_{solv} are in kcal/mol).

The solvation free energy (ΔG_{solv}) comes from ΔG_{redox} - ΔG_{sub} - $\Delta G_{I.P.}$. The difference of ΔH_f

between gas and solid phase combined with the entropy change is ΔG_{sub}. The ionization

potential of alkali metal atom (ΔH_{0K}) plus entropy change between atom and cation is $\Delta G_{I.P.}$ at

298K since the heat capacity corrections of monocation and monoatom are identical and cancel out. Enthalpies, entropies, and ionization potentials (ion-convention, Fermi-Dirac statistics) for each step are taken from the NIST chemistry webbook.[37] If 4.281 eV is used for SHE (1 atm standard state), the absolute $\Delta G_{solv}(M^+)$ ($M^+ = Li^+$, Na^+, and K^+) become -126.6, -101.1, and -83.8 kcal/mol, respectively. These values are very similar to the $\Delta G_{solv}(M^+)$ ($M^+ = Li^+$, Na^+, and K^+) at the 1 atm standard state suggested by three different cluster-pair approximation studies (Table 1 and Scheme 4).[3d,3i,31] Values that deviates by more than $\pm$ 5 kcal/mol from the cluster-pair approximation studies should be carefully reevaluated. I used the values of $\Delta G_{solv}(M^+)$ (M^+ = Li^+ (-126.5), Na^+ (-101.3), and K^+ (-84.1 kcal/mol)) reported by Kelly et al.[3i] after correcting to our standard state conversion of 1 M for solution (+1.89 kcal/mol).

The hydrolysis of SO_4^{2-} ($H_2O(l) + SO_4^{2-}(aq) \rightarrow HSO_4^-(aq) + OH^-(aq)$) is non-spontaneous at pH 7 (ΔG=16.4 kcal/mol, Appendix 2) which indicates that the anionic species formed in the dissolution of $M_2SO_4(s)$ will be SO_4^{2-} rather than HSO_4^-. Likewise, the hydrolysis of CO_3^{2-} ($H_2O(l) + CO_3^{2-}(aq) \rightarrow HCO_3^-(aq) + OH^-(aq)$) is non-spontaneous at pH 7 (ΔG=5.0 kcal/mol) which indicates that the anionic species generated in the dissolution of $M_2CO_3(s)$ will be CO_3^{2-} rather than HCO_3^-. For $M_2C_8H_8$ ($M = Li^+$, Na^+, and K^+), the step $M_2C_8H_8(s) \rightarrow 2M^+(aq) + C_8H_8^{2-}(aq)$ is not the process observed due to further reaction and formation of insoluble $C_8H_{10}(l)$ (1,3,5-cyclooctatriene) on top of water.[38] The dianion $C_8H_8^{2-}$ undergoes hydrolysis to form $C_8H_{10}(l)$. The experimental aqueous heat of reaction (ΔH_{rxn}) for the step $M_2C_8H_8(s) + 2H_2O(l) \rightarrow 2M^+(aq) + 2OH^-(aq) + C_8H_{10}(l)$ ($M = Li^+$, Na^+, and K^+) was found to be -37.3, -33.3, and -28.8 kcal/mol, respectively.[38-39] The calculated ΔG for $C_8H_8^{2-}$ hydrolysis at pH 7 ($2H_2O(l) + C_8H_8^{2-}(aq) \rightarrow C_8H_{10}(l) + 2OH^-(aq)$) is -34.7 kcal/mol (further details given below). The dianion $B_{12}H_{12}^{2-}$ does not undergo hydrolysis.

In the volumetric approach using the Jenkins Formula,[22d-22f] lattice energies (U_{POT}),

enthalpy corrections, and solid entropies were calculated by the sum of cation and anion

thermodynamic volumes (V_m) (eq 1, 2, and 3).

$$U_{POT} = 2I(\alpha V_m^{1/3} + \beta) \qquad (1)$$

$$\Delta H_L = U_{POT} + [p(n_M/2-2) + q(n_X/2-2)]RT \qquad (2)$$

$$S_{298}^o = 325*V_m + 3.6 \qquad (3)$$

For M_2X_1 crystal systems, α, β, and I are 39.55 nm·kcal/mol, -7.12 kcal/mol, constant 3 while p,

q, n_M, and n_X are constants 2, 1, 3, and 6, respectively.[22d]

The ionic volumes of Li^+, Na^+, and K^+ are 0.0067, 0.0158, and 0.0277 nm^3, respectively

while ionic volumes of CO_3^{2-} and SO_4^{2-} are 0.0426 and 0.0611 nm^3, respectively.[22h] The ionic

volume of $C_8H_8^{2-}$ and $B_{12}H_{12}^{2-}$ are 0.1868 and 0.2950 nm^3, as determined by *ab initio*

computation (0.001 e/$bohr^3$ density envelop, using Gaussian03[30] keyword "VOLUME").

Geometries and electron densities of $C_8H_8^{2-}$ and $B_{12}H_{12}^{2-}$ are taken from the *ab-initio* results by

M05-2X/6-311++G(3df,2pd) and M05-2X/aug-cc-pVTZ, respectively.

For the Born-Haber cycle, I use enthalpies from the NIST chemistry webbook followed

by entropy corrections to evaluate free energies.[37] Literature values of ΔH_f for the monoanions

(CO_3^-, SO_4^-, and $C_8H_8^-$) were combined with entropies at the G4 level of theory[40] to calcuate free

energies. If ΔH_f was not available in the literature, I applied an isodesmic equation at the G4

level of theory.[41] For the electron affinity of a monoanion, an adiabatic energy difference

between the monoanion radical and dianion was calculated at the G4 level of theory. A "bound" electron attachment was computed for CO_3^-, SO_4^-, and $C_8H_8^-$ at the CCSD(T)/G4 level of theory by using a series of dielectric medium calculations. Propagator theory (Outer Valence Green's Function), an alternative method to calculate electron attachment or detachment energies, was used to compare with CCSD(T)/G4 calculations.[42] The partial third-order (P3) of the quasiparticle theory with the aug-cc-pVQZ basis set was applied to CO_3^{2-} and SO_4^{2-} while the aug-cc-pVTZ basis set was applied to $C_8H_8^{2-}$ with geometry and ZPE corrections taken from B3LYP/GTBas3 (G4 level of theory). I used the β–LUMO orbital energy of the monoanion in the dianion geometry using the partial third-order (P3) of the quasiparticle theory for the adiabatic electron attachment.

For ΔG_{latt} of Scheme 2, I applied an atomization scheme to determine the gaseous ΔH_f for M_2CO_3 (M = Li^+, Na^+, and K^+) since the value was not available in the NIST webbook.[43] I found the most stable geometry of gaseous Li_2CO_3 to be C_{2v} symmetry[44] and used that point group to determine the geometry of Na_2CO_3 and K_2CO_3. If the crystal structure was available, I used periodic *ab initio* computations to determine the ΔE_{coh}, the energy to release one molecular unit from one unit cell of the ionic crystal (eq 4).

$$\Delta E_{coh} = E_{unit} - E_{bulk}/N_{unit} \tag{4}$$

The energy of one molecular unit is E_{unit} while E_{bulk} is the total energy of one crystal unit cell and N_{unit} is the number of molecular units in a crystal unit cell. I performed total energy calculations of a unit cell with a 4*4*4 K-point grid. The BLYP, PBE, PW91, PZ functionals and the PBE-D (PBE functional with Grimme's dispersion correction) were applied. All pseudopotentials in this

study are ultrasoft or norm-conserving.   The ΔE_{coh} calculations for M_1Cl ($M = Li^+$, Na^+, and K^+) were performed for comparison. The crystal structure of LiCl is the α-form, which is exclusively available above -30°C.[45] I selected the crystal structures of M_2SO_4 ($M = Li^+$, Na^+, and K^+) at ambient conditions.[46] The ΔE_{coh} calculations for M_2CO_3 ($M = Li^+$, Na^+, and K^+) were not performed since the Na_2CO_3 crystal is disordered[47] and the K_2CO_3 molecular geometry in the unit cell is not well reproduced. The anhydrous crystal structure of $M_2C_8H_8$ ($M = Li^+$, Na^+, and K^+) is not known but $K_2C_8H_8 \cdot$diglyme and $K_2C_8H_8 \cdot (THF)_3$ are available.[48] The crystal structures of $M_2B_{12}H_{12}$ ($M = Li^+$, Na^+, and K^+), which have recently been solved, were subjected to ΔE_{coh} calculations.[49] For the molecular unit in the gas phase, the gaseous geometry of M_2X_1 was obtained in a 20*20*20 Å box with fixed cell parameters. The geometry optimization was performed with an energy cutoff of 40 Ry. All periodic boundary calculations were done using the Quantum-Espresso Package 4.2.1.[50] For the zero-point energy (ZPE) and entropy (TΔS) contributions to the free energy of the solid, I used the PM6 semi-empirical method[51] for the cluster model of the crystal unit cell. Sherwood[52] summarizes the missing terms when I apply gas phase vibration spectra to the solid. A number of entirely new bands, which are in the low frequency region (< 800 cm^{-1}), are missed in this approach. For the metal/metal oxide couples (Ru/RuO_2 or Ir/IrO_2), *ab initio* computation for the solid ignored the ZPE and entropy correction since these contributions were less than 2.3 kcal/mol.[53] However, the ZPE contribution (ΔE_{ZPE}) for the $\Delta\Delta G_f(\Delta G_{coh})$ in Scheme 2 by PM6 is usually 1 or 2 kcal/mol while the entropy correction from the TΔS term is about 10 kcal/mol. For the cohesive free energy (ΔG_{coh}) at 298.15 K, the thermal correction energy between solid and gas phases should be applied (2RT).[54] However, given the large uncertainty in the calculation of ΔG_{coh}, the small correction is omitted from our calculations.[22g,54] The lattice free energy notation ΔG_{latt-1}, ΔG_{latt-2}, and ΔG_{latt-3} represent ΔG_{latt} (1)

obtained from the Jenkins formula (eqs. 1-3), ΔG_{latt} (2) obtained from the $(\Delta\Delta G + \Delta G_{gas})$

(Scheme 2), and ΔG_{latt} (3) obtained from the Born-Haber cycle (Scheme 1), respectively.

4.3 Results

The sum of $\Delta G_{solv}(M^+X^-)$ and ΔG_{latt} (ΔG_{latt-1}, ΔG_{latt-2}, or ΔG_{latt-3}) yields the free energies

of dissolution (ΔG^o_{diss}) for M_1X_1 ($M = Li^+$, Na^+, K^+ with $X = F^-$, Cl^-, Br^-, and I^-) salts (Table 3).

The $\Delta G_{solv}(M^+X^-)$ and ΔG_{latt-3} combination is the most reliable method of computing ΔG^o_{diss} for

M_1X_1 salt systems since it depends only on reliable experimental data. However, the

$\Delta G_{solv}(M^+X^-)$ and ΔG_{latt-2} combination also give ΔG^o_{diss} free energies which are in very close

agreement ($\pm$ 1.6 kcal/mol maximum deviation from ΔG_{latt-3}). However, Jenkins formula

substantially underestimates all ΔG_{latt} values for M_1X_1 salts except for KCl, KBr, and KI (Table

3). With the same cation, smaller anions produce larger errors, while smaller cations produce

larger errors with the same anion. For the less soluble salts, LiF and NaF, the underestimation of

ΔG_{latt-1} is substantial (-22.2 and -17.4 kcal/mol, respectively). The ΔG_{latt-1} values are determined

with eqs. 1-3 and radii from the Jenkins group.[22] However, different formula and radii have been

suggested in the past, some of which have yielded more accurate values of ΔG_{latt} for

M_1X_1.[22a,22b,22h]

Table 3. Dissolution free energy (ΔG^o_{diss}) by ΔG_{latt-1} (Jenkins formula), ΔG_{latt-2} ($\Delta\Delta G + \Delta G_{gas}$), and ΔG_{latt-3} (Born-Haber cycle) for M_1X_1 (M = Li$^+$, Na$^+$, and K$^+$; X = F$^-$, Cl$^-$, Br$^-$, and I$^-$) salts[a]

M_1X_1	ΔG_{latt-3}[b] (Born-Haber)	ΔG^o_{diss} (ΔG_{latt-1})[c,e,h]	ΔG^o_{diss} (ΔG_{latt-2})[d,f]	ΔG^o_{diss} (ΔG_{latt-3})[g]
LiF	233.1	-18.1(-22.2)	2.7(-1.4)	4.1(0.0)
LiCl	189.5	-22.4(-12.6)	-10.8(-1.0)	-9.8(0.0)
LiBr	179.6	-24.7(-11.4)	-14.9(-1.6)	-13.3(0.0)
LiI	166.5	-28.3(-10.9)		-17.4(0.0)
NaF	204.9	-16.2(-17.4)	-0.5(-1.6)	1.2(0.0)
NaCl	171.7	-9.4(-7.1)	-3.3(-1.0)	-2.3(0.0)
NaBr	163.7	-9.5(-5.6)	-4.4(-0.5)	-3.9(0.0)
NaI	152.3	-10.5(-4.2)		-6.3(0.0)
KF[i]	181.2	-17.6(-12.1)	-3.8(1.6)	-5.5(0.0)
KCl[i]	155.3	-3.6(-2.1)	-2.2(-0.7)	-1.5(0.0)
KBr[i]	148.8	-2.1(-0.5)	-2.9(-1.3)	-1.6(0.0)
KI[i]	139.2	-0.9(1.4)		-2.3(0.0)

[a]The solvation free energy of salt ($\Delta G_{solv}(M^+X^-)$) comes from reference 3i. For 1 atm standard state, 3.78 kcal/mol (1.89*2) of correction should be applied final ΔG^o_{diss}. [b]All experimental values for Born-Haber cycle are taken from the NIST chemistry webbook. [c]Ion volumes are taken from reference 22h and entropy comes from NIST chemistry webbook. [d]Free energy differences ($\Delta\Delta G$) are taken from NIST chemistry webbook while ΔG_{gas} values are taken from the average of four different DFT functionals. [e]Value in parentheses is the difference between ΔG_{latt-1} (Jenkins formula) and ΔG_{latt-3} (Born-Haber). [f]Value in parentheses is the difference between ΔG_{latt-2} ($\Delta\Delta G + \Delta G_{gas}$) and ΔG_{latt-3} (Born-Haber). [g]Value in parentheses is the difference between ΔG_{latt-3} (Born-Haber) and ΔG_{latt-3} (Born-Haber). [h]The equations of Jenkins formula for M_1X_1 salts are $U_{POT} = 2(28.0*V_m + 12.4)$, $\Delta H_L = U_{POT} - RT$ and Solid entropies of M_1X_1 salts are taken from NIST webbook. [i]ΔG_{gas} is computed at the DFT/6-311++G(3df,2pd) level for potassium-containing molecules.

Table 4 summarizes $\Delta G_{solv}(X^{2-})$ in an aqueous solution by the CPCM method with three

different cavity sets. In the same cavity set, the M05-2X functional always gives the most

negative $\Delta G_{solv}(X^{2-})$ and the Pauling cavity set always gives the most negative $\Delta G_{solv}(X^{2-})$ among

the three cavity radii sets except for $\Delta G_{solv}(B_{12}H_{12}^{2-})$. The UFF cavity set gives the smallest

$\Delta G_{solv}(X^{2-})$ for CO_3^{2-} and SO_4^{2-} while the UAKS cavity set gives the smallest $\Delta G_{solv}(X^{2-})$ for

$C_8H_8^{2-}$ and $B_{12}H_{12}^{2-}$ (Table 4).

Table 4.   Solvation free energies (ΔG_{solv}) of dianion (CO_3^{2-}, SO_4^{2-}, $C_8H_8^{2-}$, and $B_{12}H_{12}^{2-}$) with

aug-cc-pVTZ basis set by three different cavity sets for CPCM solvation in kcal/mol at

298.15 K[a]

		UFF	UAKS	Pauling
CO_3^{2-}	B3LYP	-244.4(-246.5)	-255.1(-257.4)	-262.9(-265.3)
	PBE	-241.5(-243.9)	-251.7(-254.6)	-258.6(-261.5)
	BVP86	-242.4(-244.7)	-252.8(-255.5)	-259.9(-262.7)
	M05-2X	-248.5(-250.1)	-259.9(-261.6)	-269.0(-271.0)
SO_4^{2-}	B3LYP	-225.6(-227.8)	-234.0(-236.2)	-241.5(-244.2)
	PBE	-223.7(-226.3)	-231.8(-234.4)	-238.5(-241.5)
	BVP86	-224.5(-226.9)	-232.7(-235.2)	-239.7(-242.5)
	M05-2X	-228.4(-230.2)	-237.1(-239.0)	-245.9(-248.2)
$C_8H_8^{2-}$	B3LYP	(-186.0)	(-184.2)	(-192.3)
	PBE	(-184.1)	(-182.3)	(-191.4)
	BVP86	(-187.4)	(-184.8)	(-192.8)
	M05-2X	(-192.4)	(-188.6)	(-199.4)
$B_{12}H_{12}^{2-}$	B3LYP	-148.1(-147.9)	-139.2(-139.1)	-145.8(-145.7)
	PBE	-147.2(-147.6)	-138.7(-139.5)	-145.9(-145.8)
	BVP86	-147.5(-147.8)	-138.9(-139.5)	-146.3(-146.0)
	M05-2X	-150.2(-150.4)	-140.8(-141.2)	-149.2(-149.0)

[a]Value in parentheses is done by DFT/6-311++G(3df,2pd).
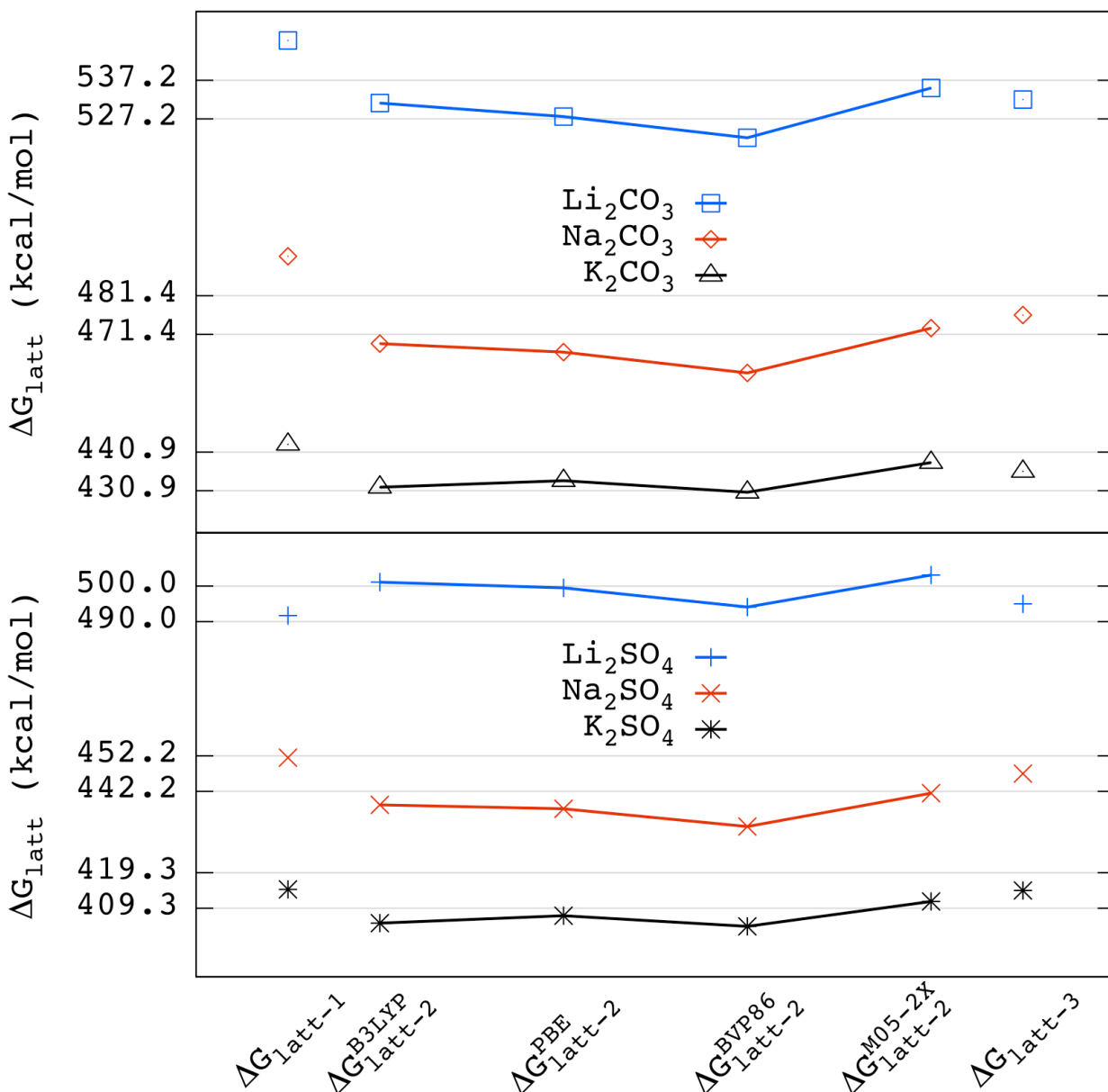
Figure 1. Lattice free energies (ΔG_{latt}) of M_2CO_3 and M_2SO_4 (M=Li^+, Na^+, and K^+) by three different methods for calculating lattice energies ($\Delta G_{latt\text{-}1}$ = Jenkins formula; $\Delta G_{latt\text{-}2}$ = $\Delta\Delta G + \Delta G_{gas}$; and $\Delta G_{latt\text{-}3}$ = Born-Haber cycle). Light lines indicate lattice energies ±5 kcal/mol from the $\Delta G_{latt\text{-}3}$ value.

The differences (ΔG_{solv}(M05-2X/Pauling) – ΔG_{solv}(M05-2X/UFF)) become smaller as the size of the dianion increases (-20.5, -17.5, -7.0, and 1.0 kcal/mol for CO_3^{2-}, SO_4^{2-}, $C_8H_8^{2-}$, and $B_{12}H_{12}^{2-}$). For $\Delta G_{solv}(X^{2-})$, the UFF and UAKS cavity sets show a strong dependence on size of the dianion but not on the shape because all dianions are highly symmetric (CO_3^{2-} in D_{3h}, SO_4^{2-} in T_d, $C_8H_8^{2-}$ in D_{8h}) or even icosahedral ($B_{12}H_{12}^{2-}$ in I_h).

The accuracy of ΔG_{latt} (relative to ΔG_{latt-3}) is presented in Figure 1 for M_2CO_3 (M = Li^+, Na^+, and K^+) where all data for ΔG_{latt-3} comes from the NIST webbook except for the ΔH_f of CO_3^-. The ΔH_f of CO_3^- (-128.7 kcal/mol) was calculated at the G4 level with the isodesmic reaction $SO_4^- + CO_2 \rightarrow SO_3 + CO_3^-$ and is close to a value reported by Wu and Tiernan[55] (-124.5±2.3 kcal/mol). The values reported for ΔH_f of CO_3^- in the NIST webbook (-116±10 kcal/mol, average of seven different estimations) is smaller by 12.7 kcal/mol.[37] Jenkins et al.[56] report a value of -76.7 kcal/mol of ΔH_f for CO_3^{2-} using the ΔH_{latt} of $CaCO_3$. From the difference in ΔH_f between CO_3^- and CO_3^{2-}, the electron affinity of CO_3^- is -52.0 kcal/mol. When the electron affinity of CO_3^- (calculated at CCSD(T)/aug-cc-pVTZ in a dielectric medium ε=100, 50, 25, 10) is extrapolated to the gas phase (ε=1, Figure 2), a value of -78.2 kcal/mol is obtained. In fact, the gas-phase extrapolated value is the same as the non-extrapolated value (see Figure 2). At highest levels of theory (CCSD(T)/aug-cc-pV5Z), the electron affinity of CO_3^- becomes -76.8 kcal/mol. For consistency, I used the electron affinity of CO_3^- at the G4 level of theory (-75.5 kcal/mol). Using an atomization scheme at the G4 level, the values of ΔH_f for gas-phase M_2CO_3 (M = Li^+, Na^+, and K^+) are -201.0, -183.4, and -188.8 kcal/mol, respectively. I computed $\Delta\Delta H_f$, which allowed the determination of $\Delta\Delta G_f$ values (74.8, 73.0, and 71.7 kcal/mol, respectively) with solid ΔH_f. The ΔG_{gas} obtained using the M05-2X functional for ΔG_{latt-2} gives the lattice free energy of M_2CO_3 (M = Li^+, Na^+, and K^+) within ±5.0 kcal/mol from the ΔG_{latt-3} value, whereas

ΔG_{latt-1} (Jenkins formula) overestimates ΔG_{latt} by 15.3, 15.2, and 7.0 kcal/mol, respectively relative to ΔG_{latt-3} (Figure 1).
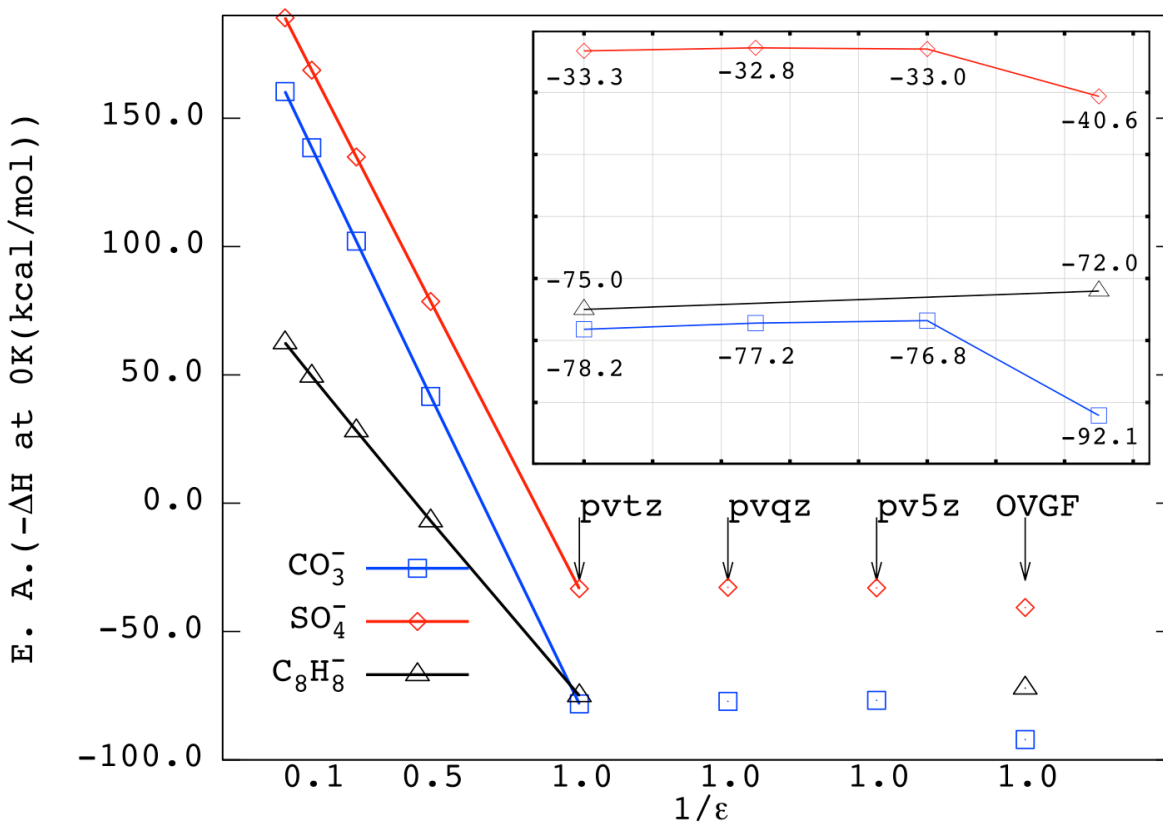
Figure 2. The electron affinity determination ($-\Delta H(0K)$ for $X^- + e^- \rightarrow X^{2-}$) of CO_3^-, SO_4^-, and $C_8H_8^-$ by three different methods (1) stabilization by solvation, (2) gaseous state using CCSD(T)/aug-cc-pV(T-5)Z, and (3) the partial third-order (P3) of quasiparticle theory with aug-cc-pVQZ for CO_3^- and SO_4^- and aug-cc-pVTZ for $C_8H_8^-$. The geometry of the monoanion is based on B3LYP/GTBas3 (part of G4 level of theory).

Figure 3 summarizes ΔG^o_{diss} of M_2CO_3 (M=Li^+, Na^+, and K^+) by three different ΔG_{latt} calculation methods combined with $\Delta G_{solv}(CO_3^{2-})$ by the Pauling cavity set and $\Delta G_{solv}(M^+)$ from

Kelly et al.[3i] The greatest consistency with experimental ΔG°_{diss} values is derived from the

M05-2X/Pauling combination, while the UFF and UAKS cavity sets give too positive values.

ΔG°_{diss} values derived from ΔG_{latt-3} and $G_{solv}(CO_3^{2-})$ from the M05-2X/Pauling method differ

from ΔG°_{diss} by 7.7, 7.7, and 5.7 kcal/mol, respectively (see $\Delta G^{\circ}_{diss}{}^{b}$ in Table 2). The M05-

2X/Pauling method computes the pK_{a2} of H_2CO_3 to be 14.3 ($\Delta G_{aq}{}^2$=19.3 kcal/mol)

corresponding to an experimental value of 10.3 ($\Delta G_{aq}{}^2$=14.1 kcal/mol), which corresponds to an

underestimation of the $\Delta G_{solv}(CO_3^{2-})$ by 5.2 kcal/mol.[10]
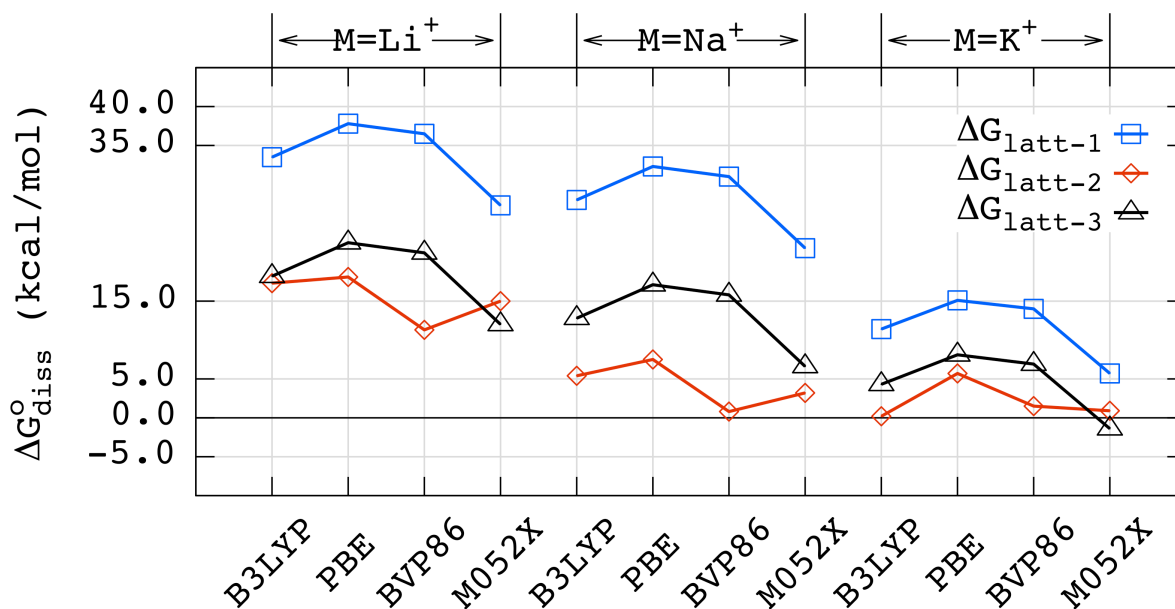
Figure 3. Dissolution free energies (ΔG°_{diss}) of M_2CO_3 ($M=Li^+$, Na^+, and K^+) by three different

methods for calculating lattice energies (ΔG_{latt-1} = Jenkins formula; ΔG_{latt-2} = $\Delta\Delta G$ +

ΔG_{gas}; and ΔG_{latt-3} = Born-Haber cycle) combined with the solvation free energy

(ΔG_{solv}) of CO_3^{2-} by the Pauling cavity set.

If this difference is applied to the ΔG°_{diss} of M_2CO_3, the difference between experimental ΔG°_{diss}

and calculated ΔG°_{diss} would be 2.5, 2.5, and 0.5 kcal/mol for M_2CO_3 ($M = Li^+$, Na^+, and K^+),

respectively. The M05-2X functional, which is an improved density functional for dispersion interaction by kinetic energy density,[29] gives the best ΔG^o_{diss} among four DFT functionals.

The instability of $SO_4^{2-}(g)$ was discussed by several groups.[19b,57] Zheng et al.[20] reported -25.4 kcal/mol for the adiabatic electron affinity of $SO_4^-(g)$ by an atomization scheme with a MP2/CBS approach. Boldyrev and Simons[57a] suggested -30.9 kcal/mol for the vertical electron detachment energy of SO_4^{2-} using QCISD(T). In the present work, the G4 level of theory gives -32.8 kcal/mol ($SO_4^- + e^- \rightarrow SO_4^{2-}$) while CCSD(T)/aug-cc-pVTZ extrapolated in varying dielectric constants gives -33.3 kcal/mol (Figure 2). At our highest level of theory (CCSD(T)/aug-cc-pV5Z), the electron affinity of SO_4^- becomes -32.8 kcal/mol.
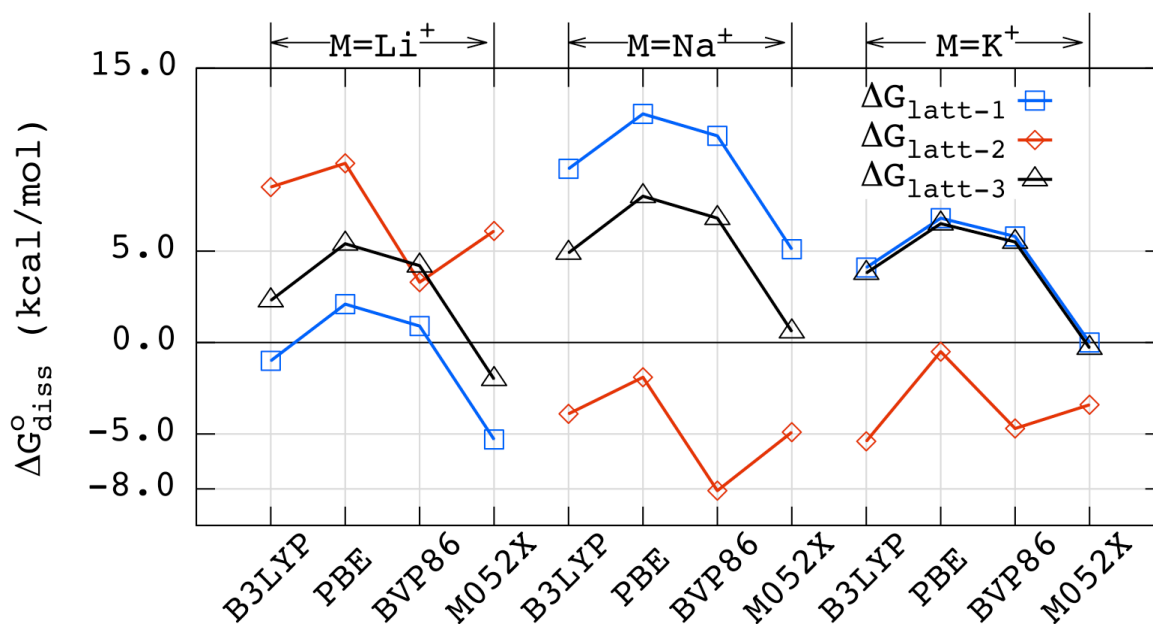
Figure 4. Dissolution free energies (ΔG^o_{diss}) of M_2SO_4 (M = Li^+, Na^+, and K^+) by three different methods for calculating lattice energies (ΔG_{latt-1} = Jenkins formula; ΔG_{latt-2} = $\Delta\Delta G$ + ΔG_{gas}; and ΔG_{latt-3} = Born-Haber cycle) combined with the solvation free energy (ΔG_{solv}) of SO_4^{2-} by the Pauling cavity set.

Relative to ΔG_{latt-3} values, ΔG_{latt-2} underestimates the lattice free energy of Na_2SO_4 and

K_2SO_4 but overestimates it for Li_2SO_4 (Figure 1), but in every case, the M05-2X functional is the

best DFT choice. For M_2SO_4 (M = Li^+, Na^+, and K^+), the Jenkins formula (ΔG_{latt-1}) is within

±5.0 kcal/mol of ΔG_{latt-3} (Figure 1). For every estimation method of ΔG_{latt}, the M05-2X/Pauling

combination yields the best prediction value of ΔG^o_{diss} for M_2SO_4 (M = Li^+, Na^+, and K^+) (Figure

4 and Table 2).

To compute ΔG_{latt-3} for $M_2C_8H_8$ (M = Li^+, Na^+, and K^+), I use $\Delta H_f(s)$ of $Na_2C_8H_8$ (-27.5

kcal/mol) and $K_2C_8H_8$ (-32.0 kcal/mol) from Stevenson et al.[39a] while $\Delta H_f(s)$ of $Li_2C_8H_8$ (-33.9

kcal/mol) comes from a private communication cited in the NIST webbook.[37] The entropy value

of $M_2C_8H_8(s)$ is calculated by Jenkins formula (eq 3).[22e] For the electron affinity of $C_8H_8^-$,

Dewar et al.[58] reported -80.9 kcal/mol by MINDO/2 method while Baik et al.[59] suggested -79.1

and -85.1 kcal/mol by DFT and Miller et al.[60] reported -61.6 kcal/mol by G2(MP2). In our

computation, CCSD(T)/aug-cc-pVTZ//G4 gives -75.0 kcal/mol (-74.3 kcal/mol at the G4 level of

theory) while the partial third-order (P3) of quasiparticle theory approach gives -72.0 kcal/mol

(Figure 2). Dominikowska and Palusiak[61] discussed the stability and aromaticity of $C_8H_8^{2-}$

including artifacts caused by using diffuse functions to describe the dianion. Despite the large

dianion size, the electron affinity of $C_8H_8^-$ (-74.3 kcal/mol) is similar to that of CO_3^- (-78.2

kcal/mol), which implies that the electronegativity of the atoms is more important than the size

of dianion (Figure 2). Sommerfeld[19a,62] reports the gas-phase lifetime of $C_8H_8^{2-}$ and CO_3^{2-} to be

6 fs and 6500 fs, respectively. For the ΔG^o_{diss} of $M_2C_8H_8$ (M = Li^+, Na^+, and K^+), the ΔG_{latt-3} and

$\Delta G_{solv}(C_8H_8^{2-})$ by the M05-2X/Pauling combination give 20.0, 19.3, and 19.7 kcal/mol,

respectively (Figure 5). While the reaction $M_2C_8H_8(s) \rightarrow 2M^+(aq) + C_8H_8^{2-}(aq)$ is very

nonspontaneous, the protonation of the $C_8H_8^{2-}$ can provide additional driving force ($C_8H_8^{2-}$(aq) + $2H_2O$(l) → $2OH^-$(aq) + C_8H_{10}(l)) (Scheme 5).
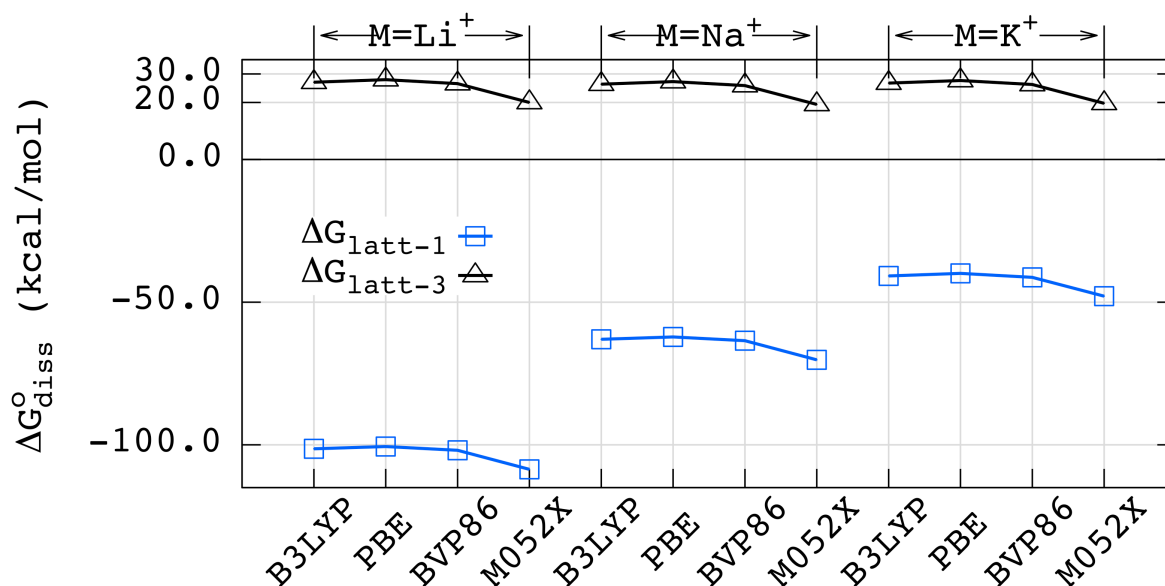
Figure 5. Dissolution free energies (ΔG°_{diss}) of $M_2C_8H_8$ (M = Li^+, Na^+, and K^+) by two different methods for calculating lattice energies (ΔG_{latt-1} = Jenkins formula; ΔG_{latt-3} = Born-Haber cycle) combined with the solvation free energy (ΔG_{solv}) of $C_8H_8^{2-}$ by the Pauling cavity set.
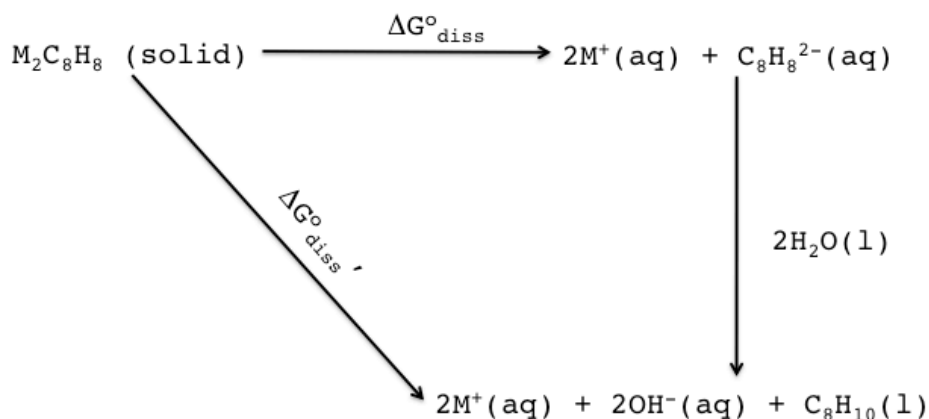
Scheme 5. Dissolution and protonation process of $M_2C_8H_8$(s) + $2H_2O$(l) → $2M^+$(aq) + $2OH^-$(aq) + C_8H_{10}(l) (M=Li^+, Na^+, and K^+).

The overall dissolution free energy (ΔG^o_{diss}') of $M_2C_8H_8$ at pH 7 ($M_2C_8H_8(s) + 2H_2O(l) \rightarrow$

$2M^+(aq) + C_8H_{10}(l) + 2OH^-(aq)$) should be evaluated to explain the dissolution of $M_2C_8H_8(s)$

(Scheme 5). Using M05-2X/6-311++G(3df,2pd) with CPCM/Pauling cavity set and -264.0

kcal/mol for $\Delta G_{solv}(H^+)$, the free energy change $-(\Delta G_{aq}^1 + \Delta G_{aq}^2)$ of $2H^+(aq) + C_8H_8^{2-}(aq) \rightarrow$

$C_8H_{10}(aq)$ is -34.7 kcal/mol at pH 7 (Appendix 2). The overall process

$\Delta G^o_{diss}{}' = \Delta G^o_{diss} - (\Delta G_{aq}^1 + \Delta G_{aq}^2)$ is predicted to be spontaneous by -14.7, -15.4, and -15.0

kcal/mol for $M_2C_8H_8(s)$, M = Li^+, Na^+, K^+, respectively (ΔG_{latt-3} and M05-2X/Pauling). On the

other hand, the ΔG_{latt-1} and $\Delta G_{solv}(C_8H_8^{2-})$ by the M05-2X/Pauling combination produces ΔG^o_{diss}

values for $M_2C_8H_8(s) \rightarrow 2M^+(aq) + C_8H_8^{2-}(aq)$ that are too much negative (-108.6, -70.2,

and -47.9 kcal/mol, respectively, Figure 5).[23a,23c] Indeed, Byrd and Rice[13d] reported that further

reoptimization of the Jenkins model would be required to reduce the error in the lattice energies

of M_2X_1 or M_2X_2 salts.
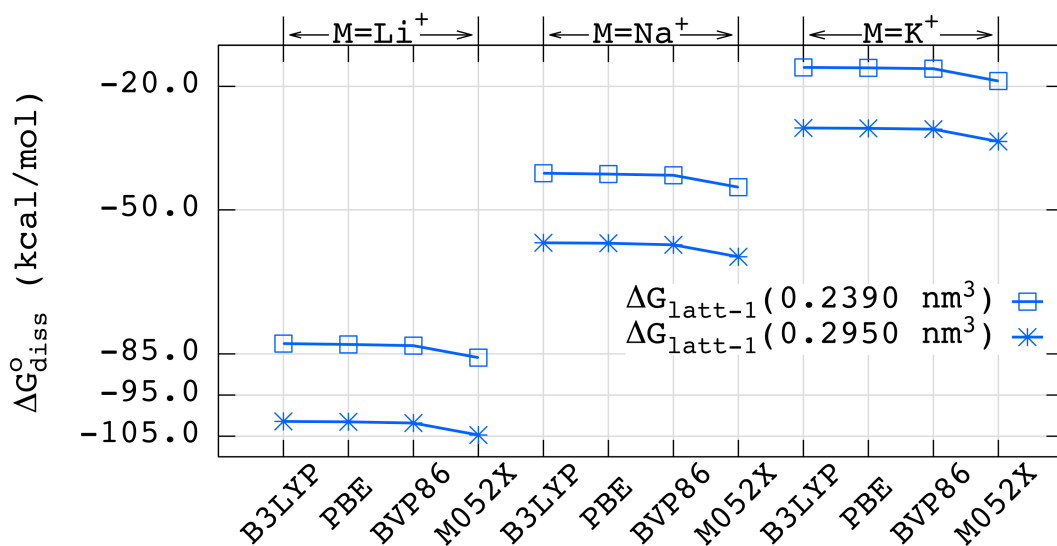
Figure 6. Dissolution free energies (ΔG^o_{diss}) of $M_2B_{12}H_{12}$ (M = Li^+, Na^+, and K^+) by lattice

energy estimation of ΔG_{latt-1} = Jenkins formula combined with the solvation free

energy (ΔG_{solv}) of $B_{12}H_{12}^{2-}$ by the Pauling cavity set.

While the $M_2B_{12}H_{12}$ salts (M = Li$^+$, Na$^+$, and K$^+$) are very stable in the solid and aqueous phase,[26c,27,63] the experimental heats of formation (ΔH_f) of the solids are still not known. A previous application of the Jenkins formula used a volume for $B_{12}H_{12}^{2-}$ of 0.2390 nm^3 that came from the 0.001 au contour of electron density,[23a] which is slightly smaller than our value of 0.2950 nm^3 (Figure 6). However, the small 0.056 nm^3 volume difference leads to more than 14.0 kcal/mol of difference in $\Delta G_{latt-1}(\Delta G^o_{diss})$ of $M_2B_{12}H_{12}$ (Figure 6).

If ΔG_{latt-1} is used with the 0.2950 nm^3 volume of $B_{12}H_{12}^{2-}$, then the ΔG^o_{diss} values for $M_2B_{12}H_{12}$ (M = Li$^+$, Na$^+$, and K$^+$) are computed to be much too spontaneous (-104.7, -61.4, and -33.4 kcal/mol, respectively) since the experimental values vary between -1.9 to -2.7 kcal/mol (Table 2). Again, the large variation in ΔG^o_{diss} for Li$^+$, Na$^+$, and K$^+$ indicates that no single modification of the $B_{12}H_{12}^{2-}$ volume can improve the ΔG^o_{diss} values using the Jenkins formula (Figure 6). Since the experimental ΔH_f of $M_2B_{12}H_{12}$(s) (M = Li$^+$, Na$^+$, and K$^+$) are not available, I could not compute ΔG_{latt-2} from $\Delta\Delta H_f$ (between solid and gas) Therefore, I computed ΔG_{latt-2} by first computing the cohesion energies ΔE_{coh} from the crystal structures (Table 5).

Using experimental $\Delta\Delta H_f$ values, I first accessed the computed ΔE_{coh} values since $\Delta E_{coh} = \Delta\Delta H_f$ - zero-point energies. The ΔE_{coh} for MCl (M = Li$^+$, Na$^+$, and K$^+$), by BLYP functional underestimates the $\Delta\Delta H_f$ of LiCl and NaCl and overestimates it for KCl. Using the dispersion-corrected PBE functional (PBE-D), the underestimation is adjusted by more than 7.5 kcal/mol for MCl (M = Li$^+$, Na$^+$, and K$^+$) (Table 5). The PZ and PW91 functionals give a reasonable ΔE_{coh} ($\Delta\Delta H_f$) estimation. However, ΔE_{coh} obtained from every DFT functional underestimates $\Delta\Delta H_f$ of Li_2SO_4 and overestimates $\Delta\Delta H_f$ of K_2SO_4 while ΔE_{coh} of Na_2SO_4 depends on the choice of DFT functional. The best ΔE_{coh} for M_2SO_4 (M = Li$^+$, Na$^+$, and K$^+$) comes from PZ, PW91, and PBE functional, respectively. The scaled dispersion corrections for M_2SO_4 (M = Li$^+$, Na$^+$,

and K$^+$) become more than 16.0 kcal/mol (PBE → PBE-D). For comparison, the dispersion

interaction in the benzene crystal is 13.3 kcal/mol from the DFT-D2 method, 12.0 kcal/mol from

the symmetry adapted perturbation theory (SAPT) whereas the experimental value is 10.3

kcal/mol.[11f,11g]

Table 5.   A comparison between experimental heats of formation differences ($\Delta\Delta H_f$, kcal/mol)

and cohesive energy (ΔE_{coh}, kcal/mol) by periodic boundary calculation

	$\Delta\Delta H_f{}^a$	(ΔE_{coh} - $\Delta\Delta H_f$)				
		BLYP	PBE	PBE-D^c	PZ	PW91
LiCl	50.8	-10.7	-26.3	-14.3	4.4	-4.3
NaCl	54.9	-11.6	-6.2	4.7	1.1	-4.8
KCl	53.1	6.9	-1.9	5.6	6.9	
Li$_2$SO$_4$	94.3	-32.4	-72.1	-55.9	-4.3	-16.5
Na$_2$SO$_4$	84.6	-19.4	-6.5	19.1	7.2	-1.9
K$_2$SO$_4$	82.1	18.2	6.9	30.8	27.5	
Li$_2$B$_{12}$H$_{12}$	61.8^b	-33.1	-45.5	-4.7	-1.4	-19.7
Na$_2$B$_{12}$H$_{12}$	54.5^b	-12.5	-1.5	36.1	18.3	-0.1
K$_2$B$_{12}$H$_{12}$	52.0^b	56.3	15.1	47.7	35.1	

^{a}The difference of ΔH_f between gas and solid state. The values for each salt come from the NIST
webbook. ^{b}The value is derived by the difference between ΔH_{gas} of M$_2$B$_{12}$H$_{12}$ (M = Li$^+$, Na$^+$,
and K$^+$) and presumable lattice enthalpies (ΔH_{latt}) (see text), where $\Delta G^o{}_{diss}$=0 is arrived with
ΔG_{solv}(B$_{12}$H$_{12}{}^{2-}$) by the Pauling cavity sets. The zero-point and entropy correction are
determined from the PM6 semi-empirical method with unit cell cluster model of M$_2$B$_{12}$H$_{12}$ (M =
Li$^+$, Na$^+$, and K$^+$). ^{c}Dispersion energy correction made by London formula. See reference 11b.

Recently, Grimme and coworkers have developed the DFT-D3 method which corrects for the

overbinding in the M$^+$·Benzene complex (M = Li$^+$, Na$^+$, and K$^+$).[12c] However, the use of DFT-

D3 in our system did not produce better results (data is not presented) and the Grimme group is

developing values suitable for ionic systems.[64] It is also possible that the interaction energy of

cations and anions is overestimated by DFT methods since it is well known that DFT

exaggerates charge equalization.[65] In this case, a dispersion correction may possibly appear to "overcorrect" and produce ΔG_{coh}, which are too binding.

To estimate ΔG_{latt} for $M_2B_{12}H_{12}$, I used the M05-2X/Pauling cavity set and assumed that $\Delta G°_{diss}=0$ (i.e. reversing the process in Scheme 3). The actual $\Delta G°_{diss}$ values for $M_2B_{12}H_{12}$ (M = Li^+, Na^+, and K^+) gathered from solubility data are slightly negative (Table 2). From ΔG_{latt}, I computed ΔH_{latt} by subtracting the ZPE and $T\Delta S$ corrections (406.6, 357.5, and 325.3 kcal/mol, respectively, Scheme 6).

$$2M^+(g) + 2e^- + B_{12}H_{12}(g)$$

$$2*\Delta H_{I.P.} \quad (5) \begin{array}{l} Li:248.7 \\ Na:237.0 \\ K: 200.2 \end{array}$$

$$-135.7 \ (6) \quad \Delta H_{E.A.}$$
$$2M^+(g) + B_{12}H_{12}{}^{2-}(g) \quad (1^{st}\&2^{nd})$$

$$2M(g) + B_{12}H_{12}(g)$$

$$\Delta H_f \quad (4) \quad 47.6$$

$$2M(g) + 12B(s) + 6H_2(g)$$

$$2*\Delta H_{sub} \quad (3) \begin{array}{l} Li:76.1 \\ Na:51.3 \\ K: 42.5 \end{array}$$

$$2M(s) + 12B(s) + 6H_2(g)$$

$$-2*\Delta H_f \quad (2) \begin{array}{l} Li:43.3 \\ Na:27.0 \\ K: 27.6 \end{array}$$

$$\begin{array}{l} Li:406.6 \\ Na:357.5 \ (7) \quad -\Delta H_{latt} \\ K: 325.3 \end{array}$$

$$2MH(s) + 12B(s) + 5H_2(g)$$

$$-\Delta H_{rxn} \quad (1) \begin{array}{l} Li:126.6 \\ Na:130.3 \\ K: 143.1 \end{array}$$
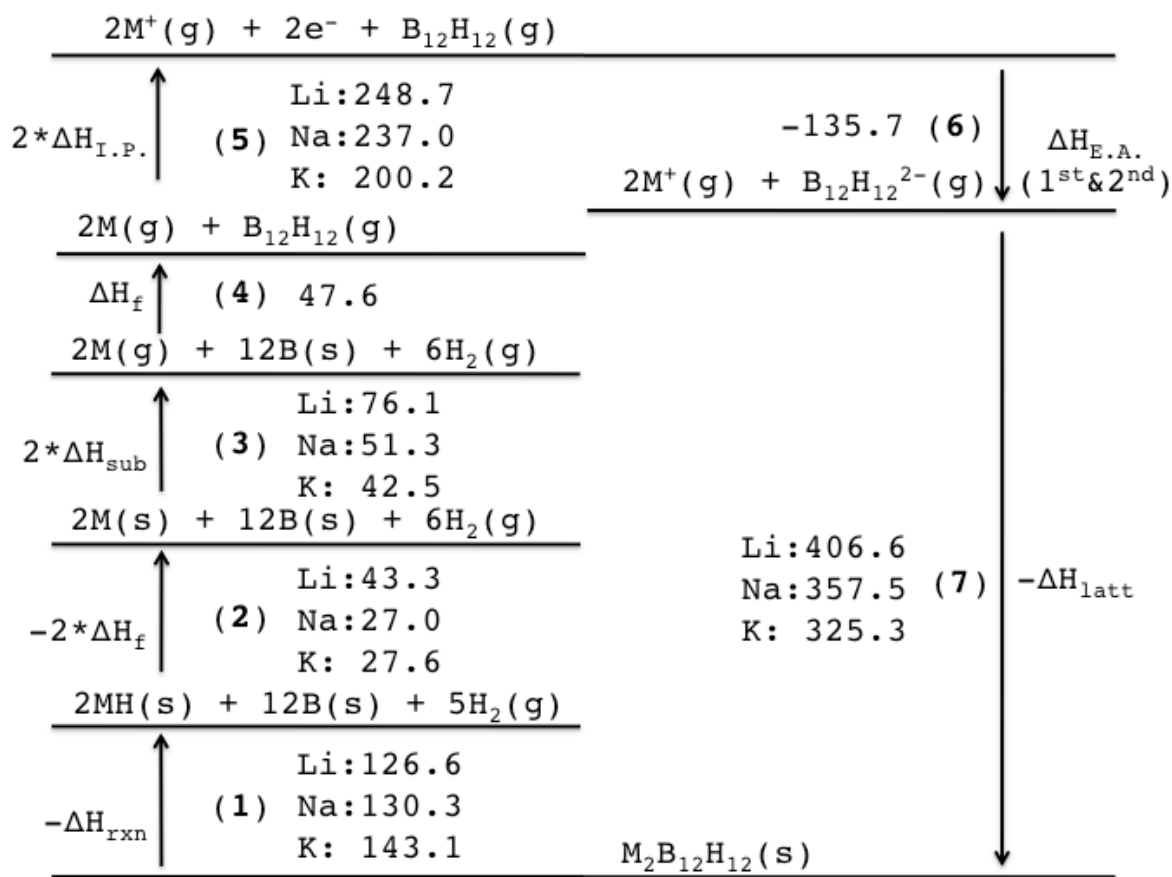
$$M_2B_{12}H_{12}(s)$$

Scheme 6. Born-Haber cycle of $M_2B_{12}H_{12}$ (M = Li^+, Na^+, and K^+) based on ΔH_{latt} values which makes $\Delta G°_{diss}=0$.

I then computed $\Delta\Delta H_f$ by combining ΔH_{latt} and computed gaseous dissociation enthalpies (ΔH_{gas})

of $M_2B_{12}H_{12}$ (M = Li^+, Na^+, and K^+; 344.8, 303.0, and 273.3 kcal/mol, respectively, average of

results by four DFT functionals) (Table 5). Based on these $\Delta\Delta H_f$ values, I find reasonable

agreement with the ΔE_{coh} of $Li_2B_{12}H_{12}$ from the PBE-D and PZ functional (Table 5). For

$Na_2B_{12}H_{12}$, the PBE and PW91 functionals give reasonable values of ΔE_{coh} while for $K_2B_{12}H_{12}$

all functionals yield too large values of ΔE_{coh}. The amount of dispersion correction from PBE to

PBE-D for $M_2B_{12}H_{12}$ (M = Li^+, Na^+, and K^+) is more than 32.0 kcal/mol and this correction is

two times larger than for M_2SO_4 (M = Li^+, Na^+, and K^+) (Table 5). However, Sedlák et al.[66]

report that the binding interaction between benzene and $B_{12}H_{12}^{2-}$ is 11.0 kcal/mol from the

CCSD(T)/CBS method and 9.2 kcal/mol from the DFT-SAPT approach. The DFT-D method

uses metal atom parameters rather than metal cations, which may exaggerate cation-cation

interactions. On the other hand, dispersion of dianion-dianion interactions may be

underestimated.

Determining the ΔH_f of $M_2B_{12}H_{12}$ (M = Li^+ and Na^+) is important because this material is

an undesirable intermediate in chemical hydrogen storage using alkali metal boranes.[25d-25f,67]

Based on the predicted crystal structure of $Li_2B_{12}H_{12}$, Ohba et al.[67] suggested 149.4 kcal/mol for

$\Delta H_{rxn}(0K)$ for the step $Li_2B_{12}H_{12}(s) \rightarrow 2LiH(s) + 12B(s) + 5H_2(g)$ while Ozolins et al.[25d] suggest

139.5 kcal/mol for ΔH_{rxn} (0K) using a different structure prediction. Scheme 6 presents a Born-

Haber cycle of $M_2B_{12}H_{12}$ (M = Li^+, Na^+, and K^+) based on ΔG^o_{diss}=0. Data for processes **2**, **3**,

and **5** are from the NIST webbook[37] while data for processes **4** and **6** are available from *ab initio*

computations. The Dixon group reported ΔH_f(298K) of $B_{12}H_{12}^{2-}$ to be -88.1 kcal/mol with a

G3B3 approach, which is the same value as I predict using G4 (-88.1 kcal/mol).[23a] The value of

$\Delta H_{rxn}(\mathbf{1})$ from Scheme 6 for $M_2B_{12}H_{12}$ (M = Li^+, Na^+, and K^+) becomes 126.6, 130.3, and 143.1

kcal/mol, respectively. The difference between our ΔH_{rxn} (**1**) and previous reported values for

$Li_2B_{12}H_{12}$ are 12.9 kcal/mol[25d] and 22.8 kcal/mol,[67] respectively.

Previous work has shown that as the size of dianion becomes larger, errors in $\Delta H_{rxn}(-\Delta H_f)$

by periodic boundary calculations become larger. For example, Ozolins et al.[25d] report 14.4

kcal/mol of ΔH_{rxn} for $MgH_2(s) \rightarrow Mg(s) + H_2(g)$ while the NIST webbook data gives 18.2

kcal/mol[37] for $-\Delta H_f$ (3.8 kcal/mol difference). By using the PBE functional, Miwa et al.[25a]

reported -38.2 kcal/mol for $\Delta H_f(0K)$ of $LiBH_4$ while the experimental value is -46.5 kcal/mol[68]

(8.3 kcal/mol difference). When the size of the anion is $B_{12}H_{12}{}^{2-}$, the difference increases to 56.2

kcal/mol. Specifically, Caputo and Züttel[25e] reported 226.1 kcal/mol for $-\Delta H_f(0K)$ of $Li_2B_{12}H_{12}$

from their standard state ($Li_2B_{12}H_{12}(s) \rightarrow 2Li(s) + 12B(s) + 6H_2(g)$) using the experimental

crystal structure[25d] while, the sum of process **1** and **2** (i.e. $-\Delta H_f$ at 298K) is 169.9 kcal/mol from

Scheme 6. Likewise, Caputo et al.[25f] reported 259.7 kcal/mol for $-\Delta H_f(0K)$ of $Na_2B_{12}H_{12}$ using

the experimental crystal structure which can be compared to 157.3 kcal/mol (i.e. $-\Delta H_f$ at 298K)

for the sum of **1** and **2** from Scheme 6 (102.4 kcal/mol difference). For $K_2B_{12}H_{12}$, our

calculations suggest 170.7 kcal/mol for $-\Delta H_f$ at 298K, which is similar to that of $Li_2B_{12}H_{12}$

(Scheme 6).

4.4 Conclusions

For the calculation of the dissolution Gibbs free energies (ΔG^o_{diss}) for M_2X_1 (M = Li^+,

Na^+, and K^+ with X = $CO_3{}^{2-}$, $SO_4{}^{2-}$, $C_8H_8{}^{2-}$, and $B_{12}H_{12}{}^{2-}$) salts, three methods for ΔG_{latt}

estimation are combined with $\Delta G_{solv}(X^{2-})$ using the CPCM solvation modeling. The $\Delta G_{solv}(X^{2-})$

obtained from the Pauling cavity set leads to a reasonable ΔG^o_{diss}. For small dianions like $SO_4{}^{2-}$,

the Jenkins formula (ΔG_{latt-1}) yields reliable ΔG^o_{diss} values when it is combined with $\Delta G_{solv}(X^{2-})$

obtained from M05-2X/Pauling cavity sets. However, the thermochemical volume of the dianion

is not easily determined by *ab initio* molecular volume calculations and the static radii cannot

yield reasonable $\Delta G^o{}_{diss}$ values when soft (large) dianions are involved. ΔG_{gas} values drived

from *ab initio* computation combined with $\Delta\Delta G_f$ values from the literature are useful to

determine ΔG_{latt} of salts but the replacement of $\Delta\Delta G_f$ by ΔG_{coh} greatly depends on the choice of

DFT functional in the periodic boundary calculations. When $\Delta G^o{}_{diss} = 0$ is assumed for

$M_2B_{12}H_{12}$ (M = Li$^+$, Na$^+$, and K$^+$), our Born-Haber cycle can be used to evaluate solid-state ΔH_f

values by computation.

4.5 References

(1)   Thompson, J. D.; Cramer, C. J.; Truhlar, D. G. *J. Phys. Chem. A* **2004**, *108*, 6532.

(2)   Conway, B. E. *Ionic hydration in chemistry and biophysics*; Elsevier: New York, **1981**.

(3)   (a) Franks, F. *Water, a comprehensive treatise*; Plenum Press: New York, **1972**. (b) Åqvist, J. *J. Phys. Chem.* **1990**, *94*, 8021. (c) Maye, P. V.; Mezei, M. *THEOCHEM* **1996**, *362*, 317. (d) Tissandier, M. D.; Cowen, K. A.; Feng, W. Y.; Gundlach, E.; Cohen, M. H.; Earhart, A. D.; Coe, J. V.; Tuttle, T. R. *J. Phys. Chem. A* **1998**, *102*, 7787. (e) Fawcett, W. R. *J. Phys. Chem. B* **1999**, *103*, 11181. (f) Rempe, S. B.; Pratt, L. R.; Hummer, G.; Kress, J. D.; Martin, R. L.; Redondo, A. *J. Am. Chem. Soc.* **2000**, *122*, 966. (g) Zhan, C.-G.; Dixon, D. A. *J. Phys. Chem. A* **2001**, *105*, 11534. (h) Asthagiri, D.; Pratt, L. R.; Ashbaugh, H. S. *J. Chem. Phys.* **2003**, *119*, 2702. (i) Kelly, C. P.; Cramer, C. J.; Truhlar, D. G. *J. Phys. Chem. B* **2006**, *110*, 16066. (j) Jensen, K. P.; Jorgensen, W. L. *J. Chem. Theory Comput.* **2006**, *2*, 1499. (k) Joung, I. S.; Cheatham, T. E. *J. Phys. Chem. B* **2008**, *112*, 9020. (l) Donald, W. A.; Williams, E. R. *J. Phys. Chem. B* **2010**, *114*, 13189. (m) Rempe, S. B.; Asthagiri, D.; Pratt, L. R. *Phys. Chem. Chem. Phys.* **2004**, *6*, 1966. (n) Burgess, J. A. *Metal Ions in Solution*; Ellis Horwood: Chichester, **1978**. (o) Noyes, R. M. *J. Am. Chem. Soc.* **1962**, *84*, 513. (p) Marcus, Y. *Biophys Chem* **1994**, *51*, 111. (q) Lamoureux, G.; Roux, B. *J. Phys. Chem. B* **2006**, *110*, 3308. (r) Yu, H.; Whitfield, T. W.; Harder, E.; Lamoureux, G.; Vorobyov, I.; Anisimov, V. M.; MacKerell Jr, A. D.; Roux, B. *J. Chem. Theory Comput.* **2010**, *6*, 774.

(4)   Latimer, W. M. *J. Am. Chem. Soc.* **1926**, *48*, 1234.

(5)   (a) Stefanovich, E. V.; Truong, T. N. *Chem. Phys. Lett.* **1995**, *244*, 65. (b) Aguilar, M. A.; Delvalle, F. J. O. *Chem. Phys.* **1989**, *129*, 439. (c) Rashin, A. A.; Namboodiri, K. *J. Phys. Chem.* **1987**, *91*, 6003.

(6)   Takano, Y.; Houk, K. N. *J. Chem. Theory Comput.* **2005**, *1*, 70.

(7)   Chipman, D. M. *J. Phys. Chem. A* **2002**, *106*, 7413.

(8)   Król, M.; Wrona, M.; Page, C. S.; Bates, P. A. *J. Chem. Theory Comput.* **2006**, *2*, 1520.

(9)   Fernandez, M. I.; Canle, M.; Garcia, M. V.; Santaballa, J. A. *Chem. Phys. Lett.* **2010**, *490*, 159.

(10)   Lee, T. B.; McKee, M. L. *Phys. Chem. Chem. Phys.* **2011**, *13*, 10258.

(11)   (a) Nabok, D.; Puschnig, P.; Ambrosch-Draxl, C. *Phys. Rev. B* **2008**, *77*, 245316. (b) Barone, V.; Casarin, M.; Forrer, D.; Pavone, M.; Sambi, M.; Vittadini, A. *J. Comp. Chem.* **2009**, *30*, 934. (c) Todorova, T.; Delley, B. *J. Phys. Chem. C* **2010**, *114*, 20523. (d) Tsuzuki, S.; Orita, H.; Honda, K.; Mikami, M. *J. Phys. Chem. B* **2010**, *114*, 6799. (e) Berland, K.; Hyldgaard, P. *J. Chem. Phys.* **2010**, *132*, 134705. (f) Beran, G. J. O.; Nanda, K. *J. Phys. Chem. Lett.* **2010**, *1*, 3480. (g) Bučko, T.; Hafner, J.; Lebègue, S.; Ángyán, J. G. *J. Phys. Chem. A* **2010**, *114*, 11814.

(12)   (a) Grimme, S.; Antony, J.; Schwabe, T.; Muck-Lichtenfeld, C. *Org. Biomol. Chem.* **2007**, *5*, 741. (b) Grimme, S. *J. Comp. Chem.* **2006**, *27*, 1787. (c) Grimme, S.; Antony, J.; Ehrlich, S.; Krieg, H. *J. Chem. Phys.* **2010**, *132*, 154104.

(13)   (a) King, C. *J. Chem. Edu.* **2005**, *82*, 1584. (b) Glasser, L.; von Szentpály, L. *J. Am. Chem. Soc.* **2006**, *128*, 12314. (c) von Szentpály, L. *J. Am. Chem. Soc.* **2008**, *130*, 5962. (d) Byrd, E. F. C.; Rice, B. M. *J. Phys. Chem. A* **2009**, *113*, 345.

(14)   Stefanovich, E. V.; Boldyrev, A. I.; Truong, T. N.; Simons, J. *J. Phys. Chem. B* **1998**, *102*, 4205.

(15)   (a) von Szentpály, L. *J. Phys. Chem. A* **2010**, *114*, 10891. (b) Cárdenas, C.; Ayers, P.; De Proft, F.; Tozer, D. J.; Geerlings, P. *Phys. Chem. Chem. Phys.* **2011**, *13*, 2285.

(16)   (a) Sablon, N.; De Proft, F.; Geerlings, P.; Tozer, D. J. *Phys. Chem. Chem. Phys.* **2007**, *9*, 5880. (b) Hajgató, B.; De Proft, F.; Szieberth, D.; Tozer, D. J.; Deleuze, M. S.; Geerlings, P.; Nyulászi, L. *Phys. Chem. Chem. Phys.* **2011**, *13*, 1663. (c) Tozer, D. J.; De Proft, F. *J. Chem. Phys.* **2007**, *127*, 034108.

(17)   (a) Puiatti, M.; Vera, D. M. A.; Pierini, A. B. *Phys. Chem. Chem. Phys.* **2009**, *11*, 9013. (b) Puiatti, M.; Vera, D. M. A.; Pierini, A. B. *Phys. Chem. Chem. Phys.* **2008**, *10*, 1394.

(18)   Jensen, F. *J. Chem. Theory Comput.* **2010**, *6*, 2726.

(19)   (a) Sommerfeld, T. *J. Phys. Chem. A* **2000**, *104*, 8806. (b) McKee, M. L. *J. Phys. Chem.* **1996**, *100*, 3473.

(20)   Zheng, W.; Lau, K.-C.; Wong, N.-B.; Li, W.-K. *Chem. Phys. Lett.* **2009**, *467*, 402.

(21)   Whitehead, A.; Barrios, R.; Simons, J. *J. Chem. Phys.* **2002**, *116*, 2848.

(22)   (a) Roobottom, H. K.; Jenkins, H. D. B.; Passmore, J.; Glasser, L. *J. Chem. Edu.* **1999**, *76*, 1570. (b) Jenkins, H. D. B.; Roobottom, H. K.; Passmore, J.; Glasser, L. *Inorg. Chem.* **1999**, *38*, 3609. (c) Jenkins, H. D. B.; Glasser, L. *Inorg. Chem.* **2002**, *41*, 4378. (d)

Jenkins, H. D. B.; Tudela, D.; Glasser, L. *Inorg. Chem.* **2002**, *41*, 2364. (e) Jenkins, H. D. B.; Glasser, L. *Inorg. Chem.* **2003**, *42*, 8702. (f) Glasser, L.; Jenkins, H. D. B. *Chem. Soc. Rev.* **2005**, *34*, 866. (g) Glasser, L.; Jenkins, H. D. B. *J. Chem. Eng. Data* **2011**, *56*, 874. (h) Glasser, L.; Jenkins, H. D. B. *Inorg. Chem.* **2008**, *47*, 6195. (i) Jenkins, H. D. B.; Liebman, J. F. *Inorg. Chem.* **2005**, *44*, 6359.

(23)   (a) Nguyen, M. T.; Matus, M. H.; Dixon, D. A. *Inorg. Chem.* **2007**, *46*, 7561. (b) Ishigaki, T.; Nikolic, Z. S.; Watanabe, T.; Matsushita, N.; Yoshimura, M. *Solid State Ionics* **2009**, *180*, 475. (c) Geis, V.; Guttsche, K.; Knapp, C.; Scherer, H.; Uzun, R. *Dalton Trans.* **2009**, 2687. (d) Boeré, R. T.; Kacprzak, S.; Keβler, M.; Knapp, C.; Riebau, R.; Riedel, S.; Roemmele, T. L.; Rühle, M.; Scherer, H.; Weber, S. *Angew. Chem. Int. Ed.* **2011**, *50*, 549.

(24)   (a) Jenkins, H. D. B.; Thakur, K. P. *J. Chem. Edu.* **1979**, *56*, 576. (b) Lide, D. R. *CRC Handbook of Chemistry and Physics*; CRC Press: New York, **2008**.

(25)   (a) Miwa, K.; Ohba, N.; Towata, S.; Nakamori, Y.; Orimo, S. *Phys. Rev. B* **2004**, *69*, 245120. (b) Frankcombe, T. J.; Kroes, G. J.; Züttel, A. *Chem. Phys. Lett.* **2005**, *405*, 73. (c) Pozzo, M.; Alfè, D. *Phys. Rev. B* **2008**, *77*, 104103. (d) Ozolins, V.; Majzoub, E. H.; Wolverton, C. *J. Am. Chem. Soc.* **2009**, *131*, 230. (e) Caputo, R.; Züttel, A. *Mol. Phys.* **2010**, *108*, 1263. (f) Caputo, R.; Garroni, S.; Olid, D.; Teixidor, F.; Suriñach, S.; Baró, M. D. *Phys. Chem. Chem. Phys.* **2010**, *12*, 15093.

(26)   (a) Patnaik, P. *Handbook of Inorganic Chemicals*; McGraw-Hill: New York, **2002**. (b) Linke, W. F.; Seidell, A. *Solubilities of Inorganic and Metal Organic Compounds*; Van Nostrand: New York, **1965**. (c) Zhukova, N. A.; Malinina, E. A.; Kuznetsov, N. T. *Zh. Neorg. Khim.* **1985**, *30*, 1292.

(27)   Kuznetso, N. T.; Klimchuk, G. S. *Russ. J. Inorg. Chem.* **1971**, *16*, 645.

(28)   (a) Kanaeva, O. A.; Kuznetsov, N. T.; Sosnovskaya, O. O. *Zh. Neorg. Khim.* **1981**, *26*, 1153. (b) Wen, W. Y.; Chen, C. L. *J. Chem. Eng. Data* **1975**, *20*, 384.

(29)   Zhao, Y.; Schultz, N. E.; Truhlar, D. G. *J. Chem. Theory Comput.* **2006**, *2*, 364.

(30)   Frisch, M. J.; Trucks, G. W.; Schlegel, H. B.; Scuseria, G. E.; Robb, M. A.; Cheeseman, J. R.; Montgomery, J. J. A.; Vreven, T.; Kudin, K. N.; Burant, J. C.; Millam, J. M.; Iyengar, S. S.; Tomasi, J.; Barone, V.; Mennucci, B.; Cossi, M.; Scalmani, G.; Rega, N.; Petersson, G. A.; Nakatsuji, H.; Hada, M.; Ehara, M.; Toyota, K.; Fukuda, R.; Hasegawa,

J.; Ishida, M.; Nakajima, T.; Honda, Y.; Kitao, O.; Nakai, H.; Klene, M.; Li, X.; Knox, J. E.; Hratchian, H. P.; Cross, J. B.; Bakken, V.; Adamo, C.; Jaramillo, J.; Gomperts, R.; Stratmann, R. E.; Yazyev, O.; Austin, A. J.; Cammi, R.; Pomelli, C.; Ochterski, J. W.; Ayala, P. Y.; Morokuma, K.; Voth, G. A.; Salvador, P.; Dannenberg, J. J.; Zakrzewski, V. G.; Dapprich, S.; Daniels, A. D.; Strain, M. C.; Farkas, O.; Malick, D. K.; Rabuck, A. D.; Raghavachari, K.; Foresman, J. B.; Ortiz, J. V.; Cui, Q.; Baboul, A. G.; Clifford, S.; Cioslowski, J.; Stefanov, B. B.; Liu, G.; Liashenko, A.; Piskorz, P.; Komaromi, I.; Martin, R. L.; Fox, D. J.; Keith, T.; Al-Laham, M. A.; Peng, C. Y.; Nanayakkara, A.; Challacombe, M.; Gill, P. M. W.; Johnson, B.; Chen, W.; Wong, M. W.; Gonzalez, C.; Pople, J. A. *Gaussian 03, Revision E.01* **2004**, *Gaussian, Inc.*, Wallingford.

(31)   Milazzo, G.; Caroli, S.; Sharma, V. K. *Tables of standard electrode potentials*; Wiley: London, **1978**.

(32)   (a) Sharpe, P.; Richardson, D. E. *Thermochim. Acta* **1992**, *202*, 173-179. (b) Bartmess, J. E. *J. Phys. Chem.* **1994**, *98*, 6420.

(33)   Cramer, C. J. *Essentials of Computational Chemistry*; John Wiley & Sons: Chiechester, **2006**.

(34)   Reiss, H.; Heller, A. *J. Phys. Chem.* **1985**, *89*, 4207.

(35)   (a) Donald, W. A.; Leib, R. D.; O'Brien, J. T.; Bush, M. F.; Williams, E. R. *J. Am. Chem. Soc.* **2008**, *130*, 3371. (b) Donald, W. A.; Leib, R. D.; Demireva, M.; O'Brien, J. T.; Prell, J. S.; Williams, E. R. *J. Am. Chem. Soc.* **2009**, *131*, 13328.

(36)   Isse, A. A.; Gennaro, A. *J. Phys. Chem. B* **2010**, *114*, 7894.

(37)   webbook.nist.gov/chemistry accessed on May 15, 2011.

(38)   Stevenson, G. R.; Valentin, J. *J. Phys. Chem.* **1978**, *82*, 498.

(39)   (a) Stevenson, G. R.; Ocasio, I.; Bonilla, A. *J. Am. Chem. Soc.* **1976**, *98*, 5469. (b) Stevenson, G. R.; Zigler, S. S.; Reiter, R. C. *J. Am. Chem. Soc.* **1981**, *103*, 6057.

(40)   Frisch, M. J.; Trucks, G. W.; Schlegel, H. B.; Scuseria, G. E.; Robb, M. A.; Cheeseman, J. R.; Scalmani, G.; Barone, V.; Mennucci, B.; Petersson, G. A.; Nakatsuji, H.; Caricato, M.; Li, X.; Hratchian, H. P.; Izmaylov, A. F.; Bloino, J.; Zheng, G.; Sonnenberg, J. L.; Hada, M.; Ehara, M.; Toyota, K.; Fukuda, R.; Hasegawa, J.; Ishida, M.; Nakajima, T.; Honda, Y.; Kitao, O.; Nakai, H.; Vreven, T.; Montgomery, J., J. A.; Peralta, J. E.; Ogliaro, F.; Bearpark, M.; Heyd, J. J.; Brothers, E.; Kudin, K. N.; Staroverov, V. N.;

Keith, T.; Kobayashi, R.; Normand, J.; Raghavachari, K.; Rendell, A.; Burant, J. C.; Iyengar, S. S.; Tomasi, J.; Cossi, M.; Rega, N.; Millam, J. M.; Klene, M.; Knox, J. E.; Cross, J. B.; Bakken, V.; Adamo, C.; Jaramillo, J.; Gomperts, R.; Stratmann, R. E.; Yazyev, O.; Austin, A. J.; Cammi, R.; Pomelli, C.; Ochterski, J. W.; Martin, R. L.; Morokuma, K.; Zakrzewski, V. G.; Voth, G. A.; Salvador, P.; Dannenberg, J. J.; Dapprich, S.; Daniels, A. D.; Farkas, O.; Foresman, J. B.; Ortiz, J. V.; Cioslowski, J.; Fox, D. J. *Gaussian 09, Revision A.02* **2009**, *Gaussian, Inc.*, Wallingford.

(41)   (a) Cheung, Y. S.; Wong, C. K.; Li, W. K. *THEOCHEM* **1998**, *454*, 17. (b) Cheung, T. S.; Law, C. K.; Li, W. K. *THEOCHEM* **2001**, *572*, 243.

(42)   (a) Ortiz, J. V. *J. Chem. Phys.* **1996**, *104*, 7599. (b) Ferreira, A. M.; Seabra, G.; Dolgounitcheva, O.; Zakrzewski, V. G.; Ortiz, J. V. *Quantum-Mechanical Prediction of Thermochemical Data*; Kluwer: Dordrecht, **2001**; Vol. 131.

(43)   (a) Nicolaides, A.; Rauk, A.; Glukhovtsev, M. N.; Radom, L. *J. Phys. Chem.* **1996**, *100*, 17460. (b) Cheng, M. F.; Ho, H. O.; Lam, C. S.; Li, W. K. *Chem. Phys. Lett.* **2002**, *356*, 109.

(44)   Ramondo, F.; Bencivenni, L. *J. Mol. Struct.* **1990**, *221*, 169.

(45)   Bach, A.; Fischer, D.; Jansen, M. *Z. Anorg. Allg. Chem.* **2009**, *635*, 2406.

(46)   (a) Alcock, N. W.; Evans, D. A.; Jenkins, H. D. B. *Acta Cryst. B* **1973**, *29*, 360. (b) Nord, A. G. *Acta Chem. Scand.* **1973**, *27*, 814. (c) Mcginnety, J. A. *Acta Cryst. B* **1972**, *28*, 2845.

(47)   Dubbeldam, G. C.; Dewolff, P. M. *Acta Cryst. B* **1969**, *25*, 2665.

(48)   (a) Noordik, J. H.; Vandenha.Te; Mooij, J. J.; Klaassen, A. A. *Acta Cryst. B* **1974**, *30*, 833. (b) Hu, N. H.; Gong, L. X.; Jin, Z. S.; Chen, W. Q. *J. Organomet. Chem.* **1988**, *352*, 61.

(49)   (a) Her, J. H.; Yousufuddin, M.; Zhou, W.; Jalisatgi, S. S.; Kulleck, J. G.; Zan, J. A.; Hwang, S. J.; Bowman, R. C.; Udovic, T. J. *Inorg. Chem.* **2008**, *47*, 9757. (b) Her, J. H.; Zhou, W.; Stavila, V.; Brown, C. M.; Udovic, T. J. *J. Phys. Chem. C* **2009**, *113*, 11187. (c) Tiritiris, I.; Schleid, T. *Z. Anorg. Allg. Chem.* **2003**, *629*, 1390. (d) Yousufuddin, M.; Her, J. H.; Zhou, W.; Jalisatgi, S. S.; Udovic, T. J. *Inorg. Chim. Acta* **2009**, *362*, 3155.

(50)   Giannozzi, P.; Baroni, S.; Bonini, N.; Calandra, M.; Car, R.; Cavazzoni, C.; Ceresoli, D.; Chiarotti, G. L.; Cococcioni, M.; Dabo, I.; Dal Corso, A.; de Gironcoli, S.; Fabris, S.;

Fratesi, G.; Gebauer, R.; Gerstmann, U.; Gougoussis, C.; Kokalj, A.; Lazzeri, M.; Martin-Samos, L.; Marzari, N.; Mauri, F.; Mazzarello, R.; Paolini, S.; Pasquarello, A.; Paulatto, L.; Sbraccia, C.; Scandolo, S.; Sclauzero, G.; Seitsonen, A. P.; Smogunov, A.; Umari, P.; Wentzcovitch, R. M. *J. Phys. Cond. Mat.* **2009**, *21*, 395502.

(51)   MOPAC2009 openmopac.net/home.html accessed on 3/31/2011

(52)   Sherwood, P. M. A. *Vibrational spectroscopy of solids*; Cambridge University Press: London, **1972**.

(53)   (a) Calle-Vallejo, F.; Martínez, J. I.; García-Lastra, J. M.; Mogensen, M.; Rossmeisl, J. *Angew. Chem. Int. Ed.* **2010**, *49*, 7699. (b) Martínez, J. I.; Hansen, H. A.; Rossmeisl, J.; Nørskov, J. K. *Phys. Rev. B* **2009**, *79*, 045120.

(54)   (a) Jenkins, H. D. B. *J. Chem. Edu.* **2005**, *82*, 950. (b) Gavezzotti, A. *Mod. Sim. Mat. Sci. Eng.* **2002**, *10*, 1. (c) Giacovazzo, C. *Fundamentals of Crystallography*; Oxford university Press: New York, **2002**.

(55)   Wu, R. L. C.; Tiernan, T. O. *Planet. Space Sci.* **1981**, *29*, 735.

(56)   Jenkins, H. D. B.; Pratt, K. F.; Smith, B. T.; Waddington, T. C. *J. Inorg. Nuc. Chem.* **1976**, *38*, 371.

(57)   (a) Boldyrev, A. I.; Simons, J. *J. Phys. Chem.* **1994**, *98*, 2298. (b) Blades, A. T.; Kebarle, P. *J. Am. Chem. Soc.* **1994**, *116*, 10761.

(58)   Dewar, M. J. S.; Harget, A.; Haselbach, E. *J. Am. Chem. Soc.* **1969**, *91*, 7521.

(59)   Baik, M. H.; Schauer, C. K.; Ziegler, T. *J. Am. Chem. Soc.* **2002**, *124*, 11167.

(60)   Miller, T. M.; Viggiano, A. A.; Miller, A. E. S. *J. Phys. Chem. A* **2002**, *106*, 10200.

(61)   (a) Dominikowska, J.; Palusiak, M. *New J. Chem.* **2010**, *34*, 1855. (b) Dominikowska, J.; Palusiak, M. *J. Comp. Chem.* **2011**, *32*, 1441.

(62)   Sommerfeld, T. *J. Am. Chem. Soc.* **2002**, *124*, 1119.

(63)   McKee, M. L.; Wang, Z. X.; Schleyer, P. v. R. *J. Am. Chem. Soc.* **2000**, *122*, 4781.

(64)   personal communication with Prof. Stefan Grimme.

(65)   Bally, T.; Sastry, G. N. *J. Phys. Chem. A* **1997**, *101*, 7923.

(66)   Sedlák, R.; Fanfrlík, J.; Hnyk, D.; Hobza, P.; Lepšík, M. *J. Phys. Chem. A* **2010**, *114*, 11304.

(67)   Ohba, N.; Miwa, K.; Aoki, M.; Noritake, T.; Towata, S.; Nakamori, Y.; Orimo, S.; Züttel, A. *Phys. Rev. B* **2006**, *74*, 075110.

(68)   Züttel, A.; Wenger, P.; Rentsch, S.; Sudan, P.; Mauron, P.; Emmenegger, C. *J. Power Sources* **2003**, *118*, 1.

Chapter 5

Redox Energetics of *Hypercloso* Boron Hydrides B_nH_n (n = 6-13) and $B_{12}X_{12}$ (X = F, Cl, OH,

and CH_3)

5.1 Introduction

Experimental studies of the electrochemistry of $B_nH_n^{-/2-}$ have been reported using

polarography and cyclic voltammetry.[1] However, polymerization or aggregation of boron

clusters during the redox reaction hinder the accurate characterization of redox species.[2] The

existence of the assumed radical anions $B_{11}H_{11}^{\bullet-}$ and $B_{12}H_{12}^{\bullet-}$ depends on solvent, but the role of

solvent itself is not well known.[2d] For example, it is known that $B_{10}H_{10}^{2-}$ and $B_{12}H_{12}^{2-}$ undergo a

stepwise one-electron oxidation to form $B_{20}H_{19}^{3-}$ or a two-electron oxidation to form $B_{20}H_{18}^{2-}$,

depending on solvent and pH conditions.[3,4] Substitution of the $B_{12}H_{12}^{2-}$ opens the possible

applications of superacidity,[5] weakly coordinating systems,[6] biological labeling system,[7] and

nanoscale pharmaceutical carriers.[8] However, the redox properties of $B_{12}X_{12}^{0/-/2-}$ (X = F, Cl, OH,

CH_3, and OCH_3) have been only partially investigated.[6a,9] Lee et al.[9g] reported $E_{1/2}$ of

$B_{12}(OR)_{12}^{0/-}$ where sixteen different -OR substituents were considered from –OCH_3

to -$OCH_2C_6H_5Br$, while the $E_{1/2}$ of $B_nH_n^{0/-}$ and the existence of neutral B_nH_n is still not known.[2]

Many *ab initio* studies of reduction potentials have been reported in the last decade.[10]

Roy et al.[10c] reported that the systematic underestimation of redox potentials with the B3LYP

functional could be corrected with a baseline shift. The medium effect is often treated with

implicit solvation models such as CPCM (Conductor-like Polarizable Continuum Model) which

was successfully applied to the redox potential in aqueous and non-aqueous solutions.[10b,10e,10h]

The linear relationship between electron affinity and reduction potential is well known, and a strong correlation is reported for various species.[10g,11] The difference between electron affinity and reduction potential is a consequence of the solvation Gibbs free energy (ΔG_{solv}) (Scheme 1).

$$
\begin{array}{ccc}
B_nH_n \ (g) \ + \ e^-(g) & \xrightarrow{\ \Delta G_{E.A.}\ } & B_nH_n^-(g) \\[1.5em]
\Big\downarrow \Delta G_{solv}\ (B_nH_n) & & \Big\downarrow \Delta G_{solv}\ (B_nH_n^-) \\[1.5em]
B_nH_n \ (aq) \ + \ e^-(g) & \xrightarrow{\ \Delta G_{sol}\ } & B_nH_n^-(aq)
\end{array}
$$
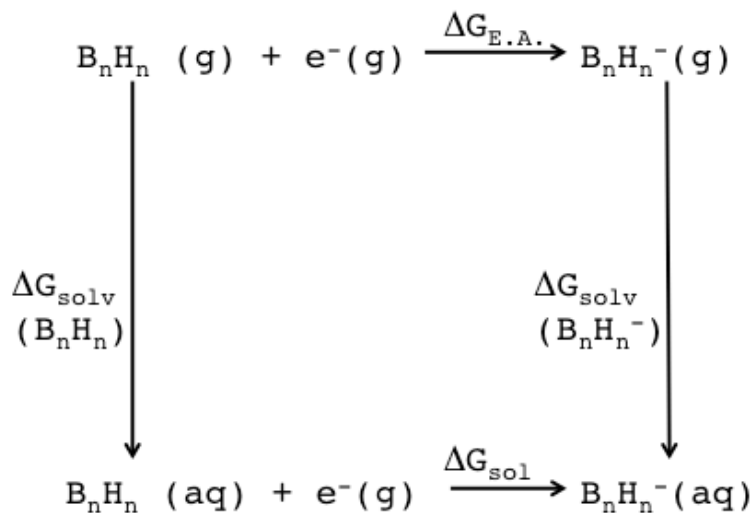
Scheme 1.   Thermodynamic cycle used to calculate reduction potential of B_nH_n species.

The PCM (polarizable continuum model) method can successfully be used to compute solvation free energies with the appropriate the choice of cavity radii.[12] Likewise, the choice of cavity radii (the boundary between solute and solvent) is critical to determine solvation free energies of dianions.[13] Many implicit solvation models such as the Born, PCM, and CPCM models have been applied to the calculation of solvation free energies of dianions.[10f,10j,14]

If the $B_nH_n^-$ intermediate is stable, the two-electron reduction process from B_nH_n may proceed with successive one-electron transfer pathways. Successive one-electron transfers versus a simultaneous two-electron transfer are governed by the ordering of reduction potentials for the first (E^o_1) and second (E^o_2) electron addition. The monoanion is unstable with respect to disproportionation to neutral and dianion species when $E^o_1 - E^o_2 < 0$ (potential inversion).[14a,15]

However, disproportionation is controlled by solvation, and the potential inversion is more often observed in solution rather than in the gas phase (eq 1).[10f,10i,14a,15a,16]

$$2B_nH_n^- \rightarrow B_nH_n + B_nH_n^{2-} \tag{1}$$

When the difference of two reduction potentials is very small, cyclic voltammetry produces single voltammetric peak for a two-electron transfer. About 98% of this potential compression is due to solvation, with a minor role from ion pairing.[15a,17] Barrière and Geiger[18] studied the two-electron transfer in $Ni(S_2C_2Fc_2)_2$ ($Fc = Fe(C_5H_5)(C_5H_4)$) which can occur either as successive one-electron transfers or as a single two-electron transfer depending on the medium. Consideration of the solvent effect is imperative to understand multi-electron transfer processes in solution.

The stability of the monoanion radical has been justified by electron delocalization.[14a,19] Mao et al.[20] reported that the extent of unpaired electron delocalization determines the solvent-dependent properties of paramagnetic organometallic complexes. In addition, several studies have shown[21] that the stability of mixed-valence ions toward disproportionation depends on solvent-induced electronic delocalization. However, electron localization in carotenoid di-ions can minimize the Coulomb repulsion and enhance solvation stabilization, while electron delocalization reduces interaction with solvent.[15b] Thus, any rationalization of potential inversion in disproportionation reactions must consider the synergistic effect of solvent on the spin/charge delocalization in the monoanion radical.

Our *ab initio* computation with implicit solvation modeling will present the details of redox energetics (E^o_{Red} versus standard hydrogen electrode (SHE)) of $B_nH_n^{0/-/2-}$ ($n = 6\text{-}13$) and

$B_{12}X_{12}^{0/-/2-}$ (X = F, Cl, OH, and CH$_3$) boron clusters. Our E^o_{Red} values will be compared to experimental oxidative stabilities ($E_{1/2}$) where $E^o_{red}(A) = E_{1/2}(B)$ in the reaction $A + e^- \rightarrow B$. Our redox energetics include the free energy of disproportionation (ΔG_{dpro}, $2B_nH_n^- \rightarrow B_nH_n + B_nH_n^{2-}$) in aqueous solution and may provide insight into the electron transfer mechanism for polyborane-containing system. All experimental $E_{1/2}$ values and all calculated E^o_{Red} values are relative to SHE in water.

5.2 Computational Details

The starting geometries of the boron clusters $B_nH_n^{0/-/2-}$ (n = 5-13) come from previous studies.[22] The B3LYP and M06-2X[23] exchange/correlation density functionals with the aug-cc-pvtz basis set were used to optimize geometries, compute vibrational frequencies, and calculate solvation free energies (Scheme 1). I also applied the G4 level of theory[24] for $\Delta G_{E.A.}$ followed by calculation of ΔG_{solv} with B3LYP/aug-cc-pvtz and M06-2X/aug-cc-pvtz method (G4/B3LYP and G4/M06-2X). Zero-point energies, thermal energies, and entropy corrections were computed in the gas phase using vibrational frequencies without scaling. For $\Delta G_{E.A.}$, I used adiabatic electron affinity calculations. The possibility of Jahn-Teller distortion and higher multiplicity electronic states of B_nH_n and $B_nH_n^-$ were considered and no electronic state issues were found. In the gas phase, the second electron binding energy (negative electron affinity) of small molecules is challenging to compute. Using a series of dielectric medium conditions (ε = 100,10,4,2, and 1), Puiatti et al.[25] extrapolated the negative electron affinities. I also found that the directly calculated electron affinity of CO_3^- and SO_4^- monoanions in the gas phase (ε = 1) gave very similar results to the extrapolated value.[26] This non-adiabatic binding energy (negative electron affinity) provided reasonable lattice energies of M_2CO_3 and M_2SO_4 salts (M = Li$^+$, Na$^+$, and

K^+).[26] I confirmed that the electron affinty of $B_6H_6^-$ in the gas phase ($\varepsilon = 1$) also gave a very similar value to the extrapolated value using a series of dielctric medium.

Among the various implicit solvation models, the CPCM[27] with the UAKS cavity set[24] and the Pauling cavity set[24] were used in our study since water has a high dielectric constant ($\varepsilon = 78.35$). The SMD (solvation model density) method with the SMD cavity set was also used because it was developed for the "universal" application of solvation modeling including charged species.[28] The UAKS and Pauling cavity sets with the CPCM method investigate the sensitivity of solvation free energies to the cavity radii for anion and dianion species. The solvation free energies with the CPCM method include cavitation, dispersion, and repulsion energies (keyword = cav, dis, rep). The solvent excluded surface (keyword = surface = SES) is applied with average density integration point 10 Å^{-2}. The cavity surface is smoothed with the keyword "Addsph". I did not apply any specific keywords for the SMD solvation modeling. All calculations were carried out using the Gaussian09 package.[24]

The absolute value of the SHE has been debated to be between 4.11 V and 4.52 V.[29] I used 4.28 V since the surface potential of water was considered.[29f,29j] I note that the absolute potential of SHE in nonaqueous solution is different from that in water.[29g] A consideration of the "liquid junction potential" (LJP) and the correction for reference electrode are necessary when converting E^o_{Red} in different solvent systems to water.[30] For example, the LJP of acetonitrile-water is 0.093 V.[1a,31] However, I did not apply the LJP since the reference electrode correction for acetonitrile has almost the same value as LJP but with opposite sign and thus the two almost cancel out.[10f] The widely used ion convention, IC (enthalpy of formation of the electron at non-zero temperatures is equal to the integrated heat capacity of the electron) is applied for the

explicit electron in Scheme 1.[32] Electron attachment energetics in the gas phase ($\Delta G_{E.A.}$) and

aqueous solution (ΔG_{sol}) in Scheme 1 can be summarized as follows (eq 2-4).

$$\Delta G_{sol} = \Delta G_{E.A.} + \Delta \Delta G_{solv} \tag{2}$$

$$\Delta G_{sol} = -nFE^o_{abs} \tag{3}$$

$$E^o_{red} = E^o_{abs} - 4.28 \tag{4}$$

The $\Delta \Delta G_{solv}$ is the difference in the free energy of solvation. The absolute reduction potential

(E^o_{abs}) is applied to the standard reduction potential (E^o_{red}) together with Faraday constant (F)

and number of moles of electrons transferred per mol of reaction (n). All experimental oxidative

stabilities from the literature are converted to E^o_{red} versus SHE unless explicitly indicated. I note

that the smaller clusters B_nH_n (n = 6-9) are reported in water while the larger clusters B_nH_n (n =

10-12) are reported in acetonitrile.[1a] Some experimental oxidative stabilities of $B_{12}X_{12}^{2-}$ (X = H,

F, Cl)[33] were determined with the Fc/Fc$^+$ reference electrode and I apply a 0.548 V correction to

convert to SHE.[10f,29a,34]

5.3 Results

  Electron affinities of B_nH_n (n=5-13) in the gas phase. The gas-phase electron

attachment free energies ($\Delta G_{E.A.}$) of $B_nH_n^{0/-/2-}$ (n = 5-13) are presented in Figure 1 where $B_{12}H_{12}$

is the only species to give a bound second electron attachment ($B_{12}H_{12}^- + e^- \rightarrow B_{12}H_{12}^{2-}$,

$\Delta G_{E.A.} < 0$). The trend of $\Delta G_{E.A.}$ in this study is similar to the reverse trend of adiabatic ionization

potential for the $B_nH_n^{2-} \rightarrow B_nH_n^- + e^-$ step using the B3LYP/6-311+G(d,p)//B3LYP/6-31G(d).[22a]
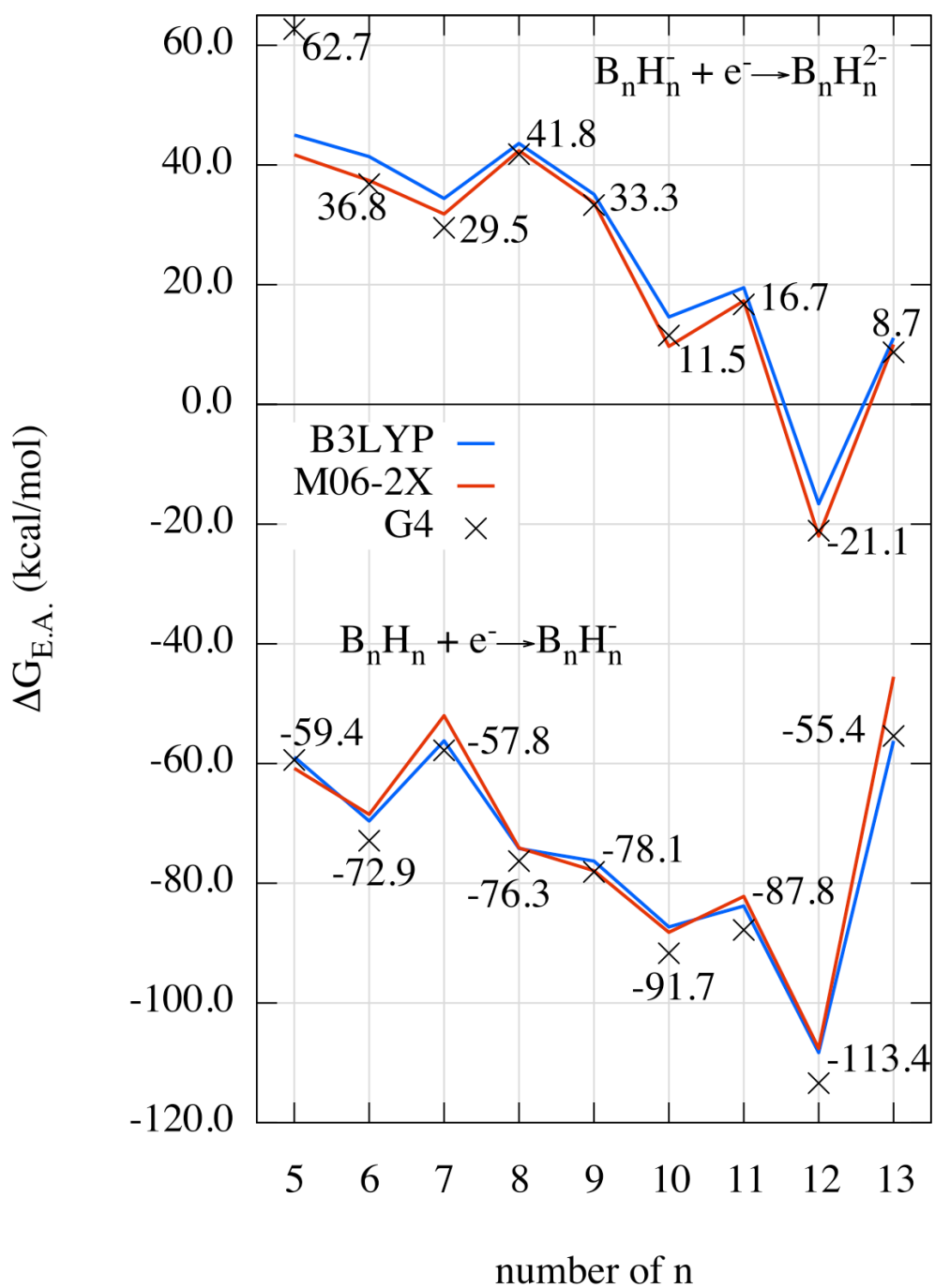
Figure 1. Electron attachment free energies ($\Delta G_{E.A.}$) of $B_nH_n^{0/-/2-}$ (n = 5-13) *hypercloso* boron

clusters in gas phase obtained on the B3LYP/aug-cc-pvtz, M06-2X/aug-cc-pvtz, and

G4 levels of theory. The values in plot are the $\Delta G_{E.A.}$ from the G4 level of theory.

Generally, the B3LYP functional yields similar attachment energies ($\Delta G_{E.A.}$) to the G4 level of

theory for the $B_nH_n + e^- \rightarrow B_nH_n^-$ step while the M06-2X functional produces attachment

energies ($\Delta G_{E.A.}$) similar to the G4 level of theory for the reaction $B_nH_n^- + e^- \rightarrow B_nH_n^{2-}$ (Figure

1). For the first and second electron attachment free energies, B3LYP and M06-2X functional

yield results that are both within 5.8 kcal/mol of the G4 results for B_nH_n (n = 6-13). The only

exception is the $B_{13}H_{13} + e^- \rightarrow B_{13}H_{13}^-$ step with the M06-2X functional which differs by 9.9

kcal/mol from the G4 result. Pathak et al.[35] reported the electron affinity (EA) of $B_{12}H_{12}$ as 4.56

eV (105.1 kcal/mol) with the B3LYP/6-311++G(d,p) method while the EA for $B_{12}H_{12}$ ($B_{12}H_{12}$ +

$e^- \rightarrow B_{12}H_{12}^-$) in our study is between 4.69 eV using B3LYP/aug-cc-pvtz and 4.92 eV for G4

(Figure 1). $B_{10}H_{10}$, $B_{11}H_{11}$, and $B_{12}H_{12}$ are superhalogen species, which means that their electron

affinities are higher than the value of a halogen atom (3.0-3.6 eV, corresponding to 69.2-83.0

kcal/mol).[36] The second electron attachment energy of B_5H_5 at the G4 level (62.7 kcal/mol) is

quite different from the DFT results (41.7 kcal/mol using M06-2X) while the first electron

attachment energies are very similar among the three methods (Figure 1). For the B_5H_5 cluster, I

used the cc-pvtz basis set rather than the aug-cc-pvtz basis set (i.e. no diffuse functions) because

diffuse functions can cause artifacts such as evaluation of the unbound second electron of small

dianions. Due to the large discrepancy of $\Delta G_{E.A.}$ values generated using different methods and

lack of literature data for the reduction process, I do not discuss B_5H_5 further (Figure 1).

Cederbaum and co-workers discussed the nature of the second electron binding in $B_6H_6^{2-}$.[37] In

contrast to the step $B_5H_5^- + e^- \rightarrow B_5H_5^{2-}$, DFT/aug-cc-pvtz and G4 methods show good

agreement for reaction $B_6H_6^- + e^- \rightarrow B_6H_6^{2-}$ (Figure 1). Electron attachment free energies of

$B_nH_n^-$ ($B_nH_n^- + e^- \rightarrow B_nH_n^{2-}$, n = 5-13) become less positive as the size of the cluster increases

(Figure 1). However, the $\Delta G_{E.A.}$ value of $B_7H_7^-$ is less positive than those of $B_8H_8^-$ and $B_9H_9^-$

while the $\Delta G_{E.A.}$ value of $B_{10}H_{10}^-$ is less positive than that of $B_{11}H_{11}^-$ ($B_nH_n^- + e^- \rightarrow B_nH_n^{2-}$ in Figure 1). Both the size and the geometry of the cluster play a role in the electron attachment process (Table 1). If one normalizes the $\Delta G_{E.A.}$ by the cluster size, $B_{13}H_{13}$ neutral presents the smallest free energy gain ($\Delta G_{E.A.}/(BH)_n$) for the first electron attachment (Table 1).

Table 1. Free energies of electron attachment per BH unit ($\Delta G_{E.A.}/(BH)_n$ kcal/mol) of B_nH_n ($n = 6$-13) boron clusters[a]

	$B_nH_n(g) + e^-(g) \rightarrow B_nH_n^-(g)$			$B_nH_n^-(g) + e^-(g) \rightarrow B_nH_n^{2-}(g)$		
	B3LYP	M06-2X	G4/M06-2X	B3LYP	M06-2X	G4/M06-2X
B_6H_6	-11.6(-18.3)	-11.4(-18.4)	-12.1(-19.1)	6.9(-17.9)	6.2(-19.1)	6.1(-18.6)
B_7H_7	-8.0(-13.4)	-7.4(-13.0)	-8.3(-13.8)	4.9(-15.4)	4.5(-16.1)	4.2(-16.1)
B_8H_8	-9.3(-13.9)	-9.3(-14.0)	-9.5(-14.3)	5.4(-11.7)	5.3(-12.2)	5.2(-11.9)
B_9H_9	-8.5(-12.5)	-8.7(-12.9)	-8.7(-12.9)	3.9(-11.0)	3.7(-11.5)	3.7(-11.2)
$B_{10}H_{10}$	-8.7(-12.3)	-8.8(-12.6)	-9.2(-12.9)	1.5(-11.7)	1.0(-12.4)	1.1(-12.0)
$B_{11}H_{11}$	-7.6(-10.8)	-7.5(-10.8)	-8.0(-11.3)	1.8(-9.8)	1.6(-10.2)	1.5(-10.1)
$B_{12}H_{12}$	-9.0(-11.9)	-9.0(-11.9)	-9.5(-12.4)	-1.4(-12.0)	-1.8(-12.5)	-1.8(-12.3)
$B_{13}H_{13}$	-4.3(-5.9)	-3.3(-4.9)	-4.3(-5.9)	0.9(-8.5)	0.8(-8.7)	0.7(-8.7)

[a]The value in parentheses is $\Delta G_{sol}/(BH)_n$ with the CPCM/Pauling method.

Solvation free energies of B_nH_n ($n = 5$-13). The solvation free energies of $B_nH_n^{0/-/2-}$ ($n = 5$-13) depend linearly on cluster size except for the neutral $B_{13}H_{13}$ species, and the value of ΔG_{solv} greatly depends on the choice of cavity set (Figure 2). The CPCM/UAKS cavity set gives the smallest ΔG_{solv}, while the SMD method gives the largest ΔG_{solv}, and the CPCM/Pauling cavity set yields values between these two (Figure 2).
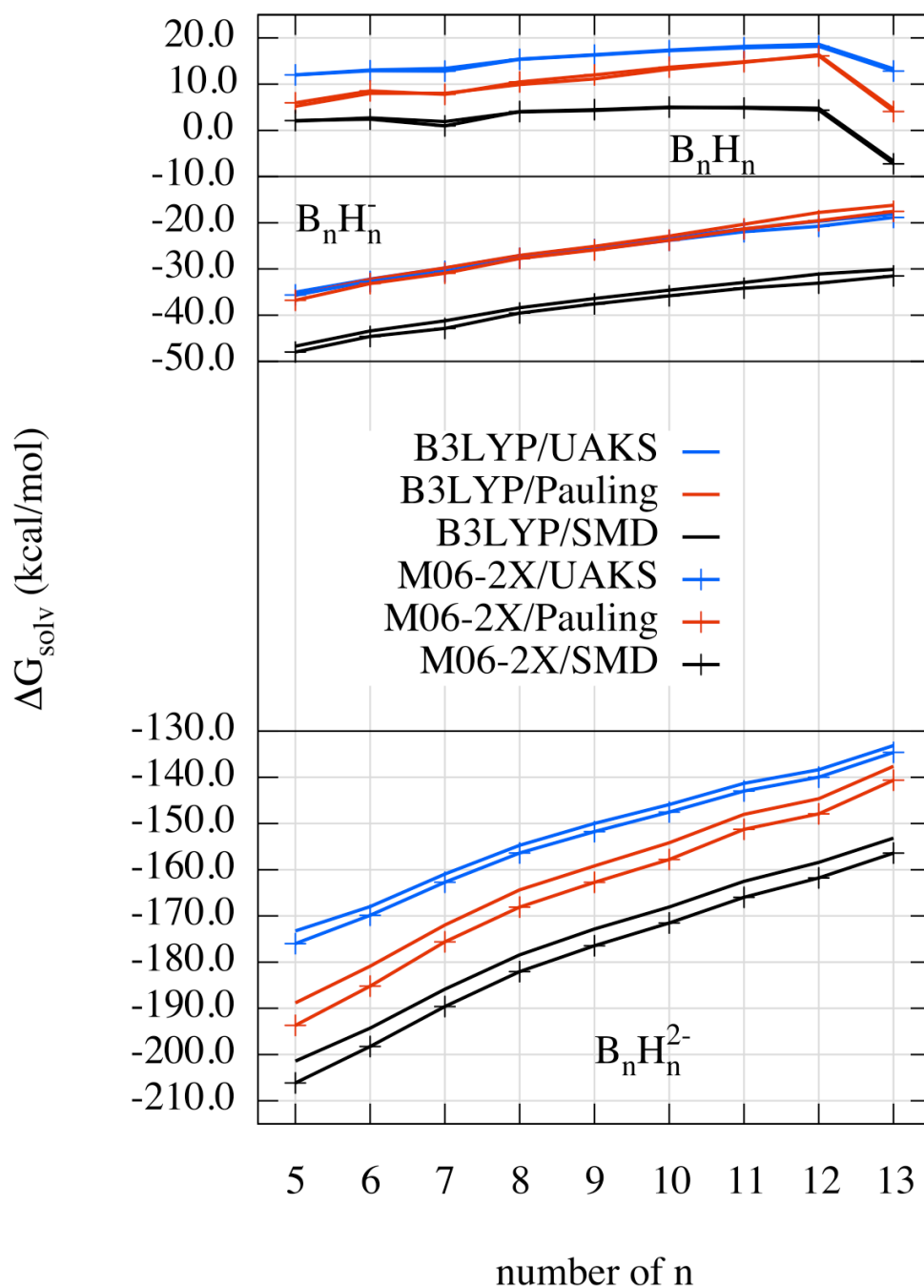
Figure 2. The solvation free energies (ΔG_{solv}) of B_nH_n, $B_nH_n^-$, and $B_nH_n^{2-}$ (n = 6-13) *hypercloso* boron clusters obtained with the CPCM/UAKS, CPCM/Pauling, and SMD solvation modeling.

The exceptional value of $B_{13}H_{13}$ is due to a much larger dipole moment (11.5 D with the M06-2X(Pauling) method) than all other dipole moments for B_nH_n (n = 6-12) species (1.6, 4.2, 0.0, 0.0, 0.6, 2.2, and 4.2 D, respectively). Because of its polar nature (a result of the electron description which has a contribution from $B_{12}H_{12}^{2-}$ with a capping BH^{2+} unit), $B_{13}H_{13}$ has a favorable solvation free energy in water. The SMD method for $B_{13}H_{13}$ gives ΔG_{solv} = -6.7 and -7.3 kcal/mol with B3LYP and M06-2X functionals, respectively, while the CPCM/UAKS and CPCM/Pauling methods yield positive values of ΔG_{solv} (Figure 2). The ΔG_{solv} of $B_nH_n^-$ (n = 6-13) with CPCM/UAKS and CPCM/Pauling cavity sets are similar, while ΔG_{solv} obtained from the SMD method gives more negative ΔG_{solv} values by about 10 kcal/mol as compared to the CPCM results (Figure 2). For the step $B_nH_n^- + e^- \rightarrow B_nH_n^{2-}$ (n = 6-13), $\Delta G_{E.A.}$ values from DFT methods and at the G4 level of theory agree within 5.0 kcal/mol (Figure 1) while ΔG_{solv} values for dianions differ by more than 20 kcal/mol depending on the size of B_nH_n (n = 6-13) (Figure 2). Thus, the solvation free energy differences ($\Delta\Delta G_{solv}$) between $B_nH_n^-$ and $B_nH_n^{2-}$ become significant factors in deciding the final E^o_{Red} values (eq 2-4). In a previous study of pK_{a2} values of diprotic acids ($HA^-(aq) \rightarrow H^+(aq) + A^{2-}(aq)$), the CPCM method with the Pauling cavity set gave better results than other cavity sets and also better than the SMD method (with SMD cavity set).[13] In addition, ΔG_{solv} of dianions with the CPCM/Pauling cavity set reproduced the dissolution free energies of alkali metal dianion salts (M_2X_1).[13,26] Therefore I decided to use the CPCM/Pauling combination to investigate the redox behavior of $B_nH_n^{0/-/2-}$ and the disproportionation of $B_nH_n^-$ (n=6-13).

The E^o_{Red} of B_nH_n (n = 6-13). Figure 3 gives E^o_{red} values for $B_nH_n^{0/-/2-}$ (n = 6-13) with the CPCM/Pauling cavity set method. The greatest variation in E^o_{red} among the four methods (B3LYP, M06-2X, G4/B3LYP, G4/M06-2X) is 0.35 V (for $B_6H_6^- + e^- \rightarrow B_6H_6^{2-}$).
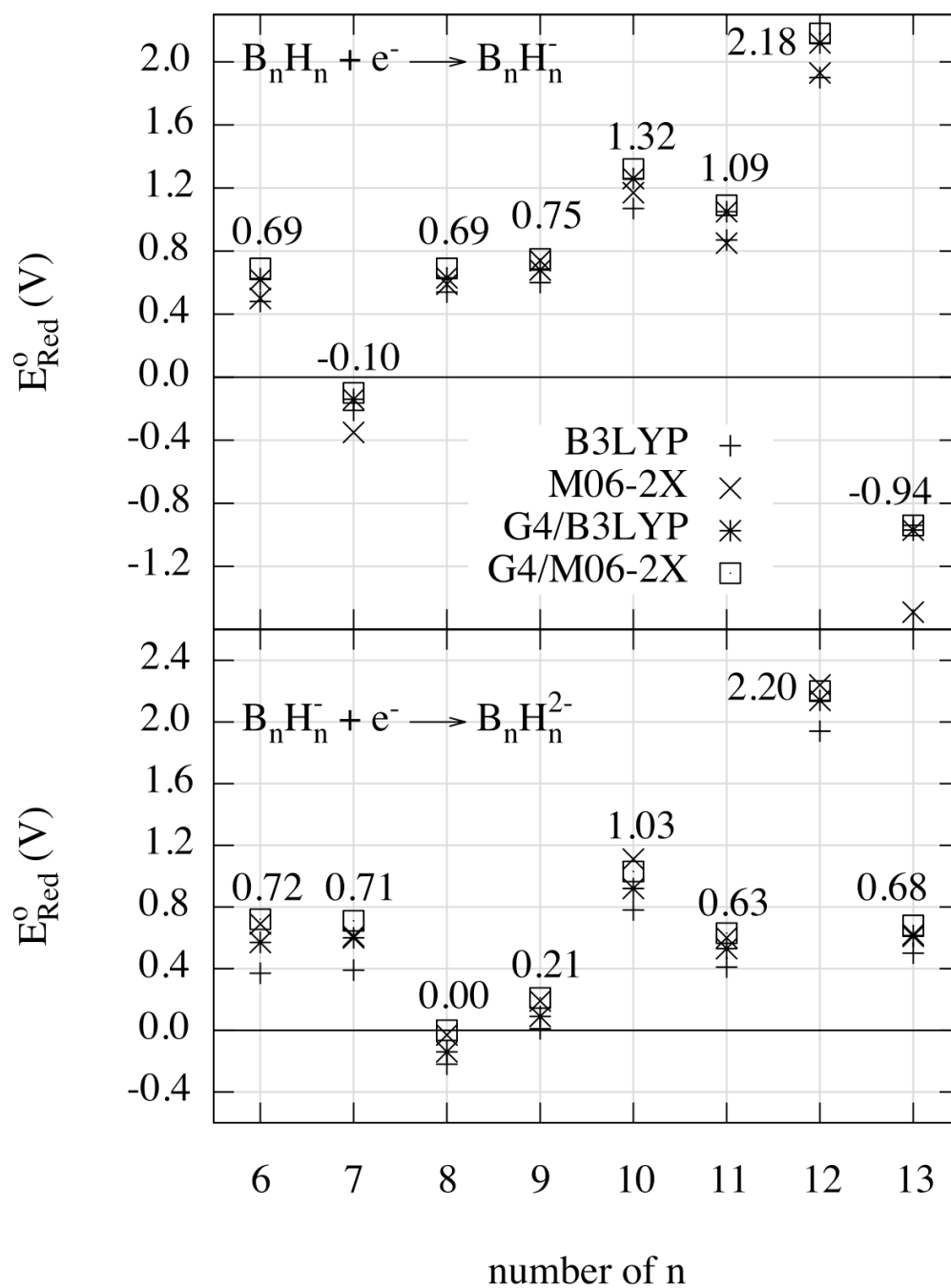
Figure 3. E^o_{red} values of $B_nH_n^{0/-/2-}$ (n = 6-13) *hypercloso* boron clusters computed on the

B3LYP/aug-cc-pvtz, M06-2X/aug-cc-pvtz, and G4 level of theory followed by

CPCM/Pauling cavity set method. The values in plot are the E^o_{red} from the G4/M06-

2X(Pauling) method.

However, the variation among the methods for all other boron clusters is less than 0.16 V except for $B_{13}H_{13}^{0/-}$ where the variation is 0.21 V (Figure 3). The larger variation of $E^o{}_{Red}$ among methods for $B_{13}H_{13}^{0/-}$ comes from the smaller $\Delta G_{E.A.}$ predicted by M06-2X relative to B3LYP and G4. Klanberg and Muetterties[1c] reported the relative order of oxidative stability ($E_{1/2}$) as $B_9H_9^{2-} < B_{11}H_{11}^{2-} < B_{10}H_{10}^{2-} < B_{12}H_{12}^{2-}$ from polarographic studies. Our $E^o{}_{red}$ values for $B_nH_n^{0/-}$ ($B_nH_n + e^- \rightarrow B_nH_n^-$, n= 6-13) and $B_nH_n^{-/2-}$ ($B_nH_n^- + e^- \rightarrow B_nH_n^{2-}$, n = 6-13) follow the same order of experimental oxidative stabilities (Figure 3). The reaction $B_7H_7 + e^- \rightarrow B_7H_7^-$ is slightly nonspontaneous while the reaction $B_{13}H_{13} + e^- \rightarrow B_{13}H_{13}^-$ is quite nonspontaneous ($E^o{}_{Red}$, -0.1 and -0.9 V respectively at G4/M06-2X(Pauling)) (Figure 3). Our $E^o{}_{Red}$ value for neutral $B_{13}H_{13}$ indicates that this is the least electron-accepting boron cluster in aqueous solution (Figure 3). It is interesting that the exceptional stability of $B_{13}H_{13}$ in the gas phase has been noted previously.[22a] The reaction $B_8H_8^- + e^- \rightarrow B_8H_8^{2-}$ is the only slightly nonspontaneous process of all the second electron attachments of the B_nH_n species (n = 6-13) (0.0 V at the G4/M06-2X level, Figure 3).

For the step $B_{12}H_{12}^- + e^- \rightarrow B_{12}H_{12}^{2-}$, our $E^o{}_{red}$ values are between 1.94 V and 2.24 V while 1.67 V and >1.4 V of oxidative stability ($E_{1/2}$) have been reported (Figure 4).[2a,38] However, a recent cyclic voltammetry study suggests a value of 2.21 V in liquid SO_2.[33] The $E_{1/2}$ for $B_{10}H_{10}^{2-}$ (1.09 V) agrees well with our $E^o{}_{red}$ predictions (1.11 or 1.03 V, using M06-2X or G4/M06-2X methods, respectively, Figure 4).[1a,38b] The polarographic study reported 0.29 V of $E_{1/2}$ for $B_{11}H_{11}^{2-}$ but the redox species was not well characterized.[1c,39] Later, a voltammetry study reported $E_{1/2} = 0.49$ V for $B_{11}H_{11}^{2-}$.[1c,39] Indeed, our $E^o{}_{red}$ values are between 0.41 V and 0.63 V. The $E_{1/2}$ of $B_9H_9^{2-}$ is 0.09 V while our $E^o{}_{red}$ values for $B_9H_9^{-/2-}$ range from 0.01 to 0.21 V.[1a,1d] The oxidative stability for the $B_9H_9^{2-}$ cluster is smaller than those of the boron clusters, $B_6H_6^{2-}$

and $B_8H_8^{2-}$. Indeed, the hydrolytic instability of $B_9H_9^{2-}$ has hindered the precise experimental
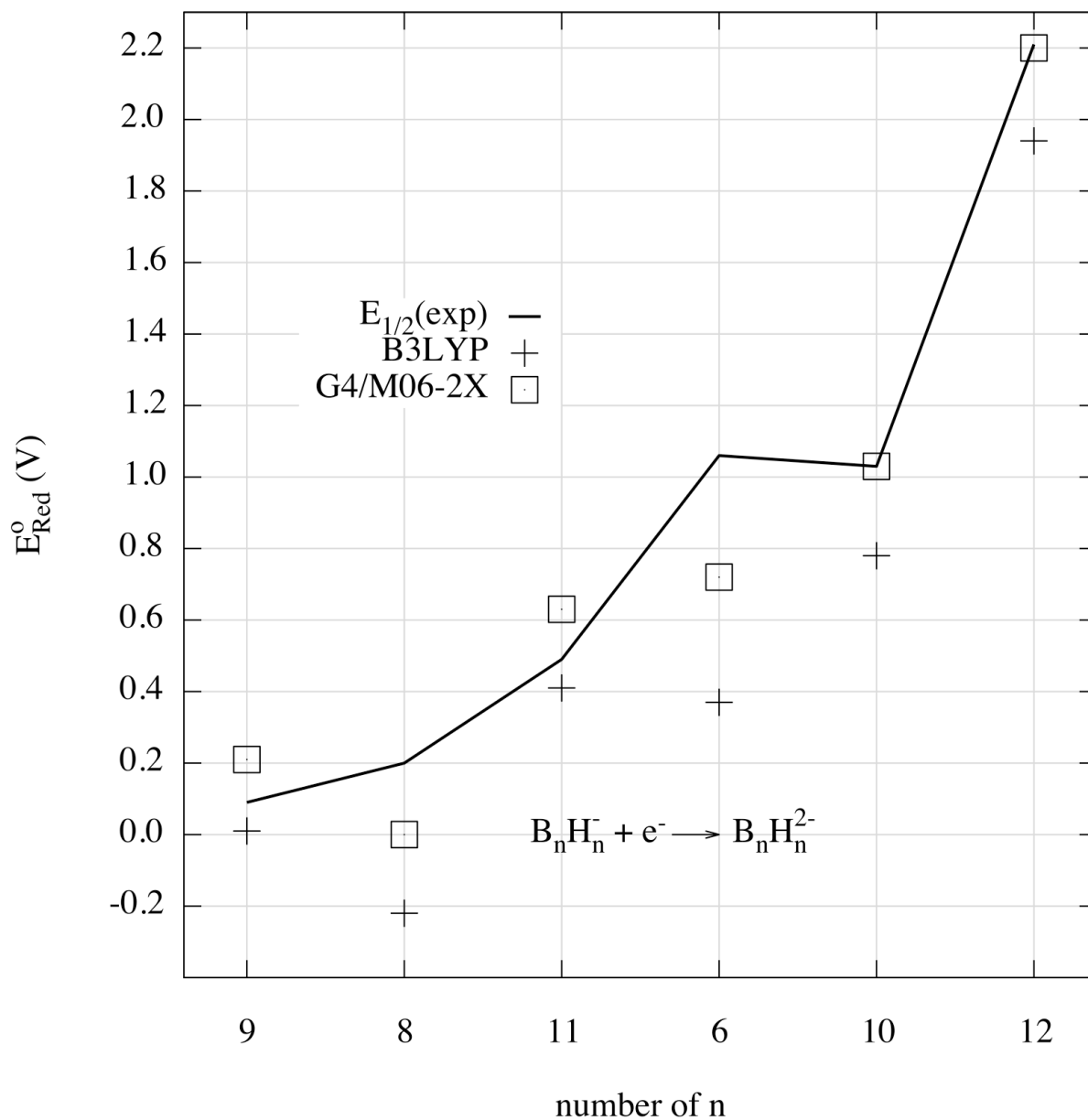
determination of $E_{1/2}$.[40]

Figure 4. The E^o_{Red} values of $B_6H_6^{-/2-}$, $B_8H_8^{-/2-}$, $B_9H_9^{-/2-}$, $B_{10}H_{10}^{-/2-}$, $B_{11}H_{11}^{-/2-}$, and $B_{12}H_{12}^{-/2-}$

obtained on the G4/M06-2X(Pauling) and B3LYP(Pauling) method including

experimental oxidative stability ($E_{1/2}$) of $B_nH_n^{2-}$.

A polarographic study of the oxidative stability ($E_{1/2}$) of $B_6H_6^{2-}$ has yielded a value of -0.09 V.[1a,1d] However, a more recent study[1e] reports a much larger value of 1.06 V in ethanol. Our predicted E^o_{red} values for reaction $B_6H_6^- + e^- \rightarrow B_6H_6^{2-}$ are between 0.37 and 0.72 V (Figure 4). The oxidative stability ($E_{1/2} = 1.06$) of $B_6H_6^{2-}$ becomes slightly larger than that of $B_{10}H_{10}^{2-}$ ($E_{1/2} = 1.03$, Figure 4). If I use ethanol as the solvent (rather than water) with the CPCM/Pauling cavity set, the E^o_{Red} values for $B_6H_6^{-/2-}$ are reduced to 0.16 (B3LYP) and 0.49 V (G4/M06-2X). Thus, I suggest that the experimental $E_{1/2}$ value of -0.09 V is too small and the value of 1.06 V is too large. Previous studies suggested that the oxidative stability of $B_7H_7^{-/2-}$ is smaller than that of $B_6H_6^{2-}$.[1a,1b,1d] Our computed E^o_{red} value for $B_7H_7^{-/2-}$ (0.71 V, G4/M06-2X) is very similar to the $B_6H_6^{2-}$ value (0.72 V, G4/M06-2X, Figure 3).

The difference between the E^o_{red} of the neutral and monoanion boron hydride clusters is related to the stability toward disproportionation. The E^o_{red} value of reaction $B_7H_7 + e^- \rightarrow B_7H_7^-$ is the smallest for the first reductions of the B_nH_n species (n = 6-13) except for $B_{13}H_{13}$ while reaction $B_8H_8^- + e^- \rightarrow B_8H_8^{2-}$ yields the smallest E^o_{red} value for the second reductions of the B_nH_n species (n = 6-13). The E^o_{red} values of $B_7H_7^{0/-}$ ($B_7H_7 + e^- \rightarrow B_7H_7^-$) show that the first reduction is more difficult than the second reduction (-0.10 - 0.71 V < 0.0, G4/M06-2X), which indicates potential inversion. However, Klanberg el $al.$[1d] reported that $B_7H_7^{2-}$ is the least stable dianion boron cluster and the most hydrolytically unstable. Except for $B_{13}H_{13}$, the E^o_{Red} of reaction $B_7H_7 + 2e^- \rightarrow B_7H_7^{2-}$ is the smallest value for the two electron attachments (0.31 V, G4/M06-2X). The computed E^o_{Red} value (reduction potential of monoanion) of $B_8H_8^-$ is 0.00 V which compares to the experimental $E_{1/2}$ (oxidative stability of dianion) of 0.2 V (Figure 4).[1a,1d] Since the calculated E^o_{red} value of reaction $B_8H_8 + e^- \rightarrow B_8H_8^-$ is 0.69 V (G4/M06-2X), B_8H_8 is predicted to have the normal ordering of potentials in aqueous solution (0.69 - 0.00 V > 0.0). The B3LYP functional

generally underestimates the oxidative stability of $B_nH_n^{2-}$ relative to experimental results and to the G4/M06-2X result by more than 0.4 V (Figure 4). Indeed, it has been reported that the B3LYP functional underestimates the experimental redox potential of transition metal complexes.[10c] However, reasonable E^o_{Red} values (within 0.2 V of the experimental value) can be obtained when the G4/M06-2X method is applied (Figure 4).

The disproportionation free energies (ΔG_{dpro}) of the processes $2B_nH_n^- \rightarrow B_nH_n + B_nH_n^{2-}$ (n = 6-13) reveal the stability of monoanion radicals (Figure 5). For example, the B_nH_n species (n = 8-11) shows positive ΔG_{dpro} values with a normal ordering of potentials while those with n=7 and 13 yields negative ΔG_{dpro} values and potential inversion ($E^o_1 - E^o_2 < 0$ for reduction) (Figure 3 and Figure 5). The ΔG_{dpro} of B_6H_6 and $B_{12}H_{12}$ are borderline potential inversion cases (-0.6 and -0.4 kcal/mol, respectively, G4/M06-2X). Thus, a positive value of ΔG_{dpro} of B_nH_n indicates that the monoanion radical should be observed. The M06-2X functional always results in the most negative ΔG_{dpro} values for every disproportionation of the B_nH_n species (n = 6-13) in this study (Figure 5). For example, the ΔG_{dpro} values for $B_{12}H_{12}^{2-}$ using B3LYP, G4/B3LYP, and G4/M06-2X methods are between -0.4 and -1.1 kcal/mol but the result from the M06-2X functional is much more negative (-7.1 kcal/mol). The variation of ΔG_{dpro} is within 2.5 kcal/mol for B_nH_n species (n = 6-13) for all methods tested except for the M06-2X functional (Figure 5).

Since the geometric changes of the B_nH_n species (n = 6-13) *hypercloso* boron clusters are subtle during the reduction process, and the solvation free energy (ΔG_{solv}) depends linearly on cluster size, the greatest effect on potential inversion comes from the electronic nature of the $B_nH_n^-$ anions (n = 6-13) (Figure 2). The best-known monanion radical is $B_8H_8^-$ where the a fluxional nature is well established.[34,50] This situation is different from other anions where fluxional behavior of the anion can induce potential inversion (i.e. $\Delta G_{dpro} < 0$).[41]
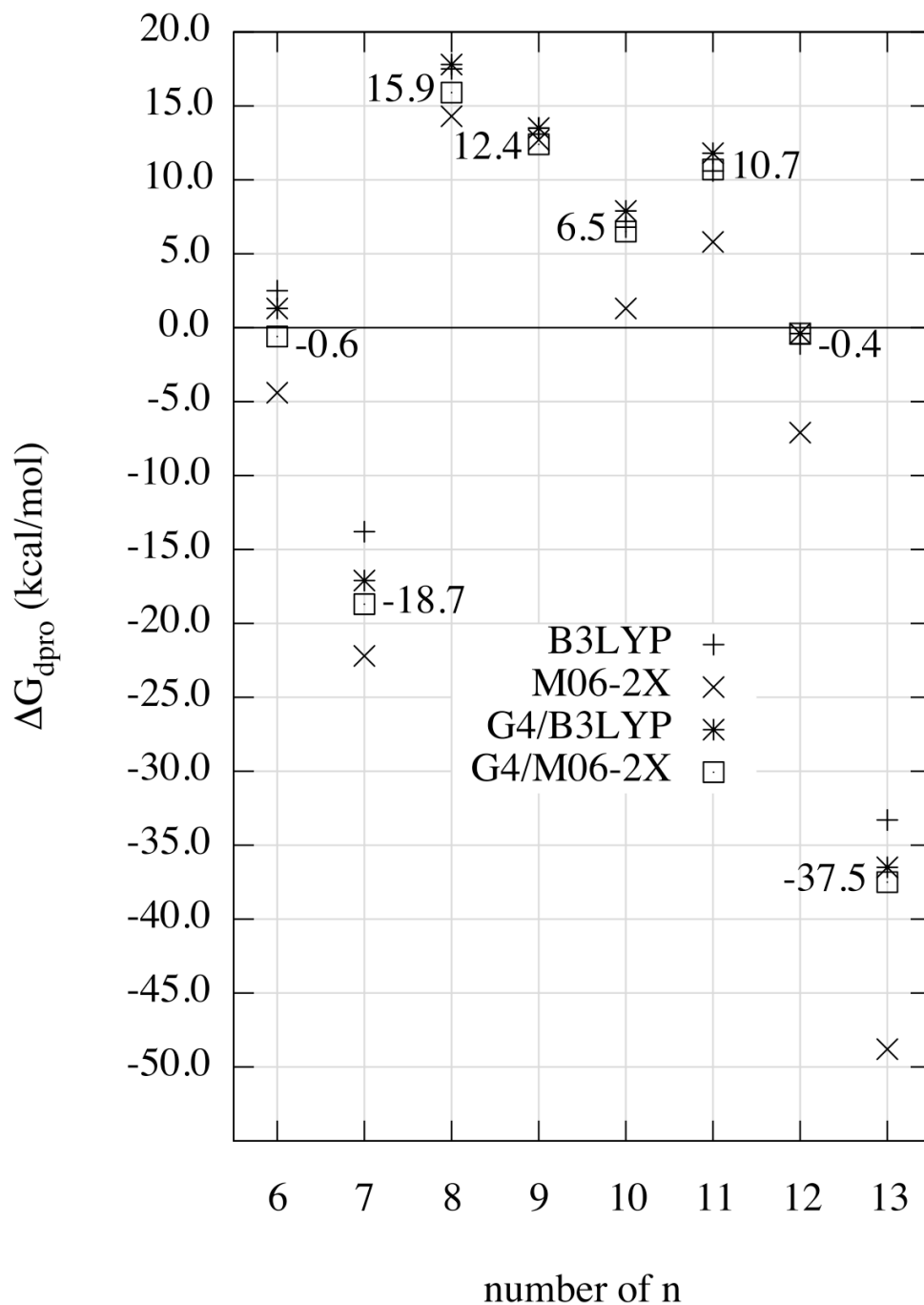
Figure 5. Disproportionation free energies (ΔG_{dpro}) of $B_nH_n^-$ (n = 6-13) *hypercloso* boron clusters computed on the B3LYP/aug-cc-pvtz, M06-2X/aug-cc-pvtz, and G4 levels of theory followed by the CPCM/Pauling cavity set method. The values in plot are the ΔG_{dpro} from the G4/M06-2X method.

Speiser et al.[42] reported that the radical monoanion $B_8Cl_8^-$ is even more stable against disproportionation than $B_9Cl_9^-$. The stable $B_8H_8^-$, $B_{10}H_{10}^-$, $B_{11}H_{11}^-$, and $B_{12}H_{12}^-$ intermediates are used to explain the formation of reduction products in the literature. Our positive ΔG_{dpro} values by G4/M06-2X combination for $2B_nH_n^- \rightarrow B_nH_n + B_nH_n^{2-}$ ($n = 8,9,10,11$) support the experimental observation of monoanion radicals (Figure 5).[1d,2d,43]

Many studies interpret the stability of monoanion radicals using delocalization of the unpaired electron.[1d,15b,19b,20,21b] The most stable monanion to disproportionation is $B_8H_8^-$ which shows strong electron delocalization in contrast to $B_{11}H_{11}^-$ (Figure 6).
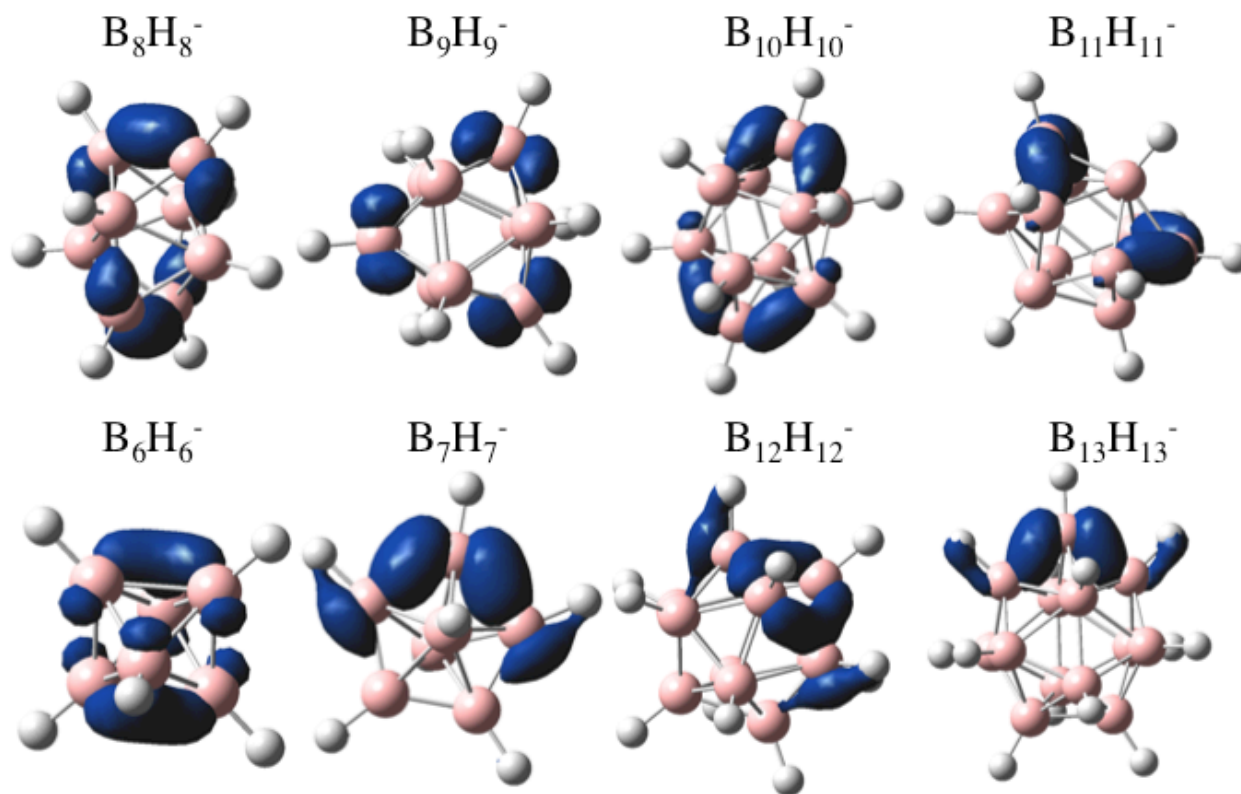

Figure 6. Spin densities of $B_nH_n^-$ ($n = 6$-13) boron clusters obtained from the M06-2X/aug-cc-pvtz level of theory (0.08 a.u. isodensity).

The monoanion radicals $B_7H_7^-$, $B_{12}H_{12}^-$, and $B_{13}H_{13}^-$ show a normal ordering of potential ($\Delta G_{dpro}<0$) which indicates that the monoanion radical should disproportionate to the neutral and dianion species (Figure 5). I interpret that the stability of $B_{11}H_{11}^-$ for disproportionation without electron delocalization comes from the smaller formation enthalpy (ΔH_f at 0 K, G4 level of theory) for $B_{11}H_{11}^{2-}$ (-4.6 kcal/mol) than those of $B_{10}H_{10}^{2-}$ (-5.6 kcal/mol) and $B_{12}H_{12}^{2-}$ (-77.8 kcal/mol).

The free energy changes per BH unit ($\Delta G_{E.A.}/(BH)_n$ and $\Delta G_{sol}/(BH)_n$) for $B_nH_n^{0/-}$ and $B_nH_n^{-/2-}$ (n = 6-13) are presented in Table 1. The stabilization by the first electron attachment of B_8H_8 in aqueous solution (-14.3 kcal/mol with G4/M06-2X) is more negative than those of B_nH_n (n = 9-13) but less negative than for B_6H_6 (-19.1 kcal/mol, Table 1).

The values of E^o_{Red} in solution and $\Delta G_{E.A.}$ in the gas phase for the first electron attachment ($B_nH_n + e^- \rightarrow B_nH_n^-$ (n = 6-12)) shows a linear relationship as found in the literature.[11a,11c-11h,15a] The value of E^o_{Red} for $B_{13}H_{13}^{0/-}$ (-0.94 V, G4/M06-2X) is about 0.2 V less than a value expected from a linear relationship (-0.7 V, Figure 7). More favorable solvation of $B_{13}H_{13}$ than those of other neutral B_nH_n clusters induces this nonlinearity (Figure 2 and 7).

The correlation between E^o_{Red} and $\Delta G_{E.A.}$ for the second electron attachment ($B_nH_n^- + e^- \rightarrow B_nH_n^{2-}$ (n = 6-12)) is given in Figure 8. Beyond the overall linear relationship, there are large deviations for several clusters, in particular $B_nH_n^-$ (n = 6 and 11). In order to understand the deviations, the decomposition of ΔG_{solv} (keyword=externaliteration) is useful. As noted previously, values of ΔG_{solv} for dianions are much larger than for monoanions or neutral species so I limit our analysis to the dianions. As the size of the cluster increases, the contribution of hydrogen atoms ($\Delta G_{solv}(H)$) to the total ΔG_{solv} of $B_nH_n^{2-}$ (n = 6-13) increases (Figure 9).

Figure 7. The correlation between gaseous electron attachment free energy ($\Delta G_{E.A.}$ by G4) and reduction potential (E^o_{Red} by G4/M06-2X(Pauling)) in aqueous solution for $B_nH_n + e^- \rightarrow B_nH_n^-$.
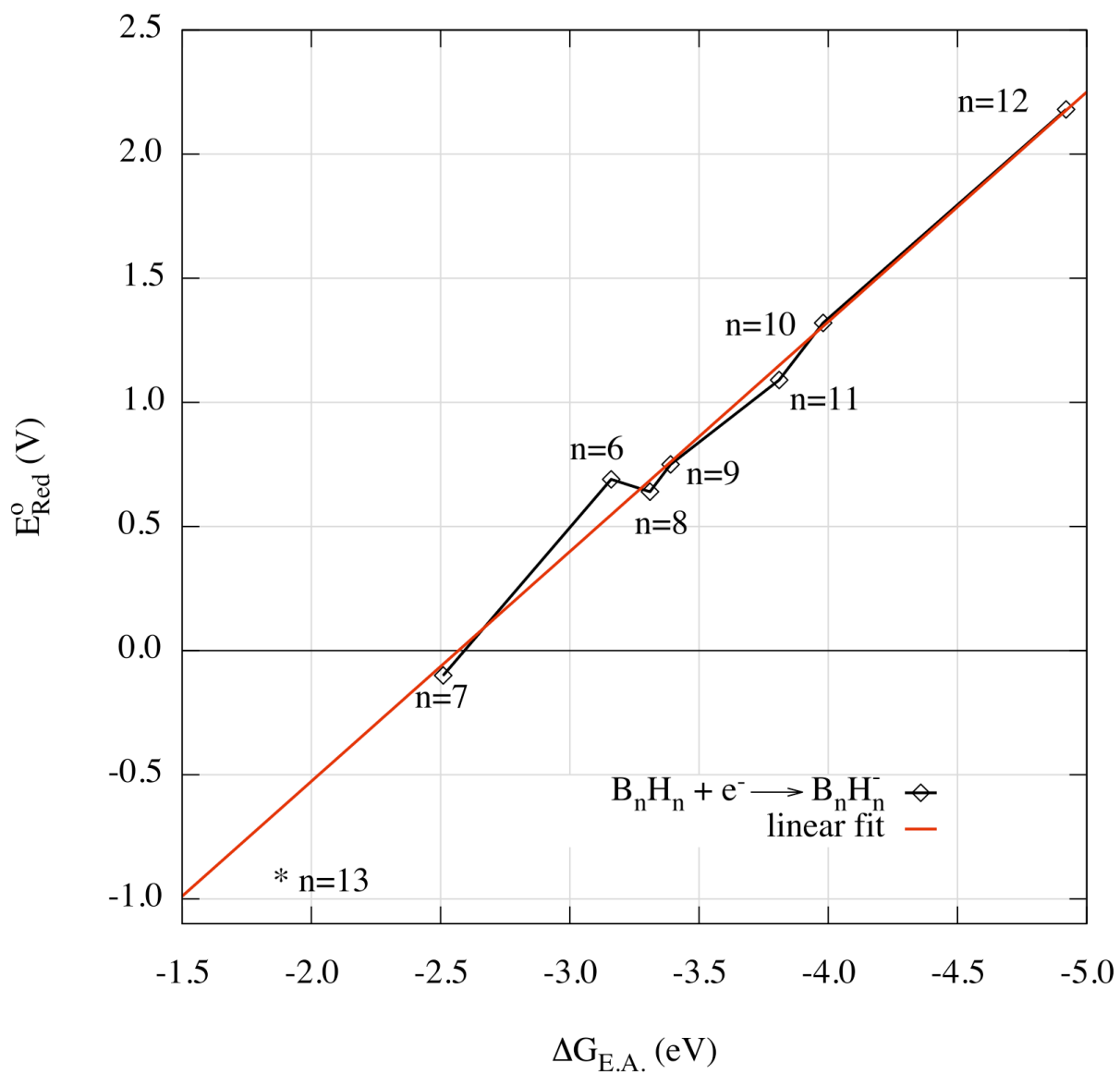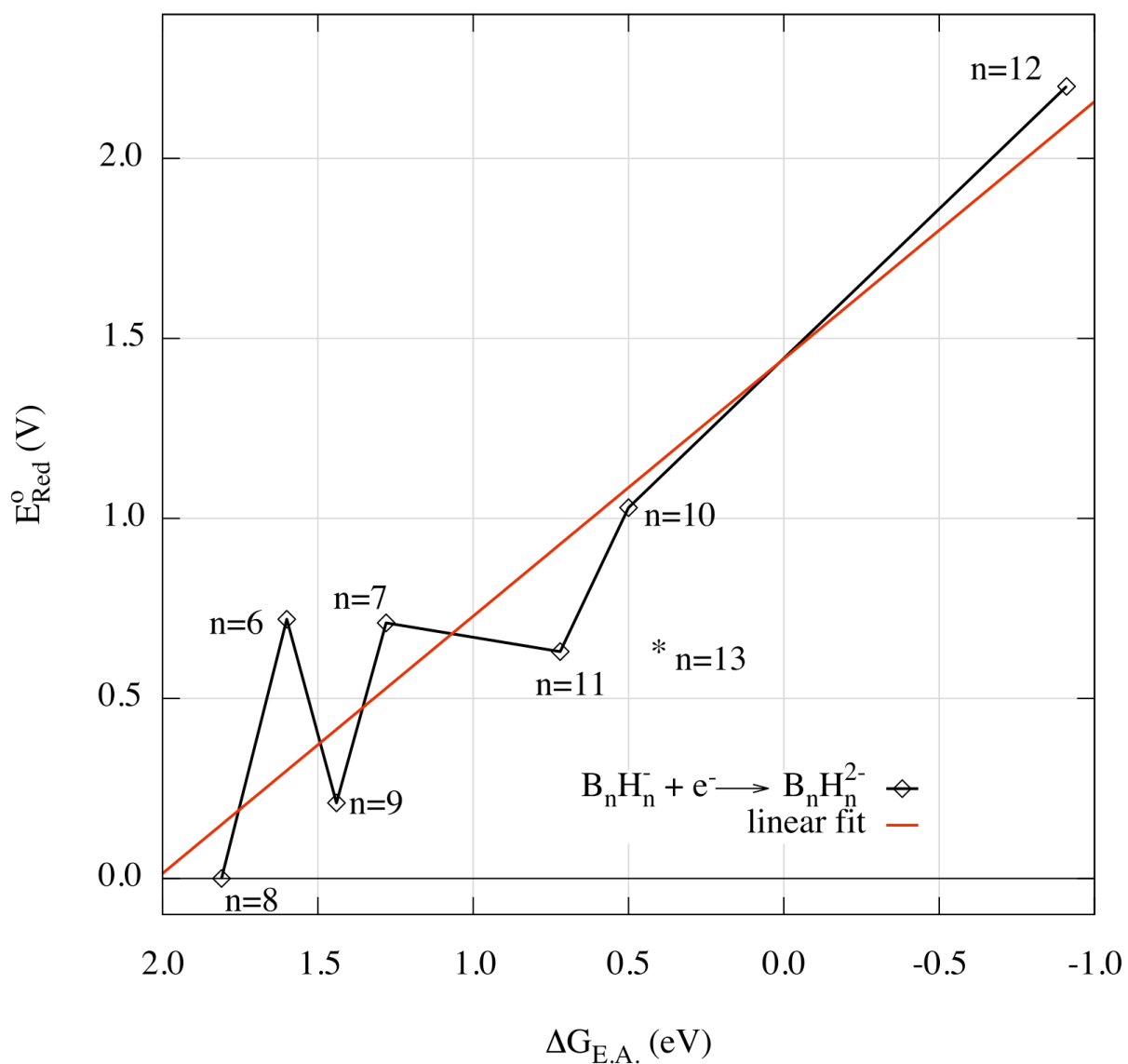
Figure 8. The correlation between gaseous electron attachment free energy ($\Delta G_{E.A.}$ by G4) and reduction potential (E^o_{Red} by G4/M06-2X(Pauling)) in aqueous solution for $B_nH_n^- + e^- \rightarrow B_nH_n^{2-}$.
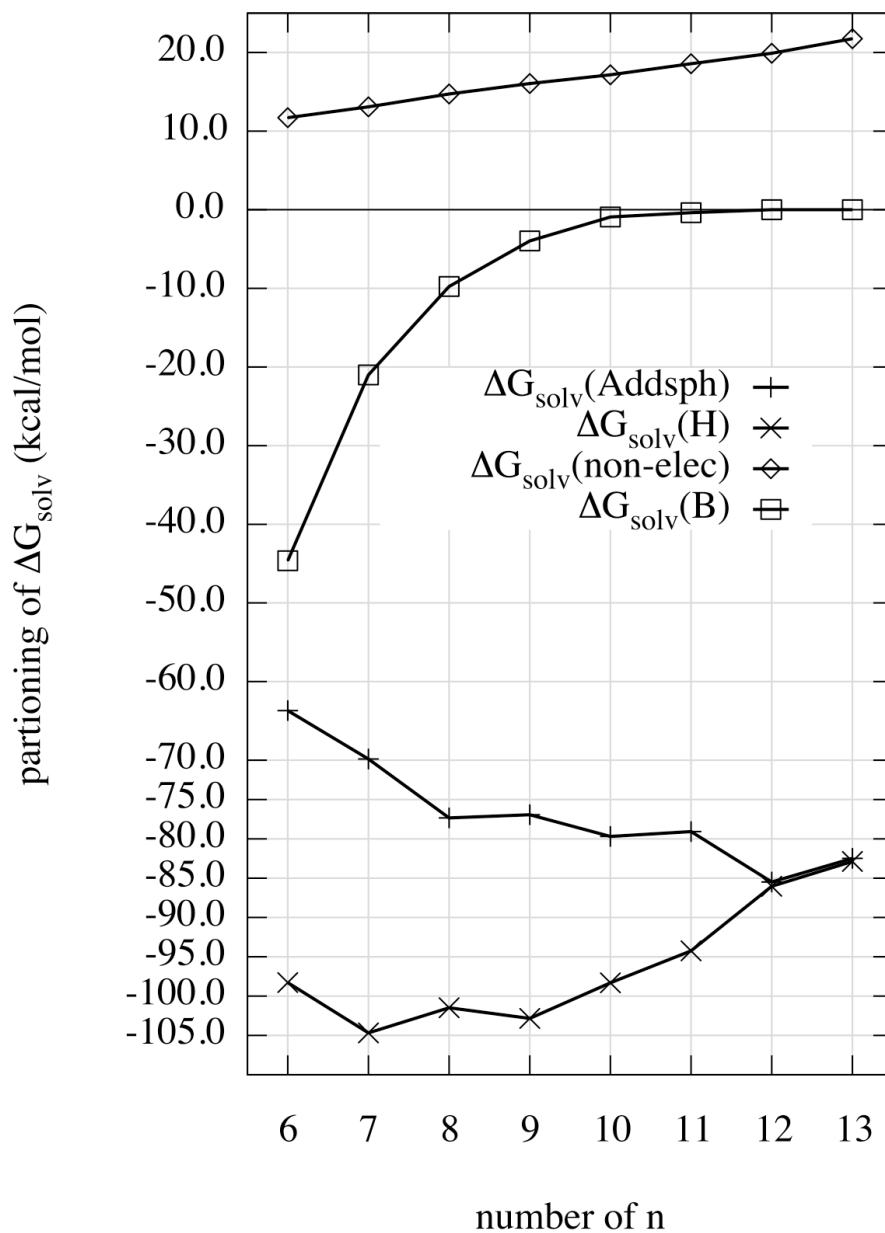
Figure 9. The partitioning of solvation free energies (ΔG_{solv}) of $B_nH_n^{2-}$ (n = 6-13) boron clusters obtained from the M06-2X/Pauling cavity set method (keyword=externaliteration) ($\Delta G_{solv}(B)$ = solvation free energy by all boron atoms, $\Delta G_{solv}(H)$ = solvation free energy by all hydrogen atoms, ΔG_{solv}(non-elec) = solvation free energy by dispersion and cavitation, and ΔG_{solv}(Addsph) = solvation free energy by smoothed surface for the cavity volume)

The contribution of the non-electrostatic terms (cavity and dispersion energy, ΔG_{solv}(non-elec)) slowly increases as the size of cluster increases while the ΔG_{solv}(B) exponentially decreases as the exposure of boron atoms in $B_nH_n^{2-}$ to solvent decreases (Figure 9). The ΔG_{solv}(B) for $B_6H_6^{2-}$ (-44.6 kcal/mol) is more than two times ΔG_{solv}(B) for $B_7H_7^{2-}$ (-21.0 kcal/mol, Figure 9). This is caused by the significant increase in accessibility of boron atoms to solvent (Figure 9). For the $B_nH_n^{2-}$ species (n = 6-8), the ΔG_{solv}(B) contributes substantially to the total ΔG_{solv} of the dianion while ΔG_{solv}(B) of $B_nH_n^{2-}$ species (n = 9-13) is relatively negligible. The deviation of $B_{11}H_{11}^{2-}$ from linearity (Figure 9) is due to the ΔG_{solv}(H) of the hydrogen attached to the seven-coordinate boron atom in $B_{11}H_{11}^{2-}$ which is about 3 kcal/mol less than ΔG_{solv}(H) from other hydrogen atoms. The smaller ΔG_{solv} of the dianion leads to a smaller E^o_{Red} value than expected (Figure 8).

E^o_{Red} of $B_{12}X_{12}$ (X = H, F, Cl, OH, and CH₃). The experimental redox chemistry of the persubstituted dodecaborates $B_{12}X_{12}$ has been reported.[1a,5,9a,9c,9g,33,44] The E^o_{Red} for the $B_{12}X_{12}^{-/2-}$ (X = H, F, Cl, OH, and CH₃, Table 2) is in the order $B_{12}Cl_{12}^{2-} > B_{12}F_{12}^{2-} > B_{12}H_{12}^{2-} > B_{12}(CH_3)_{12}^{2-} > B_{12}(OH)_{12}^{2-}$ evaluated with the B3LYP and M06-2X functional (G4/M06-2X calculations could not be carried out for X ≠ H). Ivanov *et el*.[9a] reported ca. 1.9-2.0 V for the oxidative stability of $B_{12}F_{12}^{2-}$ in ethylene carbonate:dimethyl carbonate (50:50 in volume) solution and suggested that the salts of the radical monoanion $B_{12}F_{12}^-$ might be isolable. Our positive ΔG_{dpro} for the reaction $2B_{12}F_{12}^- \rightarrow B_{12}F_{12} + B_{12}F_{12}^{2-}$ (14.4 kcal/mol, M06-2X) supports the possibility isolating $B_{12}F_{12}^-$ (Table 3). However, a more recent study of $B_{12}X_{12}^{2-}$ (X = H, F, Cl, Br, and I) in liquid SO₂ solution gives an oxidative stabilitity of 2.3 V for $B_{12}F_{12}^{2-}$, which is similar to the result with the M06-2X functional (Table 2).[33] The oxidative stability of $B_{12}(CH_3)_{12}^{2-}$ has been reported as 0.44 V (and corrected to SHE as 0.6 V)[9c,45] which can be compared to the values 0.39 V (B3LYP) or 0.67 V (M06-2X) (Table 2). The value of ΔG_{dpro} (18.9 kcal/mol) with the

158

M06-2X functional supports the well-known stability of the $B_{12}(CH_3)_{12}^-$ monoanion radical (Table 3).[9c]

Table 2. E^o_{red} values of $B_{12}X_{12}^{0/-/2-}$ (X = H, F, Cl, OH, and CH$_3$) boron clusters with the DFT/CPCM(Pauling) method

Reduction (E^o_{Red}, V)	B3LYP[a]	M06-2X[a]	$E_{1/2}$(V)	σ_p[c]
$B_{12}(OH)_{12} + e^- \rightarrow B_{12}(OH)_{12}^-$	0.79(-79.3)	1.20(-88.0)		-0.37
$B_{12}(CH_3)_{12} + e^- \rightarrow B_{12}(CH_3)_{12}^-$	1.52(-101.5)	1.80(-107.6)		-0.17
$B_{12}H_{12} + e^- \rightarrow B_{12}H_{12}^-$	1.93(-108.3)	2.12(-107.6)		0.00
$B_{12}F_{12} + e^- \rightarrow B_{12}F_{12}^-$	2.64(-129.6)	3.09(-139.2)		0.06
$B_{12}Cl_{12} + e^- \rightarrow B_{12}Cl_{12}^-$	2.92(-135.5)	3.41(-146.0)	(ca 3.1)[b]	0.23
$B_{12}(OH)_{12}^- + e^- \rightarrow B_{12}(OH)_{12}^{2-}$	0.39(5.1)	0.63(1.0)	1.3	-0.37
$B_{12}(CH_3)_{12}^- + e^- \rightarrow B_{12}(CH_3)_{12}^{2-}$	0.39(-11.0)	0.98(-24.3)	0.6	-0.17
$B_{12}H_{12}^- + e^- \rightarrow B_{12}H_{12}^{2-}$	2.24(-16.6)	2.14(-22.0)	1.7(2.2)[b]	0.00
$B_{12}F_{12}^- + e^- \rightarrow B_{12}F_{12}^{2-}$	2.03(-31.7)	2.47(-40.1)	2.0(2.3)[b]	0.06
$B_{12}Cl_{12}^- + e^- \rightarrow B_{12}Cl_{12}^{2-}$	2.54(-57.9)	2.98(-67.3)	2.6(2.7)[b]	0.23
$B_{12}(OH)_{12} + 2e^- \rightarrow B_{12}(OH)_{12}^{2-}$	0.59(-74.2)	0.92(-87.0)		-0.37
$B_{12}(CH_3)_{12} + 2e^- \rightarrow B_{12}(CH_3)_{12}^{2-}$	0.96(-112.5)	1.40(-131.9)		-0.17
$B_{12}H_{12} + 2e^- \rightarrow B_{12}H_{12}^{2-}$	2.09(-124.9)	2.13(-129.6)		0.00
$B_{12}F_{12} + 2e^- \rightarrow B_{12}F_{12}^{2-}$	2.34(-161.3)	2.78(-179.3)		0.06
$B_{12}Cl_{12} + 2e^- \rightarrow B_{12}Cl_{12}^{2-}$	2.73(-193.4)	3.20(-213.3)		0.23

[b]The $\Delta G_{E.A.}$ and ΔG_{solv} of $B_{12}X_{12}^{0/-/2-}$ are calculated with B3LYP and M06-2X functional. The value in parentheses is $\Delta G_{E.A.}$ obtained with DFT functionals. Due to the computational expense, G4 level of theory is not applied to $B_{12}X_{12}$ systems. [b]The value in parentheses is obtained from the measurement in liquid SO$_2$ solution, see reference 41. [c]The Hammett σ_p parameter comes from March, J. *Advanced Organic Chemsitry*; John & Wiley: New York, 1985.

Table 3. Disproportionation free energies in the gas phase (ΔG_{gas}, $2B_nX_n^-(g) \rightarrow B_nX_n(g) + B_nX_n^{2-}$

(g)) with DFT functionals (B3LYP and M06-2X) and in aqueous solution (ΔG_{dpro},

$2B_{12}X_{12}^-(aq) \rightarrow B_{12}X_{12}(aq) + B_{12}X_{12}^{2-}(aq)$) of $B_{12}X_{12}$ (X = H, F, Cl, OH, and CH_3)

hypercloso boron clusters with CPCM(Pauling) solvation modeling

$B_{12}X_{12}$	ΔG_{gas}[a]	ΔG_{gas}[a]	ΔG_{dpro}	ΔG_{dpro}
	B3LYP	M06-2X	B3LYP	M06-2X
$B_{12}H_{12}$	91.7	85.7	-1.1	-7.1
$B_{12}F_{12}$	97.9	99.1	14.0	14.4
$B_{12}Cl_{12}$	77.6	78.6	8.8	10.0
$B_{12}(OH)_{12}$	84.4	89.0	9.2	13.2
$B_{12}(CH_3)_{12}$	90.5	83.3	26.1	18.9

[a]G4 level of theory is not applied due to the computational expense.

The reported oxidative stability of $B_{12}Cl_{12}^{2-}$, (2.34 V, corrected to SHE as 2.6 V), can be

compared to our E^o_{Red} values of 2.54/2.98 V for $B_{12}Cl_{12}^{-/2-}$(B3LYP/M06-2X, Table 2).[1a,44] A

recent cyclic voltammetry study in liquid SO_2 solution reported a value of 2.15 V with the

ferrocene/ferrocenium reference electrode (and corrected to SHE as 2.70 V), which is between

the results obtained using the B3LYP and M06-2X functionals (Table 2).[33] The first one-

electron reduction E^o_{Red} value from the neutral ($B_{12}Cl_{12} + e^- \rightarrow B_{12}Cl_{12}^-$) evaluated with the

B3LYP and M06-2X functionals yielded 2.92 and 3.41 V respectively, which can be compared

to (corrected) the cyclic voltammetry value of 3.1 V (Table 2).[33] The identification of $B_{12}Cl_{12}$

was done by NMR and UV/Vis determinations.[33,46] The E^o_{Red} values for the $B_{12}X_{12}$ species (X =

H, F, Cl, and CH_3) are between 1.20 V and 3.41 V using the M06-2X functional (Table 2).

Knoth et al.[38b] reported that the oxidative stability decreased whenever hydroxyl groups

replaced the hydride ions of $B_{12}H_{12}^{2-}$. Recently, Van *et el.*[9f] reported the value of $E_{1/2}$ as 0.45 V

for $B_{12}(OH)_{12}^{2-}$ in CH_3CN and 0.75 V in water versus the ferrocenium/ferrocene reference

electrode couple (1.00 V in CH_3CN and 1.30 V in water versus SHE[47]). Our E^o_{Red} values for

$B_{12}(OH)_{12}^{-/2-}$ in water (using any cavity set) are much smaller than 1.00 V. The largest

calculated E^o_{Red} value of $B_{12}(OH)_{12}^{-/2-}$ (0.63 V) comes from the M06-2X functional which is 0.67

V smaller than the experimental value (1.30 V in water versus SHE, Table 2). All of the other

experimental oxidative stabilities are between the results using the B3LYP and M06-2X

functionals (Table 2). Therefore, I recommend a re-determination of $E_{1/2}$ for $B_{12}(OH)_{12}^{2-}$.

    McKee[22b] reported that the order of the Hammett (σ_p) parameter for $B_{12}X_{12}^{2-}$ agreed with

the order of gaseous stability for the process $B_{12}H_{12}^{n-} + 12HX \rightarrow B_{12}X_{12}^{n-} + 12H_2$ (n = 0,1,2; X =

H, F, OH, and CH_3), $B_{12}F_{12}^{2-} > B_{12}H_{12}^{2-} > B_{12}(CH_3)_{12}^{2-} > B_{12}(OH)_{12}^{2-}$. The trend of E^o_{Red} values

in this study also agrees well with the order of the Hammett (σ_p) parameter (Table 2). The

positive ΔG_{dpro} of $B_{12}X_{12}^{-}$ (X = F, Cl, OH, and CH_3) in our study is in agreement with the

stability of monoanion radical $B_{12}X_{12}^{-}$ (X = F, Cl, OH, and CH_3) that was observed

experimentally (Table 3).[9a-9c,9f,33,44,46]

$B_{12}H_{12}^{-}$ $B_{12}F_{12}^{-}$ $B_{12}Cl_{12}^{-}$ $B_{12}(OH)_{12}^{-}$ $B_{12}(CH_3)_{12}^{-}$
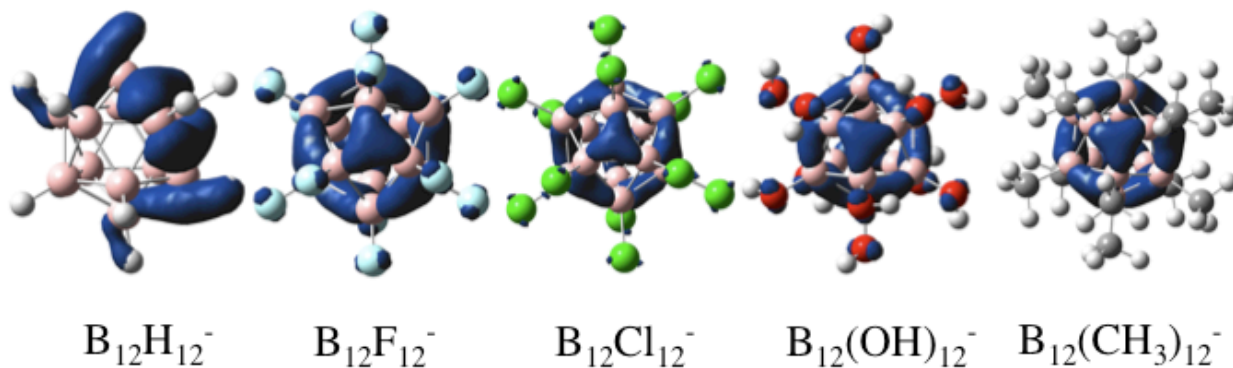
Figure 10. Spin densities of $B_{12}X_{12}^{-}$ (X=H, F, Cl, OH, and CH_3) *hypercloso* boron clusters

obtained on the M06-2X/aug-cc-pvtz level of theory (0.04 a.u. isodensity).

The unpaired spin density of the $B_{12}X_{12}^-$ species (X = F, Cl, OH, and CH$_3$) shows strong

delocalization, which is similar to that of $B_{12}H_{12}^-$ (Figure 6 and Figure 9). The unpaired electron

tends to be localized on the boron atoms of the cluster rather than on the functional groups of

$B_{12}X_{12}^-$ species (X = F, Cl, OH, and CH$_3$), in agreement with the observations from previous

studies (Figure 10).[9c,9f,33]

5.4 Conclusions

The reduction potentials (E^o_{Red}) of *hypercloso* boron hydrides B_nH_n (n = 6-13) and

persubstitiuted dodecaboron hydrides $B_{12}X_{12}$ (X = F, Cl, OH, and CH$_3$) have been studied at the

G4 level of theory and DFT methods with implicit solvation modeling. The E^o_{Red} values

obtained from the G4/M06-2X method provide the best agreement with experimental oxidative

stability ($E_{1/2}$) of the $B_nH_n^{2-}$ species (n = 6-12). Experimental oxidative stabilities of the $B_{12}X_{12}^{2-}$

species (X = F, Cl, OH, and CH$_3$) are usually located between the B3LYP and M06-2X values of

E^o_{Red}. Our oxidative stabilities for $B_6H_6^{2-}$ and $B_{12}(OH)_{12}^{2-}$ deviate more than expected from the

experimental values and I suggest that more experiments may be needed. The B3LYP functional

tends to underestimate E^o_{Red} values while the M06-2X functional tends to overestimate them.

ΔG_{solv} depends greatly on the choice of the cavity radii set while the dependence on density

functional is modest. The CPCM/UAKS cavity set gives the smallest ΔG_{solv} and the SMD

method gives the largest ΔG_{solv} for the $B_nH_n^{0/-/2-}$ species (n = 6-13). The stability of monoanion

radicals of B_nH_n (n = 6-13) to disproportionation ($2B_nH_n^- \rightarrow B_nH_n + B_nH_n^{2-}$) decreases in the

order $B_8H_8^- > B_9H_9^- > B_{11}H_{11}^- > B_{10}H_{10}^-$ while $B_7H_7^-$ and $B_{13}H_{13}^-$ are anticipated to undergo very

spontaneous disproportionation due to potential inversion. Spin density delocalization in the

$B_nH_n^-$ radical anions explains their stability but positive ΔG_{dpro} without distinct delocalization of

spin density results for $B_{11}H_{11}^-$. A good correlation between $\Delta G_{E.A.}$ and E^o_{Red} is established for the first electron attachments of the B_nH_n species (n = 6-13) but the correlation for second electron attachments of the B_nH_n species (n = 6-13) deviates from a linear relationship in the case of B_6H_6, $B_{11}H_{11}$, and $B_{13}H_{13}$. The solvation free energy differences between $B_nH_n^-$ and $B_nH_n^{2-}$ are significant factors in determining E^o_{Red} and or $E_{1/2}$ in aqueous solution. The partitioning of solvation free energies reveals why the correlation between $\Delta G_{E.A.}$ and E^o_{Red} for some $B_nH_n^{-/2-}$ species (n = 6, 7, and 11) deviates from a linear relationship.

5.5 References

(1)   (a) Morris, J. H.; Gysling, H. J.; Reed, D. *Chem. Rev.* **1985**, *85*, 51-76. (b) Muetterties, E. L.; Balthis, J. H.; Chia, Y. T.; Knoth, W. H.; Miller, H. C. *Inorg. Chem.* **1964**, *3*, 444-451. (c) Klanberg, F.; Muetterties, E. L. *Inorg. Chem.* **1966**, *5*, 1955-1960. (d) Klanberg, F.; Eaton, D. R.; Guggenberger, L. J.; Muetterties, E. L. *Inorg. Chem.* **1967**, *6*, 1271-1281. (e) Preetz, W.; Peters, G. *Eur. J. Inorg. Chem.* **1999**, 1831-1846. (f) Muetterties, E. L.; Knoth, W. H. *Polyhedral Boranes*; Marcel Dekker Inc.: New York, **1968**.

(2)   (a) Wiersema, R. J.; Middaugh, R. L. *Inorg. Chem.* **1969**, *8*, 2074-2079. (b) Watson-Clark, R. A.; Hawthorne, M. F. *Inorg. Chem.* **1997**, *36*, 5419-5420. (c) Volkov, O.; Hu, C. H.; Kolle, U.; Paetzold, P. *Z. Anorg. Allg. Chem.* **2005**, *631*, 1909-1911. (d) Volkov, O.; Paetzold, P.; Hu, C. H. *Z. Anorg. Allg. Chem.* **2006**, *632*, 945-948. (e) Zhizhin, K. Y.; Zhdanov, A. P.; Kuznetsov, N. T. *Russ. J. Inorg. Chem.* **2010**, *55*, 2089-2127.

(3)   (a) Hawthorn, M. F.; Pilling, R. L.; Stokely, P. F. *J. Am. Chem. Soc.* **1965**, *87*, 1893-1899. (b) Hawthorne, M. F.; Pilling, R. L.; Stokely, P. F.; Garrett, P. M. *J. Am. Chem. Soc.* **1963**, *85*, 3704-3705. (c) Chamberland, B. L.; Muetterties, E. L. *Inorg. Chem.* **1964**, *3*, 1450-1456. (d) Wiersema, R. J.; Middaugh, R. L. *Inorg. Chem.* **1969**, *8*, 2074-2079.

(4)   Kaczmarc.A; Kolski, G. B.; Townsend, W. P. *J. Am. Chem. Soc.* **1965**, *87*, 1413-1413.

(5)   Avelar, A.; Tham, F. S.; Reed, C. A. *Angew. Chem. Int. Ed.* **2009**, *48*, 3491-3493.

(6)   (a) Geis, V.; Guttsche, K.; Knapp, C.; Scherer, H.; Uzun, R. *Dalton Trans.* **2009**, 2687-2694. (b) Ivanov, S. V.; Davis, J. A.; Miller, S. M.; Anderson, O. P.; Strauss, S. H. *Inorg. Chem.* **2003**, *42*, 4489-4491. (c) Ivanov, S. V.; Lupinetti, A. J.; Solntsev, K. A.; Strauss, S. H. *J. Fluor. Chem.* **1998**, *89*, 65-72. (d) Peryshkov, D. V.; Popov, A. A.; Strauss, S. H. *J. Am. Chem. Soc.* **2009**, *131*, 18393-18403.

(7)   Jelen, F.; Olejniczak, A. B.; Kourilova, A.; Lesnikowski, Z. J.; Palecek, E. *Anal. Chem.* **2008**, *81*, 840-844.

(8)   Jalisatgi, S. S.; Kulkarni, V. S.; Tang, B.; Houston, Z. H.; Lee, M. W.; Hawthorne, M. F. *J. Am. Chem. Soc.* **2011**, *133*, 12382-12385.

(9)   (a) Ivanov, S. V.; Miller, S. M.; Anderson, O. P.; Solntsev, K. A.; Strauss, S. H. *J. Am. Chem. Soc.* **2003**, *125*, 4694-4695. (b) Warneke, J.; Dulcks, T.; Knapp, C.; Gabel, D. *Phys. Chem. Chem. Phys.* **2011**, *13*, 5712-5721. (c) Peymann, T.; Knobler, C. B.; Hawthorne, M. F. *Chem. Comm.* **1999**, 2039-2040. (d) Peymann, T.; Knobler, C. B.;

Khan, S. I.; Hawthorne, M. F. *J. Am. Chem. Soc.* **2001**, *123*, 2182-2185. (e) Maderna, A.; Knobler, C. B.; Hawthorne, M. F. *Angew. Chem. Int. Ed.* **2001**, *40*, 1661-1664. (f) Van, N.; Tiritiris, I.; Winter, R. F.; Sarkar, B.; Singh, P.; Duboc, C.; Muñoz-Castro, A.; Arratia-Pérez, R.; Kaim, W.; Schleid, T. *Chem. Eur. J.* **2010**, *16*, 11242-11245. (g) Lee, M. W.; Farha, O. K.; Hawthorne, M. F.; Hansch, C. H. *Angew. Chem. Int. Ed.* **2007**, *46*, 3018-3022.

(10)   (a) Baik, M. H.; Friesner, R. A. *J. Phys. Chem. A* **2002**, *106*, 7407-7412. (b) Dutton, A. S.; Fukuto, J. M.; Houk, K. N. *Inorg. Chem.* **2005**, *44*, 4024-4028. (c) Roy, L. E.; Jakubikova, E.; Guthrie, M. G.; Batista, E. R. *J. Phys. Chem. A* **2009**, *113*, 6745-6750. (d) Si, D.; Li, H. *J. Phys. Chem. A* **2009**, *113*, 12979-12987. (e) Namazian, M.; Lin, C. Y.; Coote, M. L. *J. Chem. Theory Comput.* **2010**, *6*, 2721-2725. (f) Lord, R. L.; Schultz, F. A.; Baik, M. H. *Inorg. Chem.* **2010**, *49*, 4611-4619. (g) Fry, A. J.; Davis, A. P. *J. Phys. Chem. A* **2010**, *114*, 12299-12304. (h) Gennaro, A.; Isse, A. A.; Lin, C. Y.; Coote, M. L. *J. Phys. Chem. B.* **2011**, *115*, 678-684. (i) Jiao, D.; Leung, K.; Rempe, S. B.; Nenoff, T. M. *J. Chem. Theory Comput.* **2010**, *7*, 485-495. (j) Surawatanawong, P.; Tye, J. W.; Darensbourg, M. Y.; Hall, M. B. *Dalton Trans.* **2010**, *39*, 3093-3104. (k) Blumberger, J.; Tateyama, Y.; Sprik, M. *Comp. Phys. Comm.* **2005**, *169*, 256-261. (l) VandeVondele, J.; Sulpizi, M.; Sprik, M. *Angew. Chem. Int. Ed.* **2006**, *45*, 1936-1938. (m) VandeVondele, J.; Ayala, R.; Sulpizi, M.; Sprik, M. *J. Electroanal. Chem.* **2007**, *607*, 113-120. (n) Costanzo, F.; Sulpizi, M.; Guido Della Valle, R.; Sprik, M. *J. Chem. Theory Comput.* **2008**, *4*, 1049-1056. (o) Cheng, J.; Sulpizi, M.; Sprik, M. *J. Chem. Phys.* **2009**, *131*, 154504-154520.

(11)   (a) Parker, V. D. *J. Am. Chem. Soc.* **1976**, *98*, 98-103. (b) Ballard, R. E. *Chem. Phys. Lett.* **1976**, *42*, 97-98. (c) Ruoff, R. S.; Kadish, K. M.; Boulas, P.; Chen, E. C. M. *J. Phys. Chem.* **1995**, *99*, 8843-8850. (d) Lobach, A. S.; Strelets, V. V. *Russ. Chem. Bull.* **2001**, *50*, 1593-1595. (e) Kebarle, P.; Chowdhury, S. *Chem. Rev.* **1987**, *87*, 513-534. (f) Shalev, H.; Evans, D. H. *J. Am. Chem. Soc.* **1989**, *111*, 2667-2674. (g) Nelsen, S. F.; Teasley, M. F.; Bloodworth, A. J.; Eggelte, H. J. *J. Org. Chem.* **1985**, *50*, 3299-3302. (h) Betowski, L. D.; Enlow, M.; Riddick, L.; Aue, D. H. *J. Phys. Chem. A* **2006**, *110*, 12927-12946.

(12)   (a) Sadlej-Sosnowska, N. *Theor. Chem. Acc.* **2007**, *118*, 281-293. (b) Ho, J.; Coote, M. L. *J. Chem. Theory Comput.* **2009**, *5*, 295-306. (c) Chipman, D. M. *J. Phys. Chem. A* **2002**,

106, 7413-7422. (d) Camaioni, D. M.; Dupuis, M.; Bentley, J. *J. Phys. Chem. A* **2003**, *107*, 5778-5788. (e) Ginovska, B.; Camaioni, D. M.; Dupuis, M.; Schwerdtfeger, C. A.; Gil, Q. *J. Phys. Chem. A* **2008**, *112*, 10604-10613. (f) Alexeev, Y.; Windus, T. L.; Zhan, C.-G.; Dixon, D. A. *I. J. Quant. Chem.* **2005**, *102*, 775-784. (g) Gutowski, K. E.; Dixon, D. A. *J. Phys. Chem. A* **2006**, *110*, 8840-8856.

(13)   Lee, T. B.; McKee, M. L. *Phys. Chem. Chem. Phys.* **2011**, *13*, 10258-10269.

(14)   (a) Evans, D. H.; Hu, K. *J. Chem. Soc. Faraday Trans.* **1996**, *92*, 3983-3990. (b) Felton, G. A. N.; Vannucci, A. K.; Chen, J.; Lockett, L. T.; Okumura, N.; Petro, B. J.; Zakai, U. I.; Evans, D. H.; Glass, R. S.; Lichtenberger, D. L. *J. Am. Chem. Soc.* **2007**, *129*, 12521-12530. (c) Muratsugu, S.; Sodeyama, K.; Kitamura, F.; Sugimoto, M.; Tsuneyuki, S.; Miyashita, S.; Kato, T.; Nishihara, H. *J. Am. Chem. Soc.* **2009**, *131*, 1388-1389.

(15)   (a) Evans, D. H. *Chem. Rev.* **2008**, *108*, 2113-2144. (b) Hapiot, P.; Kispert, L. D.; Konovalov, V. V.; Savéant, J.-M. *J. Am. Chem. Soc.* **2001**, *123*, 6669-6677. (c) Gileadi, E. *J. Electroanal. Chem.* **2002**, *532*, 181-189.

(16)   (a) Hush, N. S.; Blackledge, J. *J. Chem. Phys.* **1955**, *23*, 514-517. (b) Fry, A. J. *Tetrahedron* **2006**, *62*, 6558-6565.

(17)   (a) Fry, A. J. *Electrochem. Commun.* **2005**, *7*, 602-606. (b) Macías-Ruvalcaba, N. A.; Evans, D. H. *J. Phys. Chem. B.* **2005**, *109*, 14642-14647.

(18)   Barrière, F.; Geiger, W. E. *J. Am. Chem. Soc.* **2006**, *128*, 3980-3989.

(19)   (a) Yang, B.; Liu, L.; Katz, T. J.; Liberko, C. A.; Miller, L. L. *J. Am. Chem. Soc.* **1991**, *113*, 8993-8994. (b) Du, S.; Farley, R. D.; Harvey, J. N.; Jeffery, J. C.; Kautz, J. A.; Maher, J. P.; McGrath, T. D.; Murphy, D. M.; Riis-Johannessen, T.; Stone, F. G. A. *Chem. Comm.* **2003**, 1846-1847.

(20)   Mao, F.; Tyler, D. R.; Bruce, M. R. M.; Bruce, A. E.; Rieger, A. L.; Rieger, P. H. *J. Am. Chem. Soc.* **1992**, *114*, 6418-6424.

(21)   (a) Salaymeh, F.; Berhane, S.; Yusof, R.; de la Rosa, R.; Fung, E. Y.; Matamoros, R.; Lau, K. W.; Zheng, Q.; Kober, E. M.; Curtis, J. C. *Inorg. Chem.* **1993**, *32*, 3895-3908. (b) Neyhart, G. A.; Hupp, J. T.; Curtis, J. C.; Timpson, C. J.; Meyer, T. J. *J. Am. Chem. Soc.* **1996**, *118*, 3724-3729. (c) Sutton, J. E.; Taube, H. *Inorg. Chem.* **1981**, *20*, 3125-3134.

(22)   (a) McKee, M. L.; Wang, Z.-X.; Schleyer, P. v. R. *J. Am. Chem. Soc.* **2000**, *122*, 4781-4793. (b) McKee, M. L. *Inorg. Chem.* **2002**, *41*, 1299-1305.

(23)   Zhao, Y.; Truhlar, D. *Theor. Chem. Acc.* **2008**, *120*, 215-241.

(24)   Frisch, M. J.; Trucks, G. W.; Schlegel, H. B.; Scuseria, G. E.; Robb, M. A.; Cheeseman, J. R.; Scalmani, G.; Barone, V.; Mennucci, B.; Petersson, G. A.; Nakatsuji, H.; Caricato, M.; Li, X.; Hratchian, H. P.; Izmaylov, A. F.; Bloino, J.; Zheng, G.; Sonnenberg, J. L.; Hada, M.; Ehara, M.; Toyota, K.; Fukuda, R.; Hasegawa, J.; Ishida, M.; Nakajima, T.; Honda, Y.; Kitao, O.; Nakai, H.; Vreven, T.; Montgomery, J., J. A.; Peralta, J. E.; Ogliaro, F.; Bearpark, M.; Heyd, J. J.; Brothers, E.; Kudin, K. N.; Staroverov, V. N.; Keith, T.; Kobayashi, R.; Normand, J.; Raghavachari, K.; Rendell, A.; Burant, J. C.; Iyengar, S. S.; Tomasi, J.; Cossi, M.; Rega, N.; Millam, J. M.; Klene, M.; Knox, J. E.; Cross, J. B.; Bakken, V.; Adamo, C.; Jaramillo, J.; Gomperts, R.; Stratmann, R. E.; Yazyev, O.; Austin, A. J.; Cammi, R.; Pomelli, C.; Ochterski, J. W.; Martin, R. L.; Morokuma, K.; Zakrzewski, V. G.; Voth, G. A.; Salvador, P.; Dannenberg, J. J.; Dapprich, S.; Daniels, A. D.; Farkas, O.; Foresman, J. B.; Ortiz, J. V.; Cioslowski, J.; Fox, D. J. *Gaussian 09, Revision A.02* **2009**, *Gaussian, Inc.*, Wallingford.

(25)   (a) Puiatti, M.; Vera, D. M. A.; Pierini, A. B. *Phys. Chem. Chem. Phys.* **2008**, *10*, 1394-1399. (b) Puiatti, M.; Vera, D. M. A.; Pierini, A. B. *Phys. Chem. Chem. Phys.* **2009**, *11*, 9013-9024.

(26)   Lee, T. B.; McKee, M. L. *Inorg. Chem.* **2011**, *50*, 11412-11422.

(27)   Barone, V.; Cossi, M. *J. Phys. Chem. A* **1998**, *102*, 1995-2001.

(28)   Marenich, A. V.; Cramer, C. J.; Truhlar, D. G. *J. Phys. Chem. B* **2009**, *113*, 6378-6396.

(29)   (a) Reiss, H.; Heller, A. *J. Phys. Chem.* **1985**, *89*, 4207-4213. (b) Truhlar, D. G.; Cramer, C. J.; Lewis, A.; Bumpus, J. A. *J. Chem. Edu.* **2004**, *81*, 596-604. (c) Winget, P.; Cramer, C. J.; Truhlar, D. G. *Theor. Chem. Acc.* **2004**, *112*, 217-227. (d) Donald, W. A.; Leib, R. D.; O'Brien, J. T.; Bush, M. F.; Williams, E. R. *J. Am. Chem. Soc.* **2008**, *130*, 3371-3381. (e) Donald, W. A.; Leib, R. D.; Demireva, M.; O'Brien, J. T.; Prell, J. S.; Williams, E. R. *J. Am. Chem. Soc.* **2009**, *131*, 13328-13337. (f) Isse, A. A.; Gennaro, A. *J. Phys. Chem. B* **2010**, *114*, 7894-7899. (g) Kelly, C. P.; Cramer, C. J.; Truhlar, D. G. *J. Phys. Chem. B* **2007**, *111*, 408-422. (h) Tissandier, M. D.; Cowen, K. A.; Feng, W. Y.; Gundlach, E.; Cohen, M. H.; Earhart, A. D.; Coe, J. V.; Tuttle, T. R. *J. Phys. Chem. A* **1998**, *102*, 7787-7794. (i) Tissandier, M. D.; Cowen, K. A.; Feng, W. Y.; Gundlach, E.; Cohen, M. H.;

Earhart, A. D.; Tuttle, T. R.; Coe, J. V. *J. Phys. Chem. A* **1998**, *102*, 9308-9308. (j) Fawcett, W. R. *Langmuir* **2008**, *24*, 9868-9875.

(30)   Namazian, M.; Coote, M. L. *J. Phys. Chem. A* **2007**, *111*, 7227-7232.

(31)   (a) Izutsu, K. *Electrochemistry in Nonaqueous Solutions*; Wiley-VCH: New York, **2002**. (b) Diggle, J. W.; Parker, A. J. *Aust. J. Chem.* **1974**, *27*, 1617-1621.

(32)   (a) http://webbook.nist.gov/chemistry/ion accessed 10 Aug. 2011. (b) Lias, S. G.; Bartmess, J. E.; Liebman, J. F.; Holmes, J. L.; Levin, R. D.; Mallard, W. G. *J. Phys. Chem. Ref. Data* **1988**, *17*, supplement 1-861.

(33)   Boeré, R. T.; Kacprzak, S.; Keßler, M.; Knapp, C.; Riebau, R.; Riedel, S.; Roemmele, T. L.; Rühle, M.; Scherer, H.; Weber, S. *Angew. Chem. Int. Ed.* **2011**, *50*, 549-552.

(34)   Bard, A. J.; Faulkner, L. R. *Electrochemical Methods*; John Wiley & Sons, Inc.: New York, **1980**.

(35)   Pathak, B.; Samanta , D.; Ahuja, R.; Jena, P. *ChemPhysChem* **2011**, 2423-2428.

(36)   Gutsev, G. L.; Boldyrev, A. I. *Chem. Phys. Lett.* **1984**, *108*, 250-254.

(37)   Zint, N.; Dreuw, A.; Cederbaum, L. S. *J. Am. Chem. Soc.* **2002**, *124*, 4910-4917.

(38)   (a) Wiersema, R. J.; Middaugh, R. L. *J. Am. Chem. Soc.* **1967**, *89*, 5078-5078. (b) Knoth, W. H.; Sauer, J. C.; England, D. C.; Hertler, W. R.; Muetterties, E. L. *J. Am. Chem. Soc.* **1964**, *86*, 3973-3983.

(39)   Middaugh, R. L.; Wiersema, R. J. *Inorg. Chem.* **1971**, *10*, 423-424.

(40)   Wong, E. H.; Kabbani, R. M. *Inorg. Chem.* **1980**, *19*, 451-455.

(41)   (a) Grabowski, Z. R.; Rotkiewicz, K.; Rettig, W. *Chem. Rev.* **2003**, *103*, 3899-4031. (b) Shima, S.; Vogt, S.; Gobels, A.; Bill, E. *Angew. Chem. Int. Ed.* **2010**, *49*, 9917-9921. (c) Felton, G. A. N.; Petro, B. J.; Glass, R. S.; Lichtenberger, D. L.; Evans, D. H. *J. Am. Chem. Soc.* **2009**, *131*, 11290-11291.

(42)   Speiser, B.; Tittel, C.; Einholz, W.; Schafer, R. *J. Chem. Soc. Dalton Trans.* **1999**, 1741-1752.

(43)   (a) Lewis, J. S.; Kaczmarczyk, A. *J. Am. Chem. Soc.* **1966**, *88*, 1068-1069. (b) Power, P. P. *Chem. Rev.* **2003**, *103*, 789-810.

(44)   Bowden, W. *J. Electrochem. Soc.* **1982**, *129*, 1249-1252.

(45)   Peymann, T.; Knobler, C. B.; Hawthorne, M. F. *J. Am. Chem. Soc.* **1999**, *121*, 5601-5602.

(46)   Davan, T.; Morrison, J. A. *Inorg. Chem.* **1986**, *25*, 2366-2372.

(47)   Gagné, R. R.; Koval, C. A.; Lisensky, G. C. *Inorg. Chem.* **1980**, *19*, 2854-2855.

Conclusion and Future Outlook

With various computational techniques, the thermodynamical properties of condensed phase systems were investigated including reaction mechanism. The key of dehydrogenation for the ionic solid, $LiNH_2BH_3(s)$ was successfully proposed and supported with experimental data. However, the success of solid-state reaction study using gaseous *ab initio* computation comes from the non-ionic intermediates in reaction pathways. The reaction energetics of the gaseous pathway needed a qualitative justification using the lattice energy change of the solid medium. The transition state search algorithm in crystal lattice will be highly demanding to make full description of reaction in solid media.

Acid dissociations in aqueous solution could be successfully predicted when the medium effect only played a bystander role. The determination and choice of the solute-solvent boundary is critical to make quantitative predictions for pK_{a2} while the pK_{a1} prediction is relatively insensitive to the solute-solvent boundary.

Solvation free energies of the dianion were applied to the determination of lattice energies of alkali metal dianion salts and an equation using static radii of cations and anions was not successful for the alkali metal dianion salts. Non-adiabatic electron binding for the dianions works well for the construction of a Born-Habor cycle for anions of small size. The cohesive energy from the calculations using a periodic boundary condition revealed that any conventional pseudopotential approach could not reproduce well the formation enthalpy of alkali metal dianion solid salts. A dispersion correction using a classical pair-wise potential could not be an alternative way when the polarization and induction between cation and dianion were

siginificant. New density fuctional formalism is expected to deal with the strong polarization in solid medium.

The *ab initio* computation with implicit solvation modeling reproduced well the experimental oxidative stability of hypercloso polyborane clusters when the consideration of solute-solvent boundary was appropriate. Computational results revealed that some of experimental data should be reevaluated. When a two-electron transfer is envolved, the similar reduction potentials of first and second electron transfer processes (potential compression) are not easly detected using cyclic voltammetry. *Ab initio* computation with solvation modeling can be alternative way to characterize the intermediates and investigate the electron transfer mechanism.

Appendix 1

Atomic Radii for Cavity Models

	UFF	UAKS[a]	Pauling	Klmat	SMD
Hydrogen	1.443	1.000	1.200	1.300	1.200
Carbon	1.925	1.500	1.500	2.000	1.850
Nitrogen	1.830	1.500	1.500	1.830	1.890
Oxygen	1.750	1.500	1.400	1.720	1.520
Fluorine	1.682	1.500	1.350	1.720	1.730
Phosphorus	2.074	1.980	1.900	1.800	2.100
Sulfur	2.018	1.980	1.850	.2160	2.490
Vanadium	1.572	2.008	1.572	1.900	
Arsenic	2.115	2.115	2.000	1.900	
Iron	1.456	1.456	1.456	1.900	

[a]In the atom topological model (UATM), the hydrogen atoms are enclosed in the same sphere of the heavy atom they are bound to, and the sphere radii are set according to the atomic number, the charge and the hybridization of the atom, possibly corrected for first neighbor effects. The UAKS values[b] are UATM basis radii optimized for PBE0/6-31G(d). The molecular environment modifies the actual radii. [b]Barone, V.; Cossi, M.; Tomasi, J. J Chem Phys 1997, 107, 3210.
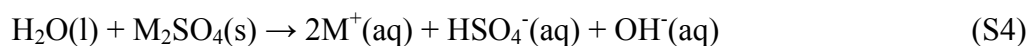
Appendix 2

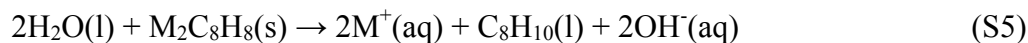-- Hydrolysis of CO_3^{2-}, SO_4^{2-}, and $C_8H_8^{2-}$ --

The dissolution of $M_2CO_3(s)$ ($M=Li^+$, Na^+, and K^+) and hydrolysis of $CO_3^{2-}(aq)$ is the sum of following three steps.

$$M_2CO_3(s) \rightarrow 2M^+(aq) + CO_3^{2-}(aq) \tag{S1}$$

$$H_2O(l) \rightarrow H^+(aq) + OH^-(aq) \tag{S2}$$

$$H^+(aq) + CO_3^{2-}(aq) \rightarrow HCO_3^-(aq) \tag{S3}$$

For eq S1, the free energy of dissolution (ΔG^o_{diss}) is computed with $\Delta G_{latt}(M_2CO_3)$, $\Delta G_{solv}(M^+)$, and $\Delta G_{solv}(CO_3^{2-})$. Eq S2 is the autoionization of $H_2O(l)$, for which $\Delta G_w=19.1$ kcal/mol at pH 7 ($\Delta G_w = -RTlnK_w$). Eq S3 is the reverse process of acid dissociation for HCO_3^- (aq). The value of $-\Delta G_{aq}^2$ for HCO_3^- is -14.1 kcal/mol using $\Delta G_{aq}^2 = 1.364*pK_{a2}$ at 298.15K where $pK_{a2}=10.3$ (R. P. Bell, The proton in chemistry, Cornell University Press, Ithaca, 1973). The overall free energy (ΔG^o_{diss}') of $H_2O(l) + M_2CO_3(s) \rightarrow 2M^+(aq) + HCO_3^-(aq) + OH^-(aq)$ is given by $\Delta G^o_{diss} + \Delta G_w + (-\Delta G_{aq}^2)$, which becomes $\Delta G^o_{diss} + 5.0$ kcal/mol and the actual anion from the dissolution of $M_2CO_3(s)$ at pH 7 is $CO_3^{2-}(aq)$. The value of ΔG^o_{diss}' for $M_2SO_4(s)$ ($M=Li^+$, Na^+, and K^+) is the sum of ΔG^o_{diss}, 19.1 kcal/mol for ΔG_w, and -2.7 kcal/mol for ΔG_{aq}^2 (eq S4).

$$H_2O(l) + M_2SO_4(s) \rightarrow 2M^+(aq) + HSO_4^-(aq) + OH^-(aq) \tag{S4}$$

The hydrolysis of SO_4^{2-}(aq) to HSO_4^-(aq) is a non-spontaneous process at pH 7 and the actual anion from the dissolution of M_2SO_4(s) at pH 7 is SO_4^{2-}(aq) (ΔG^o_{diss}' = ΔG^o_{diss} + 16.4 kcal/mol). The value of ΔG^o_{diss}' for $M_2C_8H_8$(s) (M=Li^+, Na^+, and K^+) is the sum of ΔG^o_{diss}, 2*19.1 kcal/mol for ΔG_w, and -72.9 kcal/mol for -ΔG_{aq} (eq S5).

$$2H_2O(l) + M_2C_8H_8(s) \rightarrow 2M^+(aq) + C_8H_{10}(l) + 2OH^-(aq) \qquad (S5)$$

For $2H^+$(aq) + $C_8H_8^{2-}$(aq) $\rightarrow$ C_8H_{10}(aq), the value of ΔG_{gas} with the M05-2X/6-311++G(3df,2pd), -264.0 kcal/mol of $\Delta G_{solv}(H^+)$, and ΔG_{solv} of C_8H_{10} and $C_8H_8^{2-}$ with CPCM/Pauling cavity set produce ΔG_{aq} (ΔG_{aq} = ΔG_{gas} + $\Delta\Delta G_{solv}$). At pH 7, the hydrolysis of $C_8H_8^{2-}$(aq) is very spontaneous process (ΔG^o_{diss}' = ΔG^o_{diss} -34.7 kcal/mol).

1,3,5-clcyooctatriene (C_8H_{10}) is known to isomerization to 1,3,6-cyclooctatriene (C_8H_{10}) (Baldwin, J. E.; Kaplan, M. S. *J. Am. Chem. Soc*. **1972**, *94*, 4696-4699). The hydrogenation reaction ($3H_2$(g) + C_8H_{10}(g) $\rightarrow$ C_8H_{16}(g)) of 1,3,5-cyclooctatriene is -72.4 kcal/mol while the hydrogenation reaction of 1,3,6-cyclooctatriene is -79.9 kcal/mol (Turner, R. B.; Meador, W. R.; Doering, W. V. E.; Knox, L. H.; Mayer, J. R.; Wiley, D. W. *J. Am. Chem. Soc.* **1957**, *79*, 4127-4133). Using -30.1 kcal/mol for the heat of formation (ΔH_f) of cyclooctane, the ΔH_f of 1,3,5-cyclooctatriene is 42.2 kcal/mol while the ΔH_f of 1,3,6-cyclooctriene is 49.8 kcal/mol. Thus, the 1,3,5-cyclooctatriene isomer is 7.6 kcal/mol more stable than the 1,3,6-cyclooctatriene.